

# **Microscale Approaches to the Rapid Evaluation and Specification of Microfiltration Processes**

Nigel Brynmor Jackson

A thesis submitted for the degree of  
Doctor of Philosophy  
to  
University College London

Department of Biochemical Engineering  
University College London  
Torrington Place  
London  
WC1E 7JE

## **Signed Declaration**

I, Nigel Brynmor Jackson, confirm that the work presented in this thesis is my own. Where information has been derived from other sources, I confirm that this has been indicated in the thesis.

Signed: \_\_\_\_\_

Date: \_\_\_\_\_

## Abstract

A high throughput method for the study of normal flow microfiltration operations has been established using a custom designed 8-24 well filter plate (0.8 cm<sup>2</sup>) and a commercial 96-well Multiscreen filter plate (0.3 cm<sup>2</sup>). Integration of this new approach with a typical robotic platform has enabled automation of the experimental procedure.

Membrane resistance data can be quantified using either filter plate. The accuracy of these measurements has helped to determine that plate position does not affect experimental results and applied pressure difference does not vary across either plate. Each of the two filter plate designs has been used to demonstrate that cell condition following fermentation, buffer type and media composition are all important factors influencing the specific cake resistance of *E.coli* TOP10 cells. The microscale method therefore allows parallel quantification of the impact of upstream process conditions on microfiltration performance. The custom filter plate, optimised for bioprocess studies, allows multiple membrane types to be evaluated on a single plate and the measurement of both permeate and retentate masses to ensure against cross-contamination or loss. Lower variation in specific cake resistance values is seen in the custom filter plate compared with the commercial filter plate.

These automated microscale normal flow microfiltration techniques have also been combined with factorial experimentation to identify the key factors and interactions which influence the protein transmission and specific cake resistance during filtration of an *E.coli* and protein mixture. Results indicated pH and ionic strength were important factors. The pH and ionic strength interaction was further investigated using response surface methodology and a window of operation was generated showing the pH ( $5.5 \pm 0.1$ ) and ionic strength ( $153 \pm 8$  mM) values necessary to achieve a protein transmission above 95% and a specific cake resistance below  $80 \times 10^{12}$  m.kg<sup>-1</sup>. The custom microwell filter plate cake resistance and transmission data from the response surface models scaled up by a factor of 17 to conventional

laboratory scale equipment, showing that the optimum conditions achieved in the microwell could be replicated at a larger scale. In addition to this, experiments at the laboratory scale confirmed the optimum identified by the custom microwell filter plate. This demonstrated that the combination of experimental design and the custom microwell filter plate is capable of investigation, optimisation and scale-up of a complex separation process.

Finally, the approaches established here have been expanded to a whole process sequence for the purification of plasmid DNA. A non-chromatographic process sequence, which might be used in industrial practice, involving 7 consecutive processes (4 filtration steps) has been run with 72 combinations of 8 different factors in parallel, collecting hundreds of scaleable data points. The key filtration challenges were identified as the lysis clarification and the removal of lipid removal agent (LRA). Once again the important interactions and trends were identified using microscale experimentation. A major discovery was the filter aid effect of the adsorbent; increasing LRA concentration showed a dramatic reduction in specific cake resistance. This trend was repeated in larger scale devices with different filter formats at high area (150X) and volumetric (2000X) scale-up factors. This shows that the microscale techniques developed in this thesis are capable of determining quantitative, scaleable data for early stage evaluation of whole microwell process sequences.

## Acknowledgements

Special thanks must go to my supervisor, Professor Gary Lye, for all his support and advice throughout my postgraduate and undergraduate years at UCL. Dr John Liddell has helped guide this project throughout and both his technical input and financial support through Avecia Biotechnology have been greatly appreciated. Funding for my research studentship from the Biotechnology and Biological Sciences Research Council (BBSRC) has also been vital in supporting my work.

Throughout all levels of the Department of Biochemical Engineering at UCL there have been people who have given their time to help me. Professors Mike Hoare and Nigel Titchener-Hooker have given invaluable advice on aspects of this work. I would also like to thank Gareth Mannall for his practical assistance with the HPLC, Simyee Kong and Sinyee Yau for guidance on working with plasmid DNA and Jonathan Stanway for assistance with the operation of larger scale filtration devices and LRA studies. Thanks are also due to everyone in the technical workshop who made the custom microwell filter plates that perform the important experimental work presented here.

The department gave more than just practical support. From Tuesday evening football in Regents Park to the extravagant Christmas dinners, there were many occasions to enjoy working at UCL. Thanks to everyone involved with the Beaker Society, especially the committee during the memorable year I was president.

Finally I am indebted to all my family for their support throughout my studies, especially my parents and my wife, Jen.

---

## Contents

<b>Section</b>	<b>Title</b>	<b>Page</b>
	<b>Abstract</b>	<b>3</b>
	<b>Acknowledgements</b>	<b>5</b>
	<b>Contents</b>	<b>6</b>
	<b>List of Figures</b>	<b>15</b>
	<b>List of Tables</b>	<b>19</b>
	<b>Nomenclature</b>	<b>21</b>
	<b>Abbreviations</b>	<b>25</b>
<b>1.0</b>	<b>Introduction</b>	<b>26</b>
<b>1.1</b>	<b>Overview</b>	<b>26</b>
<b>1.2</b>	<b>Bioprocessing</b>	<b>26</b>
<b>1.2.1</b>	<b>Target molecules</b>	<b>26</b>
1.2.1.1	Proteins	27
1.2.1.2	Plasmid DNA	27
<b>1.2.2</b>	<b>Upstream processes</b>	<b>28</b>
1.2.2.1	Recombinant expression systems	28
<b>1.2.3</b>	<b>Downstream processes</b>	<b>29</b>
<b>1.3</b>	<b>Microfiltration</b>	<b>31</b>
<b>1.3.1</b>	<b>Membrane processes</b>	<b>31</b>
<b>1.3.2</b>	<b>Filter media</b>	<b>33</b>
1.3.2.1	Polymeric membranes.	33
1.3.2.2	Depth filters	34
<b>1.3.3</b>	<b>Tangential flow microfiltration</b>	<b>34</b>
<b>1.3.4</b>	<b>Normal flow microfiltration</b>	<b>35</b>

---

1.3.4.1	Normal flow filtration theory	35
1.3.4.1.1	Complete blocking filtration law	38
1.3.4.1.2	Standard blocking filtration law	40
1.3.4.1.3	Intermediate blocking filtration law	42
1.3.4.1.4	Cake filtration law	43
1.3.4.1.5	Cake filtration law for constant flow operation	44
1.3.4.1.6	Combined filtration models	45
<b>1.3.5</b>	<b>Microfiltration of <i>E.coli</i></b>	<b>46</b>
<b>1.3.6</b>	<b>Microfiltration of plasmid DNA</b>	<b>47</b>
<b>1.4</b>	<b>Microscale bioprocessing</b>	<b>47</b>
<b>1.4.1</b>	<b>Scale-down of bioprocesses</b>	<b>48</b>
1.4.1.2	Microfiltration scale-down	48
1.4.1.2.1	Scale-down of normal flow filtration	49
1.4.1.2.2	Scale-down of tangential flow filtration	49
1.4.1.3	Ultra scale down of bioprocesses	49
<b>1.4.2</b>	<b>Microscale automation</b>	<b>50</b>
<b>1.5</b>	<b>Design of experiments</b>	<b>51</b>
<b>1.5.1</b>	<b>Factorial experiments</b>	<b>52</b>
1.5.1.1	Analysis of factorial experiments	53
1.5.1.2	Centre points in factorial experiments	53
1.5.1.3	Qualitative factors	54
1.5.1.4	Error analysis in factorial experiments	54
1.5.1.5	Fractional factorial analysis	54
1.5.1.6	Blocking in factorial analysis	57
<b>1.5.2</b>	<b>Response surface methodology</b>	<b>57</b>
1.5.2.1	Types of response surface	58
<b>1.5.3</b>	<b>Windows of operation</b>	<b>58</b>
<b>1.6</b>	<b>Project significance</b>	<b>59</b>
<b>1.7</b>	<b>Aims of the project</b>	<b>60</b>

---

<b>2.0</b>	<b>Materials and methods</b>	<b>62</b>
<b>2.1</b>	<b>Introduction</b>	<b>62</b>
<b>2.2</b>	<b>Chemicals</b>	<b>62</b>
<b>2.3</b>	<b>Microfiltration materials and equipment</b>	<b>62</b>
<b>2.3.1</b>	<b>Microfiltration membranes and filters</b>	<b>62</b>
<b>2.3.2</b>	<b>Tecan automation robot</b>	<b>63</b>
2.3.2.1	Vacuum manifold	63
2.3.2.2	Mixing	67
2.3.2.3	Liquid handling	67
2.3.2.4	Plate handling	67
<b>2.3.3</b>	<b>Membrane cell</b>	<b>68</b>
<b>2.3.4</b>	<b>Rotating vertical leaf filter (RVLF) scale-down device</b>	<b>70</b>
<b>2.3.5</b>	<b>Candle filter</b>	<b>70</b>
<b>2.4</b>	<b><i>E.coli</i> fermentation feed preparation</b>	<b>72</b>
<b>2.4.1</b>	<b>Fermentation conditions</b>	<b>72</b>
<b>2.4.2</b>	<b>Dry cell weight measurement</b>	<b>72</b>
<b>2.4.3</b>	<b>Sample preparation</b>	<b>73</b>
<b>2.5</b>	<b>Plasmid DNA feed preparation</b>	<b>74</b>
<b>2.5.1</b>	<b>Plasmid DNA process overview</b>	<b>74</b>
2.5.1.1	Fermentation conditions	74
2.5.1.2	Resuspension	74
2.5.1.3	Cell lysis	74
2.5.1.4	Lysate clarification	76
2.5.1.5	CTAB precipitation	76
2.5.1.6	Precipitate recovery	76
2.5.1.7	Precipitate dissolution	76
2.5.1.8	Precipitate removal	77
2.5.1.9	LRA adsorption	77
2.5.1.10	LRA adsorbent Removal	77
<b>2.5.2</b>	<b>Microscale plasmid DNA purification methods</b>	<b>78</b>

---

2.5.2.1	Lysis for microscale filtration	78
2.5.2.2	Microscale lysate clarification	79
2.5.2.3	Microscale CTAB precipitation	80
2.5.2.4	Microscale precipitate recovery	80
2.5.2.5	Microscale precipitate dissolution	81
2.5.2.6	Microscale precipitate removal	81
2.5.2.7	Microscale LRA adsorption	82
2.5.2.8	Microscale LRA removal	82
2.5.2.9	Further microscale LRA removal	82
<b>2.5.3</b>	<b>Laboratory scale plasmid DNA purification methods</b>	<b>83</b>
2.5.3.1	Lysis for laboratory scale filtration	83
2.5.3.2	Laboratory scale lysate clarification	83
2.5.3.3	Laboratory scale CTAB precipitation	83
2.5.3.4	Laboratory scale precipitate recovery	83
2.5.3.5	Laboratory scale precipitate dissolution	83
2.5.3.6	Laboratory scale precipitate removal	84
2.5.3.7	Laboratory scale LRA removal	84
<b>2.5.4</b>	<b>Pilot scale LRA adsorbent removal feed preparation</b>	<b>84</b>
2.5.4.1	Lysis for pilot scale filtration	84
2.5.4.2	Lysate clarification for pilot scale filtration	85
2.5.4.3	CTAB precipitation for pilot scale filtration	85
2.5.4.4	Precipitate recovery and dissolution for pilot scale filtration	85
2.5.4.5	Precipitate removal for pilot scale filtration	86
2.5.4.6	LRA adsorption for pilot scale filtration	86
2.5.4.7	Pilot scale LRA removal	86
<b>2.6</b>	<b>Analytical methods</b>	<b>86</b>
<b>2.6.1</b>	<b>Lysozyme assay</b>	<b>86</b>
<b>2.6.2</b>	<b>Isopropanol precipitation</b>	<b>87</b>
<b>2.6.3</b>	<b>DNA agarose gel electrophoresis</b>	<b>88</b>
<b>2.7</b>	<b>Experimental design</b>	<b>88</b>
<b>2.7.1</b>	<b>Factorial design</b>	<b>88</b>

---

2.7.1.1	<i>E.coli</i> filtration factorial design	88
2.7.1.2	Plasmid DNA purification factorial design	88
<b>2.7.2</b>	<b>Response surfaces</b>	<b>91</b>
<b>2.8</b>	<b>Data analysis</b>	<b>91</b>
<b>2.8.1</b>	<b>General error estimation</b>	<b>91</b>
<b>2.8.2</b>	<b>Comparison of means</b>	<b>94</b>
<b>2.8.3</b>	<b>Lines of best fit</b>	<b>94</b>
<b>2.8.4</b>	<b>Factorial experiments</b>	<b>95</b>
2.8.4.1	Estimation of main effects and interactions	95
2.8.4.2	Error estimation for replicated factorial experiments	96
2.8.4.3	Error estimation for non-replicated factorial experiments	98
<b>2.8.5</b>	<b>Response surfaces</b>	<b>98</b>
2.8.5.1	Response surface error estimation	100
<b>2.8.6</b>	<b>Clarification</b>	<b>100</b>
<b>2.8.7</b>	<b>Calculating flux</b>	<b>101</b>
<b>2.8.8</b>	<b>Smoothing pressure data</b>	<b>102</b>
<b>2.8.9</b>	<b>Viscosity</b>	<b>102</b>
2.8.9.1	Water viscosity correlation	102
2.8.9.2	Permeate viscosity	103
<b>2.8.10</b>	<b>Density</b>	<b>103</b>
<b>2.8.11</b>	<b>Filtration scale-up predictions</b>	<b>103</b>
2.8.11.1	Predicting flux in constant pressure filtration	104
2.8.11.2	Predicting pressure in constant flow filtration	105
<b>2.8.12</b>	<b>Protein transmission</b>	<b>106</b>
<b>3.0</b>	<b>Design and evaluation of an automated microscale microfiltration technique</b>	<b>107</b>
<b>3.1</b>	<b>Aim of the chapter</b>	<b>107</b>
<b>3.2</b>	<b>Custom filter plate design and microscale operation</b>	<b>107</b>
<b>3.2.1</b>	<b>Custom microwell filter plate design</b>	<b>108</b>

---

3.2.2	Verification of microscale performance	109
3.3	<b>Water flux and membrane resistance measurement</b>	<b>111</b>
3.3.1	Quantification of membrane resistance at microscale	111
3.3.2	Comparison of water flux data at different scales	113
3.3.3	Variation of membrane resistance across the filter plates	115
3.3.4	Importance of membrane resistance data	117
3.4	<b>Flux behaviour during microfiltration of <i>E.coli</i> fermentation broths</b>	<b>118</b>
3.4.1	Quantification of specific cake resistance at microscale	118
3.4.2	Influence of harvest time and broth age	122
3.4.3	Influence of broth pH and specific buffers	124
3.4.4	Influence of media composition	125
3.5	<b>Evaluation of microscale methods and custom filter plate design</b>	<b>129</b>
3.6	<b>Summary</b>	<b>132</b>
4.0	<b>Microfiltration optimisation using automated microscale experimentation coupled with statistical design of experiments</b>	<b>133</b>
4.1	<b>Aim of the chapter</b>	<b>133</b>
4.2	<b>Introduction</b>	<b>133</b>
4.2.1	<b>Product transmission</b>	<b>134</b>
4.2.1.1	Potential influence of membrane resistance	134
4.2.1.2	Model system	135
4.2.2	<b>Application of design of experiments</b>	<b>135</b>
4.3	<b>Factorial experiments</b>	<b>136</b>
4.3.1	<b>Factorial experiment design and implementation</b>	<b>136</b>
4.3.2	<b>Factorial results analysis of protein transmission</b>	<b>138</b>
4.3.3	<b>Factorial results analysis of specific cake resistance</b>	<b>140</b>
4.3.4	<b>Ionic strength and pH interactions</b>	<b>143</b>

---

<b>4.4</b>	<b>Response surface experiments</b>	<b>147</b>
4.4.1	Response surfaces for pH and ionic strength	148
4.4.2	Microfiltration window of operation	151
<b>4.5</b>	<b>Scale-up of optimum microfiltration conditions</b>	<b>153</b>
<b>4.6</b>	<b>Summary</b>	<b>156</b>
<b>5.0</b>	<b>Automated Microscale Plasmid DNA Purification Process Sequence</b>	<b>159</b>
<b>5.1</b>	<b>Aim of the chapter</b>	<b>159</b>
<b>5.2</b>	<b>Plasmid DNA purification</b>	<b>159</b>
5.2.1	Non-chromatographic process	160
5.2.2	Automated microwell process	162
5.2.3	Factorial design	165
<b>5.3</b>	<b>Results of microscale factorial process sequence experiments</b>	<b>168</b>
5.3.1	Lysis clarification	168
5.3.2	Precipitation process operations	175
5.3.3	LRA removal	176
5.3.4	Overall process performance: analysis of final product quality	178
<b>5.4</b>	<b>Scale-up of the key filtration steps</b>	<b>179</b>
5.4.1	Lysis clarification scale-up	180
5.4.2	LRA removal scale-up	182
5.4.2.1	RVLF scale-up	182
5.4.2.2	Candle filter scale-up	186
5.4.3	Scale-up summary	189
<b>5.5</b>	<b>Summary</b>	<b>189</b>
<b>6.0</b>	<b>Overall conclusions and future work</b>	<b>192</b>
<b>6.1</b>	<b>Overall conclusions</b>	<b>192</b>

---

<b>6.2</b>	<b>Future work</b>	<b>194</b>
<b>7.0</b>	<b>References</b>	<b>197</b>
<b>A.0</b>	<b>Appendix A: Calibration curves</b>	<b>212</b>
<b>A.1</b>	<b>Dry cell weight</b>	<b>212</b>
<b>A.2</b>	<b>Lysozyme concentration</b>	<b>212</b>
<b>B.0</b>	<b>Appendix B: Microscale calculation examples</b>	<b>215</b>
<b>B.1</b>	<b>Example <i>E.coli</i> specific cake resistance calculation</b>	<b>215</b>
<b>B.1.1</b>	<b>Raw data</b>	<b>215</b>
B.1.1.1	Shared raw data	215
B.1.1.2	Yeast extract solution	217
B.1.1.3	Cell broth supernatant	217
<b>B.1.2</b>	<b>Linearised cake formation data</b>	<b>217</b>
B.1.2.1	Yeast extract solution	217
B.1.2.2	Cell broth supernatant	218
<b>B.1.3</b>	<b>Specific cake resistance</b>	<b>218</b>
B.1.3.1	Yeast extract solution	218
B.1.3.2	Cell broth supernatant	219
<b>B.1.4</b>	<b>Flux predictions</b>	<b>219</b>
B.1.4.1	Yeast extract solution	220
B.1.4.2	Cell broth supernatant	220
<b>B.1.5</b>	<b>Summary</b>	<b>221</b>
<b>B.2</b>	<b>Example LRA specific cake resistance calculation</b>	<b>221</b>
<b>B.2.1</b>	<b>Shared raw data</b>	<b>221</b>
<b>B.2.2</b>	<b>10g.L<sup>-1</sup><sub>liquid</sub> LRA</b>	<b>223</b>
<b>B.2.3</b>	<b>50g.L<sup>-1</sup><sub>liquid</sub> LRA</b>	<b>223</b>

---

<b>B.2.4</b>	<b>Summary</b>	<b>224</b>
<b>C.0</b>	<b>Appendix C: Chapter 4 data</b>	<b>225</b>
<b>C.1</b>	<b><i>E.coli</i> and lysozyme factorial data</b>	<b>225</b>
<b>C.2</b>	<b><i>E.coli</i> and lysozyme response surface data</b>	<b>225</b>
<b>D.0</b>	<b>Appendix D: Chapter 5 data</b>	<b>230</b>
<b>D.1</b>	<b>Lysis clarification data</b>	<b>230</b>
<b>D.2</b>	<b>LRA removal data</b>	<b>230</b>
<b>D.3</b>	<b>Example plasmid DNA gels</b>	<b>236</b>
<b>E.0</b>	<b>Appendix E: Quantification of low specific cake resistances</b>	<b>238</b>
<b>E.1</b>	<b>Method for quantification of low specific cake resistances</b>	<b>238</b>
<b>E.2</b>	<b>Evaluation of precipitate removal results</b>	<b>240</b>
<b>E.3</b>	<b>Scale-up of precipitate recovery</b>	<b>243</b>
<b>E.4</b>	<b>Summary</b>	<b>243</b>

## List of Figures

Figure	Legend Summary	Page
<b>Figure 1.1</b>	Schematic demonstrating the differences between tangential flow filtration (TFF) and normal flow filtration (NFF).	36
<b>Figure 1.2</b>	Visual representation of main effects and interactions for a $2^3$ factorial experiment.	55
<b>Figure 2.1</b>	Two photographs of different configurations of the Tecan Genesis Freedom liquid handling robot.	64
<b>Figure 2.2</b>	Detail of the Tecan vacuum manifold system.	66
<b>Figure 2.3</b>	Experimental set-ups for membrane cell operation	69
<b>Figure 2.4</b>	The rotating vertical leaf filter (RVLf) scale-down laboratory filter	71
<b>Figure 2.5</b>	Overview of the non-chromatographic process for the production and purification of plasmid DNA	75
<b>Figure 2.6</b>	Details of the levels of pH and ionic strength used to generate the response surfaces described in Section 4.4.	92
<b>Figure 2.7</b>	Effect of the face centre points on the rotatability of the response surface design.	93
<b>Figure 3.1</b>	Detail of the custom filter plates designed during this work.	110
<b>Figure 3.2</b>	(a) Typical pressure profile for a water flux experiment using the custom filter plate and (b) temperature normalised water flux data determined for the different membrane geometries.	114
<b>Figure 3.3</b>	(a) Membrane resistance variation between individual wells on a single Multiscreen filter plate, (b) Repeat experiment with the same filter plate rotated through $180^\circ$ .	116
<b>Figure 3.4</b>	Illustration of the method used for determination of specific cake resistance from microscale and negative pressure experiments.	120
<b>Figure 3.5</b>	Specific cake resistance determined for an <i>E.coli</i> TOP10 fermentation broth after various broth ageing times.	123

<b>Figure 3.6</b>	Specific cake resistance of washed <i>E.coli</i> TOP10 cells resuspended in various media components.	127
<b>Figure 3.7</b>	Variation of permeate flux over time for washed <i>E.coli</i> TOP10 cells resuspended in original broth supernatant and freshly prepared yeast extract solution.	128
<b>Figure 3.8</b>	Parity plots of all the specific cake resistance data generated from the membrane cell against data generated from: (a) the Multiscreen filter plate and (b) the custom filter plate.	131
<b>Figure 4.1</b>	Effect and interaction plot for measured protein transmission levels in a $2^{5-1}$ factorial experiment.	139
<b>Figure 4.2</b>	Effect and interaction plot for measured specific cake resistance values in a $2^{5-1}$ factorial experiment.	141
<b>Figure 4.3</b>	Interaction plot showing the measured variation of protein transmission with pH at ionic strengths of 100mM and 200mM.	145
<b>Figure 4.4</b>	Interaction plot showing the measured variation of specific cake resistance with pH at ionic strengths of 100mM and 200mM.	146
<b>Figure 4.5</b>	Response surface plot of a model describing protein transmission as a function of pH and ionic strength.	149
<b>Figure 4.6</b>	Response surface plots of models describing specific cake resistance as a function of pH and ionic strength: (a) in the presence of $2 \text{ g.L}^{-1}$ protein and (b) in the absence of protein.	150
<b>Figure 4.7</b>	Overlay of the specific cake resistance (blue) and protein transmission (red) contour plots derived from the individual response surface models (Figures 4.5 and 4.6).	152
<b>Figure 4.8</b>	Overlay plot of factor ranges in and around the optimum pH and ionic strength trade-off conditions (purple shaded area) tested at laboratory scale.	154
<b>Figure 4.9</b>	Analysis of membrane cell experiments carried out in and around the optimum trade-off conditions. Figures indicate the percentage improvement of (a) lysozyme transmission and (b) specific cake resistance in comparison to the predicted optimum.	155
<b>Figure 4.10</b>	Scale-up of optimum microfiltration conditions showing permeate flux and protein transmission.	157
<b>Figure 5.1</b>	Overview of a non-chromatographic process for the production and purification of plasmid DNA.	161

<b>Figure 5.2</b>	Effect and interaction plot for measured permeate flux during the lysis clarification step of a plasmid DNA recovery process.	170
<b>Figure 5.3</b>	Interaction plot showing the variation of measured permeate flux at lysis clarification as a function of mixing speed during lysis neutralisation, using Celpure P65 and Celpure P300 filter aids.	172
<b>Figure 5.4</b>	Interaction plot showing the variation of measure permeate flux at lysate clarification with Celpure filter aid concentration following a lysis neutralisation step at mixing speeds of 400rpm and 1200rpm.	173
<b>Figure 5.5</b>	Effect and interaction plot for measured percentage clarification during the lysis clarification step of a plasmid DNA recovery process.	174
<b>Figure 5.6</b>	Effect and two-factor interactions or measured specific cake resistance during the LRA recovery step of a plasmid DNA recovery process.	177
<b>Figure 5.7</b>	Flux and pressure profiles for lysis clarification in a rotating vertical leaf filter scale-down device with custom microwell filter plate predictions.	181
<b>Figure 5.8</b>	Measured specific cake resistance and modified cake filtration constant values for LRA removal from a plasmid DNA solution at varying LRA concentrations.	183
<b>Figure 5.9</b>	Flux and pressure profiles for LRA adsorbant ( $10 \text{ g.L}_{\text{liquid}}^{-1}$ ) removal from a plasmid DNA solution in a rotating vertical leaf filter scale-down device with custom microwell filter plate predictions.	184
<b>Figure 5.10</b>	Flux and pressure profiles for LRA adsorbant ( $50 \text{ g.L}_{\text{liquid}}^{-1}$ ) removal from a plasmid DNA solution in a rotating vertical leaf filter scale-down device and custom microwell filter plate predictions	185
<b>Figure 5.11</b>	Flux and pressure profiles for LRA adsorbant ( $10 \text{ g.L}_{\text{liquid}}^{-1}$ ) removal from a plasmid DNA solution in a candle filter with custom microwell filter plate and RVLF predictions.	187
<b>Figure 5.12</b>	Flux and pressure profiles for LRA adsorbant ( $50 \text{ g.L}_{\text{liquid}}^{-1}$ ) removal from a plasmid DNA solution in a candle filter with custom microwell filter plate and RVLF predictions.	188
<b>Figure 5.13</b>	Specific cake resistance values for LRA removal at concentrations of $10 \text{ g.L}_{\text{liquid}}^{-1}$ and $50 \text{ g.L}_{\text{liquid}}^{-1}$ . Results from various scales compared: custom microwell filter plate, RVLF and candle filter.	190

---

<b>Figure A.1</b>	(a) Typical <i>E.coli</i> shake flask fermentation growth curve and (b) the calibration of optical density to <i>E.coli</i> dry cell weight.	213
<b>Figure A.2</b>	Typical Lysozyme HPLC calibration curve showing the strong linear response over the concentration range tested.	214
<b>Figure B.1</b>	The data progression from (a) example custom microwell filter plate raw mass and time data, to (b) linearised cake formation plots, through (c) specific cake resistance data, to (d) predicted laboratory scale flux decay curves.	216
<b>Figure B.2</b>	LRA data progression from (a) example custom microwell filter plate flow-through permeate mass and (b) pressure profile during flow-through to (c) specific cake resistance data.	222
<b>Figure D.1</b>	Example gel from the post LRA samples for factorial analysis, showing the very light bands and contamination, including poor standards in the first three lanes.	236
<b>Figure D.2</b>	Example gel from successful scouting tests looking at the effect of sodium chloride concentration in precipitate dissolution.	237
<b>Figure D.3</b>	Example gel from a pilot plant study including an LRA adsorption step.	237
<b>Figure E.1</b>	Effect and interactions for measured specific cake resistance during the precipitate removal step of a plasmid DNA recovery process.	242

## List of Tables

Table	Legend Summary	Page
<b>Table 1.1</b>	Various expression systems and their characteristics.	29
<b>Table 1.2</b>	Example unit operations at the various stages of downstream processing.	30
<b>Table 1.3</b>	Typical particles retained by different membrane processes.	32
<b>Table 1.4</b>	Example bioprocess applications of microfiltration and ultrafiltration.	33
<b>Table 1.5</b>	A comprehensive summary of the constant pressure filtration blocking laws.	39
<b>Table 1.6</b>	The coding for a full $2^3$ factorial experiment.	52
<b>Table 2.1</b>	Summary of the $2^{5-1}$ factorial experiment design coding for the lysozyme transmission experiments in Chapter 4.	89
<b>Table 2.2</b>	Summary of the $2^{8-2}$ factorial experiment design coding for the plasmid purification experiments in Chapter 5.	90
<b>Table 3.1</b>	Filtration equipment specifications and measured membrane resistances.	112
<b>Table 3.2</b>	Specific cake resistance of <i>E.coli</i> TOP10 cells determined in the presence or absence of 100 mM acetate buffer.	125
<b>Table 4.1</b>	Summary of the factors and levels selected for the $2^{5-1}$ factorial experiment described in Section 4.3.1.	137
<b>Table 5.1</b>	Summary of the individual unit operations involved in a typical non-chromatographic purification process for plasmid DNA showing factors and process decisions that need to be investigated.	163
<b>Table 5.2</b>	Summary of the factors and their chosen levels for the plasmid DNA process sequence $2^{8-2}$ factorial experiment.	166

---

<b>Table 5.3</b>	Summary of measured responses and illustration of the pyramidal nature of factorial design used within the plasmid DNA process sequence study.	167
<b>Table C.1</b>	Raw data and calculations for the factorial screening experiments described in detail in Section 4.3 including specific cake resistance and lysozyme transmission.	226
<b>Table C.2</b>	Raw data and calculations for the response surface experiments described in detail in Section 4.4 including specific cake resistance and lysozyme transmission.	228
<b>Table C.3</b>	Raw data and calculations for the response surface experiments in the absence of lysozyme described in detail in Section 4.4 including specific cake resistance.	229
<b>Table D.1</b>	Raw data and calculations for the lysis clarification factorial screening experiments described in detail in Section 5.3.1 including flux and clarification percentage.	231
<b>Table D.2</b>	Raw data and calculations for the LRA removal factorial screening experiments described in detail in Section 5.3.3 including specific cake resistance and modified cake filtration constant.	234
<b>Table E.1</b>	The raw data and specific cake resistance calculations from evaluation of the low specific cake resistances during the precipitate recovery stage of a plasmid DNA purification step.	241

## Nomenclature

$A$	effective filter area ( $\text{m}^2$ )
$X_A$	factorial analysis matrix
$A_0$	initial effective filtration area ( $\text{m}^2$ )
$b_i$	$i^{\text{th}}$ linear regression coefficient
$C$	volume of solids per unit volume of filtrate
$c$	number of centre-points
$c_f$	dry solids concentration in the feed ( $\text{kg}\cdot\text{m}^{-3}$ )
$CI_{95\%}$	95% confidence interval
$df_{err}$	degrees of freedom for estimating the error
$df_{tot}$	total degrees of freedom
$E$	factorial effects matrix
$E_A$	main effect A
$E_{AB}$	AB interaction
$E_I$	factorial mean
$f_i$	predicted model for the dependent variable ( $y_i$ ) at $x_i$
$G$	acceleration due to gravity ( $\text{m}\cdot\text{s}^{-2}$ )
$I$	buffer ionic strength (mM)
$J$	filtrate / permeate flux ( $\text{m}\cdot\text{s}^{-1}$ )
$J_0$	initial filtrate / permeate flux ( $\text{m}\cdot\text{s}^{-1}$ )
$k$	number of factorial experiment factors
$K$	filtration constant (various units)
$K_b$	complete blocking constant ( $\text{s}^{-1}$ )
$K_c$	cake filtration constant ( $\text{s}\cdot\text{m}^{-6}$ )
$K_c'$	modified cake filtration constant
$K_i$	intermediate blocking constant ( $\text{m}^{-3}$ )
$K_s$	standard blocking constant ( $\text{m}^{-3}$ )

---

$L$	pore length (m)
$m$	mass ratio of wet cake to dry cake
$N$	number of pores
$n$	fouling exponent
$n$	number of measurements
$OD_B$	optical density of the blank
$OD_F$	optical density of the feed
$OD_P$	optical density of the permeate
$p$	fractional factorial experiment exponent
$p_m$	number of predictors in the model
$pH$	pH
$\Delta P$	(transmembrane) pressure difference (Pa)
$Q$	filtrate / permeate flowrate ( $\text{m}^3 \cdot \text{s}^{-1}$ )
$Q_0$	initial filtrate / permeate flowrate ( $\text{m}^3 \cdot \text{s}^{-1}$ ).
$r$	number of replicates for a factorial run
$r_p$	pore radius (m)
$r_0$	initial pore radius (m)
$R^2$	coefficient of determination
$R^2_{adj}$	adjusted coefficient of determination
$R_c$	cake resistance ( $\text{m}^{-1}$ )
$R_m$	resistance of the membrane / media ( $\text{m}^{-1}$ )
$R$	total resistance ( $\text{m}^{-1}$ )
$s$	mass fraction of solids in the feed
$s^2$	unbiased estimate of the variance for the individual runs
$s_r^2$	variance for an individual replicate
$s_{eff}$	standard error of the effect or interaction
$SS_{err}$	sum of squares of the residuals

$SS_{tot}$	total sum of squares
$t$	filtration time (s)
$T$	temperature (°C)
$T_p$	percentage protein transmission
$t_{final}$	time at completion of filtration (h)
$t_{v,\alpha}$	student's t-test statistic with $\nu$ degrees of freedom for a significance level of $\alpha$
$\nu$	degrees of freedom
$V$	filtrate / permeate volume (m <sup>3</sup> )
$V_c$	liquid volume in the original feed sample (m <sup>3</sup> )
$V_{final}$	filtrate / permeate volume at completion of filtration (m <sup>3</sup> )
$V_i$	initial flow-through volume above the cake (m <sup>3</sup> )
$V_{max}$	maximum volume of feed that can be filtered before the membrane is completely blocked according to the standard blocking law (m <sup>3</sup> )
$V_{precoat}$	volume of pre-coat solution (m <sup>3</sup> )
$V_t$	cumulative filtrate / permeate collected over time $t$ (m <sup>3</sup> )
$x_i$	$i^{\text{th}}$ sample measurement or independent variable
$\bar{x}$	mean sample measurement or independent variable
$Y$	response matrix
$y_i$	$i^{\text{th}}$ dependent variable measurement
$y_{mn}$	value of the $m^{\text{th}}$ response measured for the $n^{\text{th}}$ factorial run
$\bar{y}$	mean dependent variable
$\alpha$	specific cake resistance per unit dry cake mass (m.kg <sup>-1</sup> )
$\mu$	dynamic permeate viscosity (N.s.m <sup>-2</sup> )
$\mu_T$	dynamic viscosity of water at temperature, $T$ (N.s.m <sup>-2</sup> )
$\rho_0$	mass of dry solids per unit volume of filtrate (kg.m <sup>-3</sup> )
$\rho_f$	feed density (kg.m <sup>-3</sup> )

$\rho_{ft}$	flow through solution density ( $\text{kg}\cdot\text{m}^{-3}$ )
$\rho_p$	permeate density ( $\text{kg}\cdot\text{m}^{-3}$ )
$\sigma$	sample standard deviation
$\sigma_b$	blocked area per unit filtrate volume ( $\text{m}^{-1}$ )

## Abbreviations

CCD	central composite design
CHMO	cyclohexanone monooxygenase
CTAB	cetyltrimethylammonium bromide
DCW	dry cell weight concentration
DNA	deoxyribonucleic acid
DoE	design of experiments
DSW	deep square well
<i>E.coli</i>	<i>Escherichia coli</i>
EDTA	ethylenediaminetetraacetic acid
HPLC	high pressure liquid chromatography
LRA	lipid removal agent
NaCl	sodium chloride
NFF	normal flow filtration
OD	optical density
pDNA	plasmid deoxyribonucleic acid
PVDF	polyvinylidene fluoride
RNA	ribonucleic acid (RNA)
RNaseA	ribonuclease A
RO	reverse osmosis
RSM	response surface methodology
RVLF	rotating vertical leaf filter
TFF	tangential flow filtration
USD	ultra-scale down
v/v	volume by volume
w/v	weight by volume

## **1.0 Introduction**

### **1.1 Overview**

This chapter includes introductions to the key aspects of this thesis: microfiltration (Section 1.3), microscale approaches to bioprocessing (Section 1.4) and experimental design (Section 1.5). Firstly, a brief and general summary of bioprocessing is included to place these key aspects into context and explain some of the test systems used throughout this thesis in detail.

### **1.2 Bioprocessing**

Bioprocessing is the use of living cells or their components to generate desirable products. It is a very broad ranging discipline which incorporates science and engineering techniques to harness, manipulate and optimise natural processes. In general biological processes will have environmental advantages over comparable chemical processes. It is the ability to faithfully generate the complex target molecules that are present in nature, however, which necessitates the use of bioprocesses.

#### **1.2.1 Target molecules**

There is an almost endless variety of biomolecules that can be generated by harnessing bioprocesses. The greatest interest is in complex macromolecules such as proteins and nucleic acids which can have beneficial therapeutic or diagnostic use in healthcare (Ho and Gibaldi, 2003). Recent advances in bioprocess have led to even more complex products such as viral vectors for gene delivery (Walther and Stein, 2000) and stem cells for regenerative medicine (Placzek *et al.*, 2009).

### 1.2.1.1 Proteins

Proteins comprise of one or more polypeptide chains of amino acids. Their structure and properties are largely defined by the amino acid sequence which influences the way the protein folds. Covalent post translational modifications such as glycosylation and phosphorylation can also contribute the structure and biological activity of the protein (Walsh, 2002). These complexities in folding and additional modifications make the production of fully biologically active proteins difficult to reproduce outside of the original expression system (Baneyx and Mujacic, 2004). The choice of an appropriate expression system is therefore key to the proper balance between productivity and activity.

Proteins make up almost all biopharmaceuticals which have been approved. The established categories of biopharmaceuticals are still the most common among new approvals (hormones) and the highest selling (erythropoietins) (Walsh, 2005). The market is however expanding with newer innovations in the industry such as monoclonal antibodies (Reichert and Pavlou, 2004). More complex proteins will be introduced to the market as technologies advance but it is clear proteins of all varieties will continue to be important target molecules within bioprocessing.

### 1.2.1.2 Plasmid DNA

Nucleic acids are macromolecular chains of nucleotides which encode genetic information. Deoxyribonucleic acid (DNA) and ribonucleic acid (RNA) are the building blocks of gene expression systems throughout living organisms and vital tools for the expression of recombinant proteins in bioprocessing.

Two oligonucleotides (small nucleotide polymers) have received drug approval as target molecules in their own right (Jabs and Griffiths, 2002; Ng *et al.*, 2006). Beyond this, plasmid DNA is finding increasing applications in gene therapy (Alton, 2007; Griesenbach 2007) where there is significant but as yet unrealised potential. Even once gene therapy approaches become a proven therapeutic option there will be significant challenges of scale (Prazeres *et al.*, 1999), especially in potential target

diseases such as influenza where a rapid response to pandemics at scale increases the need for novel approaches to plasmid DNA bioprocessing (Hoare *et al.*, 2005).

## 1.2.2 Upstream processes

A variety of diverse systems can be harnessed for bioprocessing, some very different in their approaches. It is the growth and utilisation of these biological systems as production factories for complex target molecules that constitutes the upstream bioprocesses. The generic approach is the growth of cells in a bioreactor which are used to generate the desired product.

This thesis does not consider in detail the complex optimisation and operation of this stage in the bioprocess, but does reference the importance of integrating upstream processes in to a study of the whole process. Upstream and downstream processes should not be treated in isolation otherwise unwanted interactions may not be detected (Kelly and Hatton, 1991; Russotti *et al.*, 1995). The nature of the upstream process will effectively determine the separation duty of subsequent downstream steps.

### 1.2.2.1 Recombinant expression systems

A vast variety of expression systems can be used in bioprocessing (Higgins and Hames, 1999). Selection is dictated by the particular target molecule of interest and how to achieve the best yields whilst still faithfully reproducing the molecule correctly (Baneyx and Mujacic, 2004). Table 1.1 contains a summary of some important expression systems.

*Escherichia coli* (*E.coli*) became the host organism of choice for the expression of many biopharmaceuticals due to long term study and use since the early inception of biotechnology (Russo, 2003). *E.coli* is a common host for both protein expression (Baneyx, 1999) and plasmid DNA production (Carnes, 2005). More recently the commercial success of monoclonal antibodies (Reichert *et al.*, 2005) has seen a rise in CHO cell host systems to achieve faithful reproduction of this complex protein.

**Table 1.1.** Various expression systems and their characteristics.

<b>Expression System</b>	<b>Cell Classification</b>	<b>Secretion Capability</b>	<b>Post-Translational Limitations</b>	<b>Example</b>
<i>Escherichia coli</i>	Gram-negative prokaryotic bacterium	Into periplasm	No glycosylation, disulphide bonds limited in cytoplasm	Goeddel <i>et al.</i> , 1979
<i>Saccharomyces cerevisiae</i>	Eukaryotic yeast	Yes, often in periplasm	Hyper-glycosylation	Shusta <i>et al.</i> , 1998
<i>Pichia pastoris</i>	Methylotrophic eukaryotic yeast	Yes	No terminal $\alpha$ 1,3 mannose.	Cregg <i>et al.</i> , 2000
Chinese Hamster Ovary	Mammalian higher eukaryote	Yes	Almost none	CMC Biotech Working Group, 2009
NS0	Mammalian higher eukaryote	Yes	Almost none	Zhou <i>et al.</i> , 1997
Tobacco	Plant higher eukaryote	Yes, size restrictions	Almost none	Staub <i>et al.</i> , 2000
Insect	Insect higher eukaryote	Yes	Almost none	Maiorella <i>et al.</i> , 1988

### 1.2.3 Downstream processes

Downstream processing is a diverse and organic field. Processes can vary considerably depending upon the nature of the expression system (see references in Table 1.1). The use of each particular product, its required dosage and therefore required product purity will also determine the level of purification required and impact on the selected process (Wheelwright, 1989). The preferences and experience of the production company can also play a part. Generic, or platform, processes are favourable for companies with a portfolio of similar products in their pipeline (Shukla *et al.*, 2007).

The methods may be different as technologies emerge and progress, but the general progression remains the same since similar impurities need to be sequentially removed regardless of the type of expression system or complexity of the upstream process:

biomass, insoluble solids, soluble components and trace impurities. Belter and co-authors (1988) split the stages of downstream processing into four main categories: removal of insolubles, isolation of products, purification and polishing. The majority of processes still fall into these categories as shown in Table 1.2. A wide variety of unit operations are shown with examples for their different functions.

**Table 1.2.** Example unit operations at the various stages of downstream processing.

Stage	Unit Operation	Function	Example
Removal of insolubles	Centrifugation	Solids removal based on relative size and density using a centrifugal force.	Jin <i>et al.</i> , 1994
	Depth filtration	Fine solids removal based on size and adsorption	Singhvi <i>et al.</i> , 1996
	Microfiltration	Solids removal by size	Riesmeier <i>et al.</i> , 1990
	Homogenisation	Product release by cell disruption	Ling <i>et al.</i> , 1998
Isolation of products	Liquid-liquid extraction	Product partitioning by relative solubility	Abbott and Hatton, 1988
	Ultrafiltration	Product concentration and contaminant removal by size	van Reis and Zydney, 2001
	Protein Precipitation	Product isolation by relative solubility	Hoare <i>et al.</i> , 1983
Purification	Affinity Chromatography	Selective product binding to affinity ligands	Roque and Lowe, 2008
	Hydrophobic Interaction Chromatography	Selective product binding based on hydrophobicity	Queiroz <i>et al.</i> , 2001
	Ion Exchange Chromatography	Selective product binding based on charge	Ishihara and Yamamoto, 2005
Polishing	Crystallisation	Selective crystal formation based on solubility	Klyushnichenko, 2003
	Lyophilisation	Water removal by freeze drying	Carpenter <i>et al.</i> , 1997
	Virus Filtration	Removal of viruses by size exclusion	Carter and Lutz, 2002

Some operations seek to combine multiple stages of separations in order to shorten the process and improve process simplicity and yield (small yield losses will compound with high numbers of processes). Expanded bed adsorption provides both insoluble

removal and product isolation in one step (Hansson *et al.*, 1994). Protein A chromatography is primarily an isolation step but provides the specificity and impurity removal consistent with purification processes (McCue *et al.*, 2003).

The overall design and structuring of downstream processes is a complex task with much literature available on the subject. The key aspects of importance to this thesis are as follows: the presence of membrane processes, particularly microfiltration, throughout the production process (Table 1.2) and the importance of process integration. As previously discussed the interface between upstream and downstream processes must be carefully evaluated to ensure changes upstream do not adversely effect the performance downstream (Kelly and Hatton, 1991; Russotti *et al.*, 1995). It is also important to take a holistic approach to the downstream process (Chhatre *et al.*, 2006).

### **1.3 Microfiltration**

Microfiltration is a separation process where a selective synthetic barrier (a membrane, usually but not exclusively polymeric) is used to permit passage or reject different feed stream components (Zeman and Zydney, 1996). The characteristic sizes involved (pore diameter, retained particle diameter) are usually used to differentiate microfiltration from other membrane processes. There are also many further ways to add detail to this definition, without full agreement in the literature. Microfiltration is best fully defined in comparison to other membrane processes.

#### **1.3.1 Membrane processes**

Membrane processes (microfiltration, ultrafiltration, nanofiltration, reverse osmosis) are widely used in many bioprocess manufacturing routes. Frequently they are also used at multiple points in a given process to carry out different functions (e.g. solid-liquid separation, fractionation, buffer exchange and sterilisation). Membranes are often defined by pore size ranges, but figures vary with differing data and opinions available (Zeman and Zydney, 1996; Cheryan, 1998; American Water Works

Association, 2005). A more useful definition is achieved by looking at the types of particles retained or permeated through the membrane. Table 1.3 summarises particle size range, types of particles and typical process operations.

**Table 1.3.** Typical particles retained by different membrane processes. Derived from various sources (van Reis and Zydney, 2007; Zeman and Zydney, 1996; Cheyran, 1998).

	Cells / Cell Debris	Colloids	Viruses	Proteins	Peptides	Antibiotics	Divalent Salts	Monovalent Salts
<b>Microfiltration</b>	R	R/P	P	P	P	P	P	P
<b>Ultrafiltration</b>	R	R	R	R/P	P	P	P	P
<b>Nanofiltration</b>	R	R	R	R	R	R	R	P
<b>Reverse Osmosis</b>	R	R	R	R	R	R	R	R

Other membrane processes exist such as gas separation (Baker, 2002) and pervaporation (Feng and Huang, 1997), which are more commonly utilised in chemical processes and not relevant to this thesis. Nanofiltration (Hilal *et al.*, 2004) and reverse osmosis (Fritzmman *et al.*, 2007) membranes are primarily used for water purification. Whilst important to the bioprocess industry, they are not directly used in downstream processing applications. The applications of microfiltration and ultrafiltration specific to bioprocessing are summarised in Table 1.4. Virus filtration is an important normal flow ultrafiltration process that is often incorrectly termed as a nanofiltration step (Burnouf and Radosevich, 2003) despite transmitting proteins such as antibodies which would be retained by nanofiltration membranes.

**Table 1.4.** Example bioprocess applications of microfiltration and ultrafiltration.

Membrane Process		Applications	Example References
Microfiltration		Cell removal	Foley, 2006.
		Cell debris removal	Bailey and Meagher, 2000.
		Product sterilisation	Jornitz <i>et al.</i> , 2002.
Ultrafiltration	Concentration Mode	Concentration	Rosenberg <i>et al.</i> , 2009.
		Purification	Kahn <i>et al.</i> , 2000.
	Diafiltration Mode	Buffer exchange	Kumik <i>et al.</i> , 1995.
		Salt removal	
	Normal Flow	Virus Filtration	Kuriyel and Zydney, 2000.

Microfiltration membranes permeate soluble product and retain the solid contaminants. In some cases they will retain product in the form of precipitates (Bentham *et al.*, 1988) or inclusion bodies (Batas *et al.*, 1999). Ultrafiltration membranes typically act to concentrate the feed by retaining particles and permeating the carrier buffer and small molecules. Diafiltration is typically used in ultrafiltration steps and involves the continuous addition of new buffer directly into the feed and thus the feed volume and concentration can be maintained while some or all of the buffer and salts can be exchanged for the new buffer.

### 1.3.2 Filter media

#### 1.3.2.1 Polymeric membranes.

A variety of methods exist for casting polymeric membranes: air casting, immersion casting, melt casting, track etching, stretching and radiation induced polymerization (Zeman and Zydney, 1996). Membranes, from these various casting conditions and disparate techniques, give the bioprocessor an array of not only pore sizes, but also pore size distributions and pore shapes (Baker, 2004). Membranes are often classified as isotropic (literally uniform in all directions), anisotropic or a composite mixture of

the two (van Reis and Zydney, 2007). Isotropic membranes are often visualised by the simplistic model of uniform cylindrical pores, but are practically membranes with little difference in pore size and structure through the depth of the membrane. Anisotropic membranes change in pore structure from one side to another, often by reducing pore size. A simplistic view is of a tapering pore, but the true structures of membranes are more complex. Different degrees of isotropy (Ulbricht *et al.*, 2007) or membrane morphology (Zydney and Ho, 2003) generate very different performance characteristics.

Modification of polymeric membranes further enhances performance, for example by increasing hydrophilicity to decrease protein binding (Yamagishi *et al.*, 1995) or adding charge for increased retention or even membranes capable of chromatographic separation (Ghosh, 2002).

#### 1.3.2.2 Depth filters

Depth filters have been used to effectively clarify cell debris by removing particles throughout the filter depth and maintaining flux (Singhvi *et al.*, 1996). Depth filters for the bioprocess industry contain cellulose or polypropylene fibers bound with an appropriate filter aid such as diatomaceous earth (van Reis and Zydney, 2007) and can be charge modified to enhance electrostatic removal of contaminants (Charlton *et al.*, 1999). Filter aids such as diatomaceous earth can be used with a guard filter to build up a retentive layer before filtration and also fed into the body of the feed to deposit a retentive layer during the course of filtration (Reynolds *et al.*, 2003).

### 1.3.3 Tangential flow microfiltration

Where fouling of microfiltration membranes is severe and high solids content is present it may be economically advantageous to use tangential flow microfiltration (TFF). Continuously pumping the feed solution across the membrane surface provides shear that removes foulant particles from the surface of the membrane. Many studies have been made into the nature of the shear forces involved (Zydney

and Colton, 1986; Belfort *et al.*, 1994) and novel filter designs to enhance shear (Light and Tran, 1981; Luque *et al.*, 1999).

This is often an approach used with ultrafiltration due to the retention of smaller particles which can concentrate at the membrane surface (Sablani *et al.*, 2001) and form gel layers on the surface of the membrane (Song, 1998).

Figure 1.1 simplistically visualises the differences between TFF and normal flow filtration, which is the focus of this thesis.

### 1.3.4 Normal flow microfiltration

In normal flow filtration (NFF) a pressure difference is applied to pass the feed directly through the membrane. Flow is therefore normal to the membrane surface. NFF is also known as ‘dead-end’ filtration, since the retained feed has nowhere to go except to block the membrane or build up at the membrane surface.

#### 1.3.4.1 Normal flow filtration theory

Fundamental NFF theory derives largely from work by Henry Darcy in the 19th century (Darcy, 1856). The filtration of pure water obeys the following equation, based on Darcy’s Law on flow through porous media:

$$Q = \frac{dV}{dt} = \frac{\Delta P \cdot A}{\mu R_m} \quad (1.1)$$

$$J = \frac{1}{A} \frac{dV}{dt} = \frac{\Delta P}{\mu R_m} \quad (1.2)$$

Where  $Q$  is the filtrate flowrate ( $\text{m}^3 \cdot \text{s}^{-1}$ ),  $J$  is filtrate flux ( $\text{m} \cdot \text{s}^{-1}$ ),  $V$  is filtrate volume ( $\text{m}^3$ ),  $t$  is time (s),  $A$  is filter area ( $\text{m}^2$ ),  $\Delta P$  is pressure difference (Pa),  $\mu$  is viscosity (Pa.s) and  $R_m$  is resistance of the media ( $\text{m}^{-1}$ ). Also of importance is the Hagen-Poiseuille equation (Poiseuille, 1840) which calculates the filtrate flowrate through a membrane consisting of  $N$  cylindrical pores of equal radius  $r$  (m) and length  $L$  (m).

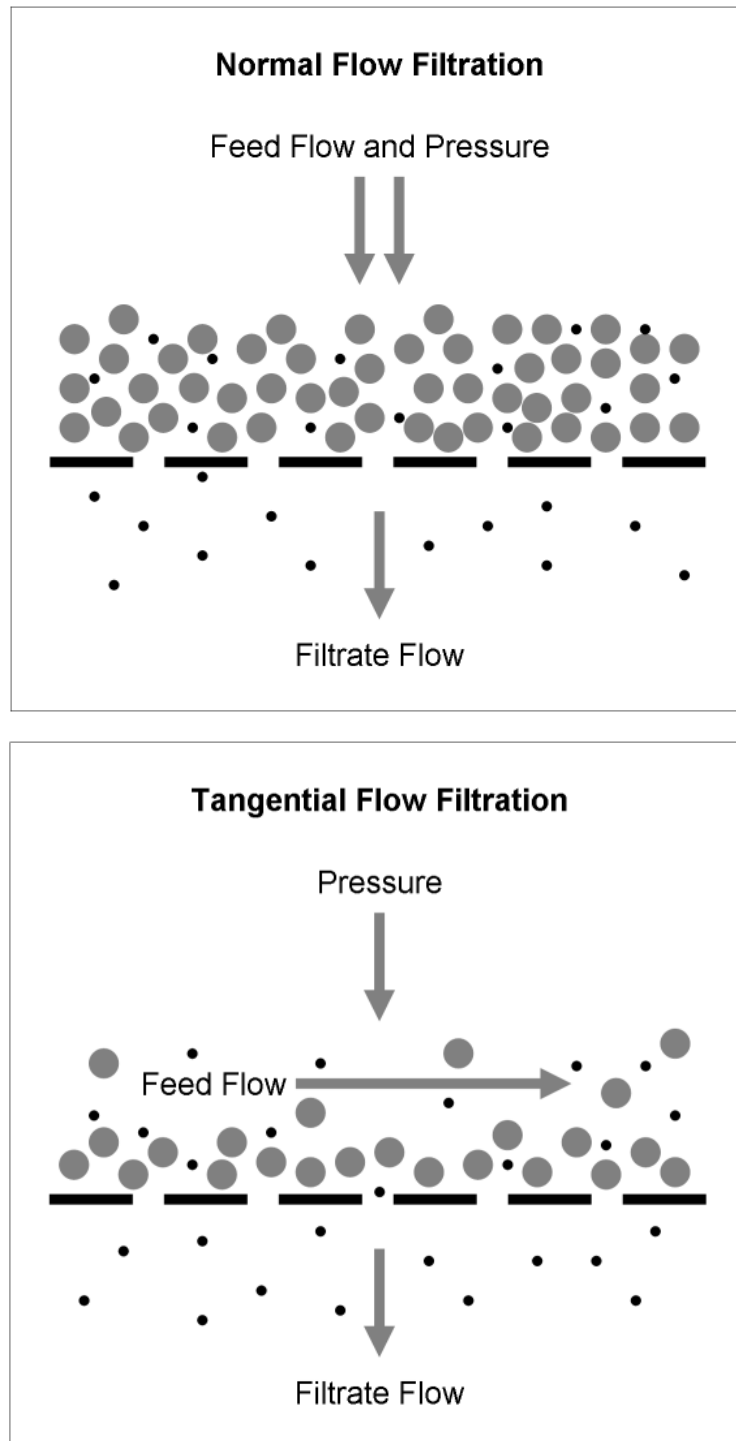


**Figure 1.1:** Schematic demonstrating the differences between tangential flow filtration (TFF) and normal flow filtration (NFF). The upstream of the membrane is the feed or retentate side. The downstream of the membrane is the filtrate or permeate side.

$$Q = N \left( \frac{\pi r^4 \Delta P}{8 \mu L} \right) \quad (1.3)$$

Early work on the laws governing normal flow filter fouling concentrated on cake filtration (Ruth *et al.*, 1933a; Ruth *et al.*, 1933b; Ruth 1935). Hermans and Bredée (1935, 1936) first studied blockage by plugging and constriction and applied analysis methods calculating the first and second derivatives of time with respect to volume which would eventually define a general equation for all the laws. The laws were further studied during the 1950s (Gonsalves, 1950; Grace, 1956). It was Hermia who finally derived a physical model for intermediate blockage (Hermia, 1966) to complete all four laws and he later combined all the derivations into one paper (Hermia, 1982). Hermia demonstrated that each law could be defined by a general equation for the resistance coefficient which is the rate of change of the instantaneous resistance (the inverse of the flowrate) with respect to volume. This equates to the second derivative of time with respect to volume and when calculated for all the laws leads to an equation of the following form:

$$\frac{d}{dV} \left( \frac{1}{Q} \right) = \frac{d^2 t}{dV^2} = K \left( \frac{dt}{dV} \right)^n \quad (1.4)$$

Where  $K$  is a constant (see Table 1.5) and  $n$  is the fouling exponent, which identifies the fouling mechanism:

- **Complete blocking** ( $n = 2$ ) is where the pores are plugged and sealed, preventing flow and reducing the effective area.
- **Standard blocking** ( $n = 1.5$ ) describes the constriction of pores, reducing the effective pore diameter and hence increasing the resistance.
- **Intermediate blocking** ( $n = 1$ ) is another plugging law, but unlike complete blocking particles can continue to fill a pore even after it is blocked.
- **Cake filtration** ( $n = 0$ ) is the build up of a cake layer on the membrane which provides an additional resistance to that of the membrane.

The derivations of these laws for the application of a constant pressure driving force are briefly outlined in the following sections and all the relevant equations are summarised in Table 1.5. All derivations are based on the assumption of a homogeneous feed solution providing a constant challenge of fouling species per unit volume of feed throughout the filtration.

#### 1.3.4.1.1 Complete blocking filtration law

The equations defining complete blockage are based on the area projected onto the membrane by the particles in a filtrate volume,  $V$ . The area blocked by this filtrate volume is  $\sigma_b V$ , where  $\sigma_b$  ( $\text{m}^{-1}$ ) is a constant evaluated by calculating the number of particles in the filtrate volume and the area projected by a single particle. The area remaining for flow is therefore  $A = A_0 - \sigma_b V$ , where  $A_0$  is the initial effective filtration area. Substituting this into Equation 1.1 yields:

$$Q = Q_0 - \frac{\Delta P \sigma_b V}{\mu R_m} \quad (1.5)$$

Where  $Q_0$  is the initial filtrate flowrate ( $\text{m}^3 \cdot \text{s}^{-1}$ ). The constant preceding the volume in Equation 1.5 is defined as the blocking constant,  $K_b$  ( $\text{s}^{-1}$ ) and hence the linear form of the equation can be written, showing that flowrate declines linearly for increasing volume:

$$Q = -K_b V + Q_0 \quad (1.6)$$

This can be rearranged to give  $\frac{Q}{Q_0} = f(V)$  and integrated by substitution to generate the  $\frac{Q}{Q_0} = f(t)$  relationship. Combining these gives the  $V = f(t)$  relationship.

Strictly speaking the volume throughout the derivations is not the filtrate volume, but the corresponding volume of feed (including the filtered particles). Hermia assumed

**Table 1.5.** A comprehensive summary of the constant pressure filtration blocking laws.

Filtration Law	(see Equation 1.4)		$\frac{Q}{Q_0} = f(t)$	$\frac{Q}{Q_0} = f(V)$	$V = f(t)$	Linear Form ( $y = mx + c$ )
	$n$	$K$				
Cake Filtration	0	$K_c$	$(1 + 2K_c Q_0^2 t)^{-\frac{1}{2}}$	$(1 + K_c Q_0 V)^{-1}$	$\frac{1}{K_c Q_0} \left( \sqrt{1 + 2K_c Q_0^2 t} - 1 \right)$	$\frac{t}{V} = \frac{K_c V}{2} + \frac{1}{Q_0}$
Intermediate Blocking	1	$K_i$	$(1 + K_i Q_0 t)^{-1}$	$e^{-K_i V}$	$\frac{1}{K_i} \ln(1 + K_i Q_0 t)$	$\frac{1}{Q} = K_i t + \frac{1}{Q_0}$
Standard Blocking	1.5	$K_s Q_0^{\frac{1}{2}}$	$\left( 1 + \frac{K_s Q_0 t}{2} \right)^{-2}$	$\left( 1 - \frac{K_s V}{2} \right)^2$	$t \left( \frac{K_s t}{2} + \frac{1}{Q_0} \right)^{-1}$	$\frac{t}{V} = \frac{K_s t}{2} + \frac{1}{Q_0}$
Complete Blocking	2	$K_b$	$e^{-K_b t}$	$1 - \frac{K_b V}{Q_0}$	$\frac{Q_0}{K_b} \left( 1 - e^{-K_b t} \right)$	$Q = -K_b V + Q_0$

the mass fraction of solids in the feed was negligible in his derivations and the filtrate and feed volumes were equivalent. The two volumes are directly proportional, however, and if the solids mass fraction is significant then this would only alter the constant  $K_b$  and the derived forms of the equations all still hold.

#### 1.3.4.1.2 Standard blocking filtration law

To derive the standard blocking law it is assumed that the membrane consists of  $N$  uniform cylindrical pores of equal initial radius  $r_0$  (m) and length  $L$  (m). The pores are constricted by even deposition of foulant over the inner surface of all the pores, keeping them uniform and cylindrical with flow declining since the area available reduces due to the decreased pore radius ( $r = r_0 + dr$ ). A volume balance on the deposited particles yields the following relationship:

$$-2N\pi Lrdr = CdV \quad (1.7)$$

Where  $C$  is the volume of solids per unit volume of filtrate. Integrating this equation gives:

$$N\pi L(r_0^2 - r^2) = CV \quad (1.8)$$

Based on the Hagen-Poiseuille equation (Equation 1.3) the flowrate is proportional to the radius to the fourth power. Rearranging Equation 1.8 to give the ratio of radii to the fourth power the  $\frac{Q}{Q_0} = f(V)$  relationship can be determined:

$$\frac{Q}{Q_0} = \left(1 - \frac{K_s V}{2}\right)^2 \quad (1.9)$$

Where the standard blocking constant,  $K_s$  ( $\text{m}^{-3}$ ), is:

$$K_s = \frac{2C}{N\pi Lr_0^2} \quad (1.10)$$

Integrating Equation 1.9 yields the following expression which is the linear form and also the  $V = f(t)$  relationship:

$$\frac{t}{V} = \frac{K_s t}{2} + \frac{1}{Q_0} \quad (1.11)$$

The  $\frac{Q}{Q_0} = f(t)$  function can then be derived by combining Equations 1.9 and 1.11.

Standard blocking is commonly used for sizing estimation and forward prediction of protein solution filtration. By rearranging Equation 1.11 it can be shown that as  $t \rightarrow \infty$  the maximum volume of feed that can be filtered before the membrane is completely blocked,  $V_{\max}$  ( $\text{m}^3$ ), is given by:

$$V_{\max} = \frac{2}{K_s} \quad (1.12)$$

The  $V_{\max}$  approach to filterability testing is to collect time and volume data over short periods, reducing the requirements for high value feed solutions (Badmington *et al.*, 1995).  $V_{\max}$  is evaluated from the linear form of the standard blocking law using a plot of  $\frac{t}{V}$  vs  $t$  and the other forms are used to forward predict and scale-up the process performance (Zydney and Ho, 2002).

The same approach can obviously be implemented using the other blocking laws, but they are not so commonly employed and the filtration constants cannot be manipulated into a constant that has a clear physical significance such as  $V_{\max}$ .

### 1.3.4.1.3 Intermediate blocking filtration law

The derivation of the intermediate blocking law is similar to that of complete blocking. The area projected onto the membrane per unit filtrate volume  $V$  is again equal to  $\sigma_b V$ . The difference is that the projected area has an equal chance to fall upon already blocked pores – filling up pores blocked to flow. Therefore the effective filtration area decreases at a rate reduced by the ratio of current ( $A$ ) to initial ( $A_0$ ) areas (the probability that particles fall upon non-blocked pores). Over a small time ( $dt$ ) and filtrate volume ( $dV = Qdt$ ):

$$dA = -\sigma_b Q dt \frac{A}{A_0} \quad (1.13)$$

Incorporating Darcy's Law (Equation 1.1) and integrating yields  $\frac{A}{A_0} = f(t)$  which is equivalent to  $\frac{Q}{Q_0} = f(t)$ .

$$\frac{Q}{Q_0} = \frac{1}{1 + K_i Q_0 t} \quad (1.14)$$

Where the intermediate blocking constant,  $K_i$  ( $\text{m}^{-3}$ ), is equal to:

$$K_i = \frac{\sigma_b \Delta P}{\mu R Q_0} = \frac{\sigma_b}{A_0} \quad (1.15)$$

The linear form can be generated by rearranging Equation 1.14:

$$\frac{1}{Q} = K_i t + \frac{1}{Q_0} \quad (1.16)$$

Integrating this yields the  $V = f(t)$  relationship:

$$V = \frac{1}{K_i} \ln(1 + K_i Q_0 t) \quad (1.17)$$

Which can then be combined with Equation 1.14 to give the  $\frac{Q}{Q_0} = f(V)$  function.

#### 1.3.4.1.4 Cake filtration law

Cake filtration theory is central to this thesis and application of the equations derived here is discussed in more detail in Section 3.4.1 in relation to microscale approaches. Forward prediction and scale-up using the equations are also detailed in Section 2.8.11.

During cake filtration the membrane maintains its properties of effective area ( $A$ ) and resistance ( $R_m$ ). A cake layer is deposited on the membrane which provides an additional increasing resistance,  $R_c$  ( $\text{m}^{-1}$ ). It is assumed that these resistances in series are additive and therefore after a filtration volume  $V$  is processed the total resistance at a given volume,  $R$  ( $\text{m}^{-1}$ ) can be given as:

$$\begin{aligned} R &= R_m + R_c \\ R &= R_m + \frac{\alpha \rho_0 V}{A} \end{aligned} \quad (1.17)$$

Where  $\alpha$  is the specific cake resistance per unit dry cake mass ( $\text{m.kg}^{-1}$ ) and  $\rho_0$  is the mass of dry solids per unit volume of filtrate ( $\text{kg.m}^{-3}$ ). Defining the cake filtration constant,  $K_c$  ( $\text{s.m}^{-6}$ ), as:

$$K_c = \frac{\alpha \rho_0 \mu}{A^2 \Delta P} \quad (1.18)$$

Equation 1.17 can be rewritten:

$$R = R_m (1 + K_c Q_0 V) \quad (1.18)$$

Since Darcy's law (Equation 1.1) shows that resistance is inversely proportional to flowrate this can be rearranged to give the  $\frac{Q}{Q_0} = f(V)$  relationship:

$$\frac{Q}{Q_0} = \frac{1}{1 + K_c Q_0 V} \quad (1.19)$$

Integrating Equation 1.19 yields the linear form of the cake filtration law:

$$\frac{t}{V} = \frac{K_c V}{2} + \frac{1}{Q_0} \quad (1.20)$$

This can also be rearranged to give  $V = f(t)$  and combined with Equation 1.19 to determine  $\frac{Q}{Q_0} = f(t)$ , both of which are summarised in Table 1.5.

For the application of this theory to quantification of microscale filtration, the linear relationship (Equation 1.20) is rewritten using Equation 1.2 and Equation 1.18 to give the unabbreviated form in terms of flux rather than throughput as quoted in Section 3.4.1. The focus is on the evaluation of the specific cake resistance, which is an intrinsic value of the resistance to flow of the cake and is effective for use in prediction of flux performance and scale-up (Section 2.8.11).

The theory of cake filtration is often extended to incorporate the effect of pressure on specific cake resistance. Under pressure some cakes will collapse and compress, leading to smaller void spaces and therefore increased restriction to flow. There are a variety of different expressions correlating the effect of pressure on specific cake resistance data (Foley, 2006).

#### 1.3.4.1.5 Cake filtration law for constant flow operation

The derivations in the preceding four sections have considered the case of a constant applied pressure as the driving force. Pumping of the feed through a filter at constant

flow is also a common approach to normal flow filtration, especially at large scale (Ball, 2000). The approach to generating equations describing the pressure increase is similar to the constant pressure derivations. For cake filtration the same expression for resistance is used (Equation 1.17) and here Darcy's law (Equation 1.1) shows that resistance is directly proportional to pressure difference, hence:

$$\frac{\Delta P}{\Delta P_0} = 1 + \frac{\alpha \rho_0 V}{AR_m} \quad (1.21)$$

With the knowledge that the flowrate,  $Q$ , is constant throughout the experiment and simply equal to volume over time and incorporating Darcy's Law at initial conditions the following expressions for pressure increase as a function of volume or time can be developed:

$$\Delta P = \Delta P_0 + (\mu \alpha \rho_0) \frac{QV}{A^2} \quad (1.22)$$

$$\Delta P = \Delta P_0 + (\mu \alpha \rho_0) \left( \frac{Q}{A} \right)^2 V \quad (1.23)$$

The cake filtration constant for constant pressure operation,  $K_c$  (Equation 1.18), can no longer be incorporated here since it includes the now variable term for pressure difference. The same is true of the intermediate and complete blocking constants. Only the standard blocking constant can be used to describe both constant pressure and constant flow behaviour. The forms of these other constant flow relationships are not derived here but are available in the literature (van Reis and Zydney, 2007).

#### 1.3.4.1.6 Combined filtration models

The extension of the classical laws derived above to consider multiple filtration mechanisms is a natural progression. Bolton and co-workers (2006) derived constant pressure and constant flow equations for combinations of blocking laws occurring simultaneously throughout the course of the filtration. Improved levels of fit were obtained with these combined models, especially the cake-complete model. However

the authors concede that this is not necessarily proof the mechanisms in the model are both occurring and that the improved fit could be due to the additional fitted parameter.

Evidence of mechanisms changing during filtration has been published for BSA (Tracey and Davis, 1994) and latex particles (Kosvintsev *et al.*, 2002) showing standard or complete blocking models fitting early data, transitioning into data that fits a cake filtration model. Plots of the derivatives in Equation 1.5 have been used to demonstrate the variation in the fouling exponent,  $n$ , over the course of BSA filtration (Bowen *et al.*, 1995), again showing a transition from complete blockage ( $n \approx 2$ ) to cake filtration ( $n \approx 0$ ). A single model describing the smooth transition from pore blockage to cake filtration was developed by Ho and Zydney (2000). The model includes three fitted parameters, but they all have a clear physical definition and could theoretically be determined independently, although not by simple methods. Ho later published a model that also incorporated internal fouling by pore constriction (Duclos-Osello *et al.*, 2006).

Whilst interesting from an academic perspective, the combined models are not simple to implement in practice and forward prediction of transition from one mechanism to another is not possible from early data. The complexities of filtration mechanisms are acknowledged when scaling up industrial filtration processes but the variability is simply accounted for in safety factors for the fitted parameters of the single mechanism models (Lutz, 2009).

### **1.3.5 Microfiltration of *E.coli***

The microfiltration of *E. coli* fermentation broths is known to be influenced by several upstream factors. Previous studies have demonstrated that cells harvested after glucose depletion within a fermentation lead to increases in cake resistance as the cells begin to lyse and degrade (Okamoto *et al.*, 2001). For other organisms, decreasing the medium pH has been shown to make *Corynebacterium* cells become more hydrophobic leading to their aggregation. During filtration this results in filter cakes with larger void spaces and hence a reduced cake resistance (Ohmori and Glatz,

1999). Fermentation media components can also increase the specific cake resistance whether using complex oil based media (Davies *et al.*, 2000) or soluble complex media with nutrients, such as tryptone (Russotti *et al.*, 1995). Factors, such as cell morphology (McCarthy *et al.*, 1998) and cell size and shape (Nakanishi *et al.* 1987) have also been shown to have an impact on microfiltration performance. The presence of extracellular matrices can also change the specific cake resistance (Hodgson *et al.*, 1993).

### **1.3.6 Microfiltration of plasmid DNA**

The increase in promising gene therapy applications (Verma and Weitzman, 2005) is driving the need for large scale DNA processing. Although not well established at process scale, a typical downstream process for plasmid DNA purification could incorporate microfiltration and ultrafiltration after lysis and precipitation and before chromatography (Ferreira *et al.*, 2000). Research has been carried out using microfiltration membranes to remove contaminants by size and adsorption while permeating the plasmid DNA (Kendall *et al.*, 2002) in contrast to concentrating the plasmid DNA (Kahn *et al.*, 2000). Normal flow sterilization of plasmid DNA solutions depends strongly on the plasmid size and solution ionic strength with higher fluxes generating increased damage (Kong *et al.*, 2006).

The high costs of chromatographic separation due to poor binding capacity (Prazeres *et al.*, 1999; Diogo *et al.*, 2005) has led to the development of non-chromatographic adsorption processes for purifying plasmid DNA (Lander *et al.*, 2002). This process involves a variety of key filtration steps for solids recovery and removal.

## **1.4 Microscale bioprocessing**

Small scale devices that allow process evaluation and optimisation with the lower volumes available in early stage product development have long been a vital tool for bioprocessing. Researchers have sought to reduce this scale further to allow studies to

be conducted earlier or in more detail. Microscale bioprocessing (Micheletti and Lye, 2006) applies scale down methods to microlitre quantities of feed.

### 1.4.1 Scale-down of bioprocesses

By scaling down a process large scale performance can be predicted without incurring the financial and timescale costs of full scale operation. Scale-down in its simplest form is the generation of a geometric mimic at a smaller scale to generate equivalent performance data to the large scale. Such geometric approaches are often used for fermentors or other reaction vessels, but even here there are significant affects of smaller scale operation that must be accounted for. For example, the key aspects for scale-down of fermentation are maintaining sufficient oxygen transfer and efficient mixing (Humphrey, 1998). In small scale geometric mimics the same impeller rotational speed will generate lower actual linear velocities and lower shear, leading to different oxygen transfer and mixing characteristics. The established scale-down techniques used are to maintain a constant tip velocity, Reynold's number, calculated power input per unit volume, oxygen mass transfer coefficient or mixing time (Junker, 2004).

For some processes geometric similarity is not beneficial. In chromatography the bed height determines the pressure drop across the column and can even affect separation performance (Carta and Jungbauer, 2010). Hence scale-down is often carried out at a constant bed height, by reducing the column diameter which vastly alters the aspect ratio (Cutler, 2004).

Knowledge of the key process drivers is required and any scale-down approach must focus on keeping the relative effects of these process drivers constant at both scales.

#### 1.4.1.2 Microfiltration scale-down

Scale-down of microfiltration involves reduction in the filtration area and maintaining the correct flux (flow per unit area). The different modes of operation and filter format used at full scale can influence the accuracy of flux scalability.

#### 1.4.1.2.1 Scale-down of normal flow filtration

In its simplistic form scale-down of normal flow filtration can be carried out by linearly scaling area. However the format of large scale filtration devices can be very different. Common formats include pleated membrane packed into a cylindrical housing. Adaptations of the technology are allowing higher membrane densities to be packed into the standard 10" cartridge format (van Reis and Zydney, 2007). The full impact of the pleating process is not fully understood, but observations have been made with sterile microfiltration media suggesting a loss in flux for pleated devices (Chandler and Zydney, 2004) and fluid dynamics studies published for pleated cartridges in other applications (Nassehi *et al.*, 2005).

Full scale normal flow filtration of feeds with high solids content include the use of candle, plate and frame, tubular and leaf filters (Sutherland, 2008). Again these formats differ from the simple cylindrical vessel and disc filter used in the laboratory and scale-up is not straight forward (Reynolds *et al.*, 2003).

#### 1.4.1.2.2 Scale-down of tangential flow filtration

Scale-down or scale-up of TFF devices cannot be easily achieved. Because of the complex variation in conditions at different positions along the membrane, this path length must be kept constant at different scales. Many other factors need to be kept constant, although this is not possible at all scales. Good scale-up data has usually been achieved by keeping path length constant (van Reis *et al.*, 1997; Ball, 2000). Membrane area and hence capacity are scaled-up by increasing the number of channels in parallel.

#### 1.4.1.3 Ultra scale down of bioprocesses

The approach of ultra-scale down (USD) was outlined by Boychyn and co-workers (2004). It allows a combination of two different small scale operations to mimic the full scale process: customised shear treatment to mimic cell breakage in the centrifuge feed zone and laboratory scale centrifugation. The key is to both predict the large

scale performance and ensure that the final output feedstream is equivalent to a sample taken from the full scale process. This not only secures process information but also allows subsequent USD steps to be carried out with the correct feed.

Similar approaches have been attempted for TFF (Lee *et al.*, 1995; Bouzerar *et al.*, 2000). A rotating disc generates shear above a small membrane disc allowing operation with millilitre quantities and mimicking the estimated shear within conventional TFF devices.

## 1.4.2 Microscale automation

Microscale processing techniques, the combination of automated experimentation and bioprocess studies carried out in microwell plate formats (Lye *et al.*, 2003), are now emerging as a means to obtain bioprocess design information early for multiple drug targets. The ability to perform representative process studies early, at small scale and with minimal human intervention also helps to reduce costs. To date the majority of microwell studies have focused on upstream operations in particular fermentation (Duetz *et al.*, 2000; Duetz and Witholt, 2001; Elmahdi *et al.*, 2003; John *et al.*, 2003) and bioconversion (Doig *et al.*, 2002). This is also true of related work on miniature stirred bioreactors (Kostov *et al.*, 2001; Lampling *et al.*, 2002; Puskeiler *et al.*, 2005; Gill *et al.*, 2008a) and automated shake flask systems (Anderlei *et al.*, 2004). For microscale processing techniques to be most effective, however, it will be necessary to integrate these upstream studies with appropriate downstream processing sequences also operated in microwell formats (Lye *et al.*, 2003). There have been initial reports on adsorption studies in microwell formats (Lye *et al.*, 2003; Welch *et al.* 2002) and the operation of linked process sequences (Ferreira-Torres *et al.*, 2005) but at present the principles of more microscale downstream processing operations need to be established.

Established automation equipment exists for microwell formats and is well established in the field of drug discovery (Gribbon and Andreas, 2005). These robotic platforms also allow high throughput operation of assays, even with filtration processes involved

(Zhang and Lynch, 2005). However the filter is there to simply perform a separation and its performance is not characterised. There is much development in the microscale automation of chemical synthesis for process development (Harre *et al.*, 1999; Pollard, 2001) and these existing platforms represent a starting point to begin development of microscale bioprocessing and start to reap similar rewards.

## 1.5 Design of experiments

Traditional experimentation focuses on exploring the effects of one factor at a time and, as we are taught early in our school science lessons, all other factors must be kept constant to ensure a fair scientific test. There are two main drawbacks of such an approach. Firstly we would not allow identification of interactions where different levels of one factor influence the measured behaviour of another factor. Secondly we would be limiting the experimental space that we test to straight lines when there are planes, cubes and even higher dimensions of experimental space to consider.

Design of Experiments (DoE) has evolved to ensure that the maximum amount of information from all the relevant experimental space is generated from the minimum resource expenditure. What is generally considered as modern experimental design derives from many of the principles developed at the Rothamsted Experimental Station founded by John Lawes in 1846. Lawes and Joseph Gilbert carried out many arrays of experiments on agricultural yields incorporating experimental designs that were factorial in nature (Yates and Mather, 1963). They employed Sir Richard Fisher to collate and analyse many of these experiments and whilst at Rothamsted he published many key texts (Fisher, 1925; Fisher, 1935). Significant developments in analysis (Yates, 1937) and designs (Plackett and Burman, 1946) and continuous refinement and study have led to the methodology summarized in key modern DoE texts (Box *et al.*, 2005; Montgomery, 2008 – both originally published in the 1970's).

### 1.5.1 Factorial experiments

Factorial experimentation is an effective and mathematically elegant approach to systematically exploring the correct regions of experimental space and defining the major variations within that space. It identifies the main effect of varying a factor and the interactions between all the factors.

A full factorial design simply incorporates all combinations of  $k$  factors at a fixed number of evenly spaced levels for each factor. Scouting using two level factorial designs is a common approach to evaluating the important factors in an experimental system. There are  $2^k$  combinations in a full two level factorial design and this expression is often used to define. Table 1.6 contains the example of a two level, three factor ( $2^3$ ) factorial design. The high and low levels are represented by +1 and -1 in the table. These levels for each factor are carefully selected to ensure that the range is not too narrow (variation is too small to measure) or too wide (includes variation outside of the typical operating range). Selection of the factor levels is the key to successful factorial design.

**Table 1.6.** The coding for a full  $2^3$  factorial experiment.

Experiment Run Number	Main Effects			Interactions			
	A	B	C	AB	AC	BC	ABC
1	-1	-1	-1	+1	+1	+1	-1
2	+1	-1	-1	-1	-1	+1	+1
3	-1	+1	-1	-1	+1	-1	+1
4	+1	+1	-1	+1	-1	-1	-1
5	-1	-1	+1	+1	-1	-1	+1
6	+1	-1	+1	-1	+1	-1	-1
7	-1	+1	+1	-1	-1	+1	-1
8	+1	+1	+1	+1	+1	+1	+1

### 1.5.1.1 Analysis of factorial experiments

Simple analysis of factorial experiments involves evaluating the main effect of each factor. This is an estimate of the change in the measured response variable going from the low level to the high level of the factor. Main effects are calculated by subtracting the average of all the responses from the low level runs from the average of the high level runs for a given factor. The calculation is visualised in Figure 1.1 and also in the coding in Table 1.6.

More complex is the evaluation of the interactions. Once again the coding in Table 1.6 shows which runs are averaged and subtracted ( $-1$ ) from the other runs ( $+1$ ). Here Figure 1.1 visually demonstrates the interactions and explains them.

The relative magnitude of effects and interactions is a good measure of how important the various factors are to the result of the measured response. Care should be taken, however, since this relies on the range of the factors being well chosen. If a very strong factor is chosen with high and low values that are too close, it could appear to be less important than minor factors.

### 1.5.1.2 Centre points in factorial experiments

The addition of multiple runs at the mean point of  $2^k$  factorial experiments is of significant use for factorial designs. By comparing the arithmetic mean of the factorial design points to that of the centre points it can be determined if the main effects and interactions are likely to be linear. Centre points can also be used to estimate the error in the response variable to allow statistical analysis without replicating the factorial points.

If attempting to fit a linear predictive model to the factorial design it is essential to have multiple replications of the centre point. Firstly the average centre point response can be statistically compared to the arithmetic mean of the factorial points to assess if a linear model is valid. Secondly the centre points ensure that the model is not being used to predict the middle of the experimental space using measurements at

the extreme. A set number of centre points can be defined that ensures an even distribution of information throughout the experimental space and gives more confidence in the model prediction.

#### 1.5.1.3 Qualitative factors

The coding and mathematics of the factorial experiment imply that only quantitative factors can be employed in such analyses. However the use of qualitative factors is entirely possible and mixtures of both qualitative and quantitative factors are possible. On the simplest level the main effect becomes the change in the response switching from one qualitative choice to the other.

Restrictions appear when taking centre points or fitting a model to the experimental space. The centre points can potentially be a mixture of the two qualitative options or two separate sets of centre points can be performed. Fitting a model (e.g. linear) can be carried out where data can be isolated at one or other of the qualitative choices. Otherwise a fitted model would assume that intermediate values exist between the discrete +1 and -1 qualitative options.

#### 1.5.1.4 Error analysis in factorial experiments

The key analysis step in factorial experiments is the evaluation of the error, which identifies which effects and interactions are statistically significant and are therefore relevant. Error estimation is often a simple comparison of the means of two groups (the +1 and -1 coding from the design matrix) using replication of each experimental condition. Other options exist including partial replication (especially replicating only the centre points) and assuming the higher order interactions are negligible and provide an estimate of the experiment variability (Montgomery, 2008).

#### 1.5.1.5 Fractional factorial analysis

In order to reduce the number of experimental runs in a factorial design it is possible to run fractional repeats. The fractional experiments are denoted  $2^{k-p}$ , where the

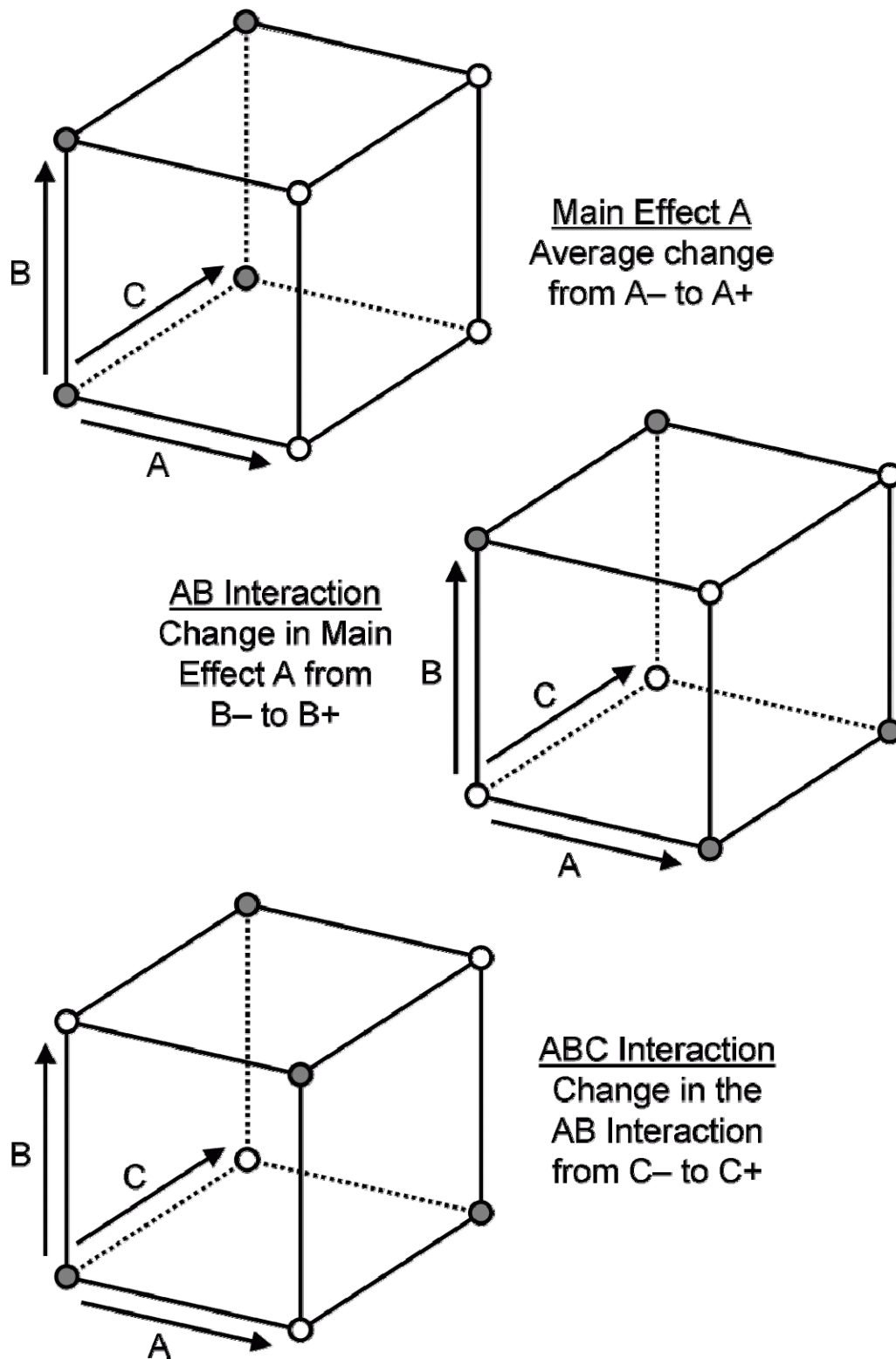


**Figure 1.2.** Visual representation of the main effects and interactions for a  $2^3$  factorial experiment. The vertices of the cube represent the high and low factorial combinations of the three factors (A, B and C). The magnitude of the effect or interaction is the average of the white points minus the average of the shaded points.

fraction of the full factorial experiment is  $\frac{1}{2^p}$ . The designs are constructed by using  $p$  groups of factors which when multiplied together equal to the identity function. This confounds main effects and interactions together. Confounded effects and interactions can not be separated and a result only a single value can be calculated sum.

For example in a  $2^{4-1}$  half factorial experiment the coding for the fourth factor (D) is constructed from the multiplication of other factor codings ( $D = ABC$ ). The defining relationship for this example is denoted as  $I = ABCD$  and involves more terms for quarter or smaller fractional designs. This leads to all two factor interactions being confounded in pairs and the result generated is the addition of these factors:  $AB + CD$ ,  $AC + BD$ ,  $AD + BC$ . If any of the three calculated interaction combinations are statistically significant it will not be possible to determine which one of the interactions is causing the change in the response without additional information. In the most extreme example the two confounded interactions could potentially be of similar magnitude and opposite sign, thus cancelling out and appearing insignificant.

The resolution of a fractional factorial experiment is defined as the minimum number of letters other than the in the defining relationship. Therefore resolution III designs have some main effects confounded with two factor interactions, resolution IV designs have main effects confounded with three factor or higher order interactions and resolution V and above designs have two factor interactions confounded with three factor or higher order interactions. This restriction still allows significant resource savings, especially when investigating higher numbers of factors. For example a  $2^8$  full factorial would take 256 runs to complete, however a  $2^{8-2}$  quarter factorial would be completed with only 64 runs at resolution V. Even when unfavourable confounding is necessary due to run limitations there are designs which can be found to minimise the number of low order interactions or main effects that are confounded (Fries and Hunter, 1980).

#### 1.5.1.6 Blocking in factorial analysis

When carrying out factorial experiments it is important not to bias the results based on restrictions to experimental operations. For example, if only the low value factor A runs were carried out in the first day of a two day trial, it would not be certain if the main effect of A was caused by varying the factor or variability from day to day. Similarly if raw material batch changes are not properly planned for there are risks the results will be biased. It is almost as if an additional factor is introduced which is not accounted for in the original design.

The simplest form of blocking is to confound the change in a block factor (e.g. different days, different raw materials) with a higher order interaction. Therefore any effects of the block factor on the response will show up in what was otherwise expected to be an insignificant interaction. Many blocking designs have been published to assist experimenters (Wu and Hamada, 2000) and modern statistical packages can be used to select the appropriate blocked designs.

Blocking is very effective in mitigating the influence of known restrictions or variations that cannot otherwise be controlled. Inside each block, or where no blocking is used the whole experiment, the runs should be randomised in order to limit the effect of any unforeseen trends or step changes in the response variable. Randomising the run order for factorial experiments is recommended where it is possible and does not complicate the execution of the runs (Box, 1990).

### 1.5.2 Response surface methodology

Response surface methodology (RSM) is simply ‘a collection of statistical and mathematical techniques useful for developing, improving and optimizing processes’ (Myers *et al.*, 2009). The whole approach is sequential in nature and requires a build up of experimental information before using sequences of experiments to ensure a response surface covers the right experimental space around the process optimum. Myers and co-authors (2009) separate RSM into three phases:

**Phase Zero:** Carry out a screening experiment to assess the important factors and interactions (see Section 1.5.1 on factorial experiments).

**Phase One:** Assess whether the optimum is close to the current factor values being investigated and, if necessary, change these using the ‘method of steepest ascent’ to determine the most likely direction to locate the process optimum.

**Phase Two:** Select and execute an appropriate response surface design in the location of the process optimum.

By following these approaches the response surface will not only give a good prediction of the relationship of multiple factors and responses, but also ensure that behaviour at and around the optimum is understood.

#### 1.5.2.1 Types of response surface

Different response surface designs with subtle variations can be selected at for different objectives. George Box was instrumental in developing effective response surface designs, including the Box-Behnken designs (Box and Behnken, 1960; 3 factors or more) and central composite designs (Box and Wilson, 1951). Central composite designs have the factorial points at their centre, with augmented star points at extended values of one factor and the centre of the other(s).

Maintaining the rotatability of the response surface design is important (Box and Hunter, 1957). This means that the predictive power of the model at any point will depend on the distance from the centre point and not the direction, essentially maintaining the symmetry of the design.

### 1.5.3 Windows of operation

There are multiple responses that must be traded off during optimisation of bioprocesses. For example required product quality must be maintained whilst keeping costs at a minimum. Overlaying different response surfaces for the same variable factors can indicate the process factor ranges which will achieve the desired

balance between these responses. Such windows of operation (Woodley and Titchener-Hooker 1996; Zhou and Titchener-Hooker, 1999) define where to operate a process. The relative size of the window can indicate how stable the process is and how easy it is to control within the required limits. The windows of operation concept has been applied to the measurement of bioprocess kinetics in high throughput robotic platforms (Nealon *et al.*, 2005)

## 1.6 Project significance

Recent advances in the life sciences and the establishment of ultra-high throughput screening technologies have led to the identification of large numbers of potentially important biopharmaceuticals. Many of these are now in the later stages of product development (Werner, 2004) and there is greater pressure than ever before on bioprocess development groups. The challenges being faced are how to deal with the larger number of new drug candidates being identified while constraining increasing bioprocess development costs which can be considerable (DiMasi *et al.*, 2003). The need is to create more efficient manufacturing routes more quickly.

Research at microscale is moving towards the goal of automated whole process sequences on the deck of a robot at microlitre scale (Lye *et al.*, 2003; Micheletti and Lye, 2006) in order to provide for this need. This is a natural progression from established principles of unit operation scale-down which have been shown to predict pilot scale performance when linked with process models (Ayazi Shamlou *et al.*, 1998). The generation of microscale downstream processing techniques is clearly vital if microscale whole process sequences are to become a reality. Some progress has been made on equilibrium-based separation techniques such as liquid-liquid extraction and solid-liquid adsorption (Lander, 2002). These have the advantage that their design is based on equilibrium parameters that are independent of the scale at which they are determined. The need now is to create microscale approaches to the more complex downstream processing techniques widely used in the biopharmaceutical sector such as microfiltration, ultrafiltration and chromatography.

## 1.7 Aims of the project

The primary objectives of the investigations in this thesis are summarized below:

- To develop an automation friendly technique for the parallel quantification of flux during normal flow microfiltration at the microscale. The technique must rapidly quantify key parameters capable of describing the filtration that are of specific use for scaling up. Currently available commercial equipment is analysed and adapted for operation of the methods where appropriate. In addition, a custom filter plate is designed, optimised for bioprocessing, to enable the most accurate assessment of microfiltration performance. Experiments relating water flux to the membrane resistance are used to indicate the initial suitability of the equipment and methods. Subsequent work tackles the more complex filtration of biological suspensions, specifically *E.coli* fermentation broth. The technique should be able to differentiate between feed samples in parallel and quantify filtration performance differences due to process changes. This work is described in Chapter 3.
- To demonstrate how automated microscale normal flow microfiltration methods developed can fully characterise a filtration process by quantifying protein transmission in addition to flux. This will utilise microscale techniques in conjunction with design of experiments methodology to optimise the filtration of an *E.coli* and protein mixture. In addition the scalability of microscale data to conventional laboratory scale equipment at optimal and non-optimal conditions is established. This work is described in Chapter 4.
- To operate an automated whole process sequence at the microscale and demonstrate that the results are scaleable. An industrially relevant and appropriate bioprocess for plasmid DNA is selected in order to investigate a significant process sequence. This will prove that such a sequence can be carried out at the microscale and demonstrate that the data generated can be

scaled in both size and format of filtration device. This work is described in Chapter 5.

This will complete the major aim of developing microscale microfiltration operations that can be incorporated into whole process purification sequences on the deck of an automation robot.

## **2.0 Materials and methods**

### **2.1 Introduction**

This chapter includes the details of materials, equipment, analytical techniques and experimental methods that have been used in the preparation of this thesis. The only exceptions are details of the design of a custom microwell filter plate and methods for data treatment of automated microscale microfiltration results. These were developed during the project and are described in detail in Chapter 3 and further adapted in Chapter 5. The newly developed microscale equipment and methods are integral to this thesis and directly relate to the discussion of the data in Chapter 3 which proves their capability.

### **2.2 Chemicals**

The yeast extract and tryptone used in the fermentation media were obtained from Oxoid Ltd. (Basingstoke, Hampshire, UK) and different batches were used in Chapters 3 and 4. All other chemicals were obtained from Sigma-Aldrich Chemical Co. (Poole, Dorset, UK) and were of analytical grade or better. Ultra-pure de-ionised water (Milli-Q Gradient, Millipore, Billerica, MA, USA) was used for the all water flux experiments and as a buffer for HPLC assays. Reverse osmosis (RO) water was used in all other experimentation (Elix 10, Millipore, Billerica, MA, USA).

### **2.3 Microfiltration materials and equipment**

#### **2.3.1 Microfiltration membranes and filters**

The majority of membranes used in this study were Millipore 0.22  $\mu\text{m}$  PVDF

(polyvinylidene fluoride) Durapore membranes in the form of 25 mm discs, Multiscreen<sup>®</sup> 96-well filter plates, or inserts from Ultrafree-CL centrifugal filters (Millipore, Billerica, MA, USA) which were used in the custom filter plate. The custom filter plate also used 0.2 $\mu$ m cellulose nitrate membranes cut to size from 47 mm discs (Whatman, Middlesex, UK).

For experiments involving filter aid a 22-26  $\mu$ m wire mesh (Betamesh 25, G Bopp & Co Ltd, Derbyshire, UK) was cut to the appropriate size in order to retain a Celpure<sup>®</sup> (Advanced Minerals, CA, USA) filter aid pre-coat. Two different grades of Celpure filter aid were used (P65 and P300). The numbers for each grade relate to the permeability of the filter aid in millidarcies and the approximate ratings of the Celpure are 0.2-0.3  $\mu$ m and 0.45-0.6  $\mu$ m respectively.

### **2.3.2 Tecan automation robot**

The automated system used in this thesis is a customised Tecan Genesis Freedom liquid handling robot (Tecan, Männedorf, Switzerland). This is capable of manipulating microwell plates and associated equipment, automated pipetting of liquids, agitation, centrifugation and vacuum filtration. The Tecan automation robot used here is shown in Figure 2.1, with various important components highlighted.

#### **2.3.2.1 Vacuum manifold**

The automated microscale normal flow filtration (NFF) technique established here is based on the use of a Tecan VacS two-position vacuum filtration manifold (Figure 2.1(b) and (d)). This was located on the deck of the Tecan Genesis Freedom liquid handling robot with Gemini software being used to control pipetting actions, plate movements and filtration manifold operation.

The system is capable of generating a vacuum up to approximately 750 mbar. The vacuum is generated and monitored in a separate vacuum chamber. Once the desired pressure is reached a valve is automatically switched connecting the vacuum chamber



**Figure 2.1.** Two photographs of different configurations of the Tecan Genesis Freedom liquid handling robot used in this work housed inside a laminar flow cabinet. (a) Integrated plate mixer, (b) VacS two-position vacuum filtration manifold, (c) 8-tip liquid handling arm, (d) VacS manifold with with 8-well custom filter plate, (e) separate RoMa robotic arm for plate manipulation, (f) entry port for integrated centrifuge (below deck).

to the vacuum manifold via tubing of approximately 0.75 m in length. The vacuum pump is turned on and off when the vacuum pressure is 5 mbar lower or higher than the set value. Hence the actual pressure profile at the vacuum manifold is variable around a set point, which is slightly lower than the requested value maintained in the vacuum chamber.

In order to allow measurements of specific cake resistance, two microwell filter plates were run in parallel on the VacS vacuum filtration manifold (Figure 2.2). A detailed cross-section of the manifold, filter plate and collection plate assembly is shown in Figure 2.2(a). A three way valve was used to vent one plate before the other as shown in Figure 2.2(b). Both plates start filtering at the same time with the same applied pressure profile. Beneath each filter plate there was a collection plate consisting of 96 removable tubes (96-well Cluster Tubes, Corning Life Sciences, Acton, MA) or 6 to 24 cuvettes (4.5 mL macro cuvette, Brand, Wertheim, Germany) so that measurements of the permeate mass from each well can be determined once filtration has stopped. This gives a single time and volume data point from each of the wells on a single plate. Vacuum pressure was monitored on one of the manifold positions by a digital manometer (Manometer 840082, SPER Scientific, Scottsdale, AZ) and logged on a PC to give the actual pressure profile seen by the microwell plates during an experimental run. The approach to the collection of flux versus time data and the calculation of membrane or specific cake resistance is developed later in Section 3.1. For water flux experiments with the Multiscreen plate, a plastic reservoir was attached above the plate in order to enable use of larger filtration volumes and hence higher pressure differences.

Once collected and weighed, the samples from both plates were stored and where required, analysed using the analytical methods detailed in Section 2.6.

To reduce measurement errors associated with the use of standard small volume Multiscreen filter plates a prototype custom microwell filter plate was designed. Details and rationale for the design are given in Section 3.2.1. All stages of the microwell filtration processes have been automated apart from the weighing operations, however many automation solutions for this are readily available. For

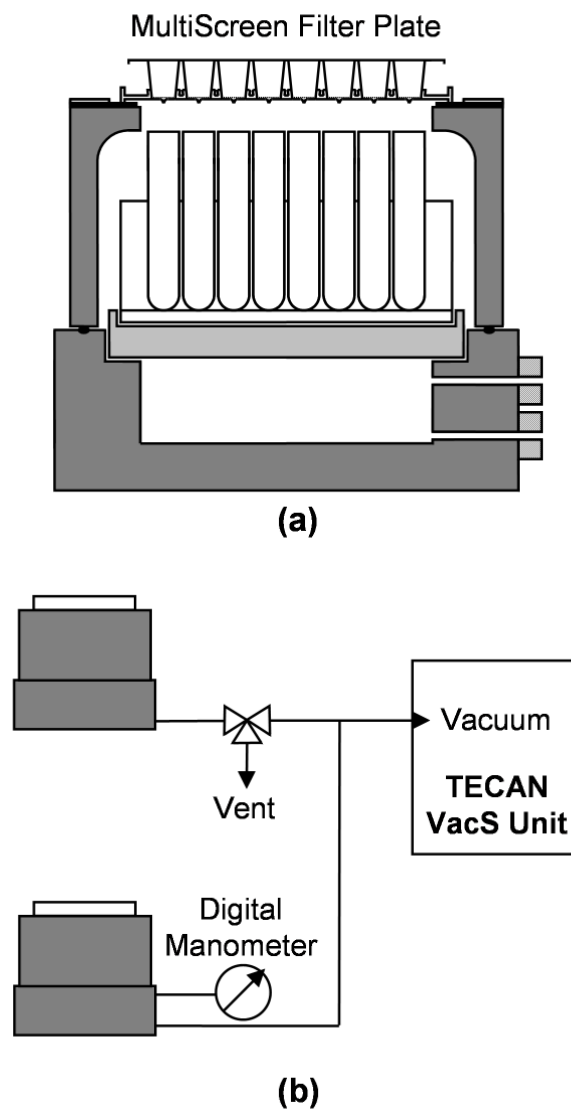


**Figure 2.2.** Detail of the Tecan vacuum manifold system showing: (a) cross-section of a single vacuum filtration manifold showing the Multiscreen filter plate on top and a deep-well collection plate below (inside) the manifold, (b) vacuum manifold equipment for parallel microscale filtration experiments using either commercial 96-well Multiscreen filter plates or the custom filter plate described in Section 3.2.1.

example, the Tecan robotic arm is able to pick up the cuvettes, filter inserts and removable tubes and could weigh them on a balance connected to the system if higher throughput operation were required. All microwell microfiltration experiments in Chapter 3 were performed at least in triplicate. Replication for the experimental designs used throughout the rest of the thesis are detailed in Section 2.7.

#### 2.3.2.2 Mixing

Any mixing or temperature control of feeds required was carried out by a Thermomixer (Eppendorf, Hamburg, Germany; see Figure 2.1(a)) which can accommodate a variety of microwell plate formats. When experiments were limited by Thermomixer numbers (in Section 2.5.2.7 where multiple plates need to be mixed for a prolonged period of time) the plates were shaken in an incubator with a microwell plate adapter (ISF-1-W, 25 mm shaking diameter, Kühner AG, Birsfelden, Switzerland). When limited by the shaking speed range of the Thermomixer, Variomag multi-position microplate mixers (Thermo Scientific, Loughborough, UK) were used.

#### 2.3.2.3 Liquid handling

All liquid handling during automated microscale processing was carried out using the Tecan's own liquid handling system consisting of an automated eight-channel pipetting system. The exception was feeds where the solids concentration is too high for the Tecan, in which case manual pipetting was used utilising pipette tips adapted with wider openings. Options do exist for handling high solids concentration samples with the Tecan, but were unavailable at the time.

#### 2.3.2.4 Plate handling

The TECAN RoMa arm was programmed to move all filter plates, collection plates and the vacuum manifold components so as to allow programs to be generated that are capable of running complete sequences of automated filtration and mixing steps.

### 2.3.3 Membrane cell

Standard laboratory scale microfiltration experiments in Chapter 3 were carried out using an unstirred normal flow membrane cell (3.8 cm<sup>2</sup>, Amicon 8010, Millipore, MA, USA) as shown in Figure 2.3(a). Nitrogen of variable pressure controlled by a regulator valve provided the driving force and permeate mass and time were logged on a PC and used to calculate water flux or specific cake resistance as necessary. This method of applying a positive gauge pressure to the feed is in contrast to the microwell scale experiments which use a vacuum pump to generate a negative gauge pressure (below atmospheric) on the permeate side of the membrane. In order to elucidate the differences of applying a positive pressure or negative pressure to drive the filtration process, the Tecan VacS vacuum pump was also used with the membrane cell as shown in Figure 2.3(b). For the negative pressure experiments, the filtration process has to be stopped and the permeate collected weighed to give a data point of time and volume, in a similar fashion to the filter plate experiments. The water flux was determined by timing the permeation of a known volume of water once a constant pressure had been reached. All pressures were monitored by a digital manometer (Manometer 840082, SPER Scientific, Scottsdale, AZ) and manually adjusted and recorded. All membrane cell experiments in Chapter 3 were performed in triplicate.

The scale-up experiments carried out in Chapter 4 used a larger membrane cell (13.2cm<sup>2</sup>, Amicon 8050, Millipore, MA, USA) and the same ancillary equipment as in Figure 2.3(a). Only the optimum condition run was duplicated, all other experiments were single evaluations.

The effective filtration areas quoted for the Amicon stirred cells were determined by measurement of *E.coli* filter cake diameters and are in close correlation to values in the literature (Wutzel and Samhaber, 2009; Akbari *et al.*, 2002) which contradict the claims of the manufacturer. This indicates that the effective filtration area may vary with the type of membrane used and the potential use of any support layers (no additional support layers were used in this thesis).

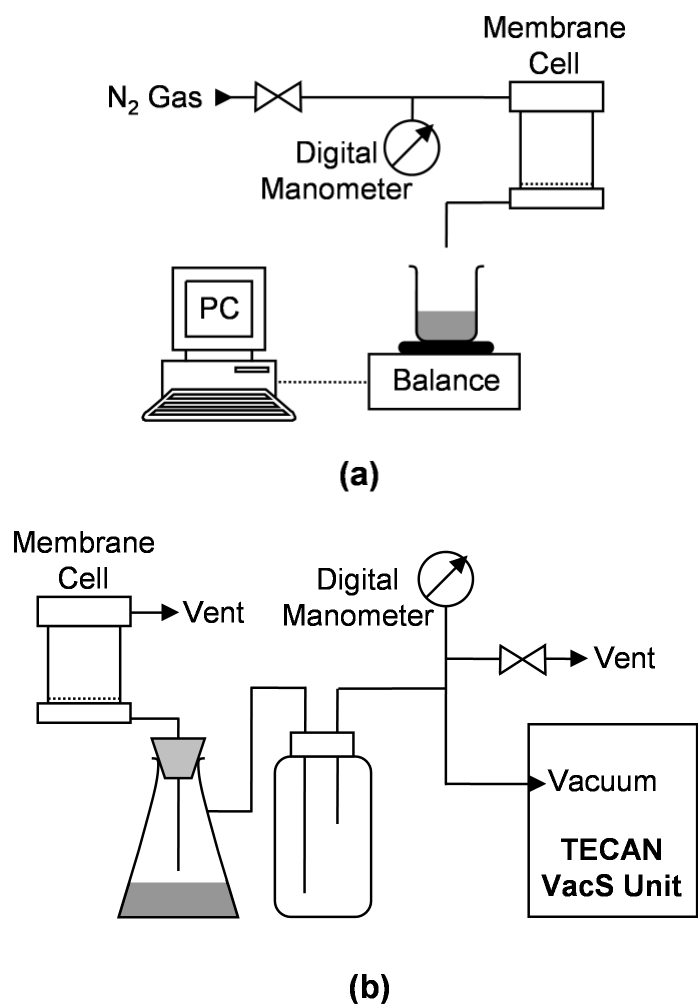


**Figure 2.3.** Experimental set-ups for membrane cell operation: (a) using nitrogen to generate a positive gauge pressure on the feed side of the membrane (b) applying a vacuum to generate a negative gauge pressure on the permeate side of the membrane.

### 2.3.4 Rotating vertical leaf filter (RVLf) scale-down device

Most simple laboratory scale filtration units consist of batch, pressure driven apparatus with a horizontal filter. Industrial filters such as the rotating vertical leaf filter (RVLf) have a vertical configuration and are also rotated on an axis perpendicular to the filter. The RVLf is also continuously fed suspension via a pump, rather than operating in batch mode. The ultra scale-down (USD) RVLf device (9cm<sup>2</sup>) was created to mimic this operation (Reynolds *et al.*, 2003). A diagram of the USD device is shown in Figure 2.4, including details of the experimental set-up. The device was rotated by means of a rubber wheel connected to a motor, which enables the filter to rotate at  $10 \pm 3$  rpm.

A peristaltic pump was connected to the inlet and used to deliver feed at a flowrate of  $0.28 \text{ mL}\cdot\text{s}^{-1}$ , based on prior work showing this is preferable for scale-up of complex solutions (Reynolds *et al.*, 2003). The filter device was filled with RO water before use, removing air from the system and ensuring the chamber was full. A wire mesh disc was used to retain the pre-coat (0.5 g of solid in 50mL of RO water) which was pumped through until finished (leaving a  $0.55 \text{ kg}\cdot\text{m}^{-2}$  pre-coat layer) and then the inlet tube was manually switched to the feed solution. Constant flow operation was maintained until the pressure reached 1.5 bar. Thereafter the flowrate was manually reduced in order to maintain a constant pressure. All feeds were kept homogeneous by the use of a magnetic stirrer.

Product was collected after the dead-volume of the system and the 50mL pre-coat water had permeated. A small amount of product can be lost with this method due to mixing in the chamber, but purity and concentration should be maintained.

### 2.3.5 Candle filter

A pilot scale candle filter (0.012 m<sup>2</sup>, Dr Muller AG, Mannedorf, Switzerland) was used for scale-up experiments during the pDNA work in Chapter 5. The same ancillary equipment was used as for the RVLf scale-down device in Figure 2.4(c). The candle filter was operated in a similar fashion to the USD RVLf device. The

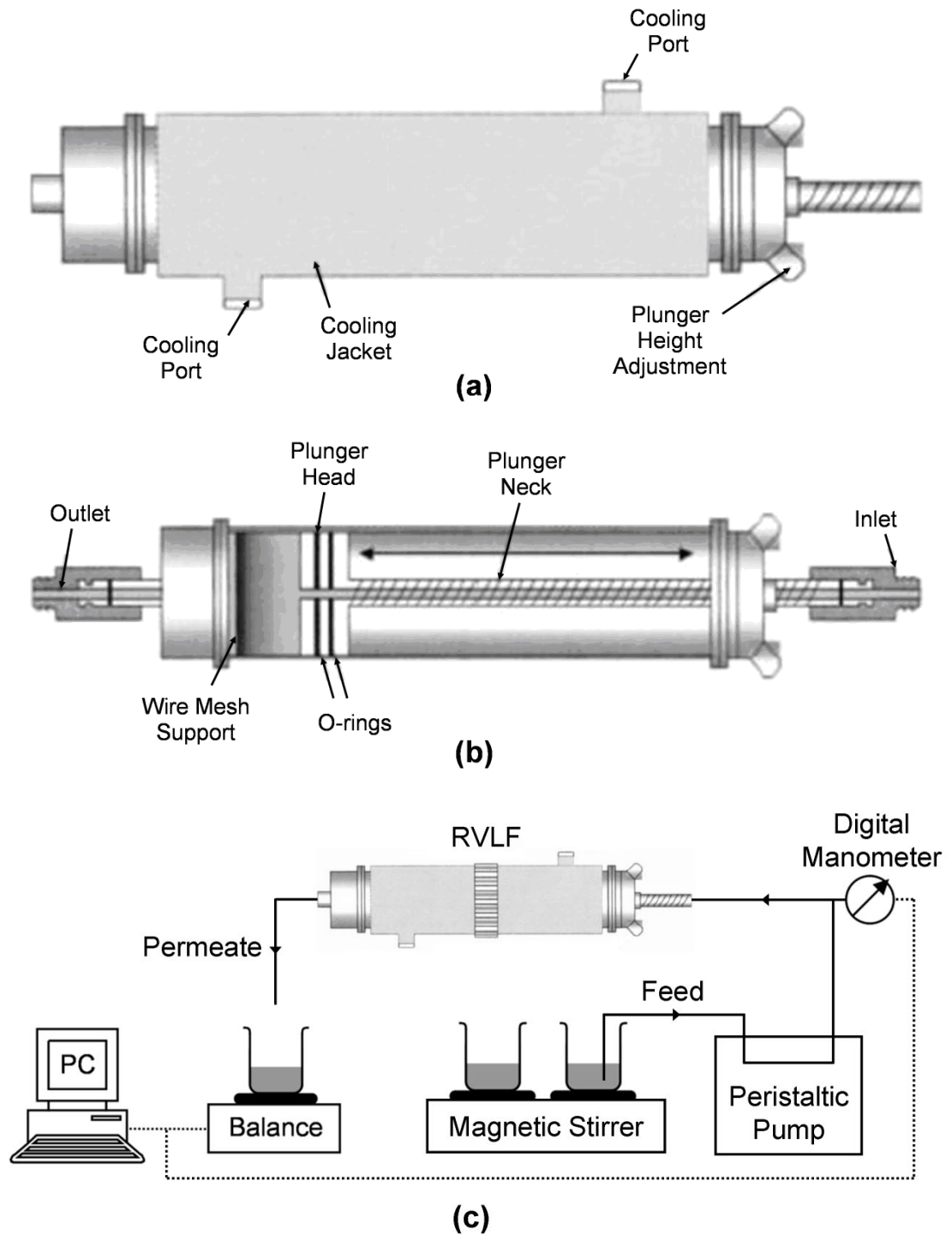


**Figure 2.4.** The rotating vertical leaf filter (RVLf) scale-down laboratory filter: (a) view of filter exterior, (b) view of filter cross section (both reproduced from Reynolds *et al.*, 2003), (c) experimental set-up used in this work.

system was filled with RO water and then the precoat (5g solids in 500mL water) was pumped through until finished and then the inlet tube was manually switched to the feed solution. The support which retained the solids was a PTFE cloth perforated with  $10 \times 30 \mu\text{m}$  openings.

## **2.4 *E.coli* fermentation feed preparation**

*Escherichia coli* TOP10 pQR239, which expresses the recombinant enzyme cyclohexanone monooxygenase (CHMO) upon induction with L-arabinose (Doig *et al.*, 2001), was used for the studies described in Chapters 3 and 4 of this thesis.

### **2.4.1 Fermentation conditions**

The soluble complex growth media used for each fermentation consisted of yeast extract, tryptone, glycerol and NaCl all at  $10 \text{ g.L}^{-1}$ . The media solution was sterilised at  $121^\circ\text{C}$  for 30 min after which  $0.2 \mu\text{m}$  filter sterilised ampicillin was added to a final concentration of  $50 \text{ mg.L}^{-1}$ . Glycerol stocks generated and stored as previously described (Doig *et al.*, 2001) were used to inoculate 40 mL of media in 250 mL baffled shake flasks, grown in an orbital shaker (ISF-1-W, 25 mm shaking diameter, Kühner AG, Birsfelden, Switzerland) at  $37^\circ\text{C}$  and 200 rpm for 14 h. These cells were then used as a 10% v/v inoculum for fermentations in 1 L baffled shake flasks (200 mL liquid volume) at  $37^\circ\text{C}$  and 200 rpm. These flasks, harvested after 4.5 h of growth, provided the feed stream used in the subsequent microfiltration studies. For cell ageing experiments, fermentations were extended maintaining the same incubation conditions with additional harvests made after a further 4 h and 24 h.

### **2.4.2 Dry cell weight measurement**

For all shake-flask fermentations, the dry cell weight concentration (DCW) of *E. coli* TOP10 cells was determined by optical density measurement at 600 nm wavelength and 10mm path length (4.5 mL macro cuvette, Brand, Wertheim, Germany; U-2001, Hitachi, Tokyo, Japan), which had been previously correlated to known DCW values

(Figure A.1 of Appendix A). These DCW measurements were determined from the weight difference between empty 1.5 mL centrifuge tubes (Eppendorf, Hamburg, Germany) dried at 100°C for 16 h and the same tubes containing dried cell pellets generated by centrifuging 1.5 mL of cell broth at 13000 rpm for 5 min followed by drying at 100°C for 16 h to achieve a constant weight. The maximum standard deviation in DCW values determined from triplicate OD<sub>600</sub> measurements was  $\pm 0.3 \text{ g}_{\text{DCW}}\cdot\text{L}^{-1}$ .

### 2.4.3 Sample preparation

Experiments in Chapter 3 examining harvest time effects on microfiltration performance used whole broth without any pre-treatment. In all subsequent experiments examining the effects of pH, ionic strength and media composition on microfiltration performance, other cell broth components were removed to eliminate the confounding effect of their interactions. Cell suspensions were centrifuged as 6 mL aliquots in Rohre centrifuge tubes (Sarstedt, Nümbrecht, Germany) at 4000 rpm and 4°C for 6 min (5810R Centrifuge, Eppendorf, Hamburg, Germany) and washed twice with 180 mM NaCl solution. The cell pellets were then stored at 4°C for a maximum of 4 h and resuspended by vortex mixing in the appropriate buffer solution prior to use. The volume that was added to each microwell is detailed in Table 3.1. All buffers used in Chapter 3 had 100 mM buffer strength and were prepared at a constant ionic strength of 180 mM with the addition of NaCl based on calculations at the buffer pH (Beynon and Easterby, 1996).

In Chapter 4 samples were prepared in a similar way. Buffers were made up using piperazine (pH 5.00, pH 5.05, pH 5.29, pH 5.50 and pH 5.95), bis-tris (pH 6.71 and pH 7.00) and MES (pH 6.00) and lysozyme from chicken egg white (approximately 50,000 units/mg protein, Sigma-Aldrich, Poole, Dorset, UK) was added to  $2 \text{ g}\cdot\text{L}^{-1}$  before resuspension of the cells. The volume added to each filter insert was 2mL.

## 2.5 Plasmid DNA feed preparation

The plasmid DNA (pDNA) purification process sequence examined in Chapter 5 of this thesis is outlined in Figure 2.5. This process was carried out at three different scales from lysis clarification through to adsorbent removal. This section is split into four, first describing the process in general and then describing the experimental methods for the microscale, laboratory scale and pilot scale processes.

### 2.5.1 Plasmid DNA process overview

The following sequences correspond to the numbered process steps indicated in Figure 2.5. Details of buffers and key chemical solutions used are also included in this section. Experimental methods for the different scales investigated are described in Section 2.5.2 (microscale), Section 2.5.3 (laboratory scale) and Section 2.5.4 (pilot scale)

#### 2.5.1.1 Fermentation conditions

The pDNA (pQR150, 20k base pairs) was transformed and propagated into *Escherichia coli* DH5 $\alpha$  as previously described (Levy *et al.*, 2000). The *E.coli* was grown in a 450L Chemap bioreactor (Chemap AG, Maennedorf, Switzerland) under previously published conditions (Levy *et al.*, 2000). The cells were then harvested by centrifugation and frozen at -80°C in bags of approximately 1kg wet cell paste.

#### 2.5.1.2 Resuspension

The clarified cells were resuspended by gentle mixing in a Tris EDTA buffer (10 mM Tris, 2 mM EDTA, pH 8) which is appropriate for subsequent cell lysis (Levy *et al.*, 2000b).

#### 2.5.1.3 Cell lysis

Chemical lysis was used to disrupt the cells and release the DNA. The alkaline-SDS

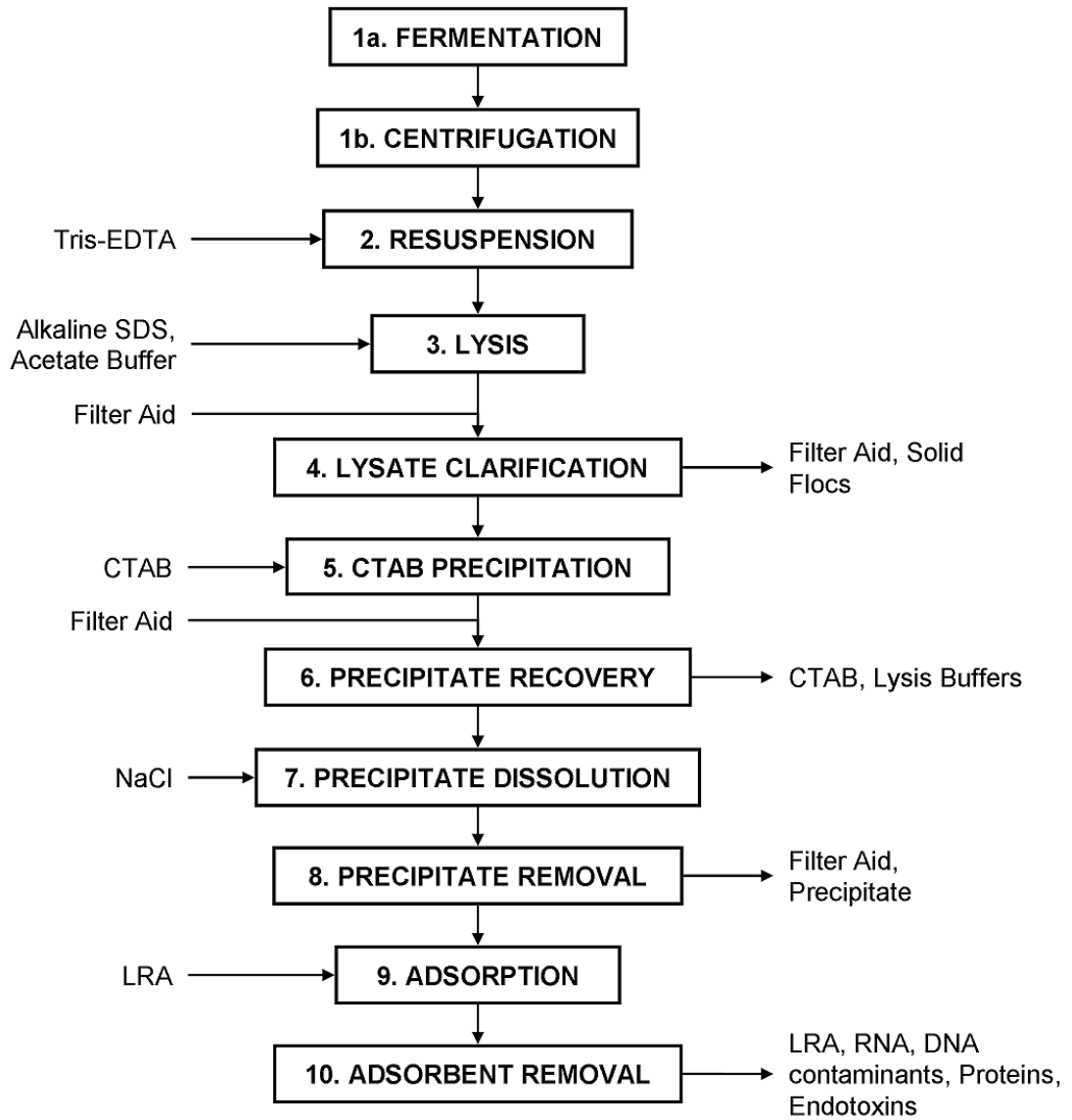


**Figure 2.5.** Overview of the non-chromatographic process for the production and purification of pDNA studied in this thesis.

solution (200mM NaOH, 1% w/v sodium dodecyl sulphate) destroys the cell surface and liberates the contents of the cell. All the nucleic acids (pDNA, genomic DNA and RNA) are denatured and thus come out of solution. A very dense potassium acetate neutralisation buffer (3M potassium acetate, 2M acetic acid, pH5.5) is used, renaturing the nucleic acids and making them soluble.

#### 2.5.1.4 Lysate clarification

The lysate is next clarified to remove solid contaminants from the nucleic acids, which are in solution. In this thesis a filtration step utilising filter aids is investigated to carry out this initial clarification step. At the largest scale centrifugation was used due to the limited availability of filter aid.

#### 2.5.1.5 CTAB precipitation

Precipitation of the target of pDNA is facilitated by the cationic surfactant cetyltrimethylammonium bromide (CTAB) binding to the negatively charged DNA phosphate backbone. A stock solution of 2% w/v CTAB in RO water was used for all scales. This stock solution was added to clarified lysate to a volume ratio of 1:4, giving a final CTAB concentration of 0.4% w/v. This is in excess of that required for complete DNA precipitation presented by Lander and co-workers (2002), who have also demonstrated that contaminants can be removed by careful control of this concentration and use of an initial low CTAB concentration removal step. These variables were not investigated in this study.

#### 2.5.1.6 Precipitate recovery

The solid precipitate was recovered by filtration (or centrifugation at the largest scale), removing soluble contaminants within the liquid phase.

#### 2.5.1.7 Precipitate dissolution

The precipitate was then dissolved to facilitate recovery of the pDNA into the aqueous

phase by the addition of salt. With careful control of this dissolution, contaminants can be left in the solid phase for subsequent removal, even unwanted conformations of pDNA. For the purposes of this microscale study a single concentration of 0.7M NaCl was chosen to recover the pDNA during all experiments. As detailed in Chapter 5, many options surround the precipitation and subsequent dissolution steps, but study of these factors in detail was beyond the scope of this work.

#### 2.5.1.8 Precipitate removal

The remaining contaminants in the precipitate and the Celpure were removed by filtration (or centrifugation at the largest scale) in order to give a clarified solution for polishing with the adsorbent.

#### 2.5.1.9 LRA adsorption

Following CTAB precipitation and precipitate re-dissolution in a sodium chloride solution there are still contaminants such as residues of CTAB and SDS, undesirable conformations of pDNA, genomic DNA, RNA and endotoxins (Lander *et al.*, 2002). Nucleic acid contaminants can be selectively adsorbed onto hydrated calcium silicate lipid removal agent (LRA) since they have a greater affinity than the conformationally constrained supercoiled pDNA (Winters *et al.*, 2003). The adsorption is a complex process in which some pDNA is initially bound but is displaced by other components (Winters *et al.*, 2003). The LRA used in this thesis was the pharmaceutical grade LRA II (Advanced Minerals, CA, USA).

#### 2.5.1.10 LRA adsorbent removal

The final step investigated is the removal of the LRA adsorbent and all the bound contaminants by the fourth and final filtration step in this process sequence, studied in detail at all scales.

## 2.5.2 Microscale plasmid DNA purification methods

The experimental design used to investigate the pDNA process at microscale is described in Section 2.7.1.2. The chosen factors and levels are shown in Table 5.2 and full details of experimental parameters, raw data and calculated responses are summarised in a series of tables in Appendix D.

### 2.5.2.1 Lysis for microscale filtration

Mixing of the very viscous lysate cannot be effectively carried out with current microscale techniques, although miniature stirred bioreactors (Lamping *et al.*, 2002; Kumar *et al.*, 2004; Gill *et al.*, 2008b) have the potential to be effective in the future when integrated with automated microscale solutions. For this study a total of  $3 \times 180$  mL of lysate was produced as described below at laboratory scale using three different stirrer speeds to provide feed for all microscale lysate experiments in Section 5.3.1.

Tris-EDTA buffer was added to 9 g of frozen *E.coli* cell paste to a total volume of 60 mL, making up a concentrated cell suspension of  $150 \text{ g.L}^{-1}$  wet cell weight. This was added to a 250 mL glass beaker with four 8 mm wide stainless steel baffles and stirred using an overhead stirrer and a 25 mm diameter 6-blade ruston impeller at various speeds from 400 rpm to 1200 rpm. The impeller disc was initially set level with the top of the cell suspension.

The lysis mixture was continuously stirred during addition of 60 mL of alkaline-SDS lysis solution at a rate of  $10 \text{ mL.min}^{-1}$  using a 5 mL pipette. Once the system was well mixed (visually determined) a further 5 minutes of mixing was carried out before neutralisation. A total of 60 mL of neutralisation buffer was then added at the same rate using fresh pipette tips. Following the final neutralisation a further 5 minutes of mixing was carried out. The lysate was carefully pipetted into separate conical flasks whilst vigorously stirring by hand to maintain homogeneity. Then the appropriate grade and concentration of Celpure was added before the final lysate solution was ready for clarification.

### 2.5.2.2 Microscale lysate clarification

The clarification of lysate at microscale was carried out using the 24-well custom microwell filter plate (Figure 3.1) using a wire mesh support (22 – 26  $\mu\text{m}$ ). A pre-coat was placed on the wire mesh by pipetting 2 mL of a 10  $\text{g.L}^{-1}$  aqueous solution of the appropriate grade of Celpure into each well. A 30kPa vacuum was then applied for 2 minutes in order to ensure removal of excess water and to leave a 0.25  $\text{kg.m}^{-2}$  pre-coat layer on the mesh. The collection cuvettes were then replaced.

In order to ensure the lysate did not settle during filtration, the custom filter plate was held at 30kPa vacuum before pipetting of the lysate, which was stirred with a magnetic stirrer at all times during the filtration. 1mL of lysate was added into each well in order, followed by a further 1mL starting again at the first well and finally a third 1mL of lysate starting at the first well again. This gave a total of 3mL lysate feed volume in each well. With a differential pressure applied immediately upon sample addition, the filtration commenced rapidly and allowed the formation of a homogeneous cake without stratification. This is in contrast to conventional laboratory filtration techniques where layering of such a complex cake can occur (Reynolds *et al.*, 2003).

Collection plates were then removed and replaced. Following this some of the clarified lysate samples were recycled through the filter cake for further solids removal, according to the experiment design described in Section 2.7.1.2. Lysate was pipetted into the feed side of the lysate cakes in the custom microwell inserts and filtered using a 30 kPa vacuum.

A 1:1:1 (v/v) mixture of Tris-EDTA buffer, alkaline-SDS lysis solution and neutralisation buffer was used to flow through the lysate cakes and determine the overall filter cake resistance at 30kPa vacuum followed by 60kPa vacuum. The same method is used as outlined in Chapter 3 for determination of membrane resistance, but in this case generating the total resistance of a pre-deposited filter cake. The calculation details are shown in Section 5.2.2.

Foaming of the filtrate did occur due to the presence of SDS in the lysate and flow-through buffer and the vacuum on the permeate side. However, outlet extensions (pipette tips cut at both ends to ~5 mm in length with a 1 – 2 mm outlet) were placed on the bottom of all custom filter plate inserts and these were delivered to the middle of the collection cuvette where any foam broke on the side of the cuvette, preventing cross contamination or loss of material. The clarified lysate samples were then frozen at -20°C for 36 h before being reused.

Due to the potential variability of this step and to ensure sufficient material was available to repeat the subsequent microscale unit operations if errors occurred, the 72 separate lysate clarification experiments outlined in the factorial design (Section 2.7.2.1) were duplicated. Only one set of samples were used for the following microscale operations, but the duplicate data set were used for lysis clarification calculations.

#### 2.5.2.3 Microscale CTAB precipitation

Clarified lysate samples (any more than 1.6 mL per microwell experimental run was discarded) were pipetted into 24 deep square well (24-DSW) microtitre plates (Sarstedt, Nümbrecht, Germany) and mixed in a Thermomixer (Eppendorf, Hamburg, Germany) at 300 rpm. 40 µL of CTAB stock solution was added every three minutes up to a total liquid volume of 2.0 mL. Mixing continued for at least 10 more minutes for each well after the final addition of CTAB.

#### 2.5.2.4 Microscale precipitate recovery

The appropriate grade and concentration of Celpure was added to the precipitate solution before using the same method as in Section 2.5.3.1 was used to filter the precipitate. In this case no permeate recycles were used, since the contaminant is in the waste stream, and a water wash was used to flow through the cake and determine the flux data. The treatment of the data collected during precipitate recovery has been described separately in Appendix E, since the resistance to flow was so low a custom technique was developed in an attempt to measure specific cake resistance.

Once the precipitate was recovered the inserts were manually taken apart and the cake removed. Tests were carried out demonstrating that the cake could potentially be removed by centrifugation, but not safely or at high throughput with the equipment available. If a well designed custom insert holder was manufactured then the high throughput automation of this step would be possible.

#### 2.5.2.5 Microscale precipitate dissolution

The precipitate cakes were placed into the individual wells of several 24-DSW microtitre plates (Sarstedt, Nümbrecht, Germany). To each well 1.6 mL of water was added and the plates were mixed in Variomag multi-position microplate mixers (Thermo Scientific, Loughborough, UK) at a high speed setting for approximately 30 minutes until the contents were homogenous. Then, while mixing at either high, medium or low speed settings, 0.4 mL of 3.5 M NaCl was pipetted into each of the wells to give a final concentration of 0.7 M NaCl. The plates were continually mixed for a further 20 minutes.

The Variomag multi position microplate mixers were used in this case because they had fine control at lower speeds. A low mixing speed was chosen to intentionally perturb the results by generating bad mixing – even at it's lowest setting the Thermomixer may have given sufficient mixing and hence it was not used during this step. The Variomag mixer speeds were not calibrated and are given as low (~100 rpm), medium (~650 rpm) or high (~1200 rpm) depending on the position of the dial (note high is not full scale deflection of the dial and therefore not the maximum 2000 rpm speed that the Variomag mixers can acheive). Precipitate dissolution speed is therefore a semi-qualitative factor since it does have a definable centre-point value, but not a quantitative scale.

#### 2.5.2.6 Microscale precipitate removal

The un-dissolved precipitate is next removed using the same method as described in Section 2.5.2.2, except that no recycle is carried out and a fresh 0.7 M NaCl solution was used to flow through the cake and determine the flux. The fresh solution is used

rather than the permeate, since the clarified permeate is the product taken on to the LRA adsorption step. The treatment of the data collected during precipitate recovery has been described separately in Appendix E.

#### 2.5.2.7 Microscale LRA adsorption

Small amounts of LRA adsorbent were next added to the individual wells of several 24-DSW microtitre plates (Sarstedt, Nümbrecht, Germany) to achieve the desired final concentration of LRA. The clarified permeate samples from the previous step were then transferred to the wells and the plates were mixed in an incubator with a microplate adapter (ISF-1-W, 25 mm shaking diameter, Kühner AG, Birsfelden, Switzerland) at 100 rpm and 4°C for the allocated time.

#### 2.5.2.8 Microscale LRA removal

The LRA solution was then filtered by the same method as in Section 2.5.3.1. The LRA was used as a pre-coat and the permeate itself was recycled in order to flow through the cake and determine the flux data. This ensured the viscosity during cake deposition and flow through specific cake resistance determination matched, allowing accurate scale-up calculations. The recycling of the product stream through the waste LRA is not expected to affect the product quality by additional adsorption since the experimental time (a matter of minutes) is small in comparison to the elapsed absorption time already completed ( $\geq 2$  hours).

#### 2.5.2.9 Further microscale LRA removal

Initial experiments into microscale LRA removal showed that the pre-coat of LRA was not being effectively retained by the wire mesh (22 – 26  $\mu\text{m}$ ). Feed generated in Section 2.5.3.6 during the laboratory scale precipitate removal was used to repeat the microscale LRA tests (Section 2.5.2.7 and Section 2.5.2.8). Repeated experiments were carried out using P300 as a pre-coat instead and these were used as scale-up to large scale experiments.

### **2.5.3 Laboratory scale plasmid DNA purification methods**

#### 2.5.3.1 Lysis for laboratory scale filtration

The same scale and methods as in Section 2.5.2.1 were used for generation of lysate for laboratory scale-up RVLf experiments in Section 5.4.1, using a stirrer speed of 1200 rpm. Then 9 g of Celpure P300 was added to the 180 mL lysate solution to give a final concentration of 50 g Celpure solids per L of lysate.

#### 2.5.3.2 Laboratory scale lysate clarification

The RVLf scale lysate clarification was carried out using the method described in Section 2.3.4 using Celpure P300 as a pre-coat and the feed generated in Section 2.5.3.1.

#### 2.5.3.3 Laboratory scale CTAB precipitation

The equipment for lysis described in Section 2.5.2.1 was used to mix the clarified lysate throughout precipitation at 400 rpm. 40 mL of CTAB stock solution was added to 160 mL of clarified lysate in 4 mL aliquots every 3 min. Mixing was continued for 10 more minutes after the final addition of CTAB.

#### 2.5.3.4 Laboratory scale precipitate recovery

Firstly, 0.4 g of Celpure P300 was added to the 200mL of precipitate solution from Section 2.5.4.2 to give a final concentration of 2 g of Celpure solids per L of liquid. Then the rotating vertical leaf filter was used as described in Section 2.3.4, with Celpure P300 as a pre-coat.

#### 2.5.3.5 Laboratory scale precipitate dissolution

The dissolution was carried out in the same vessel as the lysis and CTAB precipitation described in Section 2.5.2.1. 160mL of water was added to the recovered cake of

precipitate and Celpure. The subsequent solution was mixed for approximately 10 minutes until visually homogeneous. Then 40mL of 3.5 M NaCl was poured into the vessel whilst mixing throughout. The pDNA solution was mixed for a further 20 minutes.

#### 2.5.3.6 Laboratory scale precipitate removal

The RVLf precipitate removal was carried out using the method described in Section 2.3.4, using Celpure P300 as the pre-coat. This feed was then used to generate repeated microscale LRA data as described in Section 2.5.2.9.

#### 2.5.3.7 Laboratory scale LRA removal

The RVLf LRA removal was carried out using the method described in Section 2.3.4, using Celpure P300 as the pre-coat. For the easier to filter LRA suspensions the flow was increased to  $0.7 \text{ mL}\cdot\text{s}^{-1}$ . RVLf LRA removal experiments were carried out on the following day to the candle filter work. The feed was generated in the same way as the pilot scale experiments (Sections 2.5.4.1 to 2.5.4.6) using half the volumes and masses.

### 2.5.4 Pilot scale LRA adsorbent removal feed preparation

In order to carry out pilot scale studies of the LRA adsorbent removal step, 2L of purified pDNA was generated from the cell paste using the following steps.

#### 2.5.4.1 Lysis for pilot scale filtration

For the preparation of pDNA solution for pilot scale candle filter tests in Section 5.4.4.2, the DNA lysis was carried out at 2 L scale in a glass bottle. 100 g of *E.coli* cell paste was made up to 667 mL with Tris-EDTA buffer and mixed at 300 rpm for approximately 1 hour in an orbital shaker (ISF-1-W, 25 mm shaking diameter, Kühner AG, Birsfelden, Switzerland) to resuspend the cells. Next 667 mL of alkaline-SDS lysis solution was rapidly added to the cell suspension and then mixed by inversion

until no changes in lysate appearance were observed. Finally 667 mL of neutralisation buffer was rapidly added to the lysate mixture until no changes in neutralised lysate suspension were observed.

#### 2.5.4.2 Lysate clarification for pilot scale filtration

For the pilot scale candle filter experiments in Section 5.4.4.2, the lysate was clarified using centrifugation. The lysate was separated into 4 aliquots of 500mL and then centrifuged at 4000 rpm and 4°C for 20 minutes (JA-10 rotor, J2-MI centrifuge, Beckman Instruments, High Wycombe, UK). The supernatant was then decanted and pooled.

#### 2.5.4.3 CTAB precipitation for pilot scale filtration

For the pilot scale candle filter experiments in Section 5.4.4.2, the clarified lysate (1.6 L) and CTAB stock solution (0.4 L) were mixed together rapidly in a 2 L glass bottle which was then mixed at 300 rpm for 30 minutes in an orbital shaker (ISF-1-W, 25 mm shaking diameter, Kühner AG, Birsfelden, Switzerland).

#### 2.5.4.4 Precipitate recovery and dissolution for pilot scale filtration

For the pilot scale candle filter experiments in Section 5.4.4.2, the precipitate was recovered using centrifugation. The precipitate was separated into 4 aliquots of 500 mL and then centrifuged at 4000 rpm and 4°C for 10 minutes (JA-10 rotor, J2-MI centrifuge, Beckman Instruments, High Wycombe, UK). The supernatant was then decanted off and discarded, retaining the pDNA in the precipitate pellets. Approximately 250mL of NaCl solution was next used to dislodge the precipitate pellet from each centrifuge tube using a vortex mixer. This suspension was then decanted, pooled and made up to 2 L in total with NaCl in a 2 L glass bottle, which was then mixed at 300 rpm for 30 minutes in an orbital shaker (ISF-1-W, 25 mm shaking diameter, Kühner AG, Birsfelden, Switzerland).

#### 2.5.4.5 Precipitate removal for pilot scale filtration

For the pilot scale candle filter experiments in Section 5.4.4.2, the remaining precipitate was removed using centrifugation. The partially re-dissolved precipitate was separated into 4 aliquots of 500mL and then centrifuged at 4000 rpm and 4°C for 10 minutes (JA-10 rotor, J2-MI centrifuge, Beckman Instruments, High Wycombe, UK). The supernatant was then decanted off and pooled to give a solid-free pDNA solution.

#### 2.5.4.6 LRA adsorption for pilot scale filtration

1667 mL of the pDNA solution generated in Section 2.5.4.5 was decanted into a 2 L glass bottle and 16.67 g of LRA was added to give a final LRA concentration of 10 g.L<sub>liquid</sub><sup>-1</sup>. The remaining 333 mL of pDNA solution was decanted into a 1 L glass bottle and 16.67 g of LRA was added to give a final LRA concentration of 50 g.L<sub>liquid</sub><sup>-1</sup>. Both LRA suspensions were mixed at 150rpm and 4°C for 2 hours in an orbital shaker (ISF-1-W, 25 mm shaking diameter, Kühner AG, Birsfelden, Switzerland).

#### 2.5.4.7 Pilot scale LRA removal

The pilot scale LRA removal process follows the candle filter method detailed in Section 2.3.5, using Celpure P300 as the pre-coat and a feed flow rate of 2.4 mL.s<sup>-1</sup>.

## 2.6 Analytical methods

### 2.6.1 Lysozyme assay

The lysozyme assay used in Chapter 4 for quantification of protein transmission is based on a previously established method (Mannall *et al.*, 2006; Lee *et al.*, 2002). A 150 mm × 4.6 mm reversed phase column with a particle diameter of 5 µm and a pore size of 300 Å (Jupiter C5, Phenomenex, Macclesfield, UK) was used on a System Gold High Pressure Liquid Chromatography (HPLC) system (126 Pump Unit, 166

Detector unit, 507e Autosampler unit, System GOLD software, Beckman Coulter, High Wycombe, UK). A linear acetonitrile/water gradient with 0.1% trifluoroacetic acid (v/v) 30 to 46% acetonitrile over 12 minutes at a flow rate of 1 mL.min<sup>-1</sup> was used and the sample injection volume was 200 µL. The column was then washed in a 46% to 100% acetonitrile/water gradient over 1 minute followed by a return gradient from 100% to 30% over 1 minute and equilibration at 30% for a further minute. A standard curve was created using lysozyme in water to ensure linear response in the concentration range used (Figure A.2, Appendix A) and the original lysozyme buffers (Section 2.4.1.3) were tested and used as the initial concentration from which to calculate the transmission. Lysozyme had a retention time of  $7.94 \pm 0.35$  min, whilst UV adsorbing species from any residual cell broth or the yeast extract were eluted during the 100% acetonitrile wash step.

### **2.6.2 Isopropanol precipitation**

For sample separation prior to gel electrophoresis (Section 2.6.3), DNA was removed by precipitation with alcohol. Isopropanol was used in preference to ethanol due to its higher precipitation efficiency (Mülhardt, 2007).

Samples of 1 mL were added to 2.2 mL centrifuge tubes (Eppendorf, Hamburg, Germany) at room temperature. Then 0.7 mL of isopropanol was added and mixed with a vortex mixer. The samples were then centrifuged for 10 min at 13000 rpm in a microcentrifuge and decanted carefully without disturbing the pellet. Following this 1 ml of 70% ethanol was added to wash the pDNA pellet, removing the co-precipitated salt and replacing the isopropanol with the more volatile ethanol, making the pDNA easier to redissolve. A further centrifugation step was carried out at 13000 rpm for 15 minutes in the microcentrifuge. After the supernatant was decanted, the washed pellet was then air dried for 10 minutes. Finally the pDNA pellet was redissolved in 50 µl Tris-EDTA buffer (10 mM Tris, 2 mM EDTA, pH 8) containing 100 µg/ml RNaseA and incubated at 37°C for 30 minutes. Samples were frozen at -20°C to be loaded onto gels the following day.

### 2.6.3 DNA agarose gel electrophoresis

5 $\mu$ L from each of the samples prepared as described in Section 2.5.2 were mixed with 5 $\mu$ L of a 0.05% (w/v) bromphenol blue and 0.05% (w/v) xylene cyanole loading buffer. These samples were then loaded onto 0.8% (w/v) agarose gels containing 0.05  $\mu$ g.ml<sup>-1</sup> ethidium bromide and electrophoresed at 40V, 220 mA for 8 h in Tris-borate electrophoresis buffer (9 mM Tris, 9 mM boric acid, 1 mM EDTA). Gels were scanned using UVP 5000 Gel Documentation System and GelBase™ analysis software (Ultra Violet Products Ltd, Cambridge, UK).

## 2.7 Experimental design

### 2.7.1 Factorial design

#### 2.7.1.1 *E.coli* filtration factorial design

The design for the lysozyme transmission experiments for Chapter 4 is based on a half repeat of a five factor, 2-level factorial design using the design generator I=ABCDE. This 2<sup>5-1</sup> experiment allows the investigation of 5 factors and their interactions without aliasing main effects or two factor interactions together. Table 2.1 shows the details of the factorial experiment. Each experimental run is duplicated and the 16 mid-points are separated into 4 separate groups of 4, since Factor E is qualitative and Factor D is fixed at a single value for each microwell plate. The selection of factors and their levels is discussed later in Section 4.2.2.1.

#### 2.7.1.2 Plasmid DNA purification factorial design

The eight factors of the pDNA purification design are incorporated into a quarter repeated 2<sup>8-2</sup> design with the error estimated from the centre points. The generator for this design is I = ABCDG = ABEFH. The coding for each experiment is detailed in Table 2.2. The chosen factors, their levels and the analysis of individual responses at different stages through the process are given in Section 5.2.3.

**Table 2.1.** Summary of the  $2^{5-1}$  factorial experiment design coding for the lysozyme transmission experiments in Chapter 4. Coding shows whether the particular factor was set at the high (1), low (-1) or centre point (0) of the experimental range. Factors and their chosen values are detailed in Section 4.2.2.1. Plate position refers to the row (A-D) and column (1-6) of the well used in each of two separate pairs of custom filter plates (subscripts 1-2) and shows the randomization of experimental runs across the plates.

Experimental Run	Plate Position	Factorial Coding				
		Factor A	Factor B	Factor C	Factor D	Factor E
1	A5 <sub>1</sub> , C2 <sub>1</sub>	-1	-1	-1	-1	+1
2	B1 <sub>1</sub> , C6 <sub>1</sub>	+1	-1	-1	-1	-1
3	A3 <sub>1</sub> , C4 <sub>1</sub>	-1	+1	-1	-1	-1
4	B2 <sub>1</sub> , D5 <sub>1</sub>	+1	+1	-1	-1	+1
5	B6 <sub>1</sub> , D3 <sub>1</sub>	-1	-1	+1	-1	-1
6	A1 <sub>1</sub> , D4 <sub>1</sub>	+1	-1	+1	-1	+1
7	A6 <sub>1</sub> , D2 <sub>1</sub>	-1	+1	+1	-1	+1
8	B3 <sub>1</sub> , C5 <sub>1</sub>	+1	+1	+1	-1	-1
9	A6 <sub>2</sub> , C4 <sub>2</sub>	-1	-1	-1	+1	-1
10	A4 <sub>2</sub> , D1 <sub>2</sub>	+1	-1	-1	+1	+1
11	B2 <sub>2</sub> , D5 <sub>2</sub>	-1	+1	-1	+1	+1
12	B4 <sub>2</sub> , C6 <sub>2</sub>	+1	+1	-1	+1	-1
13	A1 <sub>2</sub> , D3 <sub>2</sub>	-1	-1	+1	+1	+1
14	B5 <sub>2</sub> , C2 <sub>2</sub>	+1	-1	+1	+1	-1
15	A3 <sub>2</sub> , D6 <sub>2</sub>	-1	+1	+1	+1	-1
16	B1 <sub>2</sub> , C5 <sub>2</sub>	+1	+1	+1	+1	+1
Midpoints M <sub>1</sub> -M <sub>4</sub>	A2 <sub>1</sub> , A4 <sub>1</sub> , D1 <sub>1</sub> , D6 <sub>1</sub>	0	0	0	-1	-1
Midpoints M <sub>5</sub> -M <sub>8</sub>	B4 <sub>1</sub> , B5 <sub>1</sub> , C1 <sub>1</sub> , C3 <sub>1</sub>	0	0	0	-1	+1
Midpoints M <sub>9</sub> -M <sub>12</sub>	B6 <sub>2</sub> , C1 <sub>2</sub> , C3 <sub>2</sub> , D2 <sub>2</sub>	0	0	0	+1	-1
Midpoints M <sub>13</sub> -M <sub>16</sub>	A2 <sub>2</sub> , A5 <sub>2</sub> , B4 <sub>2</sub> , D4 <sub>2</sub>	0	0	0	+1	+1

**Table 2.2.** Summary of the  $2^{8-2}$  factorial experiment design coding for the plasmid purification experiments in Chapter 5 Coding shows whether the particular factor was set at the high (+1), low (-1) or centre-point (0) of the experimental range. Factors and chosen values are detailed in Section 5.2.3.

Experimental Run	Factor A	Factor B	Factor C	Factor D	Factor E	Factor F	Factor G	Factor H
1	+1	+1	+1	+1	+1	+1	+1	+1
2	-1	+1	+1	+1	+1	+1	-1	-1
3	+1	-1	+1	+1	+1	+1	-1	-1
4	-1	-1	+1	+1	+1	+1	+1	+1
5	+1	+1	-1	+1	+1	+1	-1	+1
6	-1	+1	-1	+1	+1	+1	+1	-1
7	+1	-1	-1	+1	+1	+1	+1	-1
8	-1	-1	-1	+1	+1	+1	-1	+1
9	+1	+1	+1	-1	+1	+1	-1	+1
10	-1	+1	+1	-1	+1	+1	+1	-1
11	+1	-1	+1	-1	+1	+1	+1	-1
12	-1	-1	+1	-1	+1	+1	-1	+1
13	+1	+1	-1	-1	+1	+1	+1	+1
14	-1	+1	-1	-1	+1	+1	-1	-1
15	+1	-1	-1	-1	+1	+1	-1	-1
16	-1	-1	-1	-1	+1	+1	+1	+1
17	+1	+1	+1	+1	-1	+1	+1	-1
18	-1	+1	+1	+1	-1	+1	-1	+1
19	+1	-1	+1	+1	-1	+1	-1	+1
20	-1	-1	+1	+1	-1	+1	+1	-1
21	+1	+1	-1	+1	-1	+1	-1	-1
22	-1	+1	-1	+1	-1	+1	+1	+1
23	+1	-1	-1	+1	-1	+1	+1	+1
24	-1	-1	-1	+1	-1	+1	-1	-1
25	+1	+1	+1	-1	-1	+1	-1	-1
26	-1	+1	+1	-1	-1	+1	+1	+1
27	+1	-1	+1	-1	-1	+1	+1	+1
28	-1	-1	+1	-1	-1	+1	-1	-1
29	+1	+1	-1	-1	-1	+1	+1	-1
30	-1	+1	-1	-1	-1	+1	-1	+1
31	+1	-1	-1	-1	-1	+1	-1	+1
32	-1	-1	-1	-1	-1	+1	+1	-1
33	+1	+1	+1	+1	+1	-1	+1	-1
34	-1	+1	+1	+1	+1	-1	-1	+1
35	+1	-1	+1	+1	+1	-1	-1	+1
36	-1	-1	+1	+1	+1	-1	+1	-1
37	+1	+1	-1	+1	+1	-1	-1	-1
38	-1	+1	-1	+1	+1	-1	+1	+1
39	+1	-1	-1	+1	+1	-1	+1	+1
40	-1	-1	-1	+1	+1	-1	-1	-1
41	+1	+1	+1	-1	+1	-1	-1	-1
42	-1	+1	+1	-1	+1	-1	+1	+1
43	+1	-1	+1	-1	+1	-1	+1	+1
44	-1	-1	+1	-1	+1	-1	-1	-1
45	+1	+1	-1	-1	+1	-1	+1	-1
46	-1	+1	-1	-1	+1	-1	-1	+1
47	+1	-1	-1	-1	+1	-1	-1	+1
48	-1	-1	-1	-1	+1	-1	+1	-1
49	+1	+1	+1	+1	-1	-1	+1	+1
50	-1	+1	+1	+1	-1	-1	-1	-1
51	+1	-1	+1	+1	-1	-1	-1	-1
52	-1	-1	+1	+1	-1	-1	+1	+1
53	+1	+1	-1	+1	-1	-1	-1	+1
54	-1	+1	-1	+1	-1	-1	+1	-1
55	+1	-1	-1	+1	-1	-1	+1	-1
56	-1	-1	-1	+1	-1	-1	-1	+1
57	+1	+1	+1	-1	-1	-1	-1	+1
58	-1	+1	+1	-1	-1	-1	+1	-1
59	+1	-1	+1	-1	-1	-1	+1	-1
60	-1	-1	+1	-1	-1	-1	-1	+1
61	+1	+1	-1	-1	-1	-1	+1	+1
62	-1	+1	-1	-1	-1	-1	-1	-1
63	+1	-1	-1	-1	-1	-1	-1	-1
64	-1	-1	-1	-1	-1	-1	+1	+1
Midpoints (65-72)	0	0	0	0	0	0	0	0

### 2.7.2 Response surfaces

The response surfaces generated in Chapter 4 were based on an inscribed central composite design with the modifications outlined below. This type of design allows for very good predictive power, but reduces the quality of the information at the corners of the response surface. Traditional designs would have 8 centre points to give both a rotatable design and greater average information function (inverse of the design variance). However existing data has been generated at the factorial points, especially the centre, which suggests that the optimum is within the design space, but not at the centre. Therefore only 4 centre point replicates were used and the design augmented with face-centred design points (Figure 2.6). The response surface repeats many of the factorial design points, but since significant error was seen in the use of *E.coli* broths from different preparations, the two experiments were run stand-alone.

The adjustments do not significantly affect the rotatability of the design as seen in Figure 2.7. There is some variation in the information function (inverse of the design variance) depending on the direction travelled from the centre point, but not dramatically. A plot of design variance,  $\text{Var}(\hat{y})$ , was generated using Design Expert (Version 7, Stat-Ease, MN, USA) and then the ranges were converted into the information function manually.

## 2.8 Data analysis

### 2.8.1 General error estimation

The error estimated in all replicated experiments during this thesis is plus or minus one standard deviation as calculated by Microsoft Excel software (Microsoft Corporation, USA) using the following equation:

$$\sigma = \sqrt{\frac{\sum_{i=1}^n (x_i - \bar{x})^2}{n-1}} \quad (2.1)$$

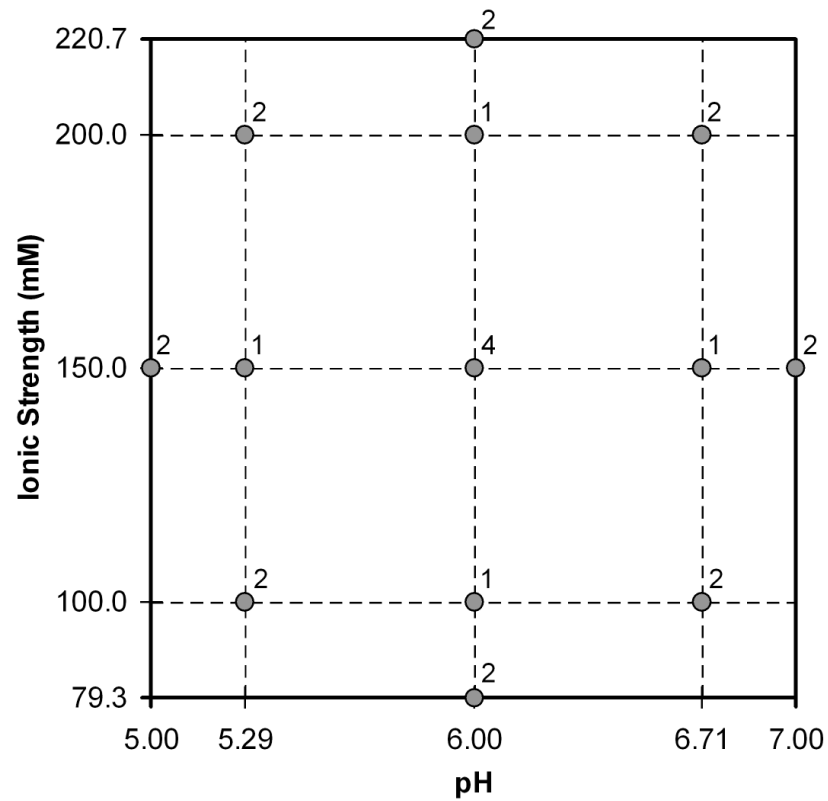


**Figure 2.6.** Details of the levels of pH and ionic strength used to generate the response surfaces described in Section 4.4. The design is an inscribed central composite design augmented with face centred points. The values next to each point represent the number of replicates carried out at that particular combination of pH and ionic strength.

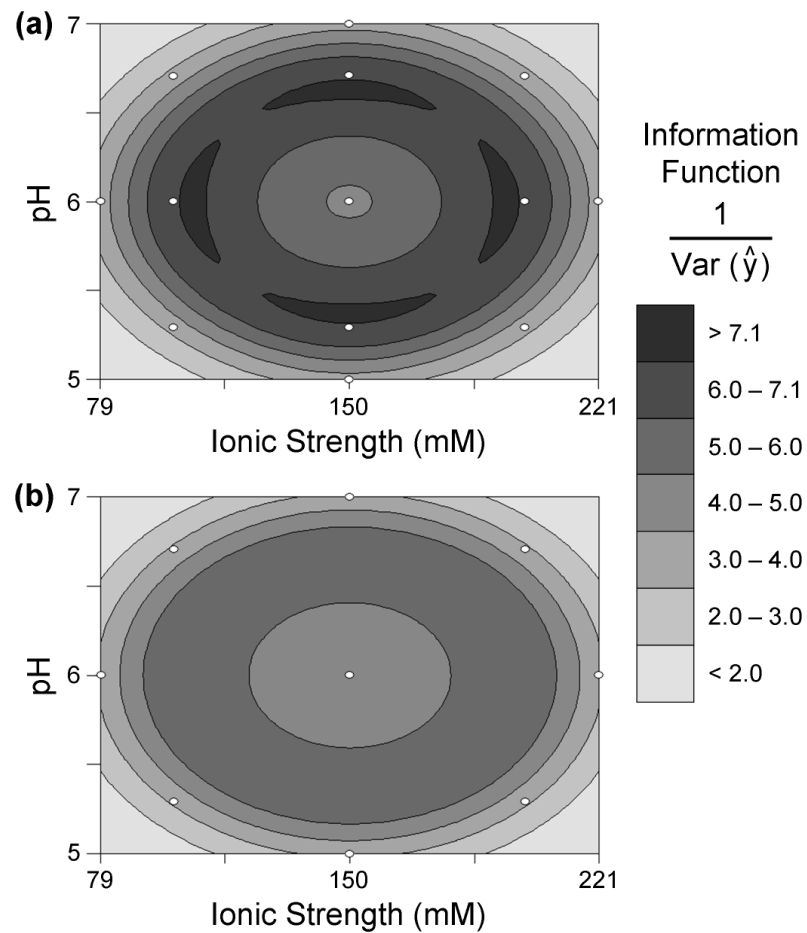


**Figure 2.7.** Effect of the face centre points on the rotatability of the response surface design. The contour plots show the variation of the information function (the inverse of the design variance): (a) with the face-centred points (b) without the face-centred points. Variance calculated as described in Section 2.7.2.

where  $x_i$  is the  $i^{\text{th}}$  of  $n$  sample measurements with a mean of  $\bar{x}$  and a sample standard deviation of  $\sigma$ .

### 2.8.2 Comparison of means

When comparing mean values to determine if there is a statistically significant chance two measurements are different, a two tailed, unequal variance t-test was used as calculated by Microsoft Excel software (Microsoft Corporation, USA). This tests the null hypothesis that the means are equal, assuming that they are both normally distributed. Although the higher mean may be clear from the data, no prediction of this could be made prior to data collection and therefore the two-tailed test is used. This makes the test more stringent for disproving the null hypothesis.

### 2.8.3 Lines of best fit

Linear mathematical relationships to describe the trends observed in the experimental data were determined by linear least squares regression using Microsoft Excel software (Microsoft Corporation, USA). A corresponding coefficient of determination ( $R^2$  value) is calculated based of the following equation:

$$R^2 = \frac{\left[ \sum_{i=1}^n (x_i - \bar{x})(y_i - \bar{y}) \right]^2}{\sum_{i=1}^n (x_i - \bar{x})^2 \sum_{i=1}^n (y_i - \bar{y})^2} \quad (2.2)$$

where  $x_i$  is the  $i^{\text{th}}$  of  $n$  selected independent variable levels yielding a dependent variable measurement of  $y_i$  and  $\bar{x}$  and  $\bar{y}$  are the respective averages of the independent and dependant variables. This is equivalent to the following expressions:

$$R^2 = 1 - \frac{SSR_{err}}{SSR_{tot}}$$

$$R^2 = 1 - \frac{\sum (y_i - f_i)^2}{\sum (y_i - \bar{y})^2} \quad (2.3)$$

where  $SS_{err}$  is the sum of squares of the residuals,  $SS_{tot}$  is the total sum of squares, and  $f_i$  is the predicted model for the dependent variable. These expressions show how the coefficient of determination is often interpreted as the proportion of variation that can be described by the model.

## 2.8.4 Factorial experiments

### 2.8.4.1 Estimation of main effects and interactions

In order to estimate the main effects and interactions an analysis matrix,  $X_A$ , is generated from the design coding (e.g. Table 2.1). The analysis matrix has columns  $2^{k-p}$  rows high, where  $k$  is the number of factor,  $p$  denotes the size of the fractional repeat  $\left(\frac{1}{2^p}\right)$  and  $2^{k-p}$  is the number of individual factorial runs carried out (excludes centre-points). The first column is used for calculating the mean and is therefore all populated with +1 values. Each subsequent column contains +1/-1 coding for either a main effect or an interaction. The following equation can then be used to generate effects matrix,  $E$ , containing the mean ( $E_I$ ), main effects (e.g.  $E_A$ ) and interactions (e.g.  $E_{AB}$ ) for two different responses:

$$E = \frac{1}{2^{k-p-1}} YX_A \quad (2.4)$$

$$E = \begin{bmatrix} E_{I1} & E_{A1} & \cdots & E_{AB1} & \cdots \\ E_{I2} & E_{A2} & \cdots & E_{AB2} & \cdots \end{bmatrix}$$

$$X_A = \begin{matrix} & I & A & B & \cdots & AB & \cdots \\ \begin{bmatrix} +1 & -1 & -1 & \cdots & +1 & \cdots \\ +1 & +1 & -1 & \cdots & -1 & \cdots \\ +1 & -1 & +1 & \cdots & -1 & \cdots \\ +1 & +1 & +1 & \cdots & +1 & \cdots \\ \cdots & \cdots & \cdots & \cdots & \cdots & \cdots \\ +1 & +1 & +1 & \cdots & +1 & \cdots \end{bmatrix} \end{matrix}$$

$$Y = \begin{bmatrix} y_{11} & y_{12} & \cdots & y_{1n} \\ y_{21} & y_{22} & \cdots & y_{2n} \end{bmatrix}$$

where  $Y$  is the response matrix with  $y_{mn}$  being the value of the  $m^{\text{th}}$  response measured for the  $n^{\text{th}}$  factorial run. More responses can be added by extending the number of rows in  $E$  and  $Y$ , but the specific case of two responses is shown here since this is the maximum number of responses calculated during this thesis for a given number of experimental runs.

#### 2.8.4.2 Error estimation for replicated factorial experiments

For replicated factorial experiments, the error estimate for factorial experiments is based on a t-test comparing the means of two halves of the experimental data.

If each of  $2^{k-p}$  factorial runs is replicated  $r$  times then  $s^2$  is an unbiased estimate of the variance for the individual runs with  $\nu = r - 1$  degrees of freedom:

$$s^2 = \frac{1}{r-1} \sum_{i=1}^r (y_i - \bar{y})^2 \quad (2.5)$$

where  $y_i$  is the individual response replicate and  $\bar{y}$  is the mean response for that factorial run. Since all these estimates have the same degrees of freedom then they can be pooled together to provide a single estimate of the variance for any individual replicate,  $s_r^2$ :

$$s_r^2 = \frac{1}{2^{k-p}} \sum_{i=1}^{2^{k-p}} s_i^2 \quad (2.6)$$

The effects and interactions are simply the difference between the averages of two halves of the data (as defined by the +1/-1 coding of the design matrix) with  $2^{k-p-1} \cdot r$  experimental observations each. The variance of each half is the replicate variance divided by the number of experimental observations in that half. The standard error

of the effect or interaction,  $s_{eff}$ , can therefore be evaluated from the sum of the variances of these two halves of data since the degrees of freedom match:

$$s_{eff} = \frac{s_r}{\sqrt{2^{k-p-2} \cdot r}} \quad (2.7)$$

The standard error,  $s_{eff}$ , is used to calculate a 95% confidence interval,  $CI_{95\%}$ , for all the effects and interactions is calculated as follows:

$$CI_{95\%} = s_{eff} t_{v, \alpha=0.05} \quad (2.8)$$

where  $t_{v, \alpha=0.05}$  is the student's t-test statistic with  $v = 2^{k-p}(r - 1)$  degrees of freedom for a significance level,  $\alpha$ , of 0.05. If a main effect or interaction is greater than this confidence interval then it is statistically significant.

For the factorial experiments in Chapter 4, where two different methods were used to calculate the volume permeated in a given time (increase in cuvette volume and decrease in filter insert volume) there were four different specific cake resistances generated for a given duplicate run. However the results for the two different measurement techniques must first be averaged before being treated as above, otherwise the degrees of freedom would be over-estimated. Hence the degrees of freedom are the same as for any other duplicated factorial experiment analysis.

The approach outlined in this section does not take into account any error introduced by the fit to the centre points. In this thesis there is no model or response surface generated by the initial screening analysis and therefore the fit to a linear model is not considered. The statistical test is only being used to compare the factors (or interactions thereof) at their extremes in order to determine if there is an effect of changing them by the specified ranges.

### 2.8.4.3 Error estimation for non-replicated factorial experiments

Equations 2.7 and 2.8 are used to determine a confidence interval, as with the replicated factorial design, but the replicate variance and degrees of freedom are determined from the replicated centre-points. The following is an unbiased estimator of the variance from  $c$  centre-points with  $\nu = c - 1$  degrees of freedom:

$$s_c^2 = \frac{1}{c-1} \sum_{i=1}^c (y_i - \bar{y})^2 \quad (2.9)$$

where  $y_i$  is the individual centre point replicate and  $\bar{y}$  is the mean of the centre points. The above variance is used as an estimate of replicate variance,  $s_r^2$ , and used to calculate the standard error for the factorial analysis,  $s_{eff}$ , using Equation 2.7. This is then used in Equation 2.8 with  $\nu = c - 1$  degrees of freedom to determine the confidence interval.

## 2.8.5 Response surfaces

Responses of cake resistance and lysozyme transmission were generated at various values of ionic strength and pH as described in Section 4.4. The responses were modelled using both linear and quadratic models calculated using multiple linear regression with least squares fit. The linear and quadratic models were then compared for fit in order to determine the most appropriate model (Section 2.8.5.1).

Ionic strength (I) and pH are used in the following linear equation to model a given response (y):

$$y = b_0 + b_1 pH + b_2 I + b_{12} pH.I \quad (2.10)$$

where  $b_0 - b_3$  are the constant regression coefficients. The regression is performed on  $n$  different data points using the following equation and matrices to yield a vector of all the regression coefficients:

$$b = (X'X)^{-1} X'y \quad (2.11)$$

$$b = \begin{bmatrix} b_0 \\ b_1 \\ b_2 \\ b_{12} \end{bmatrix}$$

$$X = \begin{bmatrix} 1 & pH_1 & I_1 & pH_1 I_1 \\ 1 & pH_2 & \dots & \dots \\ \dots & \dots & \dots & \dots \\ 1 & pH_n & I_n & pH_n I_n \end{bmatrix}$$

$$y = \begin{bmatrix} y_1 \\ y_2 \\ \dots \\ y_n \end{bmatrix}$$

where  $y_n$  is the response from the  $n^{\text{th}}$  experiment carried out with buffer conditions of  $pH_n$  and  $I_n$ . The quadratic model is defined as follows:

$$y = b_0 + b_1 pH + b_2 I + b_{12} pH.I + b_{11} pH^2 + b_{22} I^2 \quad (2.12)$$

Equation 2.11 is again used for the linear regression with the following vectors and matrix:

$$b = \begin{bmatrix} b_0 \\ b_1 \\ b_2 \\ b_{12} \\ b_{11} \\ b_{22} \end{bmatrix}$$

$$X = \begin{bmatrix} 1 & pH_1 & I_1 & pH_1 I_1 & pH_1^2 & I_1^2 \\ 1 & pH_2 & I_2 & \dots & \dots & \dots \\ 1 & pH_3 & \dots & \dots & \dots & \dots \\ \dots & \dots & \dots & \dots & \dots & \dots \\ \dots & \dots & \dots & \dots & \dots & \dots \\ 1 & pH_n & I_n & pH_n I_n & pH_n^2 & I_n^2 \end{bmatrix}$$

### 2.8.5.1 Response surface error estimation

Error for the response surface is represented by a coefficient of determination ( $R^2$  value) that is adjusted to account for the use of two variables to predict the response, which reduces the degrees of freedom. The following equation is used:

$$R_{adj}^2 = 1 - \frac{SS_{err} df_{tot}}{SS_{tot} df_{err}}$$

$$R_{adj}^2 = 1 - (1 - R^2) \frac{n-1}{n-p-1} \quad (2.13)$$

where  $df_{err}$  are the degrees of freedom for estimating the error,  $df_{tot}$  are the total degrees of freedom,  $n$  is the data point sample number and  $p_m$  is the number of predictors in the model (not including the constant, so 5 for the quadratic models used in the response surfaces). Equation 2.3 is used to calculate the unadjusted  $R^2$  value to insert into Equation 2.13.

### 2.8.6 Clarification

The clarification of lysate is determined by the following equation using optical density (OD) measurements:

$$\% \text{ clarification} = \frac{OD_F - OD_P}{OD_F - OD_B} \times 100 \quad (2.14)$$

Where  $OD_F$  is the optical density of the feed,  $OD_P$  is the optical density of the permeate after filtration clarification, and  $OD_B$  is the optical density of the blank (flow through buffer described in Section 2.5.2.2). All OD values were measured at 600 nm wavelength and in a Sapphire II microplate reader (Tecan, Männedorf, Switzerland). An estimate for the OD of the lysate feeds was attempted from serial dilutions of the lysate in the blank buffer. Significant error was seen due to variation in the amount of flocs carried over in each serial dilution. The final value used for all calculations was fixed as the OD of the high neutralisation stirrer speed (finest flocs) to the nearest OD unit: 50. This is not an accurate estimation and trends of different factors are more important than absolute values.

### 2.8.7 Calculating flux

Flux,  $J$ , is defined as the flowrate,  $Q$ , per unit area,  $A$ :

$$J = \frac{Q}{A} = \frac{1}{A} \cdot \frac{dV}{dt} \quad (2.15)$$

where  $V$  is the permeate volume and  $t$  is the filtration time. Using SI units ( $Q$  [=]  $\text{m}^3 \cdot \text{s}^{-1}$ ,  $V$  [=]  $\text{m}^3$ ,  $t$  [=]  $\text{s}$ ,  $A$  [=]  $\text{m}^2$ ), flux has units of  $\text{m} \cdot \text{s}^{-1}$  and can be considered as a superficial velocity. Commonly in the literature fluxes are calculated from a mixture of units ( $Q$  [=]  $\text{L} \cdot \text{h}^{-1}$ ,  $V$  [=]  $\text{L}$ ,  $t$  [=]  $\text{h}$ ,  $A$  [=]  $\text{m}^2$ ) leading to values of flux in  $\text{L} \cdot \text{m}^{-2} \cdot \text{h}^{-1}$ . This has the advantage that typical fluxes are  $\gg 1 \text{ L} \cdot \text{m}^{-2} \cdot \text{h}^{-1}$ , as opposed to  $\ll 1 \text{ m} \cdot \text{s}^{-1}$ . In this thesis fluxes in SI units are used for calculations, but all quoted fluxes are converted into  $\text{L} \cdot \text{m}^{-2} \cdot \text{h}^{-1}$  by multiplying by  $3.6 \times 10^6 \text{ L} \cdot \text{s} \cdot \text{m}^{-3} \cdot \text{h}^{-1}$ .

Many methods can be employed to evaluate  $\frac{dV}{dt}$ . For this thesis  $\frac{dV}{dt}$  at time  $t$  is evaluated as the linear slope of the volume and time data in the range  $t \pm \Delta t$ , where  $\Delta t$  is up to 10 seconds and is selected based on the rate of change in flux and general variability of the data. The slope is a simple and good approximation of the gradient where the flux decay rate during the time interval  $t \pm \Delta t$  is low. For constant flow tests this data is then smoothed by averaging flux data over a time period of up to 15

seconds, selected to be greater than the period of the peristaltic pump and therefore smooth out the fluctuations.

### 2.8.8 Smoothing pressure data

During constant flow tests in this thesis the pressure fluctuates due to the peristaltic pumps used. In order to smooth this pressure data, the pressure is averaged over a time period of up to 15 seconds, selected to be greater than the period of the pump and therefore reduce fluctuations in pressure and reveal the true trend.

During all calculations, SI units of pressure ( $\text{N}\cdot\text{m}^{-2}$  or Pa) are used. When the data is reported in text or graphs, units of kilopascals (kPa) are used to reduce the number to a manageable number of digits.

### 2.8.9 Viscosity

#### 2.8.9.1 Water viscosity correlation

All water viscosities are calculated as follows, according to the following correlation which has < 1% error in the range 0 – 100°C (Gray, 1972):

$$\mu_T = \mu_{20} \times 10^{\frac{1.37023 \times (20-T) - 0.000836 \times (20-T)^2}{109+T}} \quad (2.16)$$

where  $\mu_T$  is the dynamic viscosity of water ( $\text{N}\cdot\text{s}\cdot\text{m}^{-2}$ ) at temperature  $T$  (°C). Water fluxes can then be normalised (as in Section 3.3.2) to 25°C as follows:

$$J_{25} = J_T \frac{\mu_T}{\mu_{25}} \quad (2.17)$$

### 2.8.9.2 Permeate viscosity

The viscosities of permeates do not have literature correlations and are difficult to measure accurately, especially during high throughput experimentation. They are approximated to that of water for the purposes of cake resistance calculations. A fixed value of  $0.001 \text{ N}\cdot\text{s}\cdot\text{m}^{-2}$  is used for all permeate viscosities, rounding up the value of water viscosity at typical laboratory temperatures ( $22 \pm 2^\circ\text{C}$ ) to one significant figure since the soluble components will, if anything, act to raise the viscosity of water. Since the correlation in Section 2.8.9.1 can only be asserted as valid for pure water, no temperature correction is applied to permeate viscosity. This will lead to slight inaccuracies in the absolute values of specific cake resistances, but the comparative differences and measures of precision will remain relatively accurate.

### 2.8.10 Density

For all solutions the permeate density is assumed to be  $1.00 \text{ g}\cdot\text{mL}^{-1}$ . This overestimates the literature values for the density of water by less than 1% in the range  $0.0$  to  $45.2^\circ\text{C}$  (Perry and Green, 1997). For scale-up calculations any inaccuracies in the assumed density are eliminated since permeate volume is quantified by mass at all scales.

### 2.8.11 Filtration scale-up predictions

To scale up and account for pressure variations between scales or for using constant pressure derived data to predict constant flow experiments, an adaptation of the cake filtration constant from established cake filtration theory (Equation 1.18) is required. By eliminating the terms for pressure and area the modified cake filtration constant,  $K_c'$  ( $\text{N}\cdot\text{s}\cdot\text{m}^{-4}$ ), is generated:

$$K_c' = K_c A^2 \Delta P = \mu \alpha \rho_0 \quad (2.18)$$

where  $\mu$  is the dynamic permeate viscosity ( $\text{N}\cdot\text{s}\cdot\text{m}^{-2}$ ),  $\alpha$  is the specific cake resistance per dry cake mass ( $\text{m}\cdot\text{kg}^{-1}$ ), and  $\rho_0$  is the dry mass of cake solids per unit volume of

permeate ( $\text{kg}\cdot\text{m}^{-3}$ ). To evaluate  $K_c'$  from constant pressure data the cake resistance fouling model is used as described in Section 1.3.4.1.4. Combining Equations 1.18, 1.20 and 2.18 and then rearranging to include flux in the expression yields:

$$\frac{At}{V} = \frac{K_c'V}{2A\Delta P} + \frac{1}{J_0} \quad (2.19)$$

where  $t$  is the measurement time (s),  $V$  is the collected permeate volume ( $\text{m}^3$ ),  $A$  is the effective filtration area ( $\text{m}^2$ ),  $\Delta P$  is the pressure drop across the filter ( $\text{N}\cdot\text{m}^{-2}$ ), and  $J_0$  is the the initial flux ( $\text{m}\cdot\text{s}^{-1}$ ). Equation 2.19 shows that a plot of  $\frac{At}{V}$  vs  $\frac{V}{2A\Delta P}$  yields a linearised plot of the data where the gradient is equal to the modified cake filtration constant.

#### 2.8.11.1 Predicting flux in constant pressure filtration

For constant pressure experiments the modified cake filtration constant,  $K_c'$ , is used for scale up since it is theoretically independent of scale where filter format does not restrict the formation of the cake layer. The main assumption in the scale-up prediction is that the cake is not significantly compressible between the pressure of the larger scale filtration run and the pressure at which  $K_c'$  is evaluated during smaller scale studies. Larger scale flux,  $J$  ( $\text{m}\cdot\text{s}^{-1}$ ), is predicted using the following equation, as modified from the  $\frac{Q}{Q_0} = f(t)$  expression in Table 1.5:

$$J = J_0 \left( 1 + \frac{2K_c'J_0^2t}{\Delta P} \right)^{-\frac{1}{2}} \quad (2.20)$$

which gives the predicted flux at any chosen time for a specified  $\Delta P$ . SI units are used throughout the calculations for simplicity and then the flux is converted to  $\text{L}\cdot\text{m}^{-2}\cdot\text{h}^{-1}$  as described in Section 2.8.7. For experiments in Chapter 3, where predictions are made up to completion of the larger scale filtration run, the time ( $t_{final}$ ) to process that volume ( $V_{final}$ ) is predicted by rearranging Equation 2.19:

$$t_{final} = \frac{V_{final}}{A} \left( \frac{K_c' V_{final}}{2A\Delta P} + \frac{1}{J_0} \right) \quad (2.21)$$

### 2.8.11.2 Predicting pressure in constant flow filtration

To predict the increase in pressure drop across the filter during constant flow filtration the following base equation is used, modified from Equation 1.23 in Section 1.3.4.1.5 to incorporate the modified cake resistance constant and change flowrate for flux:

$$\Delta P = \Delta P_0 + K_c' J^2 t \quad (2.22)$$

where  $\Delta P_0$  is the initial pressure at the start of filtration ( $\text{N}\cdot\text{m}^{-2}$ ). Predictions are made on the assumption that there is plug-flow in the filter device and therefore the pre-coat and feed solutions are filtered one after the other with the resistances additive. Therefore the final pressure when the total volume of pre-coat,  $V_{precoat}$  ( $\text{m}^3$ ) has been filtered becomes  $\Delta P_0$  for the feed solution. It is assumed that the original resistance provided by the wire mesh and cloth supports is negligible.

$$\Delta P = K_c'_{precoat} \frac{JV_{precoat}}{A} + K_c'_{feed} J^2 t \quad (2.23)$$

In reality there will be mixing in the pump, tubing and filter housing which will lead to a curved transition between the pre-coat and feed solution slopes. This has not been accounted for in these simple scale-up predictions. It is also assumed that there is no variation in cake resistance within the pressure range. The validity of this assumption is raised in Chapter 5 during discussion of the scale-up data. This allows data determined at constant pressure to be used. The method outlined in Section 3.3.1 is adapted to calculate  $K_c'$  for a pre-deposited filter cake as detailed in Section 5.2.2.

In order to determine the data for the pre-coat an experiment was carried out to determine the water flux through a fully deposited pre-coat layer.

$$K_c'_{precoat} = (\mu\alpha\rho_0)_{precoat} = \frac{\Delta P}{J\left(\frac{V}{A}\right)_{precoat}} \quad (2.24)$$

A value of  $2.5 \times 10^8 \text{ N.s.m}^{-4}$  was determined for Celpure P300 tested at a variety of fluxes. When scaling from the RVLf scale-down device to the pilot scale candle filter the modified cake resistance constant from the RVLf is determined from the pressure and time data using Equation 2.20.

It is assumed that there is a maximum allowable pump pressure (150 kPa) during constant flow operation, beyond which the flow is reduced to maintain constant pressure (at 150 kPa). The time at which this maximum pressure is reached was calculated from Equation 2.23, thereafter Equation 2.20 was used to predict the decline in flux.

### 2.8.12 Protein transmission

The observed protein transmission,  $T_p$ , is calculated using the following equation:

$$T_p = \frac{c_p}{c_b} \quad (2.25)$$

where  $c_p$  is the protein concentration of the filtrate ( $\text{g.L}^{-1}$ ) and  $c_b$  is the initial bulk feed protein concentration ( $\text{g.L}^{-1}$ ). All samples are taken from the pooled filtrate and are therefore the overall transmission at the time the sample is taken. All transmission values are converted from fractions to percentages for data presentation by multiplying by 100.

## **3.0 Design and evaluation of an automated microscale microfiltration technique\***

### **3.1 Aim of the chapter**

The aim of this chapter is to develop an automation friendly technique for the rapid and parallel quantification of permeate flux during microfiltration operations at the microscale. The specific objectives are as follows:

- To establish an automated technique that can rapidly quantify key process parameters, such as permeate flux, which are capable of describing filtration performance and are of specific use for scale-up.
- To calculate water fluxes and clean membrane resistances in addition to determination of the flux behaviour of more complex biological suspensions. These measurements need to differentiate between feed samples in parallel and quantify filtration performance differences due to process changes.
- To quantify the precision and accuracy of the automated technique and demonstrate that these are at least equivalent to laboratory scale approaches.

### **3.2 Custom filter plate design and microscale operation**

Conventional approaches to laboratory scale microfiltration use an applied “positive pressure” (i.e. greater than atmospheric pressure, achieved by the application compressed air or nitrogen delivered to the feed side of the membrane) to enable the continuous collection of data on the volume/mass of permeate over time. This is the

---

\* Part of the work presented in this chapter has been published as: N.B. Jackson, J.M. Liddell, G.J. Lye (2006) An automated microscale technique for the quantitative and parallel analysis of microfiltration operations, *J. Membr. Sci.* 276, 31-41.

advantage of the microwell filtration technique first described by Chandler and Zydney (2004), who used a manifold designed to seal around and pressurise each well of a conventional filter plate from above. It also enables larger pressure differences to be obtained (Vandezande *et al.*, 2005). For high throughput operation, however, such an approach is currently difficult to implement in an automation friendly and cost-effective manner. Consequently, the approach adopted here involves the use of a microplate vacuum filtration manifold already widely used for solid phase extraction steps in high throughput screening applications (Harrison and Walker, 1998). While such devices are readily integrated into the operation of any liquid handling robot, filtration occurs under an applied “negative pressure” (i.e. a vacuum is generated on the permeate side of the membrane leading to a pressure below atmospheric). The initial steps taken in this work to allow flux measurement and improve the accuracy of data collection have been described in Section 2.3.2. In order to enable quantitative measurements on the filtration performance of complex biological suspensions, two microwell filter plates need to be run in parallel on the automation platform, providing two different data points of time and volume. The treatment of this data to yield useful parameters describing filtration performance is presented in Sections 3.3 and 3.4.

### 3.2.1 Custom microwell filter plate design

To reduce measurement errors associated with the use of standard small volume (300  $\mu\text{L}$  maximum) Multiscreen filter plates, a prototype 8-well microwell filter plate was initially designed during this work. The filter block is based on a standard microwell plate footprint, as shown in Figure 3.1(b), containing holes for removable membrane inserts. The inserts used here were taken from Ultrafree-CL centrifugal filters as shown in Figure 3.1(a). The choice of membranes available in each of Millipore’s Multiscreen, Ultrafree-CL and disc formats restricted comparative work to their Durapore membrane and a 0.22  $\mu\text{m}$  rating was selected as it lies within the range of pore sizes used in similar studies (30 kDa, Okamoto *et al.*, 2001; 0.45  $\mu\text{m}$ , Nakanishi *et al.* 1987). Silicone rubber o-rings are used to seal the filter inserts once a vacuum is applied. A collection block, similar to that shown in Figure 2.1(a), located in the base of the VacS manifold holds removable tubes for collecting the permeate

from each individual insert. This custom filter plate design is able to accommodate a variety of membrane types on a single plate and also enables both permeate and retentate masses to be measured independently neither of which is possible with existing filter plate designs. The ability to measure permeate and retentate masses independently for each well also makes it possible to mass balance each microfiltration process in order to verify there has been no cross contamination or notable measurement errors.

Further design improvements were made after initial proof of concept studies and a full 24-well custom filter plate was constructed (Figure 3.1(c)), increasing experimental throughput by three-fold compared to the previous design. A ledge to tightly hold the silicone o-ring for each individual well is countersunk into the top of the plate and a 2mm high edge is added to the base, giving a smaller area of contact with the rubber seal of the manifold and improving plate sealing. In addition the inserts were modified so that they could be taken apart and allow any membrane or filter that could be cut to size to be used. This removes the constraints of using only Millipore membranes, allowing the direct comparison of membranes from different manufacturers (Chapter 4) and the use of a wire mesh filter and filter aids (Chapter 5).

For the custom filter plate, as with the commercial Multiscreen filter plate (Section 2.3.2), all stages of the microwell filtration processes have been automated apart from the weighing of the removable collection tube and filter inserts. Many automation solutions for this are already available, however they were not explored during this study. For example, the Tecan RoMa arm is capable of picking up the filter inserts and removable collection tubes and could weigh them on a balance connected to the system if higher throughput operation were required.

### **3.2.2 Verification of microscale performance**

For verification of microscale data, comparable experiments were carried out using a small laboratory scale membrane cell (described in Section 2.3.3). In order to elucidate the differences of applying a positive pressure or negative pressure to drive the filtration process, the same TecanVacS vacuum pump was also used for the

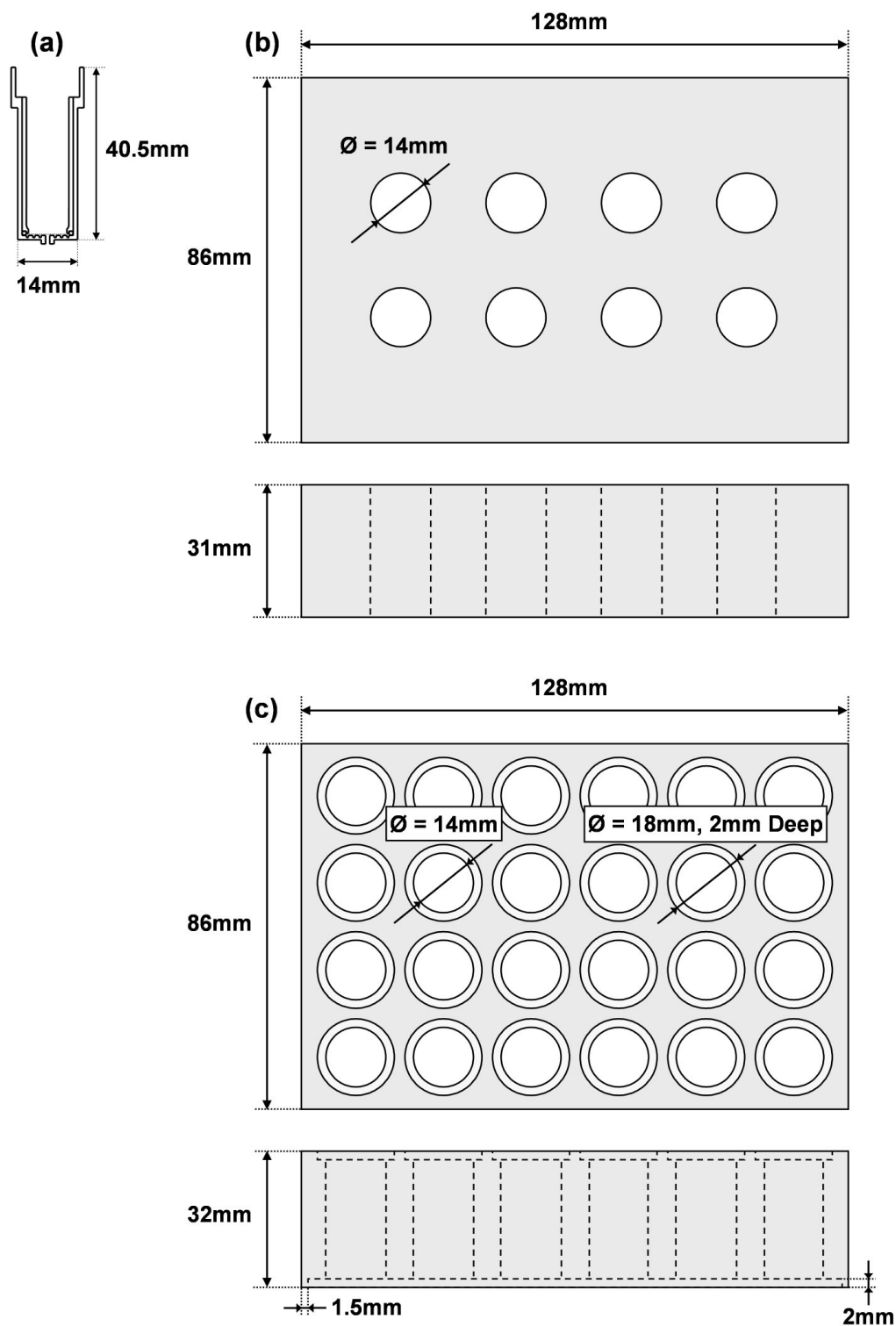


**Figure 3.1.** Detail of the custom filter plates designed during this work showing: (a) the commercially available removable membrane inserts; (b) plan and elevation views of the 8-well custom filter plate housing (capable of holding eight separate inserts); (c) plan and elevation views of the 24-well custom filter plate housing designed to maximise experimental throughput and improve sealing of the inserts. Note that each housing has the footprint of a standard microwell plate. Further details are given in Section 3.2.1.

membrane cell studies. For the negative pressure experiments, the filtration process has to be stopped and the collected permeate weighed to give a single data point of time and volume, in a similar fashion to the filter plate experiments. The four different experimental set-ups compared in this chapter are summarised in Table 3.1.

### 3.3 Water flux and membrane resistance measurement

In order to validate the automated microscale filtration concept, initial experiments focused on the measurement of water flux data for experiments performed under both positive and negative applied pressures at microwell and conventional laboratory scales. A numerical approach to the quantification of membrane resistance was also established.

#### 3.3.1 Quantification of membrane resistance at microscale

The basic equation for flow through a filtration membrane is described by a variation of Darcy's law (Section 1.3.4.1.4) relating flux behaviour to the membrane resistance,  $R_m$  ( $\text{m}^{-1}$ ):

$$\frac{1}{A} \frac{dV}{dt} = \frac{\Delta P}{\mu R_m} \quad (3.1)$$

where  $A$  is the effective filtration area ( $\text{m}^2$ ),  $V$  is the permeate volume ( $\text{m}^3$ ),  $t$  is the filtration time (s),  $\Delta P$  is the transmembrane pressure drop ( $\text{N.m}^{-2}$ ) and  $\mu$  is the dynamic permeate viscosity ( $\text{N.s.m}^{-2}$ ). Integrating Equation 3.1 over a variable pressure range allows the membrane resistance to be expressed in terms of the integral of transmembrane pressure difference with respect to time:

$$R_m = \frac{A \int \Delta P . dt}{\mu V_t} \quad (3.2)$$

**Table 3.1.** Filtration equipment specifications and measured membrane resistances. The custom filter plate was designed during this work (Section 3.2.2) to allow the simultaneous use of different membrane types on the same plate and to minimise the errors associated with microscale experimentation; values in brackets represent maximum sample volume and number of wells on a single plate; membranes are Millipore 0.22 $\mu$ m Durapore PVDF. Membrane resistance determined as described in Section 3.3.1 (error stated is one standard deviation about the mean).

<b>Filtration Equipment</b>	<b>Pressure Application</b>	<b>Sample Volume, V (mL)</b>	<b>Effective Filtration Area, A (cm<sup>2</sup>)</b>	<b>V/A Ratio (mL.cm<sup>-2</sup>)</b>	<b>Sample Throughput</b>	<b>Membrane Resistance (<math>\times 10^{-10}</math> m<sup>-1</sup>)</b>
Multiscreen Filter Plate	Negative	0.30	0.28	1.06	96	4.79 $\pm$ 0.32 (n=480)
Custom Filter Plate	Negative	0.83 (2.50)	0.79	1.06 (3.16)	8 (24)	5.16 $\pm$ 0.20 (n=40)
Membrane Cell	Positive	4.00 (12.00)	3.80	1.05 (3.16)	1	5.04 $\pm$ 0.09 (n=15)
Membrane Cell	Negative	4.00 (12.00)	3.80	1.05 (3.16)	1	5.15 $\pm$ 0.10 (n=15)

where  $V_i$  is the cumulative permeate collected ( $\text{m}^3$ ) over the filtration time.

By determining the total volume of liquid permeated and monitoring the variation in pressure difference over time it is possible to accurately determine the membrane resistance, since the integral is by definition the area under a pressure versus time profile. This area can easily be evaluated from a sufficiently detailed pressure profile.

Figure 3.2(a) shows a typical pressure profile for a water flux experiment using the custom filter plate in which the total volume of water permeated was an average of 3.57 mL for 8 filter inserts. From Equation 3.2 this corresponds to a membrane resistance of  $5.12 \times 10^{10} \text{ m}^{-1}$ . The permeate viscosity used for calculating membrane resistances was determined using correlations from the literature (Section 2.8.9.1) accounting for any changes in laboratory temperature ( $\pm 1^\circ\text{C}$ ) between individual filtration experiments.

### 3.3.2 Comparison of water flux data at different scales

Water flux data for the Multiscreen filter plate, custom filter plate and the membrane cell operated using both positive and negative applied pressure is shown in Figure 3.2(b). For the two filter plate designs, average pressure and water flux are used to plot the data points. Each data point is an average generated from experiments using all 96 or 8 wells on the Multiscreen and custom filter plates respectively. In the case of the membrane cell each data point is an average from three experiments using different membrane discs. All flux values are normalised to correspond to the flux at  $25^\circ\text{C}$ . The flux versus transmembrane pressure data for each format is seen to be very linear ( $R^2 > 0.993$ ) demonstrating a constant membrane resistance over the pressure range investigated. Since all experiments used the same  $0.22 \mu\text{m}$  PVDF membranes there is also a close correlation between the flux values determined for all the membrane formats and scales of operation. Closer inspection of the membrane cell data suggests that there is a small reduction ( $\sim 3\%$ ) in permeate flux when operating under negative as opposed to positive pressure. This slight discrepancy could be due to pressure losses along the connecting tubing from the vacuum flask to the membrane cell or could be simply a difference associated with applying a pressure below

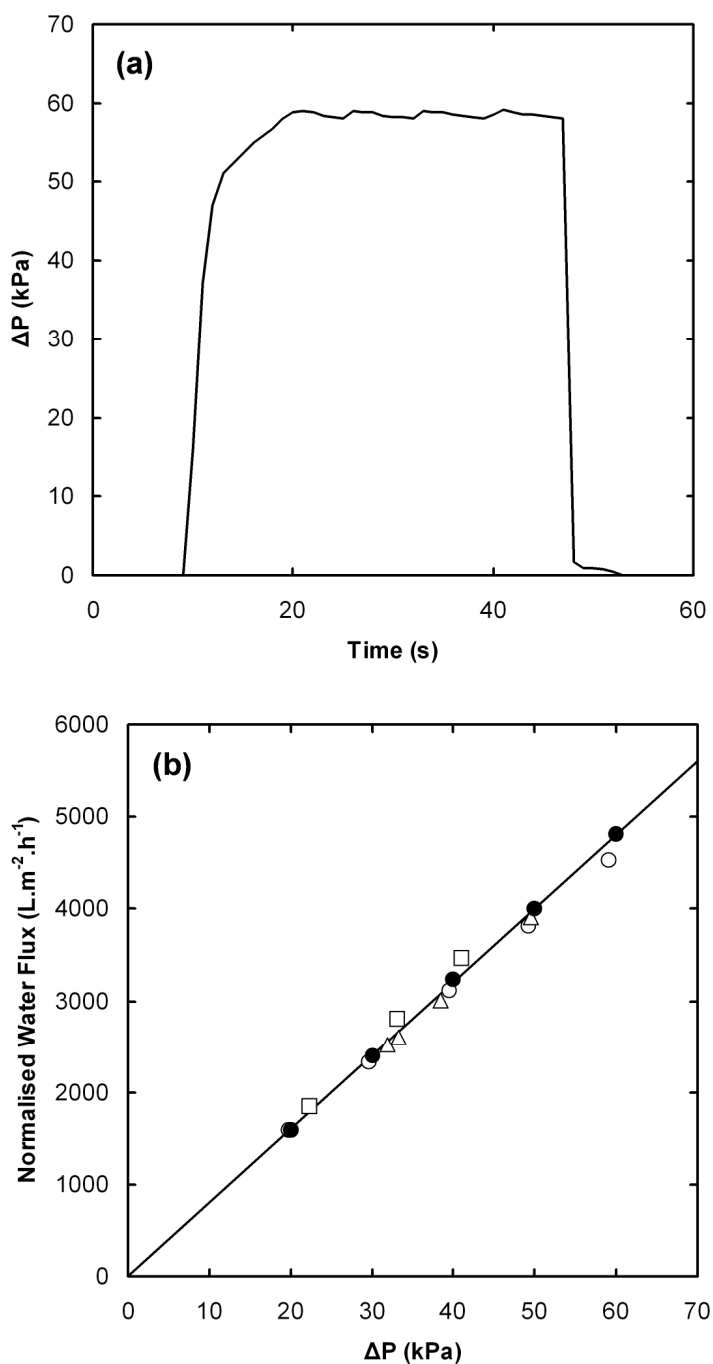


**Figure 3.2.** (a) Typical pressure profile for a water flux experiment using the custom filter plate and (b) temperature normalised water flux data determined for the different membrane geometries using 0.22  $\mu\text{m}$  Durapore PVDF membranes: ( $\square$ ) Multiscreen filter plate (0.3  $\text{cm}^2$ ) under negative pressure, ( $\Delta$ ) custom filter plate (0.8  $\text{cm}^2$ ) under negative pressure, ( $\bullet$ ) membrane cell (3.8  $\text{cm}^2$ ) under positive pressure, ( $\circ$ ) membrane cell (3.8  $\text{cm}^2$ ) under negative pressure. Solid line in (b) fitted by linear regression of all data. Membrane equipment as described in Table 3.1 and experiments performed as described in Sections 3.3.1 and 3.3.2.

atmospheric on the permeate side of the membrane. Similarly, the water flux values for the 96-well filter plate are seen to be slightly higher than for all the other formats. The water flux data shown in Figure 3.2(b) can be translated into membrane resistance values for each membrane format using Equation 3.2. As shown in Table 3.1, very similar  $R_m$  values of the order of  $5 \times 10^{10} \text{ m}^{-1}$  are calculated for the custom filter plate and membrane cell operated under both positive and negative pressure. With the 96-well Multiscreen filter plate the calculated membrane resistance is around 7% lower than for the other three membrane formats (statistically significant difference by two tailed t-test, unequal variance,  $p < 0.05$ ). This overall variation in  $R_m$  for the Multiscreen filter plate could arise from the methods involved in securing the membranes to the base of each acrylic well and small differences in the effective membrane area.

### 3.3.3 Variation of membrane resistance across the filter plates

While the membrane resistance for the Multiscreen filter plate given in Table 3.1 is an average value across *all* 96 wells, the variation in  $R_m$  values between *individual* wells on a single plate is shown in Figure 3.3(a). This pattern was obtained from 96 simultaneous water flux experiments and is representative of experiments performed on a number of different plates. It indicates that membrane resistance is relatively constant along each row (letters A – H) but is more variable along columns (numbers 1 – 12). This might suggest that strips of membrane from different sources are used along each row during filter plate construction or may be representative of the variability across larger sheets of membrane. Figure 3.3(b) shows the membrane resistances generated from a separate experiment where the same filter plate was rotated 180° on the vacuum manifold. The arrows on Figure 3.3 show the position of the vacuum source relative to the Multiscreen filter plates. An almost identical pattern of membrane resistances can be seen. This means that the position of a well in relation to the vacuum source does not affect the measured membrane resistance and that the applied pressure difference is uniform across the Multiscreen filter plate. Discrepancies occur at the edge columns where higher incidences of droplets hitting the edges of the collection tubes were observed experimentally. Despite improvements seen by decreasing the distance between filter plate and collection

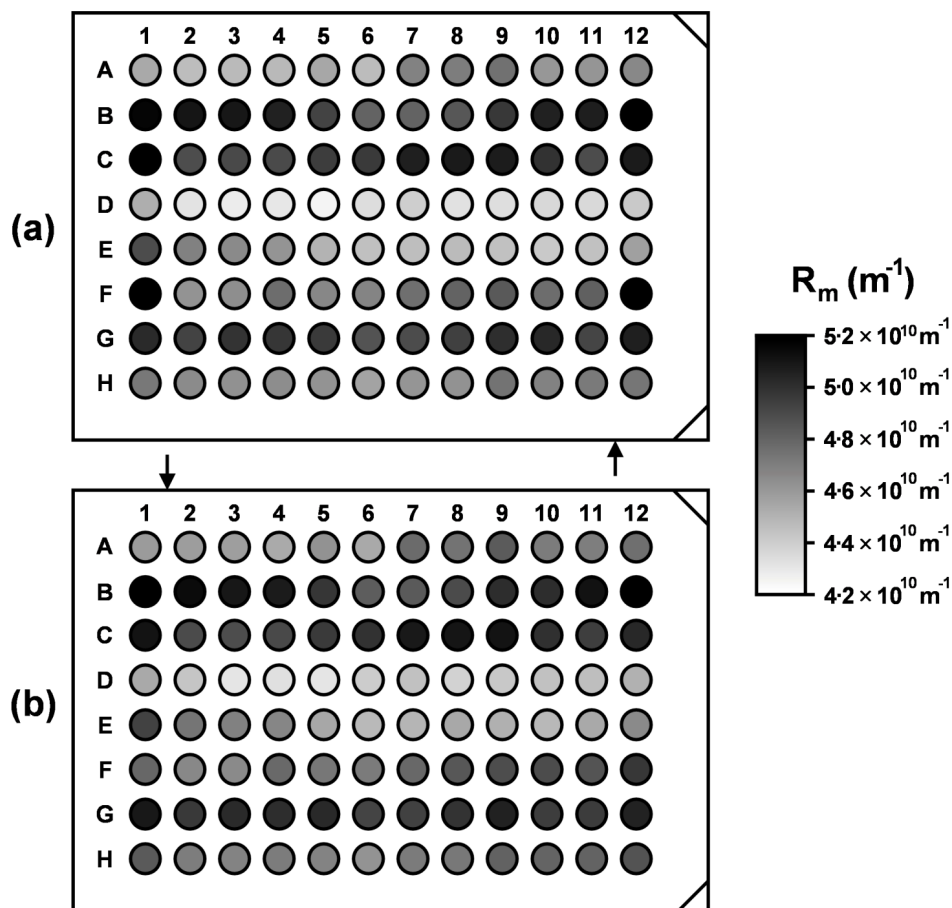


**Figure 3.3.** (a) Membrane resistance variation between individual wells on a single Multiscreen filter plate ( $0.3 \text{ cm}^2$ ). Plan view of a filter plate where the shading of each well corresponds to the scale of measured membrane resistances on the right hand side of the figure. (b) Repeat experiment with the same filter plate rotated through  $180^\circ$ . Arrows represent the relative position of the vacuum source. Experiment performed as described in Section 3.3.3, using a  $0.22 \text{ }\mu\text{m}$  Durapore PVDF membrane.

tubes, this discrepancy continued for the 96-well Multiscreen filter plate. Consequently, for this commercial filter plate design, the edge columns were not used in subsequent experiments.

Similar control experiments were carried out with the custom filter plate. Data from hundreds of individual measurements of membrane resistance determined using the custom filter plates was analysed. It was shown that no row, column or type of well (corner, edge, centre) gives an average membrane resistance significantly different from the overall mean (one sample t-test,  $p > 0.05$ ). It should be noted that these statistical conclusions are not due to poor accuracy in the experimental technique. In a series of 5 experiments, 8 filter insert positions were randomly changed. No significant variation occurred due to plate position, but the average calculated membrane resistance for each individual insert was significantly different from the overall mean (one sample t-test,  $p < 0.05$ ) since each had its own distinct average membrane resistance. This shows that the measurement of membrane resistance is accurate enough to discover any meaningful variation. It can be concluded that the position of a filter insert within the plate does not have a significant effect on the calculated membrane resistance and that the applied pressure difference is uniform across the entire custom filter plate.

### **3.3.4 Importance of membrane resistance data**

It should be noted that although interesting with respect to the consistency of filter plate manufacture, the impact of these variations in membrane resistance on subsequent determinations of specific cake resistance can generally be neglected. Theory predicts that specific cake resistance is independent of membrane resistance, as shown in Equation 3.3 (and explained in Section 1.3.4.1.4). In the experiments described here this is likely to be true since the membrane resistance is always a small part of the total resistance to flow. However, changes in membrane resistance may affect the high flux values during the initial part of a filtration run and so comparison of volume and time data from membranes of similar resistance is the best option. Measurement of membrane resistances may also be important when considering transmission of a target molecule, as discussed later in Chapter 4. Overall, the results

presented in this section show that membrane resistance can be rapidly and accurately determined in microplate formats and that the results obtained are comparable to laboratory scale processes performed using both positive and negative applied pressures.

### **3.4 Flux behaviour during microfiltration of *E.coli* fermentation broths**

Although it was shown in Section 3.3 that comparable membrane performance was obtained as when using positive applied pressures, the amount of permeate flux data that can be collected from each well during negative pressure operation is limited. During the normal flow filtration of complex biological suspensions there is a variable flux due to the increase in resistance to flow over time as a filter cake is deposited. A more sophisticated approach is required to determine the specific cake resistance of the filter cake. Specific cake resistance is an intrinsic measurement of the resistance to flow generated by a particular solid-liquid suspension (Section 1.3.4.1.4). It can be used to predict the flux throughout a normal flow filtration experiment (Section 2.8.11). This section details the approach to the automated and parallel measurement of specific cake resistance at the microscale and then shows how this is used to explore the changes in *E.coli* filtration performance due to several process changes.

#### **3.4.1 Quantification of specific cake resistance at microscale**

As described previously in Section 2.3.2 and illustrated in Figure 2.1(b), the method established here collects permeate data from two identical filter plates run in parallel from the same vacuum source. One manifold is vented before the other to give two permeate masses at two different filtration times. These can then be used to estimate specific cake resistance of broth derived *E.coli* TOP10 cells.

Established cake filtration theory (Section 1.3.4.1.4) links the measurement time ( $t$ ) and collected permeate volume ( $V$ ) data in a linearised equation:

$$\frac{At}{V} = \frac{\mu\alpha\rho_0}{2\Delta P} \frac{V}{A} + \frac{\mu R_m}{\Delta P} \quad (3.3)$$

where  $\alpha$  is the specific cake resistance per dry cake mass ( $\text{m.kg}^{-1}$ ) and  $\rho_0$  is the dry mass of cake solids per volume of permeate ( $\text{kg.m}^{-3}$ ) which is determined from the following equation:

$$\rho_0 = \frac{s\rho_p}{1-sm} \quad (3.4)$$

where  $s$  is the mass fraction of solids in the feed,  $\rho_p$  is the permeate density ( $\text{kg.m}^{-3}$ ) and  $m$  is the mass ratio of wet cake to dry cake. Alternatively,  $\rho_0$  can be expressed in terms of the dry solids concentration as:

$$\rho_0 = \frac{c_f}{\rho_f} \cdot \rho_p \cdot \frac{1}{\left(1 - \frac{c_f}{\rho_f} m\right)} \quad (3.5)$$

where  $c_f$  is the dry solids concentration in the feed ( $\text{kg.m}^{-3}$ ) and  $\rho_f$  is the feed density ( $\text{kg.m}^{-3}$ ). For the *E.coli* filtration feeds used during this work, the product of solids fraction and mass ratio is very low and the feed is only slightly denser than the permeate. Hence the term  $\rho_0$  approximates to the dry solids concentration in the feed. This assumption allows specific cake resistance to be calculated from data obtainable in high throughput operation.

For each experiment performed in the filter plate, a plot of  $t/V$  versus  $V$  produces a linear portion following initial pressure application and cake build-up. By controlling the time over which each plate is filtered it is possible to ensure that the two data points collected lie on the straight line portion of the  $t/V$  versus  $V$  plot as shown schematically in Figure 3.4. The selected times will give a measurable range of specific cake resistance which will typically cover up to two orders of magnitude. The times can be selected based on initial trial experiments at a typical feed composition, published cake resistance values, prior process knowledge or acceptable process boundaries.

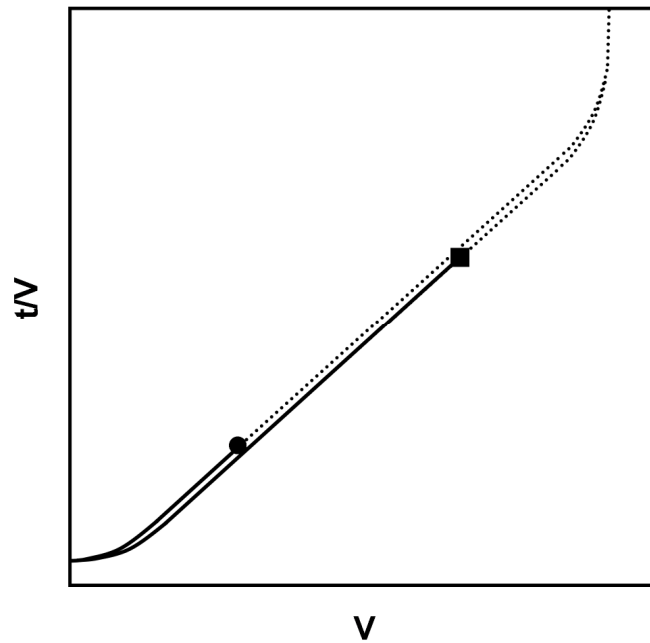


**Figure 3.4.** Illustration of the method used for determination of specific cake resistance from microscale and negative pressure experiments. The solid lines represent the progress of a filtration process up to the collection of the data points (●, ■) from two identical, parallel experiments. The dotted lines represent what would have been the course of each filtration process if the pressure had not been released to take a measurement of permeate (and retentate) volume. A gradient can then be determined from these two points on the straight line portion of the graph and used to calculate the cake resistance as described in Section 3.4.1.

Experimentally, it is necessary to ensure that filtration occurs for a sufficient time that the pressure difference has reached steady state and cake formation is in the linear region. Using this approach, real volume and time data during cake deposition from whole fermentation broths can be quantitatively analysed.

By using the two data points collected to generate the gradient of a straight line, an equation for specific cake resistance can be formed:

$$\alpha = \frac{\left( \frac{t_2}{V_2} - \frac{t_1}{V_1} \right)}{(V_2 - V_1)} \cdot \frac{2A^2 \Delta P}{\mu c_f} \quad (3.6)$$

The numeric subscripts represent data from the separate microwell filter plates where plate 1 is the first to have the applied pressure vented at time  $t_1$ . Equation 3.6 will be valid for feeds that demonstrate a constant cake resistance and which do not filter to completion before  $t_2$ . If this does occur, the second data point will be easily identified as being above a critical volume and thus not valid for analysis. This would, however, require a reduction in cake resistance of at least an order of magnitude to what was expected. In addition, any feed where the calculated cake resistance increases during the filtration process, such as when pore blocking also occurs (Ho and Zydney, 2000), can be identified from a high x-intercept.

For scale up predictions of permeate flux described in Section 2.8.7.1 and implemented in this chapter in Figure 3.7, the modified cake filtration constant,  $K_c'$  ( $\text{N.s.m}^{-4}$ ), is required and is readily calculated from the same data set:

$$K_c' = \mu \alpha \rho_0 = 2A^2 \Delta P \frac{\left( \frac{t_2}{V_2} - \frac{t_1}{V_1} \right)}{(V_2 - V_1)} \quad (3.7)$$

In the following sections the variation of specific cake resistance of *E.coli* TOP10 cells is explored as a function of medium composition and microfiltration conditions. All specific cake resistance values reported for the Multiscreen plate, custom filter

plate and the membrane cell under negative pressure were calculated using Equation 3.6. Values for the Multiscreen filter plate are derived from 8 replicate experiments while values for the custom filter plate are derived from 3 replicate experiments. In both cases replicates were performed in parallel on the same plate. For the membrane cell, 3 replicates for specific cake resistance calculation were carried out in sequential experiments. Example specific cake resistance calculations showing the progression of raw data to calculated values and through to flux prediction are shown in Appendix B.

### 3.4.2 Influence of harvest time and broth age

An important consideration in the development of every process is timing and scheduling between each unit operation. Delays within a single process step can lead to consequential scheduling problems. Equipment may still be in use or tied up in turnaround tasks such as cleaning or sterilisation. By simulating such delays microscale filtration techniques demonstrate an ability to test the robustness of a process to scheduling changes as well as enabling the optimum filtration conditions to be identified for a given broth. Figure 3.5 shows three different sets of specific cake resistance data for fermentations in which harvesting is delayed by 0 h, 4 h or 24 h. Fermentations were performed as described in Section 2.4. At each harvest time identical fermentation broth samples were filtered using the Multiscreen filter plate, custom filter plate and the membrane cell under positive and negative applied pressures. The results in Figure 3.5 clearly indicate the expected increases in specific cake resistance with broth ageing time and also show very similar results for each of the filtration devices. Even allowing for the variation seen in the microwell experiments, t-tests (two-tailed, unequal variance,  $p < 0.05$ ) show that the mean specific cake resistance is significantly different for cells harvested on time ( $t = 4.5$  h) compared to cells harvested 4 h later ( $t = 8.5$  h). These results further demonstrate that comparable filtration performance is achieved between both the microwell filter plate designs and the conventional laboratory membrane cell. They also show that the microwell filtration techniques are able to quantitatively distinguish the performance of different feed streams with different properties.

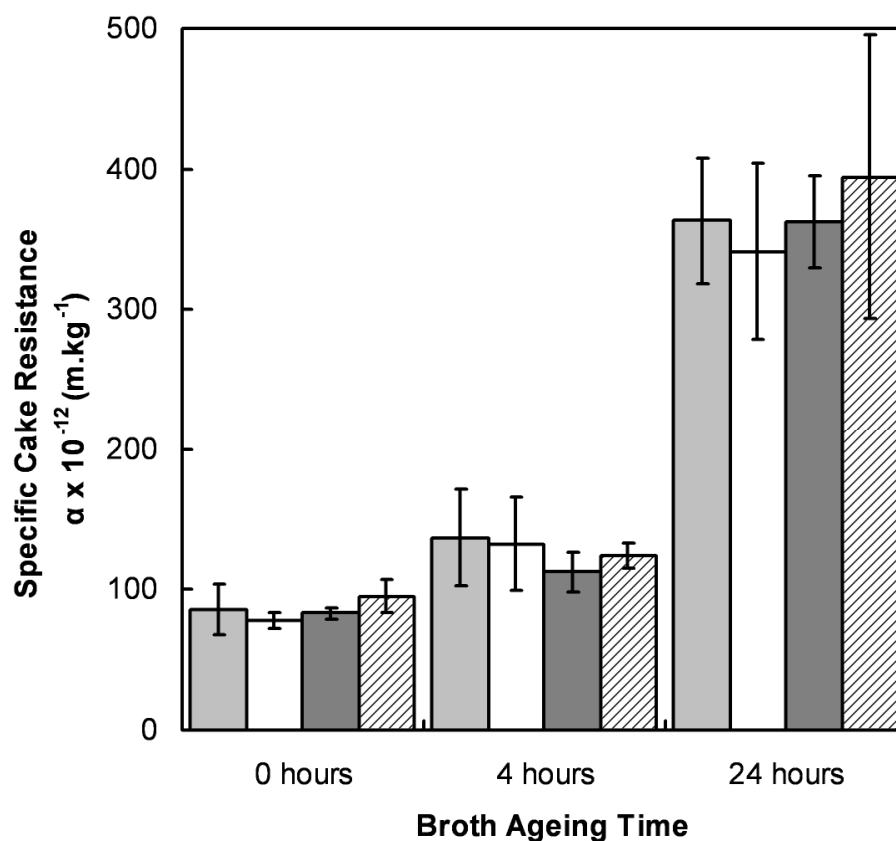


**Figure 3.5.** Specific cake resistance determined for an *E.coli* TOP10 fermentation broth after various broth ageing times: (■) Multiscreen filter plate (0.3 cm<sup>2</sup>) under negative pressure, (□) custom filter plate (0.8 cm<sup>2</sup>) under negative pressure, (▣) membrane cell (3.8 cm<sup>2</sup>) under positive pressure, (▨) membrane cell (3.8 cm<sup>2</sup>) under negative pressure. Membrane equipment described in Table 3.1 and experiments performed as described in Section 3.4.2: pressure difference 60 kPa. Error bars represent one standard deviation about the mean (n = 8 for the Multiscreen filter plate, n = 3 for other formats).

Previous work with *E.coli* (Okamoto *et al.*, 2001) has shown that the measured increase in cake resistance of aged cells is due to their deterioration and the release of intracellular components caused by insufficient nutrients. The values of specific cake resistance generated here for the broth aged 24 h are of a similar order of magnitude to other literature values. Cake resistance values for freshly harvested cells however, are considerably lower than those previously quoted in the literature for NFF at the same pressure difference of 60 kPa (Okamoto *et al.*, 2001; Nakanishi *et al.*, 1987). This is probably a consequence of the previous studies having used different media for the culture of wild type *E.coli* strains and cultivation times up to 10 times longer than used here in the case of freshly harvested broth. The extended fermentation times would tend to increase the proportion of older or lysed cells in the broth while the strong influence that complex media components can have on *E.coli* cake resistance values is described later in Section 3.4.5.

### 3.4.3 Influence of broth pH and specific buffers

The interaction of solid particles in the feed stream can be significantly affected by their pH and ionic environment. These, in turn, are known to influence microfiltration performance (Ohmori and Glatz, 1999). Buffers at a constant ionic strength of 100 mM were used to control the pH of the *E.coli* TOP10 suspension during filtration studies. These would avoid the use of strong acids or bases which might otherwise damage the cells and obscure the true behaviour.

Certain buffers used to control the pH of the feed stream (phosphate, citrate, succinate, piperazine, MES, and tris-bis) showed no change in measured specific cake resistance values when used to vary the pH over a range of 2 – 7. There was also no observed lysis of the cells. During the experiments, however, it was discovered that the use of acetate as a buffer resulted in an approximately 3-fold reduction in specific cake resistance as shown in Table 3.2. The introduction of this small molecule can be seen to have an emphatic effect on the cake resistance, most likely from the result of aggregation of larger particles. For all the other buffers used, the specific cake resistance of the *E.coli* TOP10 cells was of the order of  $2 \times 10^{14}$  m.kg<sup>-1</sup>. Compared to

the membrane cell experiments that were carried out sequentially, all the microscale experiments investigating pH could be conducted in parallel on the same plate.

**Table 3.2.** Specific cake resistance of *E.coli* TOP10 cells determined in the presence or absence of 100 mM acetate buffer. Cake resistances determined as described in Section 3.4.3. Experimental variation indicated represents one standard deviation about the mean, n = number of individual wells or experiments.

Filtration Equipment	Specific Cake Resistance, $\alpha$ ( $\times 10^{-12}$ m.kg <sup>-1</sup> )	
	Without Acetate	With Acetate
Multiscreen Filter Plate	176 $\pm$ 42 (n = 48)	63 $\pm$ 7 (n = 8)
Custom Filter Plate	186 $\pm$ 26 (n = 18)	61 $\pm$ 1 (n = 3)
Membrane Cell (Positive Pressure)	179 $\pm$ 52 (n = 18)	62 $\pm$ 4 (n = 3)

#### 3.4.4 Influence of media composition

The optimisation of microbial fermentation processes routinely involves the evaluation of many different types and concentrations of media components to enhance cell growth rates and/or product titre (Demain and Davies, 1999; Doig *et al.*, 2006). For the efficient optimisation of the *overall* process sequence, which is of most relevance to industry, the influence of these different media components, especially on the early product recovery stages (Davies *et al.*, 2000) must also be considered. Previous published data has suggested a reduction in *E.coli* specific cake resistance when cells are washed and resuspended in buffer (Okamoto *et al.*, 2001). In contrast our initial experiments indicated an increase in the specific cake resistance using *E coli* TOP10 cells. To examine this in more detail, along with the influence of individual medium components on microfiltration performance, washed cell pellets were resuspended in the original supernatant, buffer alone or buffer containing 10 g.L<sup>-1</sup> of either tryptone, yeast extract or glycerol. The buffer species used in these

experiments was piperazine which, at pH 5.5, matches the final pH of the whole cell broth at harvest. By washing the cells and resuspending them in the original supernatant, any effects due to the processing of the cells before the microfiltration experiments are removed from the comparison.

Figure 3.6 shows the previously noted increase in specific cake resistance for the cells resuspended in buffer compared to cells resuspended in the original supernatant. When the resistance of the cells in solutions of all the individual media components is examined, it can be seen that glycerol and tryptone have no significant effect when the pH is maintained constant. By comparison, when the *E.coli* TOP10 cells are resuspended in a 10 g.L<sup>-1</sup> yeast extract solution the specific cake resistance of the cells is determined to be approximately 3 times lower than when cells are resuspended in buffer alone and about half that of the whole supernatant. The mechanism by which the yeast extract reduces the specific cake resistance is unclear but is likely to be a specific interaction with the cells leading to a more open cake structure through cellular aggregation (the yeast extract itself is completely soluble so will not in itself contribute to the cake composition).

The variation in flux over time for single replicates of the membrane cell is shown in Figure 3.7 comparing results from 4 mL of cells resuspended in freshly prepared yeast extract to 4 mL of cells resuspended in the original broth supernatant (V/A ratio of 1.05 mL.cm<sup>-2</sup>). The data is included up to the completion of each filtration and highlights a 1.8-fold difference between membrane cell processing times. Specific cake resistance data collected from Multiscreen filter plates and custom filter plates are used to generate predicted flux data up to the same V/A ratio based on cake filtration theory (Section 2.8.7.1). The predictions for both microwell formats show good agreement with the membrane cell flux data. In addition, similar differences in processing time are predicted by both the Multiscreen (2.1-fold) and custom filter plates (1.7-fold). Similar figures can readily be produced for every feed composition presented in this chapter (not shown).

The influence of media components on microfiltration performance was again found to be the same for all three membrane configurations studied and, as with the pH

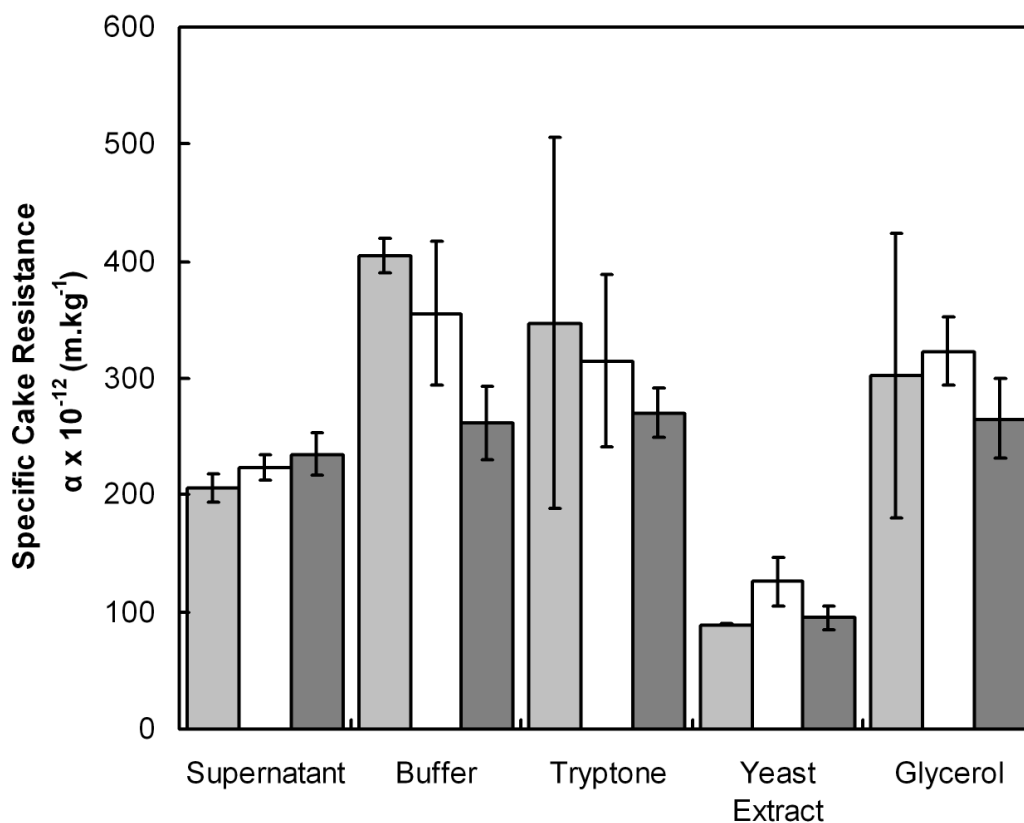


**Figure 3.6.** Specific cake resistance of washed *E.coli* TOP10 cells resuspended in various media components: (■) Multiscreen filter plate (0.3 cm<sup>2</sup>) under negative pressure, (□) custom filter plate (0.8 cm<sup>2</sup>) under negative pressure, (▣) membrane cell (3.8 cm<sup>2</sup>) under positive pressure. Membrane equipment as described in Table 3.1 and experiments performed as described in Section 3.4.4: pressure difference 60 kPa. Error bars represent one standard deviation about the mean (n = 8 for the Multiscreen filter plate, n = 3 for other formats).

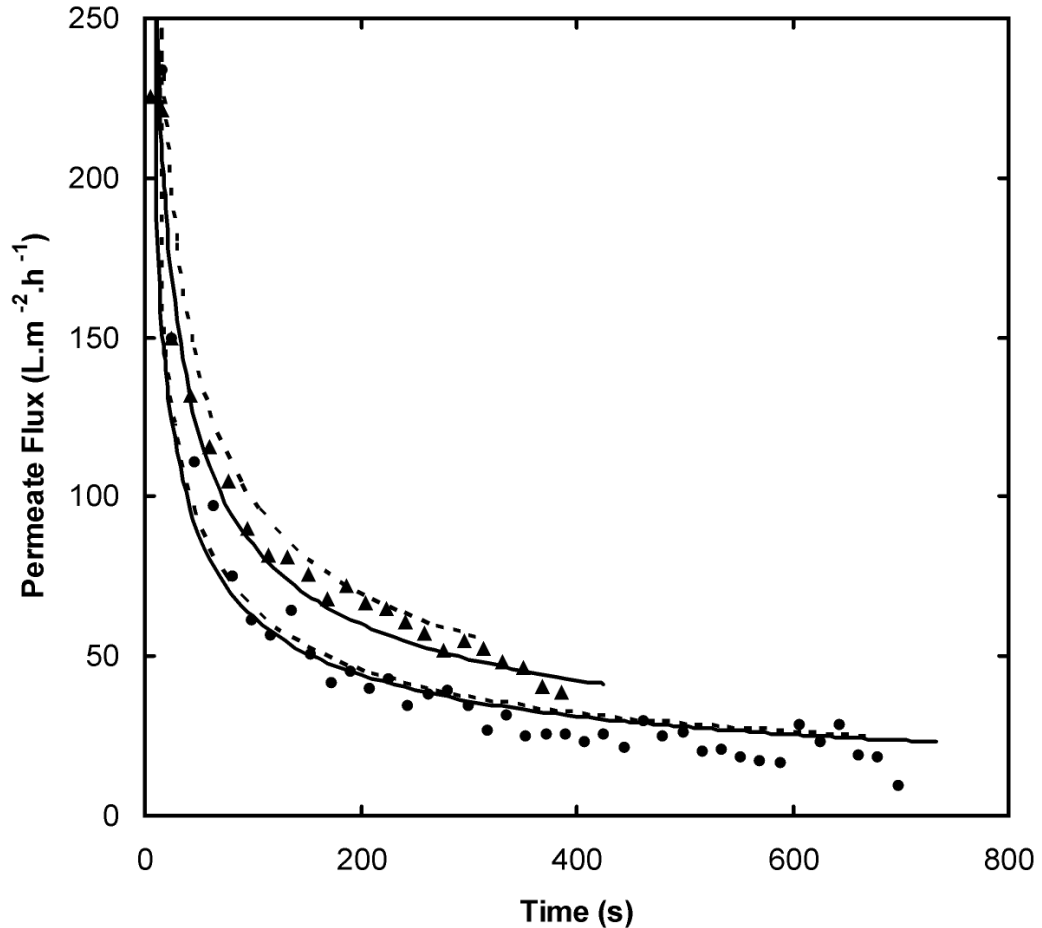


**Figure 3.7.** Variation of permeate flux over time for washed *E.coli* TOP10 cells resuspended in original broth supernatant (●) and freshly prepared yeast extract solution (▲) using the membrane cell (3.8 cm<sup>2</sup>) under positive pressure. Lines show the predicted flux generated from specific cake resistance data determined using the Multiscreen filter plate (0.3 cm<sup>2</sup>) under negative pressure (dashed) and the custom filter plate (0.8 cm<sup>2</sup>) under negative pressure (solid). Membrane equipment as described in Table 3.1 and experiments performed as described in Section 3.4.4: pressure difference 60 kPa. Flux predictions calculated using Equation 2.20 as described in Section 2.8.11.

studies described in Section 3.4.3, both microwell filter plate designs enabled the influence of the different media components to be examined in parallel. This also improved the experimental methodology in that any variation of the feed stream due to ageing of the cells between sequential experiments, as with the membrane cell studies, was removed.

### **3.5 Evaluation of microscale methods and custom filter plate design**

The microscale experiments investigating the influence of harvest time (Section 3.4.2), buffers (Section 3.4.3) and media composition (Section 3.4.4) on microfiltration performance have shown how several different feeds can be analysed in parallel, usually on a single plate. The ability to process all these feeds in parallel, rather than in series as with the membrane cell, leads to many advantages in terms of experimental throughput and the range of process variables it is possible to investigate in a given time. The results in all the previous sections for both filter plate designs have shown that membrane resistance and specific cake resistance data are similar to those obtained in the conventional lab scale NFF experiments. Figure 3.8 shows parity plots of the specific cake resistance values generated in this study. A small number of outlying results are evident for both the Multiscreen filter plate (Figure 3.8(a)) and the custom designed filter plate (Figure 3.8(b)). Analysis of these particular values showed them to be from the media component experiments where sample variation when preparing the resuspended cell solutions resulted in a large degree of variability. The lines of best fit to the experimental data (solid lines) indicate that both filter plate designs generate slightly higher cake resistances, by about 10%, compared to the membrane cell. This is a consequence of the outlying media component results and probably also small errors in determination of the membrane area which, being a squared term in Equation 3.6, can have a large influence on the calculated cake resistance values. The one limitation in the use of a vacuum manifold for these microscale membrane studies is that only transmembrane pressure differences up to approximately 75 kPa can be studied unlike the values of up to 200 kPa reported when positive pressure is applied (Chandler and Zydney, 2004).

Overall, however, the agreement between the filter plate and membrane cell experiments is very good and would result in identical interpretations with regard to membrane process performance.

Finally, comparing the two filter plate designs, Figure 3.8 shows that there is more variation in the cake resistance values determined with the commercial Multiscreen filter plate (Figure 3.8(a)) than with the custom designed filter plate (Figure 3.8(b)). It should also be remembered here that the data and errors generated using the Multiscreen filter plate are from 8 separate replicates compared to only 3 replicates with the other membrane formats. This greater variation is perhaps not surprising in that the design of the Multiscreen filter plate is optimised for high throughput screening applications rather than bioprocess studies. For each well the applied sample volume is very small (Table 3.1) and any problems in the collection and gravimetric analysis of the permeate fractions can have a significant impact on calculation of the specific cake resistance. In contrast the custom filter plate shown in Figure 3.1 has been specifically designed for bioprocess studies. The applied sample volume is up to 8 times larger than for the commercial plate (Table 3.1) minimising analysis errors and giving the best correlation with the laboratory scale membrane cell results (Figure 3.8(b)). The removable membrane inserts (Figure 3.1 (a)) enable analysis of individual retentate samples and calculation of a process mass balance. Additionally they would facilitate study of different types of membrane in a single experiment something that is not possible with the commercial Multiscreen plate. Although the experimental throughput of the custom plate is 4-fold less than with the commercial plate (Table 3.1) the number of experiments required in bioprocess studies is considerably less than for drug screening and requires the collection of more precise and quantitative data (Lye *et al.*, 2003; Micheletti and Lye, 2006).

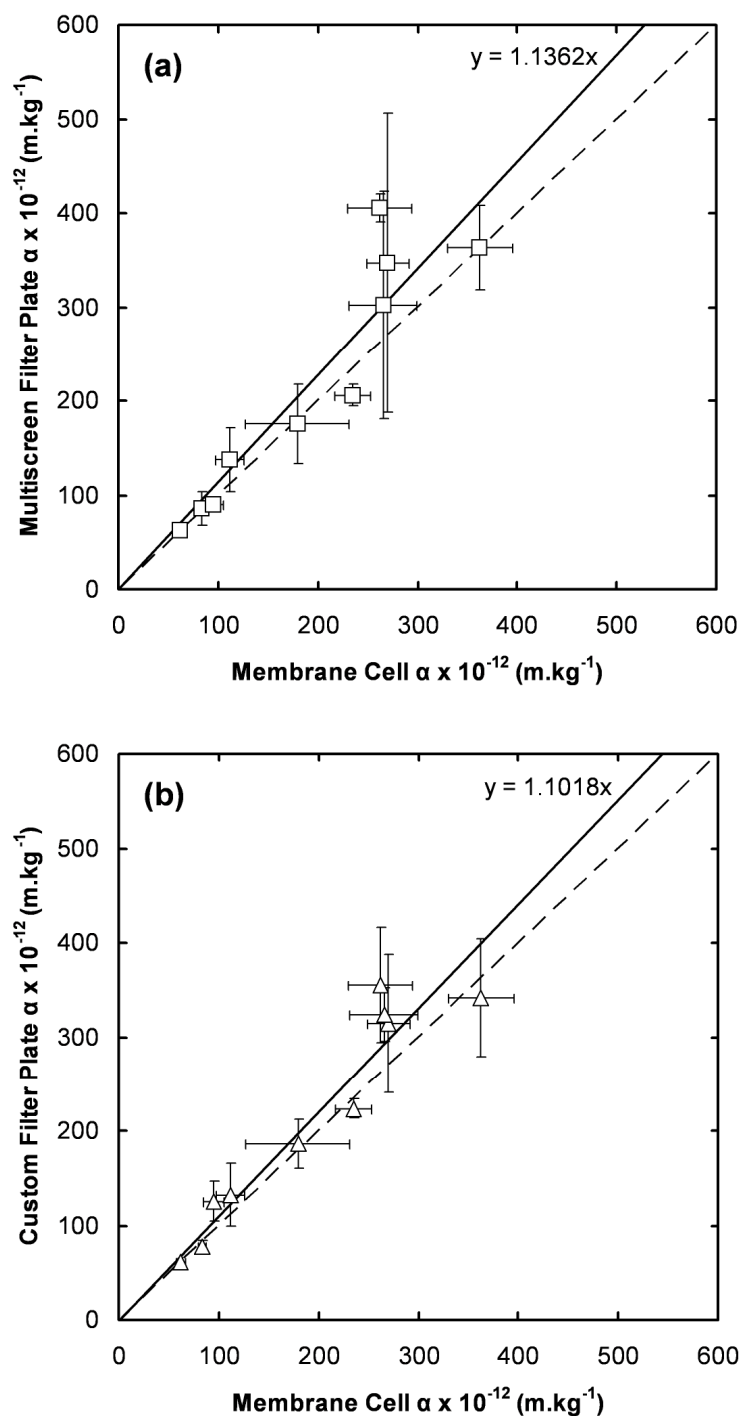


**Figure 3.8.** Parity plots of all the specific cake resistance data generated from the membrane cell under positive pressure ( $3.8 \text{ cm}^2$ ) against data generated from: (a) the Multiscreen filter plate ( $0.8 \text{ cm}^2$ ) under negative pressure and (b) the custom filter plate ( $0.3 \text{ cm}^2$ ) under negative pressure. Solid lines fitted by linear regression while dashed line denotes parity. Error bars represent one standard deviation about the mean ( $n = 8$  for the Multiscreen filter plate,  $n = 3$  for other formats).

### 3.6 Summary

In this chapter a high throughput method for the study of normal flow microfiltration operations has been established using a custom designed 8 to 24 well filter plate and a commercial 96-well Multiscreen filter plate. Integration of this new approach with a typical robotic platform has enabled automation of virtually all the experimental procedure (Section 2.3.2).

Membrane resistance values can be accurately quantified using either filter plate design (Table 3.1). The accuracy of these measurements has helped to determine that plate position does not affect experimental results and applied pressure difference does not vary across either plate (Figure 3.3, Section 3.3.3).

Each of the two filter plate formats has been used to demonstrate that cell condition following fermentation, buffer type and media composition are all important factors influencing the specific cake resistance of *E.coli* TOP10 cells (Figure 3.5, Table 3.2 and Figure 3.6). The microscale method therefore allows parallel quantification of the impact of upstream process conditions on microfiltration performance.

The custom filter plate designed here, specifically optimised for bioprocess studies, allows multiple membrane types to be evaluated on a single plate and the measurement of both permeate and retentate masses to ensure against cross-contamination or material losses. Lower variation in specific cake resistance values is seen in the custom filter plate compared with the commercial filter plate (Figure 3.8). Having established the microscale method here, its application to the optimisation of permeate flux and soluble protein transmission is considered in Chapter 4.

---

## **4.0 Microfiltration optimisation using automated microscale experimentation coupled with statistical design of experiments**

### **4.1 Aim of the chapter**

The aim of this chapter is to demonstrate how the automated microscale microfiltration technique established in Chapter 3 can be used to fully characterise filtration process performance by quantification of both permeate flux and protein transmission. The specific objectives of this chapter are:

- To use the automated microwell technique described in Chapter 3 for the simultaneous collection of both permeate flux and protein transmission data.
- To demonstrate the utility of combining microwell scale experimentation with statistical Design of Experiments (DoE) techniques for rapid process optimisation and analysis of process trade-offs.
- To illustrate the scale-up of microwell data to conventional laboratory scale for the prediction of permeate flux and protein transmission over time.
- To demonstrate that the optimum design space location is equivalent between microscale and conventional laboratory scale techniques.

### **4.2 Introduction**

The results described previously in Chapter 3 focused solely on the quantification of permeate flux. Here the additional measurement of protein transmission during automated microscale microfiltration and the concept of experimental design for high throughput bioprocessing are introduced.

### 4.2.1 Product transmission

The transmission of extracellular products and impurities can be assessed during automated microscale microfiltration in a very similar way as for conventional filtration experiments. Quantification of transmission levels is important since they vary with process operating conditions (Persson *et al.*, 2003) and will impact on product yield and therefore the performance requirements of subsequent downstream processing operations. Permeate and retentate samples from identical wells run for different times (already necessary for the analysis of permeate flux as described in Section 3.4.1) can also be assayed to give an indication of the cumulative observed transmission of extracellular material over time. The assays required for this duty should be rapid, robust and suitable for working with the small sample volumes generated using the microwell approach. They should also be capable of integrated automation in order to ensure that analysis does not become a bottleneck for high throughput bioprocess investigation.

#### 4.2.1.1 Potential influence of membrane resistance

Solute transmission through a membrane can theoretically be influenced by the membrane pore size (Zeman and Zydney, 1996). Variations in water flux that can be effectively measured in parallel at microscale (Section 3.3.3) could represent differences in the average pore size of a membrane but may also be due to variations in porosity or thickness. Protein transmission can also depend on more subtle membrane differences, which can vary despite constant water flux measurements (Fane *et al.*, 1983). In addition, the size of the model protein to be used in this chapter is small compared to the membrane pore size and so small variations in membrane resistance are unlikely to have a significant impact on transmission. In order to confirm this, membrane resistances were determined for every individual membrane used during the work described in this chapter. No correlation could be found between the transmission values and the corresponding membrane resistance. Transmission values presented here have therefore not been normalised by membrane resistance in this chapter, although this remains an option for other combinations of feed and membrane type in other applications.

#### 4.2.1.2 Model system

The model system chosen for investigation in this chapter is an *E.coli* TOP10 fermentation broth (average dry cell weight of  $7.4 \pm 0.4 \text{ g.L}^{-1}$ ) spiked with  $2 \text{ g.L}^{-1}$  of lysozyme. Lysozyme is used since it is cheap, has a quantitative assay available and may be likely to interact with the *E.coli*, thus producing interesting effects to challenge the experimental design and methods. The optimisation procedure is carried out as if the protein of interest is a high value product and good yield is imperative for success of the separation. The method of feed preparation for all the samples used in this chapter is detailed in Section 2.4.3.

Lysozyme acts by breaking up peptidoglycans in bacterial cell walls. The gram negative *E.coli* cells can still be susceptible to lysis by lysozyme, but only if the outer membrane can be weakened by, for example, mild osmotic shock in the presence of EDTA (Witholt *et al.*, 1976; Pierce *et al.*, 1997). Control experiments carried out using a membrane cell showed no change in the filtration characteristics of the model system over a 2 h period indicating little or no lysis occurs. All experiments reported here were began almost immediately after resuspension of the cells and each experiment was concluded within a 2 h time window.

#### 4.2.2 Application of design of experiments

Initially the use of Design of Experiments (DoE) techniques with high throughput processes may seem counter-intuitive. Once techniques are developed to allow multiple experiments to occur in parallel then it appears not to be necessary to use methods that reduce the number of experiments that are carried out. There are several reasons, however, that demonstrate how automated microscale experimentation and DoE methodology complement each other very well in order to facilitate rapid bioprocess development and support a quality by design approach (Rathore and Mhatre, 2009). DoE seeks to expand the experimental space that can be explored, by considering multiple factors and their interactions. When considering only a few factors from one or two processes, traditional experimental approaches may be adequate in conjunction with high throughput automation systems. However, when

whole process sequences with several factors for each unit operation are studied then the required number of experiments increases far beyond that which can be explored using conventional experimentation, even with high throughput capabilities. DoE is also sequential in nature, focusing on the important areas of experimental space and progressively seeking optimal conditions. Automated processes are ideally suited to this due to their ability to easily repeat experiments with only slight variations to the operating conditions. It is important that any automated microscale process is capable of application to DoE methodology in order for whole process sequences to be effectively studied at the microscale.

### **4.3 Factorial experiments**

This section analyses the important process factors that determine high protein transmission and low specific cake resistance (high flux) during microfiltration of an *E.coli* fermentation broth containing an extracellular protein. It also determines the significance of each factor for the process as a whole and how analysis of initial results can be used to focus further experiments to determine optimum processing conditions.

#### **4.3.1 Factorial experiment design and implementation**

The factorial experiment presented in this Chapter is a half repeat of a 2-level factorial experiment examining five factors (design detailed in Section 2.7.1.1) affecting flux behaviour and transmission during the filtration of an *E.coli* fermentation broth containing an extracellular protein. The factors and their chosen levels are summarised in Table 4.1.

The high and low levels for pH are chosen to match the range over which pH may vary during batch fermentation, as observed in shake flask fermentations. The ionic strength is varied relatively closely around the salt concentration used in the standard growth media. The change in pH and ionic strength will influence charge based interactions between the cell, membrane and protein. This may lead to changes in the

filter cake structure (Ohmori and Glatz, 1999) and influence protein transmission through the microfiltration membranes (Persson *et al.*, 2003). The yeast extract concentration is studied at the levels previously shown to significantly reduce cake resistance in Chapter 3. A varying pressure difference will show any potential change in filter cake compressibility (Nakanishi *et al.*, 1987; Foley, 2006) and the levels are chosen within the range achievable using the available vacuum manifold. The two membranes are chosen due to their similar pore size allowing different manufacturers and different membrane polymers to be compared.

All experiments at a given pressure were carried out in parallel using the 24-well custom microwell filter plate (Section 3.2.1) according to the method described in Section 3.4.1. Samples were prepared as described in Section 2.4. In addition to this method, the permeate samples collected were assayed as described in Section 2.6.1 and protein transmissions calculated as described in Section 2.8.12. Each factorial run was duplicated and 4 repeats of the centre-point values for pH, ionic strength and yeast extract concentration were carried out at each combination of pressure and membrane type as prescribed by the design in Section 2.7.1.1. Separate centre-points are required for each membrane type since this is a qualitative factor and no centre-point pressure was used since this would require a separate plate to be run.

**Table 4.1.** Summary of the factors and levels selected for the  $2^{5-1}$  factorial experiment described in Section 4.3.1.

Factor	Factorial Code	Low Value	High Value
pH	A	5	7
Ionic Strength	B	100 mM	200 mM
Yeast Extract Concentration	C	0 g.L <sup>-1</sup>	10 g.L <sup>-1</sup>
Transmembrane Pressure Difference	D	40 kPa	70kPa
Membrane Type	E	Cellulose nitrate (0.2µm)	PVDF (0.22µm)

The measured raw data, protein transmission and calculated specific cake resistance responses for each individual experiment are summarised in Table C.1 of Appendix C. These response data were then used to calculate the main effects and interactions using the methods described in Section 2.8.4.

#### 4.3.2 Factorial results analysis of protein transmission

Protein transmission levels were initially shown to be lower during microscale filtration when measured over short time periods ( $t \leq 90$  s). This was attributed to the presence of water in the hold-up volume of each filter insert that would dilute the permeate sample and also to low levels of protein adsorption that can rapidly occur in the early stages of microfiltration (Bowen and Gan, 1991). Time points towards the end of the filtration experiments ( $t \geq 300$  s) showed higher transmission levels and clearer variation between experiments. The single values of transmission quoted in this chapter are therefore from the latest time point available within the experiment.

Figure 4.1 shows the calculated effects and interactions for the measured protein transmission response during filtration. Each effect or interaction greater in magnitude than the dashed lines (95% confidence interval) is statistically significant. Whilst the magnitude can indicate the relative importance of an effect or interaction it is also dependant on the factor ranges investigated. The main effects, which quantify the influence of each individual factor on the calculated protein transmission, are summarised below.

- Increased pH (A) reduces the protein transmission considerably. This is a dominant effect since the magnitude is high.
- High ionic strength (B) improves protein transmission.
- The presence of yeast extract (C) acts to reduce the level of protein transmission. The magnitude of the effect is also high compared to the confidence intervals.
- Pressure (D) has no significant effect on protein transmission, as would be expected if the cake is not compressible over the range of transmembrane pressures investigated.

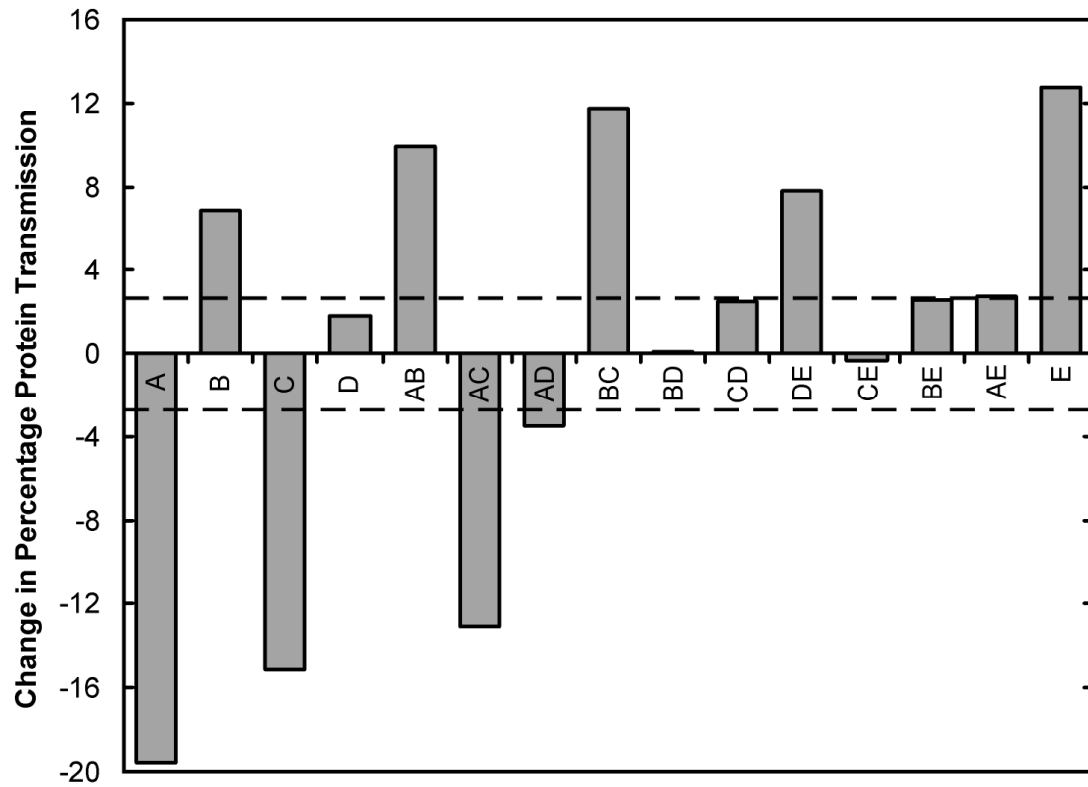


**Figure 4.1.** Effect and interaction plot for measured protein transmission levels in a  $2^{5-1}$  factorial experiment. Factors investigated are as follows: A = pH, B = ionic strength, C = yeast extract concentration, D = transmembrane pressure difference, E = Membrane Type. Factor levels detailed in Table 4.1. Experiments performed using a custom microwell filter plate ( $0.8 \text{ cm}^2$ ) as described in Section 4.3.1. The dashed lines represent 95% confidence intervals inside which effects and interactions are not statistically significant.

- The PVDF membrane gives better transmission than the cellulose nitrate membrane (E). This is easily explained since the cellulose nitrate membrane is specified as high protein binding by the manufacturer.

The interactions shown in Figure 4.1 give an indication of more complicated relationships between the individual factors. The AD and AE interactions are comparatively small in magnitude to the other main effects and interactions and are not significant at a 99% confidence interval. The DE interaction (transmembrane pressure / membrane type) is unexpected since the pressure does not influence transmission. Due to the half repeat in the factorial experiment design this interaction is also combined with the 3-factor interaction between pH, ionic strength and yeast extract (ABC). This rare three factor interaction is seen to be present when the raw data is examined. Two extreme outlying results (30.6%, 42.5%; as shown in Table C.1 of Appendix C) occur at pH 7 and 100 mM ionic strength only in the presence of yeast extract. These outliers also influence the individual interactions between yeast extract, pH and ionic strength (AB, AC, BC) which are shown to be clearly significant in Figure 4.1. The presence of yeast extract always acts to reduce protein transmission and does so to a much greater detriment at certain combinations of other factors.

In summary, optimal protein transmission should be achieved when the process is operated in the absence of yeast extract. Since pressure and membrane type do not interact with any other factors it can be concluded that the best transmission can be achieved anywhere within the pressure range 40 kPa – 70 kPa using the PVDF membrane. This leaves the ionic strength and pH interaction (AB) for further investigation and optimisation. This interaction is discussed in more detail in Section 4.3.4 with reference to the electrostatic forces that both factors will influence.

### **4.3.3 Factorial results analysis of specific cake resistance**

The calculated effects and interactions for the measured specific cake resistance response are summarised in Figure 4.2 in the same fashion as for the protein transmission results described in the previous section. High specific cake resistances

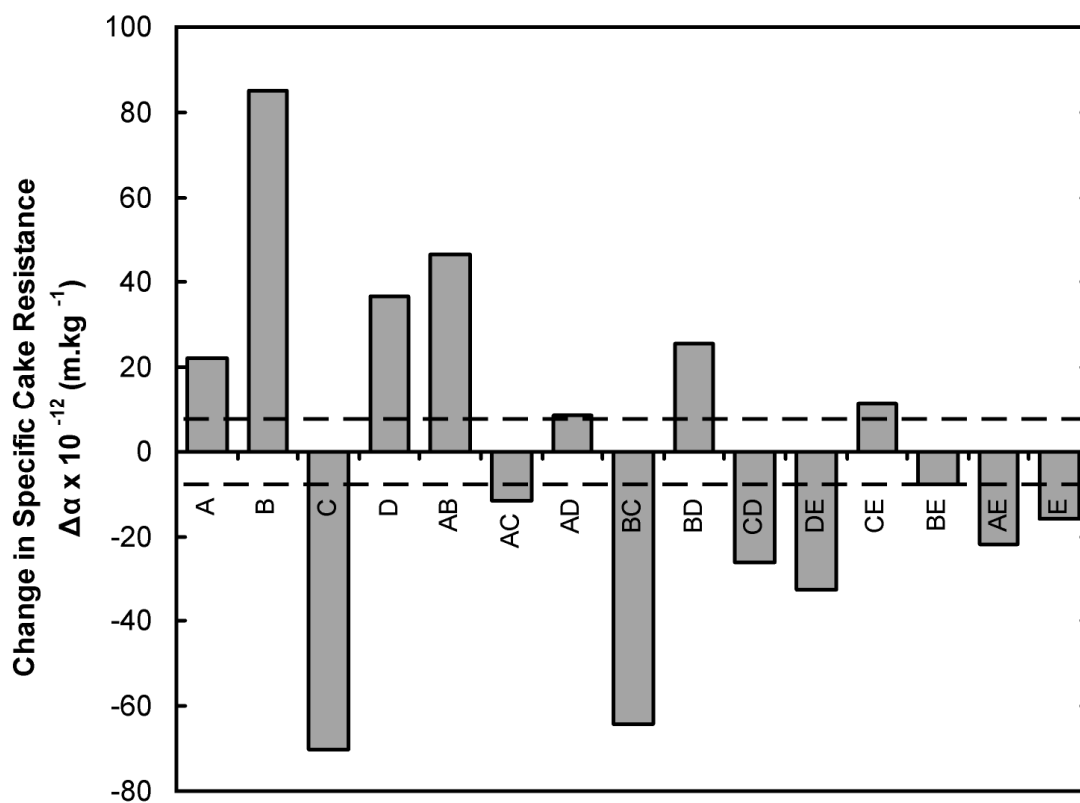


**Figure 4.2.** Effect and interaction plot for measured specific cake resistance values in a  $2^{5-1}$  factorial experiment. Factors investigated are as follows: A = pH, B = ionic strength, C = yeast extract concentration, D = transmembrane pressure difference, E = membrane type. Factor levels detailed in Table 4.1. Experiments performed using a custom microwell filter plate ( $0.8 \text{ cm}^2$ ) as described in Section 4.3.3. The dashed lines represent 95% confidence intervals inside which effects and interactions are not statistically significant.

are undesirable as they lead to reduced fluxes and longer overall processing times, as described in Section 1.3.4.1.4. The main effects, which quantify the influence of each individual factor on the calculated protein transmission are summarised below.

- pH (A) acts to increase the specific cake resistance at higher levels.
- High ionic strength (B) clearly increases the cake resistance and this effect has the highest magnitude.
- As described in Section 3.4.4, high yeast extract concentration (C) decreases the cake resistance and clearly allows higher permeate fluxes.
- The *E.coli* filter cakes formed during the experiments are compressible, but not to an excessive extent since high pressures (D) lead to only a moderate increase in specific cake resistance and collected volumes are always higher overall at the higher pressure.
- The main effect of membrane type (E) is the lowest in magnitude and shows that the PVDF membrane gives slightly lower specific cake resistance.

All of the interactions shown in Figure 4.2 exceed the confidence intervals and require interpretation. Despite the main effect of pH not being strong, there is a clear interaction with ionic strength (AB). Again yeast extract concentration interacts clearly with ionic strength (BC) which is likely to be due to a contribution to the overall ionic strength from components in the yeast extract. High ionic strengths and the absence of yeast extract lead to more compressible cakes (BD, CD) although compression is never severe enough to prevent the highest pressure in the range giving the highest permeate fluxes. Despite generally reducing cake resistance, the best filtration performance measured here is achieved in the absence of yeast extract at a particular combination of pH and ionic strength values (pH 7, 100mM), reversing the general trend and causing the three factor interaction (ABC = DE).

There is also another three factor interaction (BCD = AE) likely to be important. Given the three strongest main effects are ionic strength (B), yeast extract concentration (C) and pressure (D) this is also likely to be a three factor interaction. Examining the data it can be seen that the cakes appear to be more compressible at

combinations of high ionic strength and low yeast extract concentration. Data at this combination (factorial runs 3, 4, 11 and 12) dominates the interaction. For this interaction to be explained by a pH and membrane type (AE) it would require an explanation of why the specific cake resistance for cellulose nitrate increases at high pH. Since only a small portion of the cake is in contact with the membrane such a change is most likely to result from additional fouling at the surface or within the membrane. However, checks on the  $t/V$  against  $V$  intercept values from high pH and cellulose nitrate runs show no significant variation from other factorial runs and therefore suggests that no significant plugging or constriction is taking place (see Section 3.4.1) and the BCD interaction is more likely.

The remaining interactions (AC, AD, CE, BE) are all marginally significant and small in magnitude in comparison to the others discussed.

For optimal permeate flux performance the PVDF membrane should be used at the upper pressure limit. There is a more complex relationship between pH, ionic strength and yeast extract concentration and it is not obvious from the factorial experiment what the optimal conditions are for these factors. In a process where product recovery is important, high transmission will be essential. The improvements in flux from the presence of yeast extract are not studied further, due to its detrimental effect of transmission. Just as with the measured protein transmission response, the interaction between pH and ionic strength on specific cake resistance requires more examination and is described further in Section 4.3.4.

#### **4.3.4 Ionic strength and pH interactions**

With the dramatic changes in filtration performance that are possible by manipulating the electrostatic environment (van Reis *et al.*, 1999) it is not surprising that there is significant interaction between the pH (which can vary the charge on a species) and the presence of ionic species (which can mediate charge interactions) for this factorial study. The pI of lysozyme is at pH 10.7 (Walsh, 2002) and it will retain a net positive charge at all pH values used here. Millipore's Durapore PVDF has a slightly negative zeta-potential over the pH range of this study which increases in magnitude with

increasing pH (Raghavan *et al.*, 1996). The cellulose nitrate membranes also typically exhibit negative zeta-potentials over a wide pH range (Tarleton and Wakeman, 1994). Electrostatic interactions between the membrane and target protein are possible but there are also the complex *E.coli* cells to consider.

The interaction plots shown in Figures 4.3 and 4.4 provide a graphical representation of the interaction values for pH and ionic strength summarised in the earlier effects plots (Figures 4.1 and 4.2). There is a clear interaction for the protein transmission response as similar transmissions measured at low pH reduce to different extents depending upon the ionic strength level (Figure 4.3). The worst transmission is at the combination of high pH and low ionic strength. This appears as if it could be explained by an interaction between lysozyme and the membranes, but later data (Section 4.4) will link the poor lysozyme transmission to an interaction with a component within the cake layer. The centre-point value, which lies away from the linear interpolations, also suggests this is a non-linear interaction. More data points are required to show the behaviour of protein transmission over the entire range of pH and ionic strength combinations.

As previously discussed, the interaction for transmission is strongly influenced by the outlying data at pH 7, 100mM ionic strength and 10g/L yeast extract concentration. Examining the data for PVDF membrane and 0g/L yeast extract shows that the two lowest protein transmission values are the replicates for pH 7 and 100mM and the same interaction as shown in Figure 4.3 is indicated, however statistical significance cannot be proved. These factors may still interact in the absence of yeast extract with the PVDF membrane, with the centre-point variation still suggesting an interesting non-linear response.

Figure 4.4 demonstrates the effect of the pH and ionic strength interaction on the measured specific cake resistance. At low ionic strength the cake resistance reduces with increasing pH, yet at high ionic strength it increases with increasing pH. Once more the centre-point of the experiments indicates a non-linear relationship and further experiments must be performed to determine the full shape of the interaction.

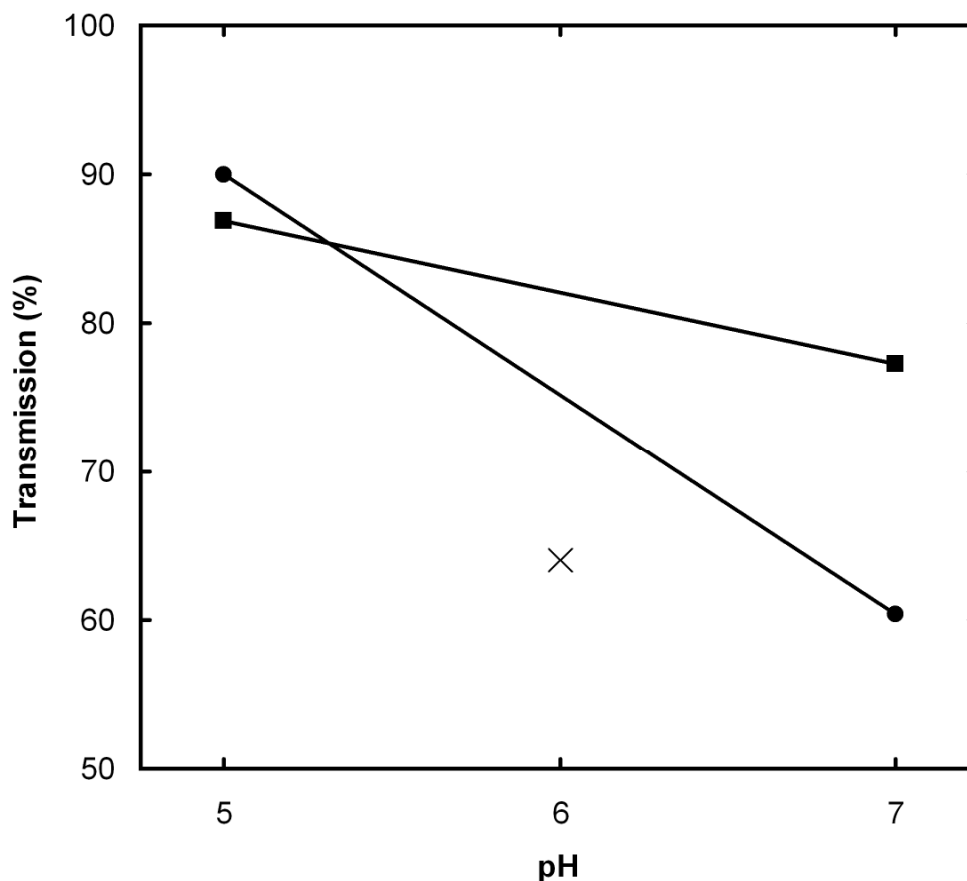


**Figure 4.3.** Interaction plot showing the measured variation of protein transmission with pH at ionic strengths of 100mM (●) and 200mM (■). Data points represent the average from runs during a  $2^{5-1}$  factorial experiment. The centre-point of the factors in the experiment is also included (×). Solid lines indicate assumed linear relationships which should pass close to the centre point if this assumption holds. Experiments performed using a custom microwell filter plate ( $0.8 \text{ cm}^2$ ) as described in Section 4.3.4.

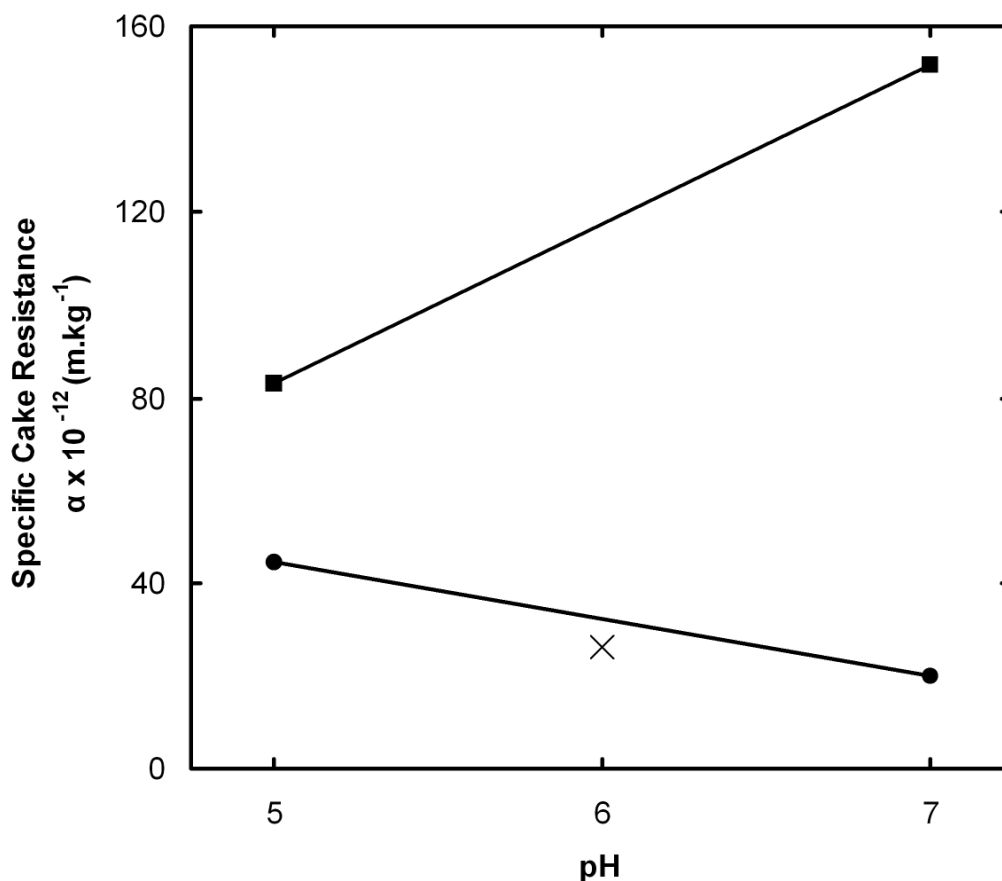


**Figure 4.4.** Interaction plot showing the measured variation of specific cake resistance with pH at ionic strengths of 100mM (●) and 200mM (■). Data points represent the average from runs during a  $2^{5-1}$  factorial experiment. The centre-point of the factors in the experiment is also included (×). Solid lines indicate assumed linear relationships which should pass close to the centre point if this assumption holds. Experiments performed using a custom microwell filter plate ( $0.8 \text{ cm}^2$ ) as described in Section 4.3.4.

It is notable that from the factorial data it appears that the best filtration performance coincides with the worst transmission at the combination of pH 7 and 100 mM ionic strength. A trade-off is thus likely to be required between the differing optimum values for protein transmission and permeate flux.

#### **4.4 Response surface experiments**

The factorial experiments described in Section 4.3 have focused in on the pH and ionic strength interaction as the important experimental space for further examination. The previous interaction plots from the screening experiments (Figures 4.3 and 4.4) suggest that whilst these areas may be of interest for the individual protein transmission and specific cake resistance responses, a trade-off between the two giving optimal process performance is unlikely to be located in the corners of the response surfaces. Consequently an inscribed central composite design (CCD) design was selected to give more predictive power in the centre of the design space compared to the edges. Response surfaces of protein transmission and specific cake resistance were generated using an inscribed CCD as described in Section 2.6.2.

Based on the earlier factorial data, experiments here were operated in the absence of yeast extract, using the 0.22 $\mu$ m PVDF membrane under a 60 kPa transmembrane pressure difference.

All experiments were carried out in parallel using the 24-well custom microwell filter plate (Section 3.2.1) according to the method described in Section 3.4.1. Samples were prepared as described in Section 2.4. In the same way as for the factorial experiments, the longer time permeate samples collected were assayed as described in Section 2.6.1. The response surface was replicated with samples in the absence of lysozyme.

The measured raw data, protein transmission and calculated specific cake resistance responses for each individual well are summarised in Tables C.2 and C.3 of

Appendix C. These response surface data were then fitted to linear or quadratic models using the methods described in Section 2.8.4.

#### 4.4.1 Response surfaces for pH and ionic strength

The measured variation in protein transmission due to pH and ionic strength changes within the CCD experimental space is shown in Figure 4.5. The response surface shows a broad optimal transmission level (>95%) occurs at low pH and mid-range ionic strengths. A clear interaction is shown since a large drop in transmission occurs (to <70%) at the combination of low ionic strength and high pH as previously suggested in the screening experiments (Figure 4.3). The following quadratic model is used in Figure 4.5 to describe percentage protein transmission ( $T_p$ ) as a function pH ( $pH$ ) and ionic strength ( $I$ , mM) in the range pH 5 – 7 and 79.3 mM – 220.7 mM:

$$T_p = 5.84 \times 10^1 + 1.20 \times 10^1 pH + 1.30 \times 10^{-1} I + 7.74 \times 10^{-2} pH \cdot I - 2.45 \times 10^0 pH^2 - 1.69 \times 10^{-3} I^2 \quad (4.1)$$

The corresponding specific cake resistance response surface from data collected in parallel in the same automated microwell experiments is shown in Figure 4.6(a). Again a clear interaction can be seen similar to that predicted from the factorial data (Figure 4.4). At high ionic strength increasing pH increases cake resistance, whereas the opposite is true at low ionic strength. Cake resistance decreases sharply towards low ionic strengths and high pH values where an area of low cake resistance and consequently high permeate flux can be seen. The values of cake resistance here (some lower than  $10^{13}$  m.kg<sup>-1</sup>) are much lower than those seen in Chapter 3 and correspond to the poorest transmission levels. It is likely that the lysozyme is influencing the low cake resistance by forming part of the cake itself or influencing cake structure, which explains the low transmission. This is confirmed by Figure 4.6(b), which shows the variation in specific cake resistance with pH and ionic strength in the absence of lysozyme. Little or no variation occurs due to pH (as described in Section 3.4.3) and cake resistance decreases with ionic strength. No interaction is evident, since the response surface is mostly constant across the pH axis. The data is described by a linear model, since it gives a better fit than the quadratic

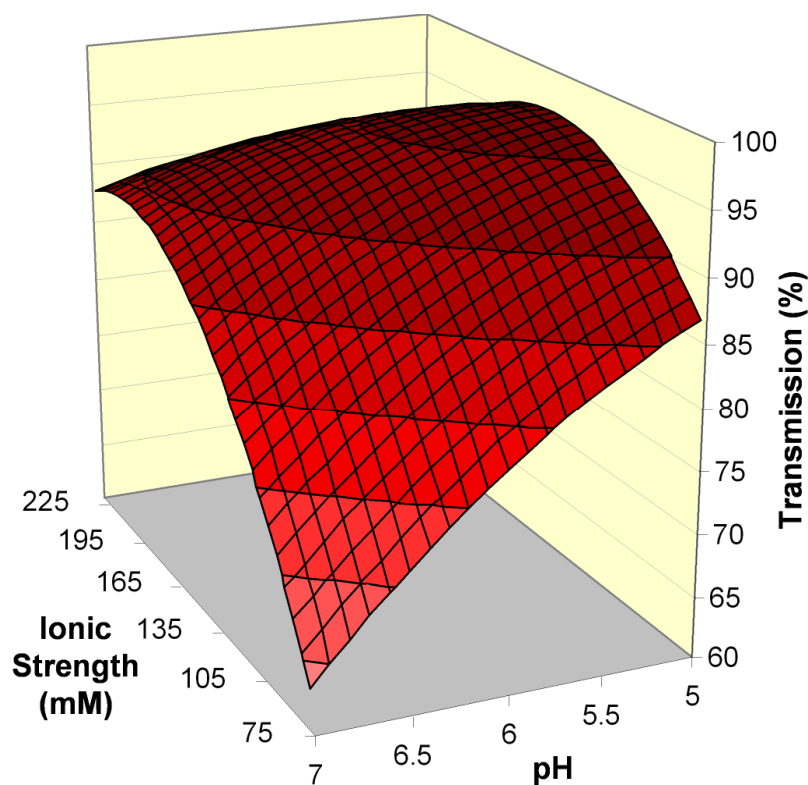


**Figure 4.5.** Response surface plot of a model describing protein transmission as a function of pH and ionic strength. Surface generated using an inscribed central composite design and applying a quadratic model fitted by multiple regression ( $R^2_{\text{adj}} = 0.508$ ). Response surface model calculated as described in Section 2.8.5. Experiments performed using a custom microwell filter plate ( $0.8 \text{ cm}^2$ ) as described in Section 4.4.

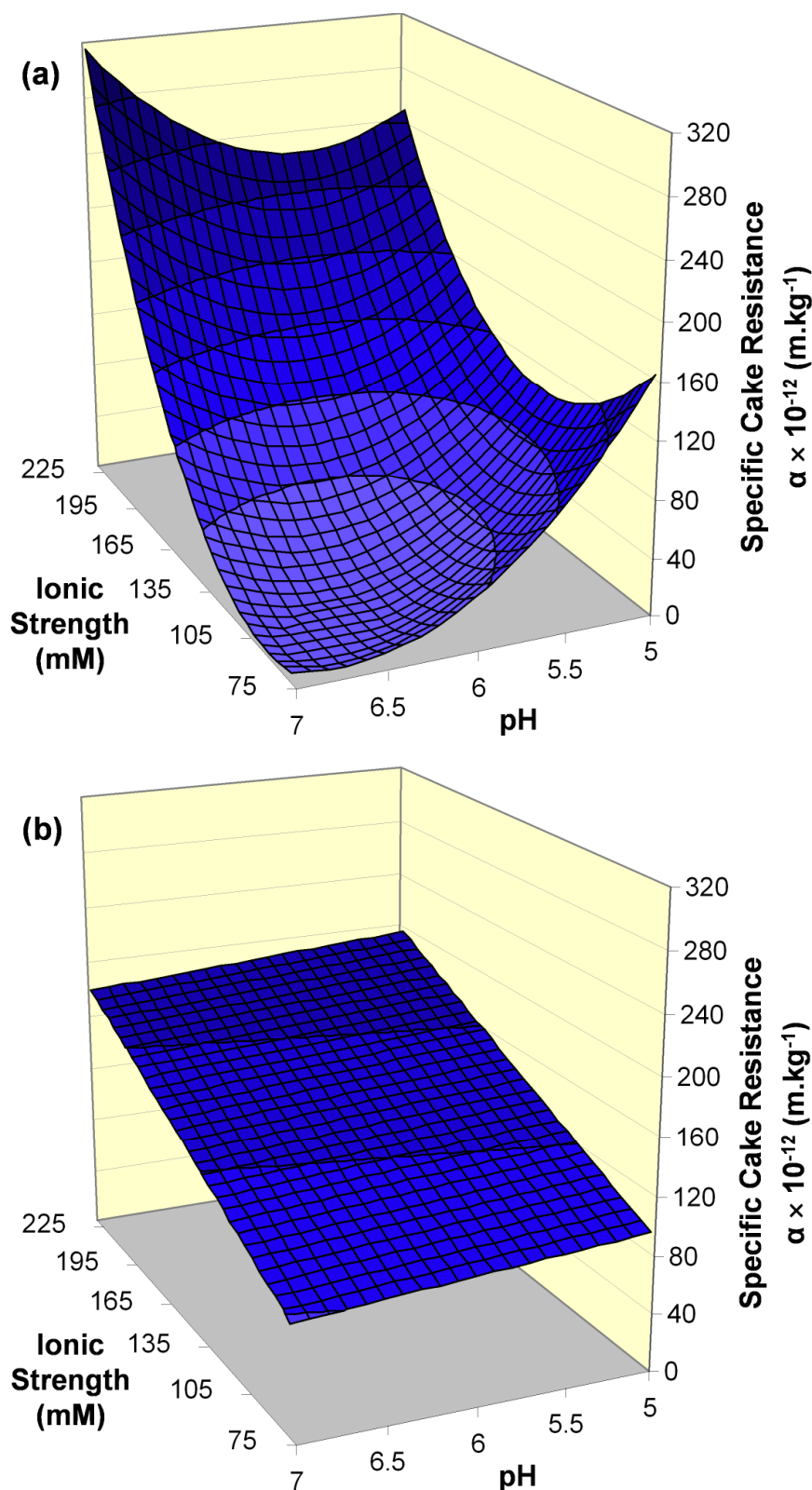


**Figure 4.6.** Response surface plots of models describing specific cake resistance as a function of pH and ionic strength. Surfaces generated using central composite designs and fitted by multiple regression: (a) in the presence of  $2 \text{ g.L}^{-1}$  protein (quadratic model,  $R^2_{\text{adj}} = 0.901$ ) and (b) in the absence of protein (linear model,  $R^2_{\text{adj}} = 0.531$ ). Response surface models calculated as described in Section 2.8.5. Experiments performed using a custom microwell filter plate ( $0.8 \text{ cm}^2$ ) as described in Section 4.4.

model according to the adjusted R-squared values (Section 2.8.5.1). Values of cake resistance in the absence of lysozyme are also consistent with the results in Chapter 3. Clearly the lysozyme is required to reach the low cake resistances seen in Figure 4.6(a) and must directly influence the cake formation. The following quadratic model is used in Figure 4.6(a) to describe specific cake resistance ( $\alpha$ ) in  $\text{m.kg}^{-1}$  as a function pH ( $pH$ ) and ionic strength ( $I$ , mM) in the range pH 5 – 7 and 79.3 mM – 220.7 mM:

$$\alpha = 2.91 \times 10^{15} - 7.59 \times 10^{14} pH - 8.41 \times 10^{12} I + 7.40 \times 10^{11} pH.I + 5.22 \times 10^{13} pH^2 + 1.76 \times 10^{12} I^2 \quad (4.2)$$

Comparing Figures 4.5 (protein transmission) and 4.6(a) (specific cake resistance) there are conflicting trends between the optimum operating conditions for high protein transmission and low specific cake resistance (high permeate flux). A process trade-off is therefore required between high protein transmission at an acceptable permeate flux.

#### 4.4.2 Microfiltration window of operation

By overlaying the two-dimensional contour plots derived from the response surfaces shown in Figure 4.5 and Figure 4.6(a) it is possible to visualise a window of operation (Woodley and Titchener-Hooker 1996; Zhou and Titchener-Hooker, 1999) where certain trade-off conditions are satisfied. This overlay plot is shown in Figure 4.7. Excellent recovery of the target protein is a high priority in most bioprocess applications and so a minimum 95% transmission is chosen. An acceptable specific cake resistance is considered to be below  $8 \times 10^{13} \text{ m.kg}^{-1}$ , corresponding to an average permeate flux of approximately  $30 \text{ L.m}^{-2}.\text{h}^{-1}$  for a 1 h process. The Window of Operation in which both these criteria are satisfied is highlighted in purple on Figure 4.7. In terms of experimental space it is small, but the pH and ionic strength are factors that can be accurately controlled. Feed streams having an ionic strength of  $153 \pm 8 \text{ mM}$  and a pH of  $5.5 \pm 0.1$  thus represent the optimum conditions for operation of the microfiltration process.

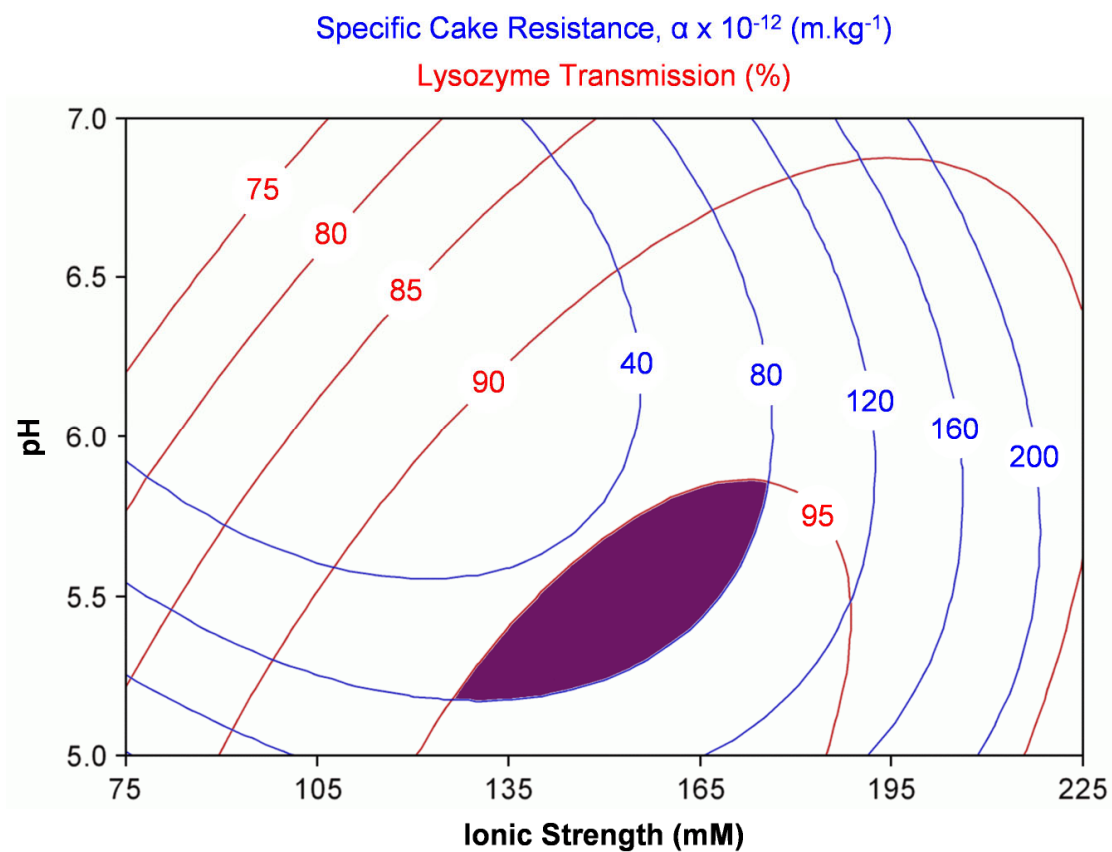


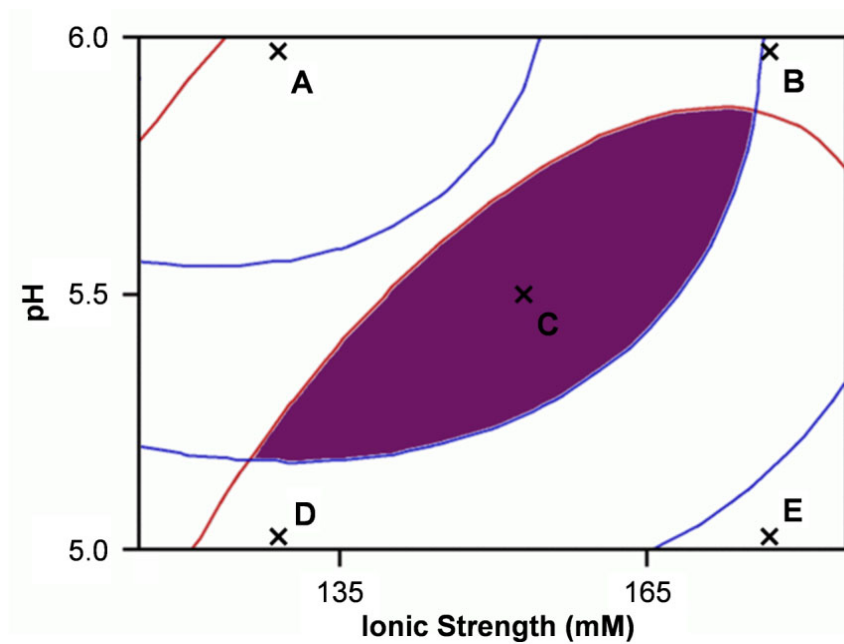
**Figure 4.7.** Overlay of the specific cake resistance (blue) and protein transmission (red) contour plots derived from the individual response surface models (Figures 4.5 and 4.6). Shaded area indicates feasible Window for Operation for the chosen optimum trade-off conditions (purple). Further discussion in Section 4.4.2.

## 4.5 Scale-up of optimum microfiltration conditions

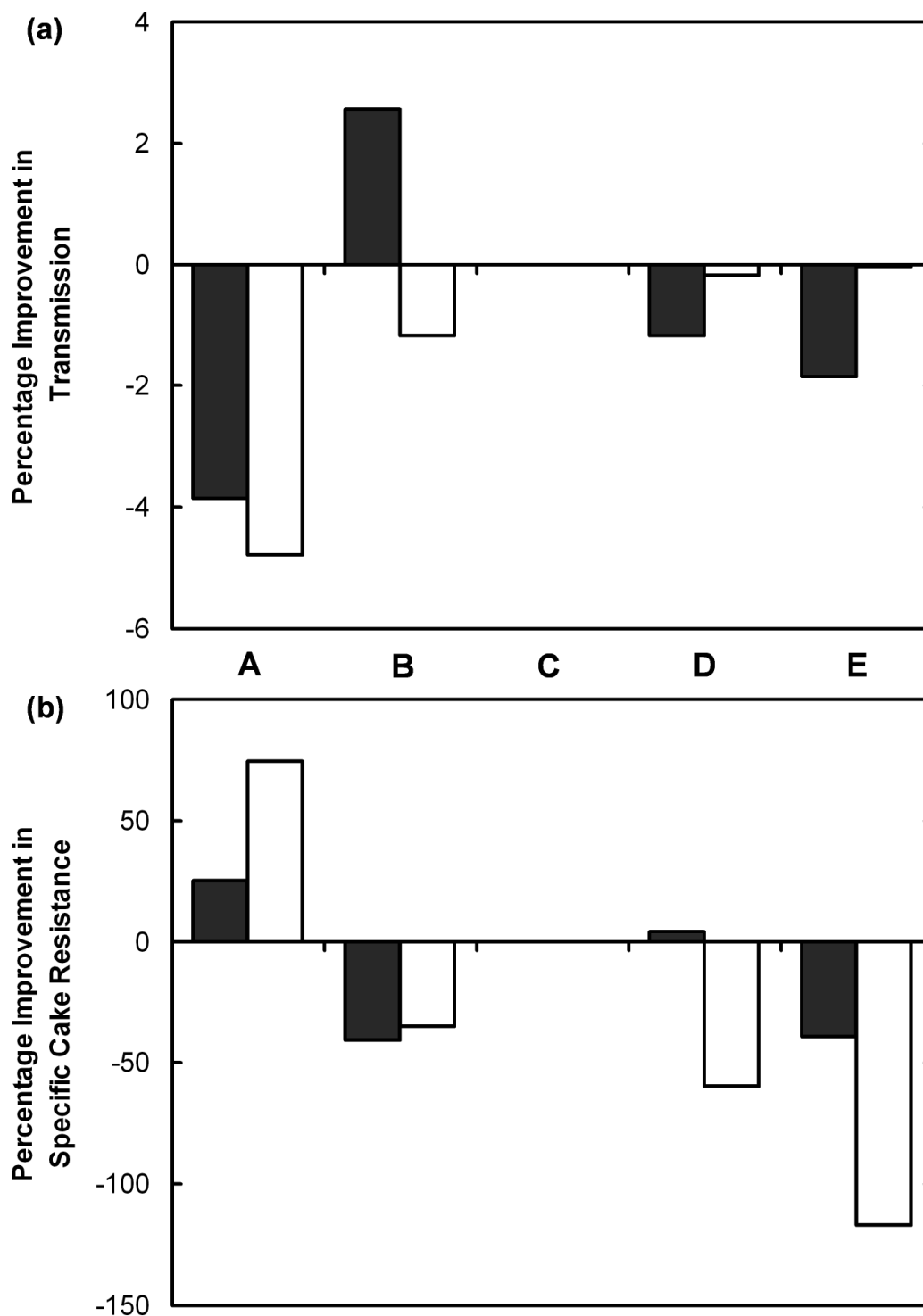
To demonstrate the scalability of the microwell data, experiments were carried out in and around the Window of Operation identified in Section 4.4.2 using a membrane cell with a filtration area of  $13.2 \text{ cm}^2$ . This is approximately 17 times the area of the custom microwell filter plate insert used in the previous response surface experiments. Figure 4.8 shows the 5 chosen experimental verification conditions tested at laboratory scale labelled A-E. If the microscale data are correct they will accurately predict the performance of the laboratory scale equipment and in addition the membrane cell will show that experiment C (pH 5.5, 153 mM) gives the optimum balance between protein transmission and specific cake resistance. No point outside the window of operation should give both better transmission and flux behaviour than the optimum conditions (C). Experiments were carried out as described in Section 2.3.3, using feeds prepared as described in Section 2.4. The custom microwell filter data are derived from the quadratic models fitted to the response surface data in Section 4.4 (Equations 4.1 and 4.2).

Figure 4.9 shows the percentage improvement in the measured protein transmission and specific cake resistance for each experiment with reference to experiment C for the membrane cell and the same data predicted from the response surface models. The results clearly show that when the conditions deviate from the optimum levels the performance of the microfiltration process declines. Where the transmission increases (B) there is a corresponding increase in the resistance to filtration and a decrease in flux. Where the specific cake resistance and flux improves (A) there is an unacceptable reduction in transmission. These results confirm that the process is best carried out within the Window of Operation defined by Figure 4.7.

Figure 4.9 also shows that the microwell predictions show a close correlation to the membrane cell experiments and although variations are seen, it should be noted that the data shown here depends heavily on the values of transmission and cake resistance at C, against which the other data is compared. The prediction of the optimum levels of pH and ionic strength are thus considered scalable from microwell to laboratory scale.



**Figure 4.8.** Overlay plot of factor ranges in and around the optimum pH and ionic strength trade-off conditions (purple shaded area) tested at laboratory scale using a membrane cell (13.2 cm<sup>2</sup>). Experiments described in Section 4.5 and subsequent results presented in Figure 4.9. Contours as indicated on Figure 4.7.



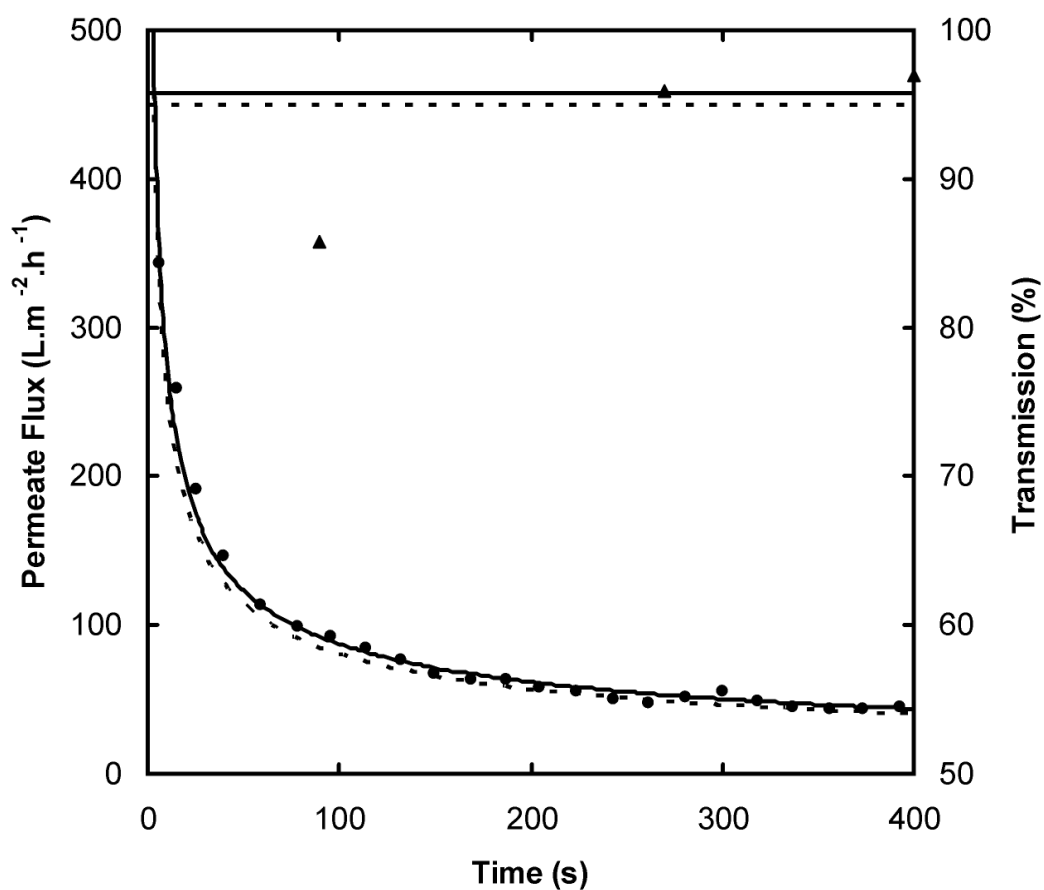
**Figure 4.9.** Analysis of membrane cell experiments carried out in and around the optimum trade-off conditions. Figures indicate the percentage improvement of (a) lysozyme transmission and (b) specific cake resistance in comparison to the predicted optimum, C. Dark bars are the membrane cell (13.2 cm<sup>2</sup>) data and light bars are the custom microwell filter plate (0.8 cm<sup>2</sup>) predictions. Conditions for experiments A-E shown in Figure 4.8 and experiments performed as described in Section 4.5. Pressure difference 60 kPa.

Figure 4.10 shows more detailed filtration characteristics for the optimum conditions of pH 5.5 and 153mM ionic strength using a Millipore 0.22 $\mu$ m PVDF membrane in the absence of yeast extract operated at 60kPa pressure difference. Scale-up data from the membrane cell is presented alongside microscale predictions, calculated using Equations 4.1 and 4.2 and the scale up equations in Section 2.8.7.1. The transmission starts low, as previously noted at the microscale in Section 4.3.2, and then rises above 95% to the levels predicted by the custom microwell filter plate. The flux shows close correlation between the two scales and is above the values corresponding to the maximum specific cake resistance of  $80 \times 10^{12} \text{ m.kg}^{-1}$ . In addition to the close agreement of the dynamic variation of process performance at the optimum shown in Figure 4.9, the optimum conditions predicted at the microscale also scale-up to predict the protein transmission and flux during a laboratory scale membrane cell experiment.

## 4.6 Summary

The automated microscale normal flow microfiltration techniques established in Chapter 3 have been combined here with factorial experimentation to identify the key factors and interactions which influence protein transmission and specific cake resistance during filtration of an *E.coli*-protein mixture. Both permeate flux and protein transmission could be determined in parallel from the same microwell experiments, increasing the process insight that can be gained from each experiment.

The initial factorial scouting experiments (Section 4.3) identified pH and ionic strength to be the most significant factors and showed the existence of a strong 2-factor interaction (Figures 4.3 and 4.4). The pH and ionic strength interaction was further investigated using response surface methodology (Section 4.4) and a Window of Operation was generated showing optimum operating conditions (Figure 4.7). The pH and ionic strength values necessary to achieve a transmission above 95% and a specific cake resistance below  $80 \times 10^{12} \text{ m.kg}^{-1}$  were pH  $5.5 \pm 0.1$  and  $153 \pm 8 \text{ mM}$ . The ability to rapidly perform the necessary experiments using only millilitres of feed material (288mL in total for scouting of 5 factors and response surface optimisation)



**Figure 4.10.** Scale-up of optimum microfiltration conditions showing permeate flux (●) and protein transmission (▲) during a membrane cell ( $13.2 \text{ cm}^2$ ) experiment. Solid lines represent predictions from custom microwell filter plate ( $0.8 \text{ cm}^2$ ) data using Equation 2.20. Dashed lines represent the minimum acceptable values selected for successful operation of the process. Experiments performed as described in Section 4.5. Pressure difference 60 kPa.

further confirms the utility of parallel microscale experimentation. The application of DoE methodology enables a reduction in the number of experiments to be performed and also identifies factor interactions which are missed in conventional experimental approaches.

Finally, the custom microwell filter plate specific cake resistance and protein transmission values predicted from the response surface models were shown to scale up by a factor of 17 to conventional laboratory scale equipment. The results showed that the optimum permeate flux and protein transmission conditions achieved in the microwell could be replicated at a larger scale (Figure 4.10). In addition, drops in process performance predicted at the microscale when process conditions deviated from the optimum were also observed at laboratory scale (Figure 4.9).

In summary, the combination of experimental design and automated microwell experimentation has been shown to be capable of investigation, optimisation and scale-up of a complex separation step. In Chapter 5, this utility of the combined DoE-microwell microfiltration approach is applied to the investigation of a whole process sequence using multiple filtration operations and an industrially relevant product.

---

## **5.0 Automated microscale plasmid DNA purification process sequence**

### **5.1 Aim of the chapter**

The aim of this chapter is to illustrate the operation of an automated microscale process sequence and demonstrate that the results obtained are scaleable. The specific objectives are as follows:

- To apply the combination of statistical experimental design and automated microwell experimentation demonstrated in Chapter 4 to a whole bioprocess sequence.
- To quantify the interdependancies and effects of multiple factors spread throughout 7 consecutive stages of an appropriate non-chromatographic process for plasmid DNA purification that might be used in industrial practice.
- To illustrate that performance and key process trends in laboratory and pilot scale filtration equipment can be predicted from data generated at microscale.

### **5.2 Plasmid DNA purification**

The potential application of plasmid DNA (pDNA) in the area of gene therapy and DNA vaccination has led to the need for scalable recovery and purification strategies. Large-scale purification of pDNA from clarified cell lysate has been attempted by a wide range of chromatographic techniques, such as ion-exchange, reverse-phase and affinity resins (Ferreira *et al.*, 2000). However, at large manufacturing scale (>10 m<sup>3</sup>) such chromatographic techniques might be prohibitively expensive due to the low

binding capacity of most resins for large pDNA molecules (Prazeres *et al.*, 1999; Diogo *et al.*, 2005).

The continued threat of a bird flu pandemic (Abbott and Pearson, 2004) is driving the need for rapid production of a vaccine in sufficient quantities. One viable option is the use of a pDNA vaccine which could be produced in large quantities using existing facilities (Hoare *et al.*, 2005). Investigating different pDNA purification operations along with their scale-up characteristics is of importance to gain insight into alternative process routes and the likely purity and yield of pDNA that could be obtained. A suite of scaleable microscale unit operations would allow the rapid evaluation of multiple process options if coupled with appropriate liquid handling robotic platforms (Micheletti and Lye, 2006).

This chapter will evaluate precipitation and adsorption based processes for the isolation of a pDNA vaccine, such as H5NI (Claas *et al.*, 1998), using microscale normal flow filtration (NFF) as the solid-liquid separation method of choice. Scale-up studies to investigate the ability of microwell filtration to predict up to pilot scale will also be carried out.

### 5.2.1 Non-chromatographic process

A typical process for a non-chromatographic pDNA purification strategy is shown in Figure 5.1. More details about the individual unit operations are listed in Section 2.4.2. One of the main characteristics of the process is that the volume of process fluid remains relatively constant throughout, allowing the entire process sequence to be run at microscale without sample volumes falling to a level from which it is impossible to obtain accurate and reliable quantification of key process variables.

The high purification duties carried out by chromatographic systems is achieved by using selective cetyltrimethylammonium bromide (CTAB) precipitation to capture the pDNA (Lander *et al.*, 2002) and by polishing using hydrated calcium silicate lipid removal agent (LRA) to remove contaminants (Winters *et al.*, 2003).

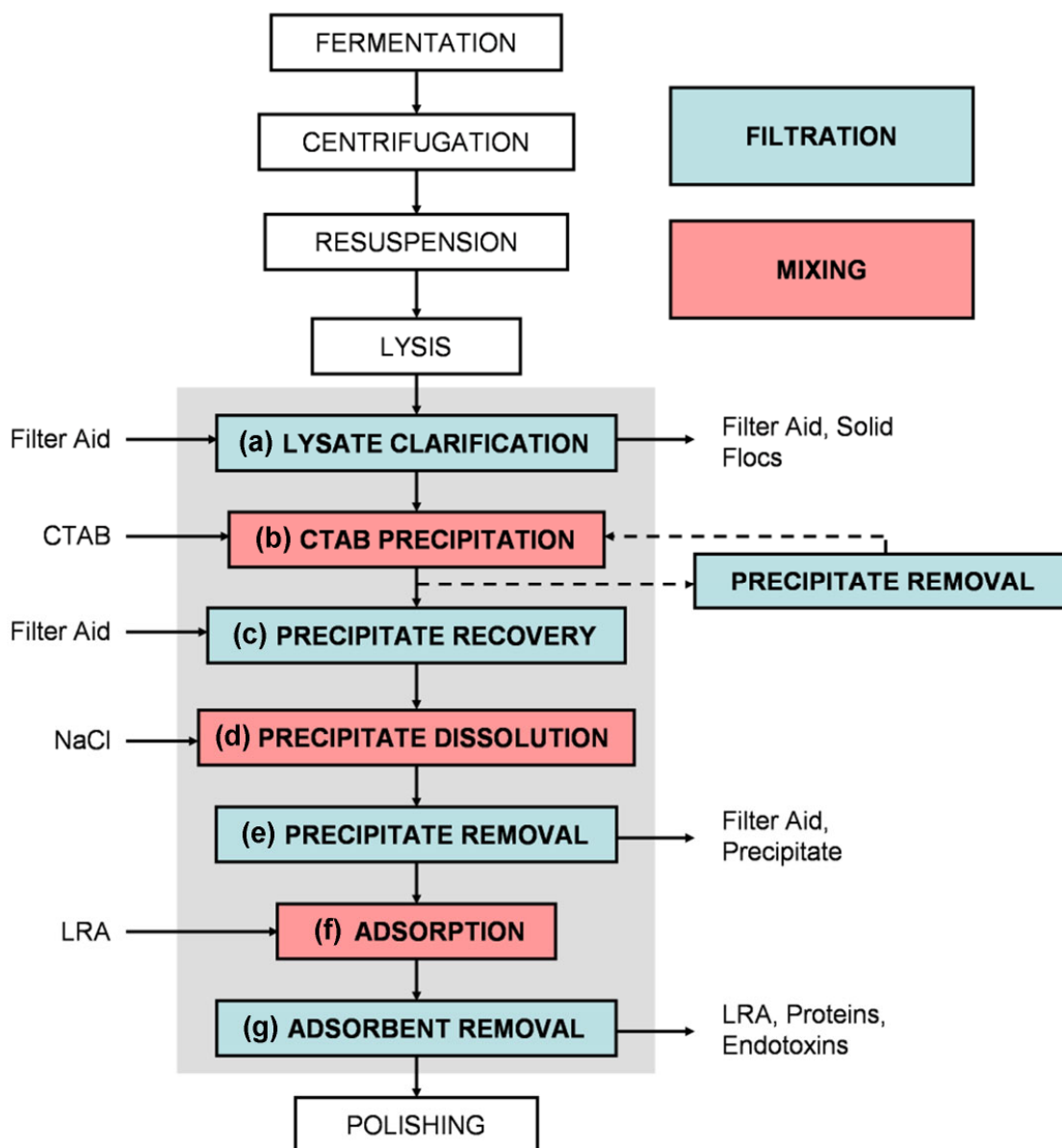


**Figure 5.1.** Overview of a non-chromatographic process for the production and purification of plasmid DNA. The shaded area represents the process sequence examined in this chapter using microwell filtration (blue) and microwell mixing (red) operations. CTAB = cetyltrimethylammonium bromide, LRA = lipid removal agent.

### 5.2.2 Automated microwell process

A summary of the individual processes involved in the whole plasmid purification sequence is shown in Table 5.1. Available methods for mimicking the large scale process using automated microscale techniques are also listed. At the heart of the 7-step process are the CTAB precipitation and LRA adsorption steps. Both of these can be investigated using the microscale microfiltration technique established in Chapter 3 to determine the flux performance of solids removal / recovery steps and the yield and purity of the purified pDNA. Along with microscale mixing operations, this allows a whole process sequence to be automated on the deck of the Tecan robotic platform (Section 2.3.2).

One difficulty in adapting automated microwell operations to the purification process is the recovery of precipitate. Separation of the precipitate by filtration is simple, subsequent recovery of the cake, however, is not easily achieved in an automated manner. During the studies described in this chapter, the automated experiment was stopped and the cake was carefully removed manually. Test experiments have been carried out demonstrating that the removal of these filter cakes is simply achieved by inverting the custom filter inserts and gently centrifuging. Design and construction of appropriate centrifuge holder plates could allow the safe, automated and integrated removal of filter cake in the future. This precipitate recovery stage also requires a flow through of buffer for quantification of cake resistance, but this is not a large departure from the full scale process since a washing step may often occur here to remove excess waste entrained in the cake.

Cake resistance calculations developed in Chapter 3 are not directly applicable here when adapting the pDNA process to microscale. This is due to the settling nature of the feeds involved which would skew the filterability profiles due to a higher solids challenge at earlier times, leading to inaccurate results. The method adopted in this chapter therefore involves completion of the filtration and measurement of flux through a pre-deposited cake to determine the specific cake resistance. The technique outlined in Section 3.3.1 for the quantification of membrane resistance is used to calculate the total cake, pre-coat and wire mesh resistance. Assuming that the mesh

**Table 5.1.** Summary of the individual unit operations involved in a typical non-chromatographic purification process for plasmid DNA showing factors and process decisions that need to be investigated. Chosen factors to investigate in this chapter are shown in bold.

<b>Unit Operation</b>	<b>Automated Microscale Process Mimic</b>	<b>Factors and Process Decisions Requiring Investigation</b>
Fermentation	Incubated, shaken microwell plate	Temperature, media composition, feed strategy, time, oxygen transfer, mixing conditions, inoculation conditions.
Cell Recovery	Centrifuged microwell plate or custom filter plate	Choice of operation, centrifuge type, rotational speed, flowrate, additions, concentration factor, washing.
Resuspension	Difficult to achieve due to handling of cell pastes.	Buffer conditions, mixing conditions, final concentration.
Lysis	Difficult to achieve due to high viscosities involved and mixing requirements	Lysis buffers, <b>mixing speed</b> , addition rates, mixing times.
Lysate Clarification	Custom filter plate	<b>Filter aid type, filter aid concentration, permeate recycling</b> , pre-coat thickness and type, settling.
CTAB Precipitation	Shaken microwell plate	Mixing speed, CTAB concentration and solution conditions, addition rate, mixing time, two cut process.
Precipitate Recovery	Custom filter plate and centrifugation for solids recovery	<b>Filter aid type, filter aid concentration</b> , washing, pre-coat thickness and type.
Precipitate Dissolution	Shaken microwell plate	Salt concentration, salt type, addition rate, <b>mixing speed</b> , mixing time.
Precipitate Removal	Custom filter plate	Cake washing, extra filter aid addition, pre-coat thickness and type.
LRA Adsorption	Shaken microwell plate or packed adsorption plate	<b>LRA concentration, time</b> , buffer conditions, addition rate, temperature, mixing conditions, batch or flow-through.
LRA Removal	Custom filter plate	Filter aid additions, pre-coat thickness and type, partial settling.
Final Polishing	Limited solutions	Factors dependant on process choices

and pre-coat resistances are negligible compared to the cake resistance, Equation 1.17 for the cake resistance can be combined with Equation 3.2 to calculate the specific cake resistance,  $\alpha$  ( $\text{m.kg}^{-1}$ ):

$$\alpha = \frac{A^2 \int \Delta P . dt}{\mu \rho_0 V_t V_c} \quad (5.1)$$

The following symbols relate to the properties of the feed during deposition of the cake:  $\rho_0$  is the mass of solids per unit volume of liquid ( $\text{kg.m}^{-3}$ ),  $V_c$  is the liquid volume in the original feed sample ( $\text{m}^3$ ). The following symbols relate to the properties during flow-through evaluation of the cake resistance:  $\int \Delta P . dt$  is the area under the pressure-time profile generated ( $\text{N.s.m}^{-2}$ ),  $\mu$  is the viscosity of the solution used for flow through the deposited cake ( $\text{N.s.m}^{-2}$ ) and  $V_t$  is the flow-through permeate volume.  $A$  is the effective filtration area, common to both cake deposition and flow-through ( $\text{m}^2$ ). If the viscosity of the permeate generated during cake deposition and the viscosity of the flow-through solution are approximately equal then the modified cake filtration constant,  $K_c'$  ( $\text{s.m}^{-2}$ ), can be used for scale-up when evaluated as follows:

$$K_c' = \mu \alpha \rho_0 = \frac{A^2 \int \Delta P . dt}{V_t V_c} \quad (5.2)$$

Details of the appropriate flow-through solutions used at the various microscale filtration steps are given in Section 2.5.2. The difficulties in evaluating  $\rho_0$  for the complex lysate feed necessitates the use of average flow-through flux, normalised to the equivalent flux at 60 kPa, as the measured response for lysate clarification. This does not interfere with accurate scale-up since Equation 5.2 does not require determination of the solids mass content.

The approach adopted for sample collection is to only assay the final product material at the end of the entire process sequence. This allows volumes to be maintained during the whole process sequence and prevents the need for sacrificial experiments run only up until a specific point in the process. This also has the advantage that it

limits the analysis burden and total number of experiments significantly. There is some risk that certain process combinations might cause significant reductions in product in the middle of the process that might be difficult to pick up. However, the coding of the experiments (described in Section 2.7.1.2) will be likely to reveal the exact factor responsible for a failure, even if it occurs in the middle of the process.

Finally, selections of some of the factors or process decisions that can be investigated in this whole process sequence are also listed in Table 5.1. This is by no means a comprehensive list and there are over 50 items listed to investigate. Experimental design (as used in Chapter 4) coupled with high-throughput automated microscale techniques (as established in Chapter 3) will be key to enabling the investigation of all these variables and their interactions across individual unit operations in the sequence. Prior process knowledge must also play a part to focus these designs and to select the most appropriate factors and ranges at each step.

### 5.2.3 Factorial design

The large number of experiments necessary to investigate a whole process sequence clearly calls for Design of Experiments (DoE) methods to be employed. The chosen factors highlighted in Table 5.1 for investigation are detailed, with their coding and selected factor ranges in Table 5.2. The fractional factorial design employed is described in Section 2.6.1.2. The chosen ranges expand on existing experience of pilot scale work (Hoare *et al.*, 2005) and try to vary the nature of the process streams to demonstrate that the microwell approach can correctly identify quantitative differences in process performance. The Celpure filter aid used in this design is available in discrete grades corresponding to the coarseness of the particles. The Celpure grade number is a quantification of permeability in millidarcies, but there is no intermediate grade and therefore the factor is qualitative, with the centre-point using a 50/50 mixture of each grade.

As can be seen in Table 5.3, a factorial design for a process sequence forms an approximately pyramidal structure. The key responses measured throughout the

**Table 5.2.** Summary of the factors and their chosen levels for the plasmid DNA process sequence  $2^{8-2}$  factorial experiment. Experiments performed as described in Section 2.5.2, according to the factorial design in Section 2.7.1.2.

Factor	Factorial Code	Low Value (-1)	High Value (+1)	Centre-Point (0)
Celpure Grade	A	P65	P300	50% P65 / 50% P300
Lysis Neutralisation Mixing Speed	B	400 rpm	1200 rpm	800rpm
Celpure Concentration for Lysis Clarification	C	30 g.L <sub>lysate</sub> <sup>-1</sup>	50 g.L <sub>lysate</sub> <sup>-1</sup>	40 g.L <sub>lysate</sub> <sup>-1</sup>
Number of Permeate Recycles During Lysis Clarification	D	0	2	1
Celpure Concentration for Precipitate Removal	E	2 g.L <sub>liquid</sub> <sup>-1</sup>	10 g.L <sub>liquid</sub> <sup>-1</sup>	6g.L <sub>liquid</sub> <sup>-1</sup>
Dissolution Mixing Speed	F	Low	High	Medium
LRA Concentration	G	6.7 g.L <sub>liquid</sub> <sup>-1</sup>	33.3 g.L <sub>liquid</sub> <sup>-1</sup>	20.0 g.L <sub>liquid</sub> <sup>-1</sup>
LRA Adsorption Time	H	2 h	24 h	13 h

**Table 5.3.** Summary of measured responses and illustration of the pyramidal nature of the factorial design used within the plasmid DNA process sequence study. Experiments performed as described in Section 2.5.2, according to the factorial design in Section 2.7.1.2.

<b>Response</b>	<b>Active Factors</b>	<b>Factorial Analysis</b>	<b>Error Estimate</b>
Lysis Clarification Flux	ABCD	$2^4$	4 Replicates
Lysate Clarification	ABCD	$2^4$	4 Replicates
Precipitate Recovery Specific Cake Resistance	ABCDE	$2^5$	Duplicates
Precipitate Removal Specific Cake Resistance	ABCDEF	$2^6$	Centre points
LRA Removal Specific Cake Resistance	ABCDEFGH	$2^{8-2}$	Centre points
Plasmid Yield	ABCDEFGH	$2^{8-2}$	Centre points
Plasmid Purity	ABCDEFGH	$2^{8-2}$	Centre points

process sequence are: the flux and percentage clarification for the lysis clarification step; the specific cake resistance during precipitate recovery, precipitate removal and LRA removal; and the plasmid process yield and purity. The early stage responses are governed by simple factorial designs with a high number of repeats producing the necessary material for the later stages in the sequence. As the process continues the number of replicates reduces and the complexity of the factorial analysis increases. A greater understanding of variation is generated towards the start of the process, where there are more degrees of freedom for error estimation. In the case of pDNA this helps due to the variable nature of the lysate feed which is at high solids concentration and difficult to accurately manipulate. The larger number of repeats required for upstream processes in a factorial design for process sequences would be conducive to the use of miniature bioreactor technologies (Lamping *et al.*, 2002; Kumar *et al.*, 2004; Gill *et al.*, 2008a) to feed the microwell downstream processes sequence.

### **5.3 Results of microscale factorial process sequence experiments**

#### **5.3.1 Lysis clarification**

Following fermentation the cell lysis step (Figure 5.1(a)) requires a delicate balance between high stirrer speed to maintain homogeneity in a complex, viscous solution and a low tip speed to limit damage to the shear labile plasmid (Hoare *et al.*, 2005). The cell lysis experiments and subsequent clarification tests are described in Section 2.4.2.2 and the raw data is detailed in Appendix D. Visual observations highlighted that changes in the lysis mixing speed also impacted very noticeably on the nature of the solid flocs that were collected. At the lower stirrer speed (400 rpm) the flocs were large and a substantial amount floated to the liquid surface when given time to settle. In contrast the higher mixing speed (1200 rpm) caused smaller, more defined spherical flocs to form which mainly settled at the bottom of the liquid. The centre-point speed generated a mixture between these situations with a variation in floc density. The clear difference in floc size and density would obviously impact on the filtration characteristics of the lysate. The filter aid used is denser than water, so it settles in a similar fashion to the flocs obtained at the medium and high stirrer speeds.

In order to ensure settling did not occur during microscale filtration to form a layered cake, lysate feed was mixed using a magnetic stirrer to maintain homogeneity and then pipetted as three separate 1 mL aliquots into the wells whilst a vacuum was already applied. Instantaneous filtration, separated into three additions, helped to reduce the time available for settling and create an even cake. This is a distinct advantage of the custom filter plate combined with the Tecan robot in comparison to traditional small scale laboratory equipment such as the membrane cell which has been shown to poorly predict industrial normal flow filtration equipment due to an uneven distribution of solids along the axis of flow (Reynolds *et al.*, 2003).

Figure 5.2 shows the effects and interactions for the response detailing permeate flux through the filter cake generated during the lysate clarification step. Each effect or interaction greater in magnitude than the dashed lines is statistically significant. Whilst the magnitude can indicate the relative importance of an effect or interaction it is also dependant on the chosen factor ranges just discussed. The interpretation of the main effects is summarised below:

- A higher Celpure permeability grade (A) generates a much better flux and is therefore more suited as a filter aid for the solids generated in the lysis experiments.
- High stirrer speed during neutralisation (B) gives a clear higher flux which is due to the defined and dense nature of the flocs described above.
- A high concentration of Celpure (C) gives a small increase in flux. This may be due to excess Celpure merely increasing the thickness of the cake and no longer contributing to the reduction in specific cake resistance.
- Recycling the permeate (D) causes a limited reduction in flux which must be compared to any improvement in clarification or subsequent processes.

In summary it is clear that the key factors are Celpure grade and neutralisation stirrer speed. The use of Celpure P300 and a high stirrer speed during lysis neutralisation is important to generate high fluxes during lysis clarification.

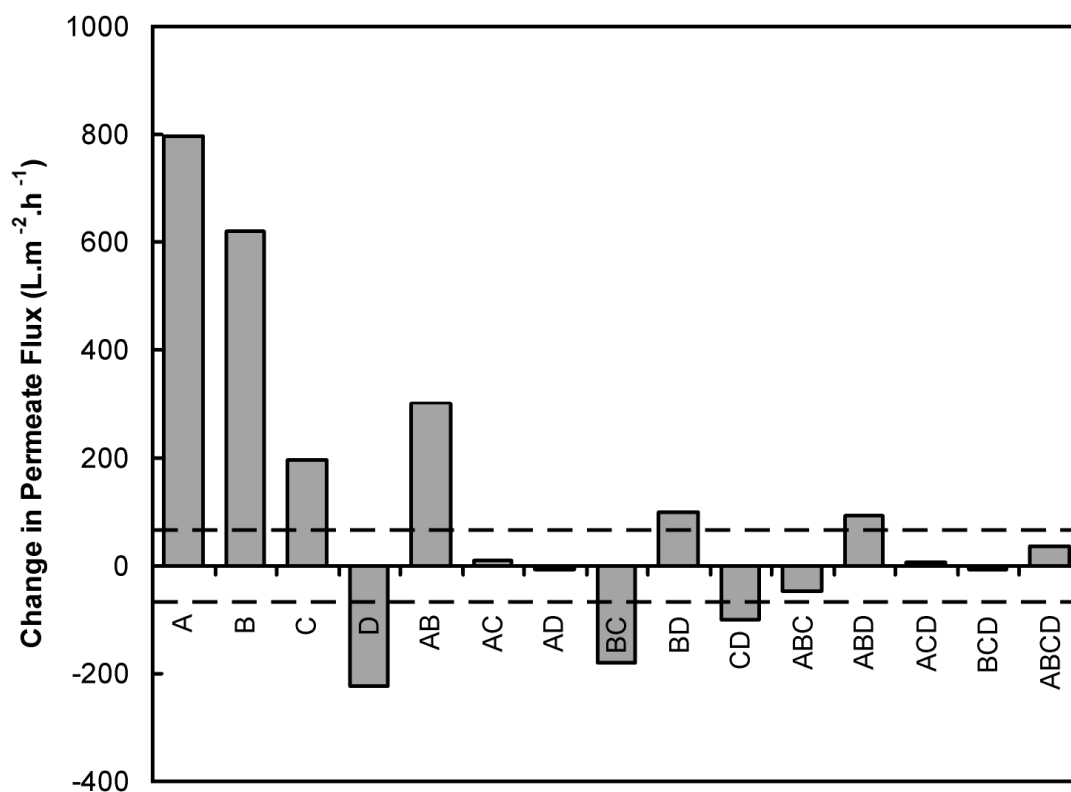


**Figure 5.2.** Effect and interaction plot for measured permeate flux during the lysis clarification step of a plasmid DNA recovery process. Factors investigated are as follows: A = Celpure grade, B = neutralization stirrer speed, C = Celpure concentration, D = number of permeate recycles. Experiments performed using a custom microwell filter plate (0.8 cm<sup>2</sup>) as described in Section 5.3.1. The dashed lines represent 95% confidence intervals inside which effects and interactions are not statistically significant.

The clearly significant AB and BC two-factor interactions shown in Figure 5.2 are described in more detail in Figures 5.3 and 5.4. The interaction between Celpure grade and lysis neutralisation speed (AB) is a simple combination interaction as shown in Figure 5.3. The positive effects on flux of each factor are increased at their highest levels. This demonstrates that Celpure P300 shows a greater improvement in compatibility compared with Celpure P65 for the morphology of the flocs from the high lysis neutralisation stirrer speed. Celpure P300 is the more appropriate grade for lysis clarification at all process combinations.

The interaction of lysis neutralisation stirrer speed and Celpure concentration (BC) is more interesting. Figure 5.4 shows that an increase in Celpure concentration increases the flux for the more complex low stirrer speed lysate due to the need for more filter aid to reduce the specific cake resistance. At the high stirrer speed, however, the smaller, more defined and rigid flocs that are formed mean that increased Celpure concentration shows limited change in flux performance. It is likely that the filter aid is both decreasing the specific cake resistance and also increasing the amount of total cake mass, with these opposing changes balancing out to give a similar flux. These results clearly demonstrate the impact of process variables in one operation impacting on the performance of subsequent steps, specifically the material requirements for it.

Interactions BD and CD and ABD are only marginally significant and small in comparison to the major effects. They are therefore not examined further here. The interactions do not overturn the overall trends of the main effects and as suggested in Figure 5.2, the best flux data point is achieved with  $50 \text{ g.L}_{\text{liquid}}^{-1}$  of Celpure P300, a lysis mixing speed of 1200 rpm and no permeate recycle (see Table D.1 in Appendix D).

Figure 5.5 shows the calculated effects and interactions for the percentage lysate clarification response. Percentage clarification was calculated as detailed in Section 2.8.6. Again, ignoring those that are marginally significant, the major effects and interactions greater in magnitude than the confidence intervals (dashed lines) are the number of recycles (D) and its interaction with Celpure concentration (CD). The impact of recycling is greater at the lower concentration of Celpure, where there is

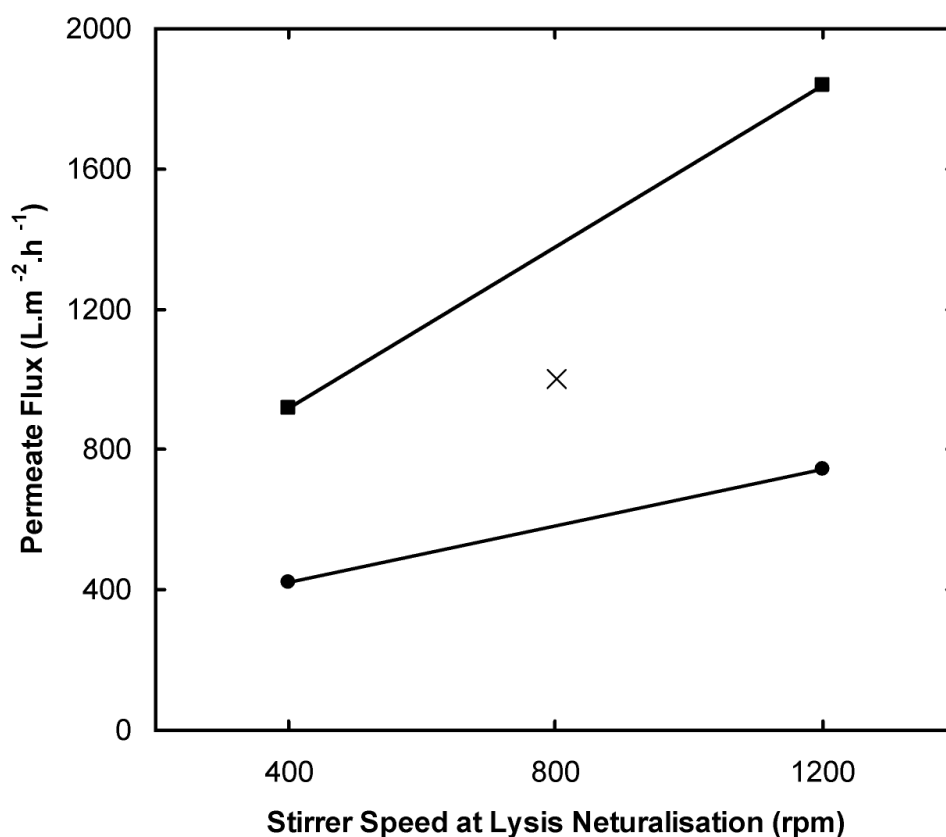


**Figure 5.3.** Interaction plot showing the variation of measured permeate flux at lysis clarification as a function of mixing speed during lysis neutralisation, using Celpure P65 (●) and Celpure P300 (■) filter aids. Data points represent the average from replicated runs during a factorial experiment. The centre-point of the factors in the experiment is also included (×). Solid lines indicate assumed linear relationships which should pass close to the centre point if this assumption holds. Experiments performed using a custom microwell filter plate (0.8 cm<sup>2</sup>) as described in Section 5.3.1.

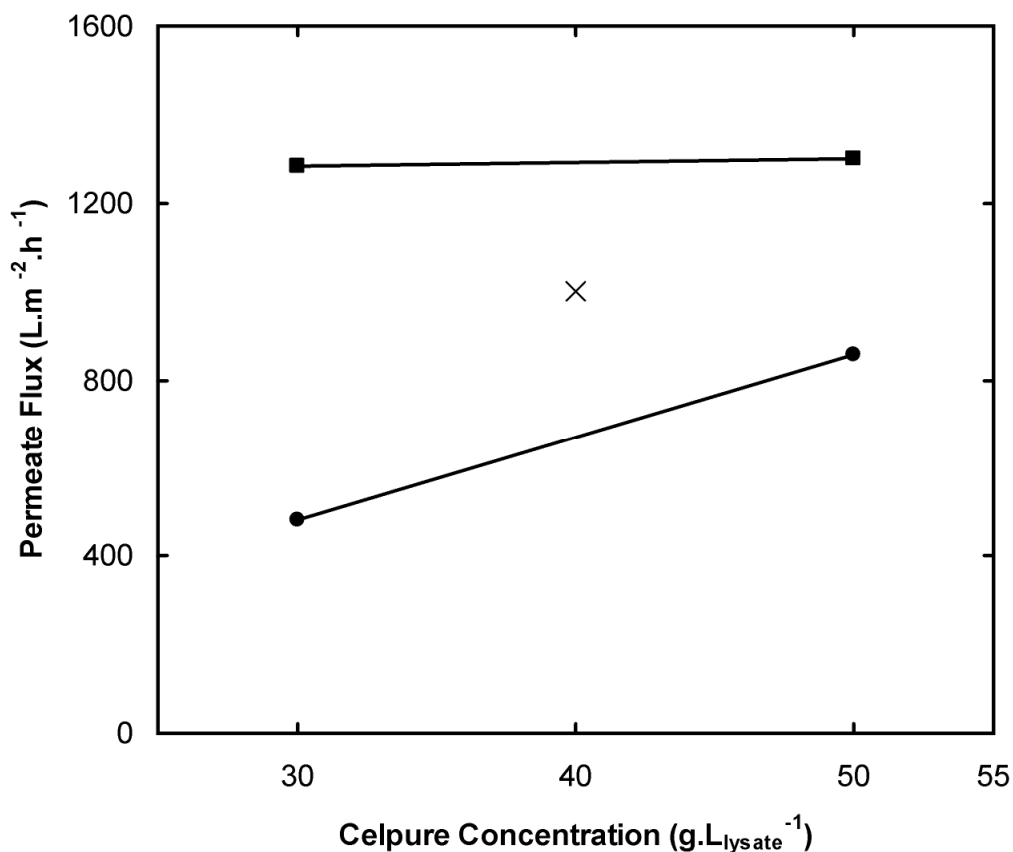


**Figure 5.4.** Interaction plot showing the variation of measure permeate flux at lysate clarification with Celpure filter aid concentration following a lysis neutralisation step at mixing speeds of 400rpm (●) and 1200rpm (■). Data points represent the average from replicated runs during a factorial experiment. The centre-point of the factors in the experiment is also included (×). Solid lines indicate assumed linear relationships which should pass close to the centre point if this assumption holds. Experiments performed using a custom microwell filter plate (0.8 cm<sup>2</sup>) as described in Section 5.3.1.

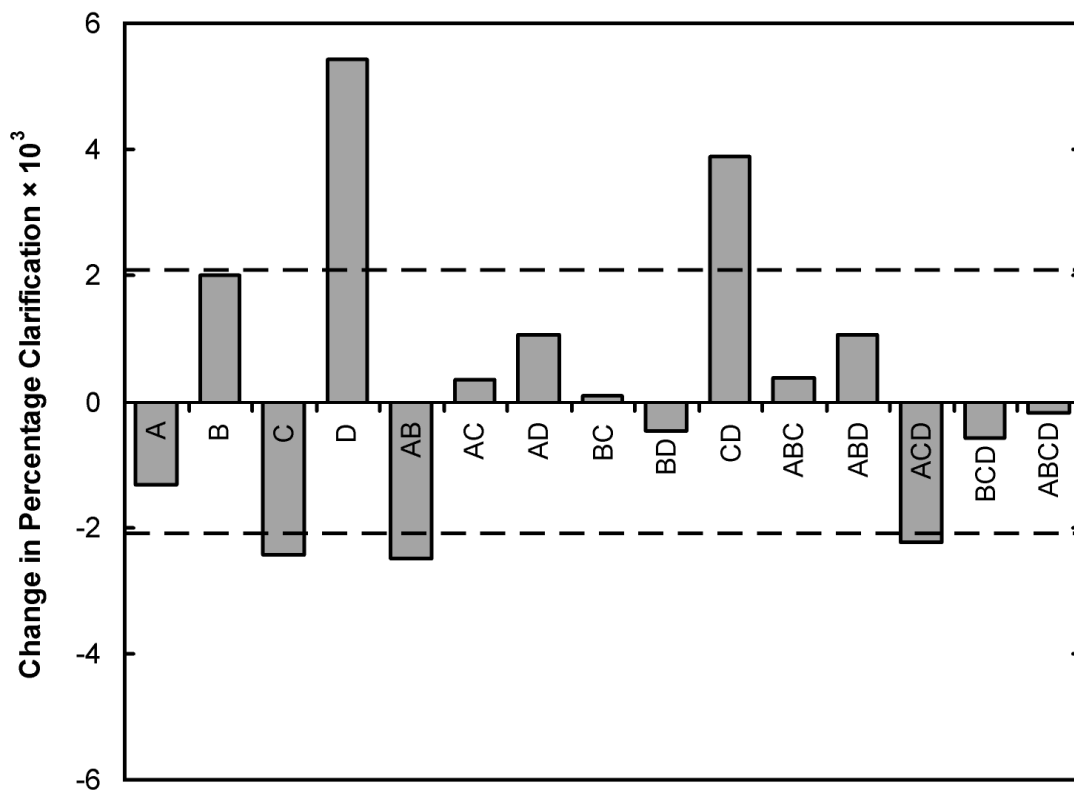


**Figure 5.5.** Effect and interaction plot for measured percentage clarification during the lysis clarification step of a plasmid DNA recovery process. Factors investigated are as follows: A = Celpure grade, B = lysis neutralization stirrer speed, C = Celpure concentration, D = number of recycles. Experiments performed using a custom microwell filter plate (0.8 cm<sup>2</sup>) as described in Section 5.3.1. The dashed lines represent 95% confidence intervals inside which effects and interactions are not statistically significant.

less total filter aid in the cake. Recycling permeate at the lower Celpure concentration does lead to a statistically significant increase in clarification, however the average magnitude of this increase is only 0.01% at the lower Celpure concentration. Unless the small increase in solids caused by not recycling the permeate effects subsequent filtration steps, then the process already achieves adequate clarification throughout the experimental space investigated and will operate quicker without the decrease in flux and extra throughput required to recycle the permeate.

### **5.3.2 Precipitation process operations**

The CTAB precipitation process (Figure 5.1(b)) was successfully carried out in microwells and microwell filtration was used to recover the precipitate (Figure 5.1(c)). The precipitate was then selectively redissolved in microwells (Figure 5.1(d)) and microwell filtration was used a second time to remove unwanted precipitate (Figure 5.1(e)). The details of these methods are described in Sections 2.4.2.3 and 2.4.2.4.

The testing of filtration performance for these two steps was not possible due to the extremely low resistance of the precipitate cakes. The cake was not capable of holding any test fluid in place before a vacuum was applied since the force of gravity alone was capable of relatively fast permeate rates, ensuring that measurement of flux under an applied pressure was not possible. The level of the cake resistance is therefore so low that processing the precipitate becomes more a question of solids content as the back pressures generated will not be significant. The possibility also exists that the precipitate can be processed without the need for filter aid. In any case, the process knowledge gained by microwell evaluation of CTAB precipitation suggests this is a robust process and will not cause filtration problems at large scale. This is useful as it allows development effort to be focused on the more challenging unit operations.

A method for the determination of precipitate cake resistance was subsequently developed and tested for the precipitation recovery phase. The results of that analysis are detailed in Appendix E.

### 5.3.3 LRA removal

Host cell DNA contaminants generated during the cell lysis step can be selectively adsorbed onto hydrated calcium silicate LRA (Figure 5.1(f)) since the linear fragments have a greater affinity than the conformationally constrained supercoiled pDNA (Winters *et al.*, 2003). Once this purification step has taken place the LRA, loaded with the contaminant DNA, is removed by filtration (Section 5.1(g)) to give a purified pDNA solution. These experiments are described in Section 2.4.2.5.

The DNA-laden LRA suspensions proved to be much more difficult to filter than the protein precipitates described in Section 5.3.2. Despite being rigid particles in a comparatively clean solution, they displayed modified cake filtration constants of the same order of magnitude to the lysate, suggesting similar flux characteristics. The factorial analysis of the measured specific cake resistance response is shown in Figure 5.6.

It shows that almost all effects and interactions are significant. Before assigning conclusions to these values, the analysis as a whole should be considered. There are multiple 2-factor interactions that appear to be higher in magnitude than the relevant main effects. A more plausible explanation is that variability at the factorial combinations is underestimated by the centre points. There are at least 23 different two or three-factor interactions that are higher in magnitude than all the main effects except F and G. Pooling the higher order interactions to estimate error is an accepted approach – although this must be an *a priori* decision based on process knowledge. However, were this approach to be used then it is clear that all interactions and effects, except for LRA concentration (Factor G), would no longer be significant. Regardless of the level of error, the concentration of LRA dominates process performance in comparison to the conditions used in the previous processing steps (as represented by Factors A-F) since the main effect for LRA concentration is 4.4 times greater in magnitude compared to the nearest other effect. The negative value of this main effect shows that specific cake resistance decreases significantly with increasing LRA concentration. This suggests that the LRA is acting as a filter aid. Either fouling particles still present in the feed are further dispersed throughout a rigid LRA

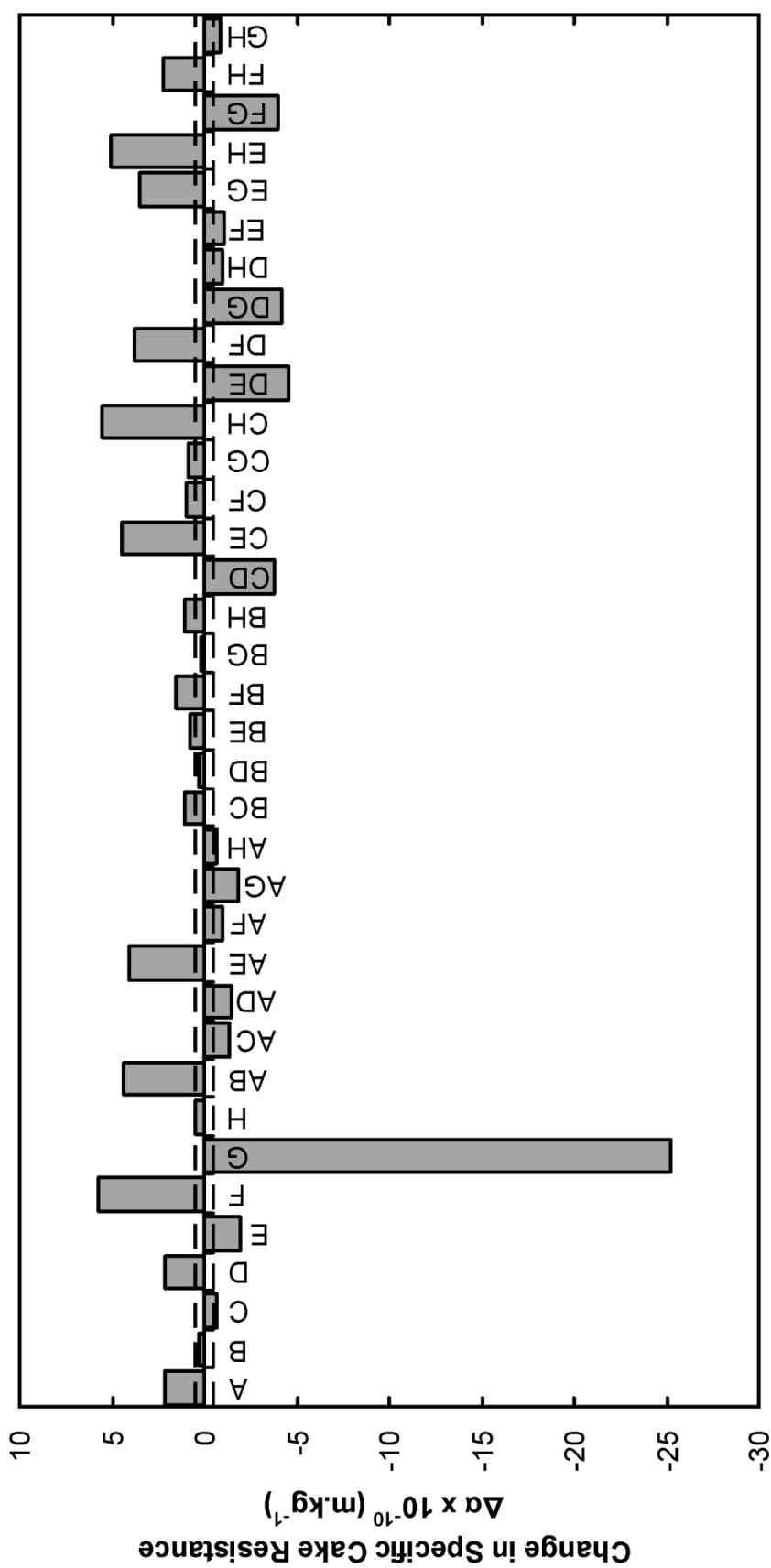


**Figure 5.6.** Effect and two-factor interactions for measured specific cake resistance during the LRA recovery step of a plasmid DNA recovery process. Factors investigated are as follows: A = Celpure grade, B = lysis neutralization stirrer speed, C = Celpure concentration for during lysate clarification, D = number of permeate recycles during lysate clarification, E = Celpure concentration during precipitate recovery, F = precipitate dissolution stirrer speed, G = LRA concentration, H = LRA adsorption time. Experiments performed using a custom microwell filter plate ( $0.8\text{cm}^2$ ) as described in section 5.3.3. The dashed lines represent 95% confidence intervals inside which effects and interactions are not statistically significant.

cake, or the LRA with bound nucleic acid has a greater resistance to flow and this is at a lower proportion the higher the LRA concentration.

Problems were caused in this experiment by the use of LRA as a pre-coat. There was some unexpected passage of LRA through the 22-26  $\mu\text{m}$  wire mesh (see section 2.3.1) during the main filtration run and this may have led to the variation seen as well as the poor assay performance outlined in the following section. Some wire mesh discs appeared to be clogged with LRA after filtration. This observation was made after the custom inserts were dismantled for cleaning and it was not possible to assign these observations to particular experiments. It is possible that this added to the variability of the process and may potentially not have been seen with the 8 out of 72 experiments that were run at the centre-points used for error estimation. These centre-points were carried out at intermediate time (Factor H) and were therefore carried out in a separate block to the other data.

The use of LRA as a pre-coat may have influenced the results of the factorial analysis, but it did not prevent discovery of a clear reduction in specific cake resistance at higher concentrations of LRA. This response was further investigated during scale-up studies (Section 5.4.2) using Celpure P300 as a pre-coat.

#### **5.3.4 Overall process performance: analysis of final product quality**

The quantification of product yield and purity was difficult. The isopropanol precipitation method employed is unable to remove the small levels of dissolved LRA that had permeated through the final filtration step (see Section 5.3.3). This may have caused the low quality of agarose gels generated. Other contributing factors may have led to the resulting poor gels such as the concentration of standards and general quality of the gel cast. There is therefore limited data and a full factorial analysis of product pDNA yield and purity responses could not be performed. pDNA is certainly present following the isopropanol precipitation in all samples since a visible pellet was formed, but the gels did not show clearly the relative content or intensity of the DNA species expected (genomic DNA, supercoiled pDNA, open-circular pDNA,

linear pDNA). Details of these analytical techniques are in Sections 2.5.2 and 2.5.3. Example gels and further discussion can be found in Section D.3 of Appendix D.

Reliance on a robust assay technique makes microscale automated experiments subject to failure when the assay does not work as expected. Spare samples can not easily be kept due to the small volumes involved. Improvements and tests, or alternatives to the assay such as anion exchange HPLC (Winters *et al.*, 2003), are required in the future. A sacrificial approach to the microscale process could have been used where many more experiments are performed in parallel but some sacrificed for analysis throughout the process. This would have given more opportunity for successful analysis but also increased the burden on the number of experiments (1224 individual microscale operations as opposed to 504) and especially the assay numbers (432 as opposed to 72). In such a detailed and long process sequence it is important to avoid putting strain on the analytical methods and causing the assay to be a bottleneck for microscale operations.

## **5.4 Scale-up of the key filtration steps**

Scale-up experiments were carried out for the key filtration steps of lysis clarification and LRA removal, as determined by microscale (0.8 cm<sup>2</sup>) filtration. Two devices were used: a scaled down rotating vertical leaf filter (RVLf) device (9 cm<sup>2</sup>) which is detailed in Section 2.3.4 and a pilot scale candle filter (120 cm<sup>2</sup>) which is detailed in Section 2.3.5.

All scale-up calculations are made using the modified cake filtration constant,  $K_c'$ , calculated as described in Section 5.2.2 and applying the scale-up equations detailed in Section 2.8.7.

### **5.4.1 Lysis clarification scale-up**

The microwell approaches adopted to limit settling of the filter cake and layering that were detailed in Section 5.3.1 ensure that the resistance to filtration is not

overestimated and accurate scale-up can be achieved based on microscale results. Figure 5.7 shows how the data carefully generated from the custom microwell filter plate (Appendix D, Equation 5.2, Equations 2.23 and 2.20) can both scale-up and predict different formats that are better suited to dealing with high solids concentration feeds. The lysis carried out for both microscale and RVLFF experiments used the same equipment and scale, as detailed in Section 2.4.2.2.

The permeate flux data shown is taken from a filtration run using the rotating vertical leaf filter (RVLFF) scale-down device and predictions from the custom microwell filter plate data. The best conditions from the microscale scouting experiments (Section 5.3.1) were used for scale-up studies. The lysis neutralisation speed used was 1200 rpm, with 50 g.L<sub>liquid</sub><sup>-1</sup> of Celpure P300. The permeate was not recycled. A constant flux is maintained, as predicted by the microscale data, for the majority of the filtration until it begins to drop off at approximately 600 seconds. This is due to fluctuations in pressure which caused the peak pressure to exceed 150 kPa and the control method employed which reduced the flowrate to compensate. This is therefore an artefact of the pump used and not an indication of poor scalability.

The pressure rises more quickly than predicted in the initial phase of the experiment until about 250 seconds. This is due to the mixing in the RVLFF device which causes the transfer from filtering pre-coat to filtering lysate feed to become gradual rather than immediate. The microscale prediction shown is made on the assumption of no mixing between the fronts of the two feed solutions. After this period the custom filter plate prediction shows very good correlation with the RVLFF pressure profile all the way until the reduction in flowrate previously explained which overcompensates for the increase in pressure.

#### **5.4.2 LRA removal scale-up**

Experiments performed in the microscale factorial experiment used LRA as a precoat, although this was not properly retained by the mesh support as described previously in Section 5.3.3. Large scale experiments switched to the use of Celpure 300 as a filter aid and additional experiments were carried out at the microscale to use for scale-up

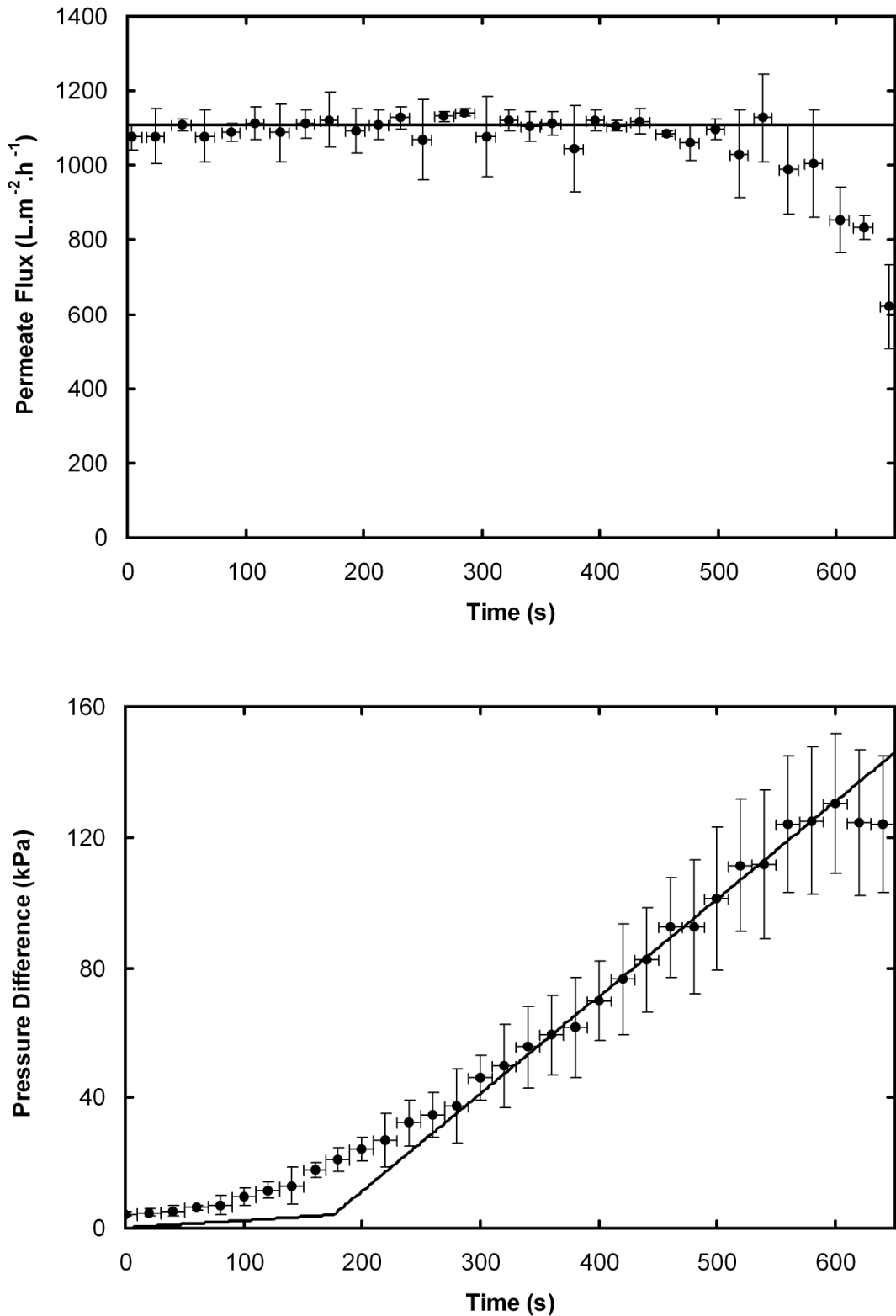


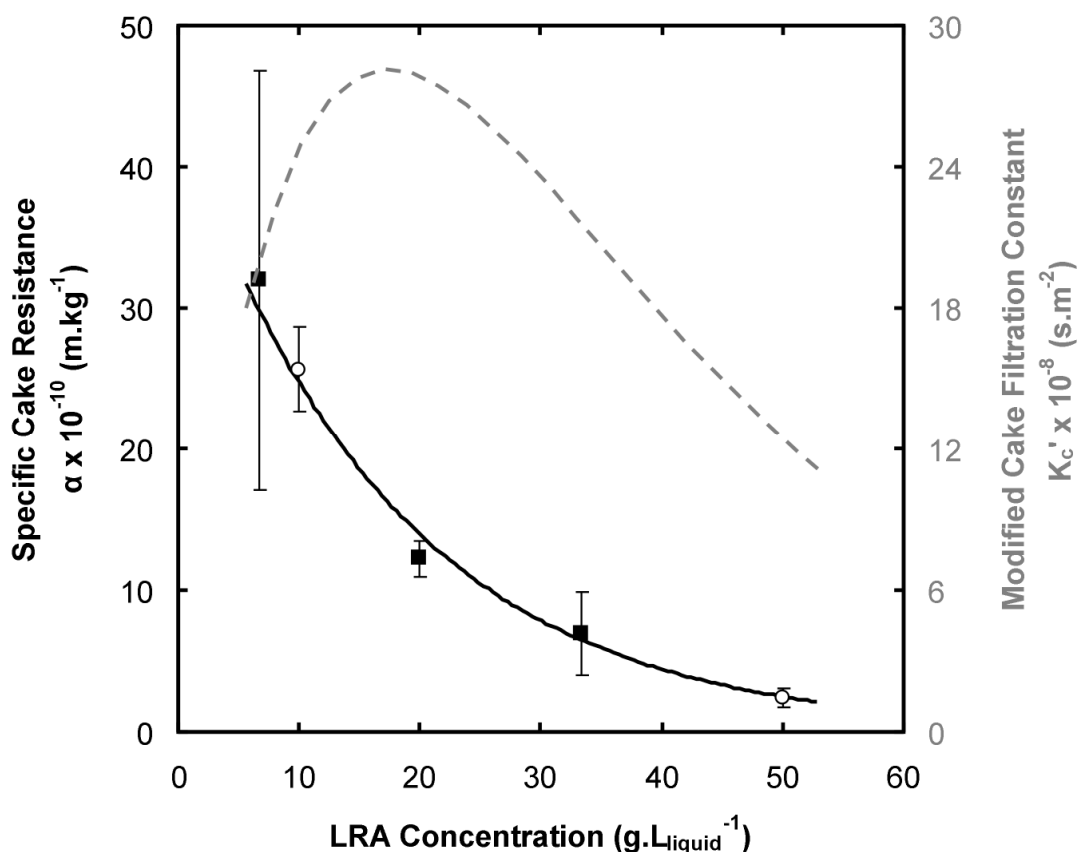
**Figure 5.7.** Flux and pressure profiles for lysis clarification in a rotating vertical leaf filter scale-down device ( $9 \text{ cm}^2$ ). Solid lines represent the custom microwell filter plate ( $0.8 \text{ cm}^2$ ) predictions according to Equations 2.23 and 2.20. Error bars for the y-axis represent one standard deviation ( $n > x$ ) over the range denoted by the x-axis bars. Experiment carried out as described in Sections 2.5.3.2 and 5.4.1.

evaluation. Different values of LRA concentration were chosen for study and the microscale data is compared in Figure 5.8. Note that the factorial run data is averaged from all different combinations of the other factors listed in Table 5.2, which explains the high variability. The two sets of results match well and show a relationship between cake resistance and LRA concentration which is consistent with the action of LRA as a filter aid. Also included in Figure 5.8 is the modified cake filtration constant ( $K_c'$ ), which is used to calculate the rate of pressure increase for scale-up calculations (Section 2.8.7). The decrease in specific cake resistance is not sufficient to give a meaningful reduction in  $K_c'$  over the range tested during the factorial scouting experiments, but the factorial data predict the potential reduction which is indeed seen at  $50\text{g.L}_{\text{liquid}}^{-1}$ . This suggests that a slower increase in pressure will be seen at large scale at the higher concentration and is the reason that  $10\text{g.L}_{\text{liquid}}^{-1}$  and  $50\text{g.L}_{\text{liquid}}^{-1}$  concentrations were selected. Details of the generation of feed for the LRA scale-up experiments are given in Section 2.5.3 (RVLF) and Section 2.5.4 (candle filter). The filtration equipment was operated as described in Section 2.3.4 (RVLF) and Section 2.3.5 (candle filter).

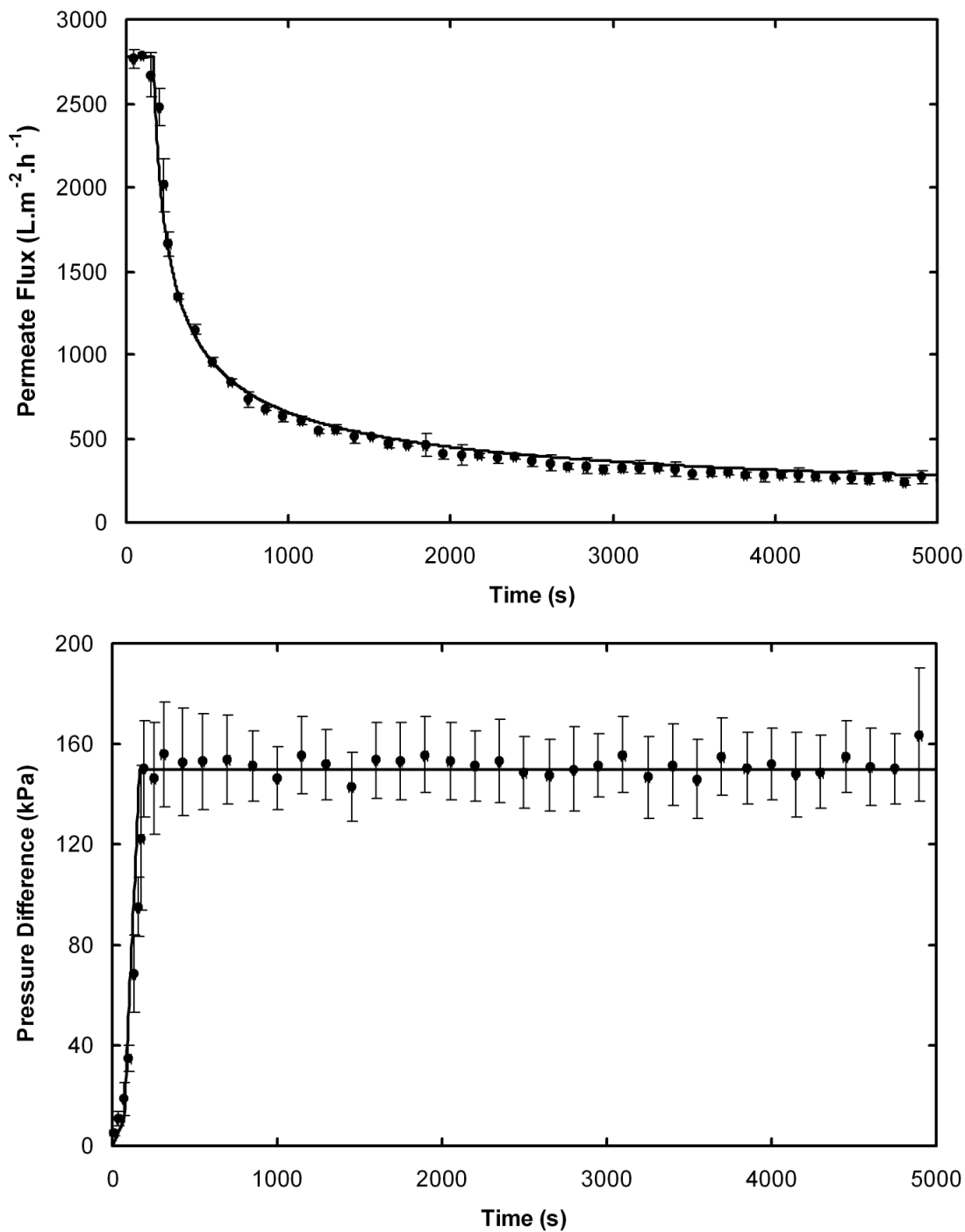
#### 5.4.2.1 RVLF scale-up

Figure 5.9 shows the RVLF scale down filter device performance for  $10\text{g.L}_{\text{liquid}}^{-1}$  of LRA adsorbent in a plasmid DNA solution. The data shows excellent correlation with the predictions from the custom microwell filter plate, especially considering that the volumetric scale up factor is 250. The LRA is filtered to a throughput in excess of  $800\text{L.m}^{-2}$  and the pressure increases to the set upper limit of 150 kPa after approximately 200 seconds of filtration. After this point the flux decays according to filtration theory and the microwell predictions.

The corresponding data for  $50\text{g.L}_{\text{liquid}}^{-1}$  of LRA in the feed suspension is shown in Figure 5.10. The microscale filter plate underpredicts the increase in pressure at the higher concentration, however it still predicts the distinct difference in cake resistance between the two concentrations. Since the rate of pressure rise is not predicted, the corresponding time that the RVLF reaches 150 kPa and the flowrate is reduced to compensate is much shorter than predicted.



**Figure 5.8.** Measured specific cake resistance (■,●) and modified cake filtration constant (---) values for LRA removal from a plasmid DNA solution at varying LRA concentrations. Data is taken from two different sources for comparison: a factorial experiment with many other different factors using LRA as a pre-coat (■,.) and separate experiments carried out with Celpure P300 as a pre-coat (●, ). Solid line is an exponential line of best fit of the form  $y = ae^{bx}$  ( $R^2 = 0.91$ ). Experiments carried out as detailed in Section 5.4.2 and Section 5.3.3.



**Figure 5.9.** Flux and pressure profiles for LRA adsorbant ( $10 \text{ g}\cdot\text{L}_{\text{liquid}}^{-1}$ ) removal from a plasmid DNA solution in a rotating vertical leaf filter scale-down device ( $9 \text{ cm}^2$ ). Solid lines represent the custom microwell filter plate ( $0.8 \text{ cm}^2$ ) predictions according to Equations 2.23 and 2.20. Error bars for the y-axis represent one standard deviation ( $n=11$ ) over the range denoted by the x-axis bars. Experiment carried out as described in Sections 2.5.3.7 and 5.4.2.1.

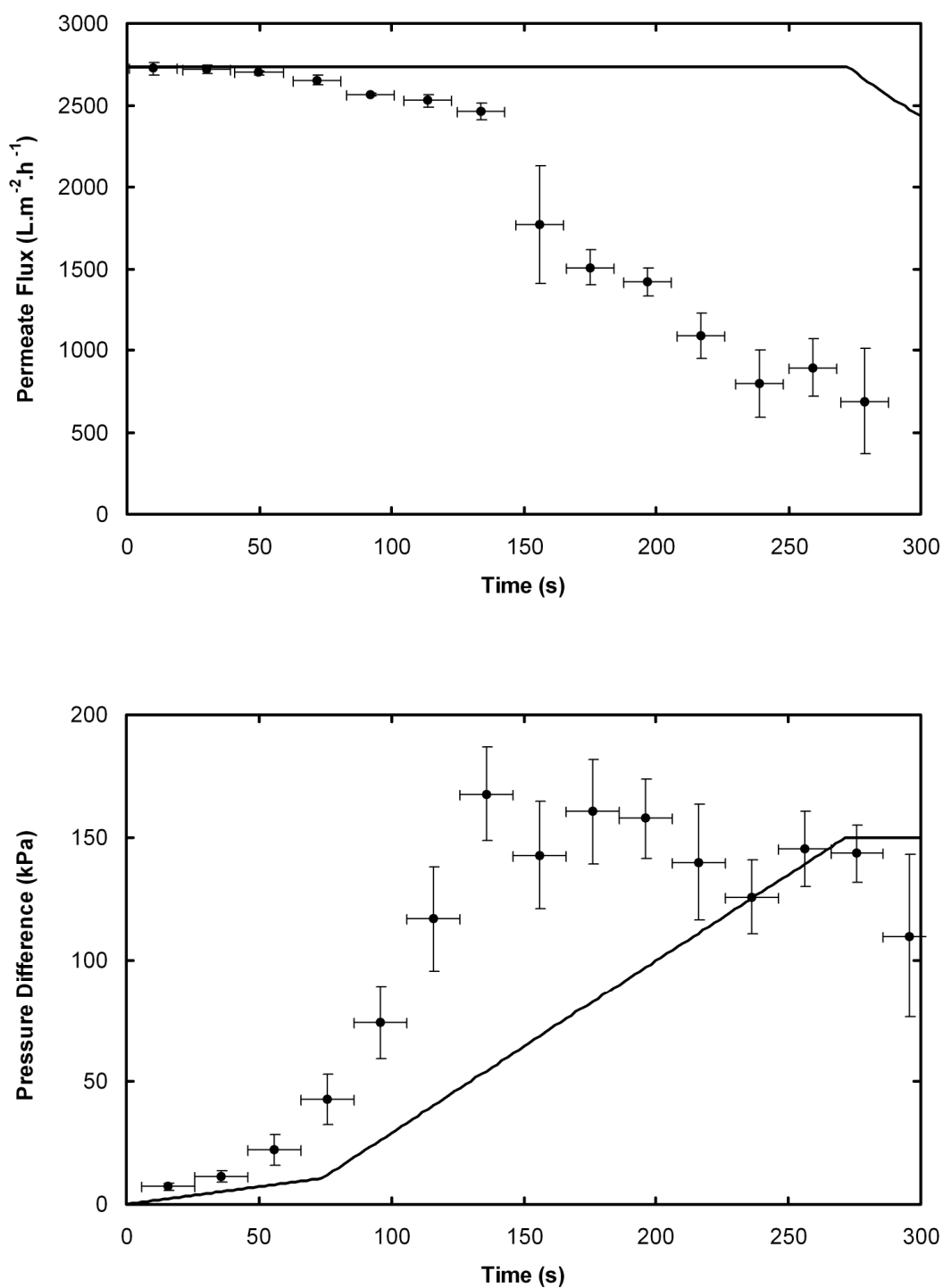


**Figure 5.10.** Flux and pressure profiles for LRA adsorbant ( $50 \text{ g}\cdot\text{L}_{\text{liquid}}^{-1}$ ) removal from a plasmid DNA solution in a rotating vertical leaf filter scale-down device ( $9 \text{ cm}^2$ ). Solid lines represent the custom microwell filter plate ( $0.8 \text{ cm}^2$ ) predictions according to Equation 2.23 and 2.20. Error bars for the y-axis represent one standard deviation ( $n=11$ ) over the range denoted by the x-axis bars. Experiment carried out as described in Sections 2.5.3.7 and 5.4.2.1.

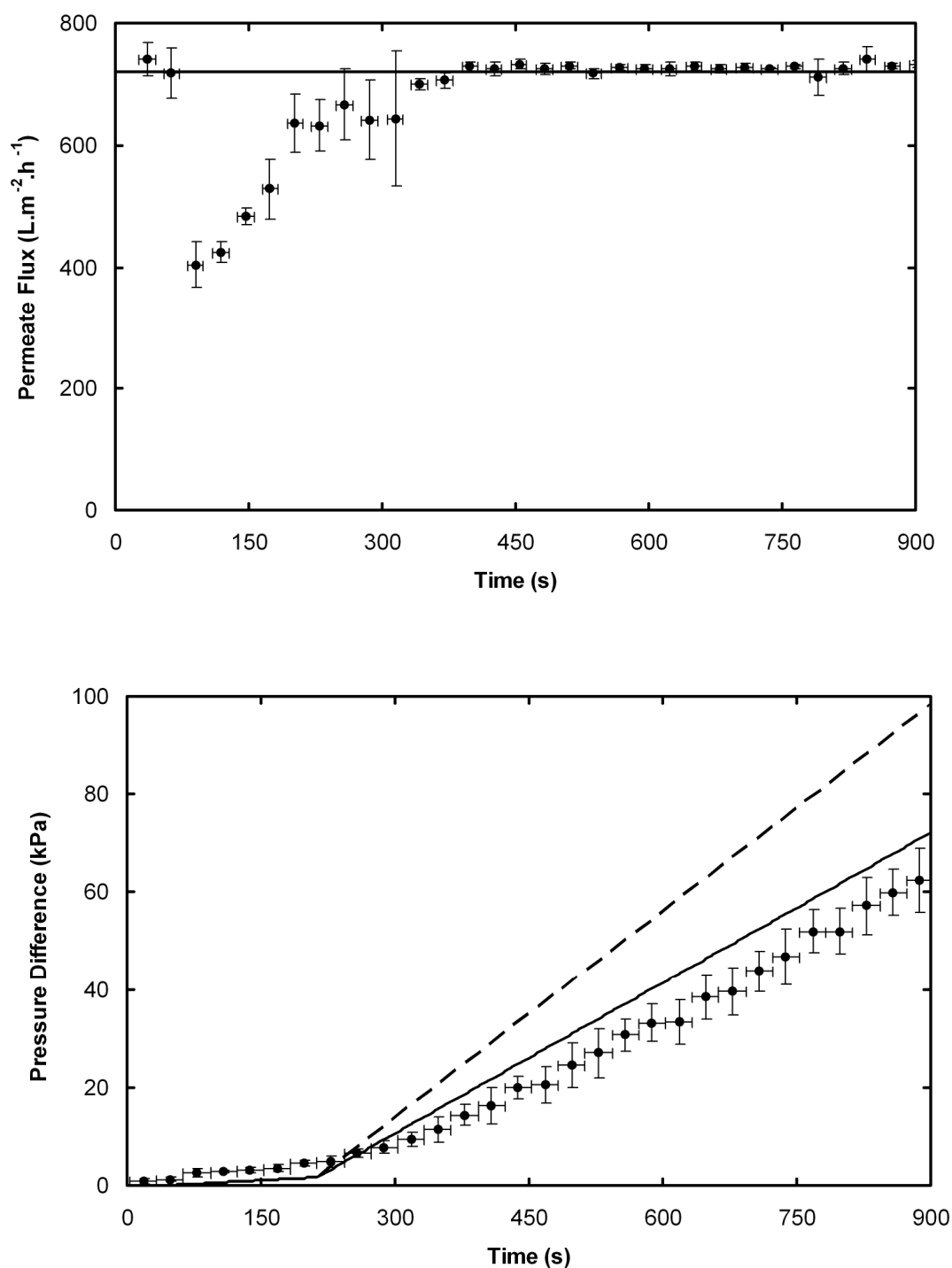
The scale-up factor in terms of filtration area is just over 11, however in terms of volume the process has been scaled by a factor of 65 ( $50 \text{ g.Liquid}^{-1}$ ) and 250 ( $10 \text{ g.Liquid}^{-1}$ ). In addition the data has been scaled from a simple constant pressure vertical flow through NFF process to a horizontal constant flow system with a rotating chamber.

#### 5.4.2.2 Candle filter scale-up

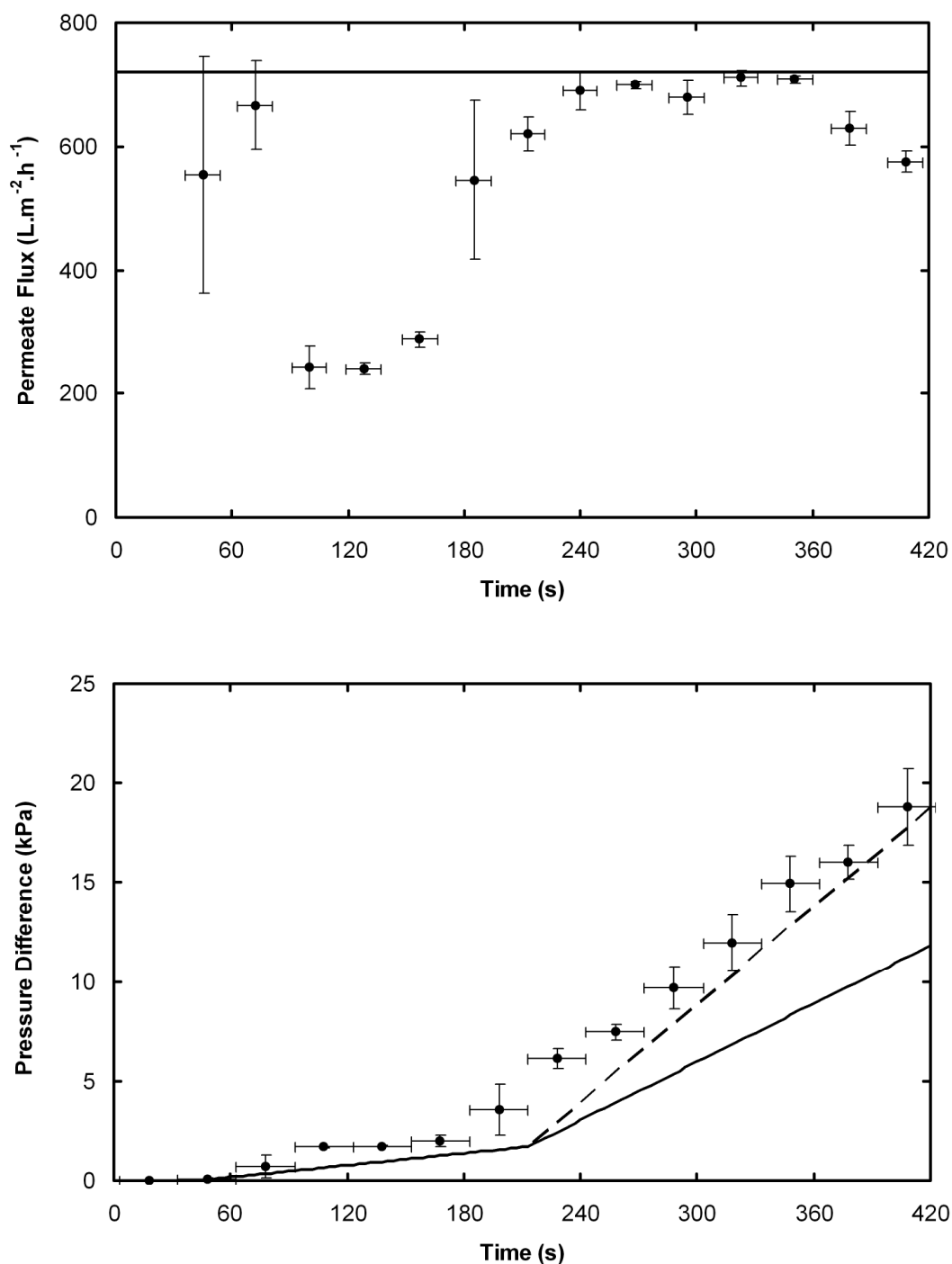
Both the custom microscale filter plate and the RVLf data were used for comparison to the candle filter performance. Scale-up calculations were carried out using Equation 2.23. For the RVLf the same equation was applied to the straight line portions pressure profiles in Figures 5.9 and 5.10 in order to calculate the necessary modified cake filtration constant values for the feeds required to complete the scale-up calculations.

Figure 5.11 shows the candle filter device performance for  $10 \text{ g.Liquid}^{-1}$  of LRA adsorbent in a plasmid DNA solution. An initial drop in flux is seen in all the candle filter data since there is dead volume on the filtrate side. The flux recovers well before significant product filtration begins and the pump was fully calibrated. The pressure data shows excellent correlation with the predictions from the custom microwell filter plate at a volumetric scale up factor of over 2000. At this concentration the RVLf scale-down device appears to not scale particularly well but the calculated cake resistances are still relatively close.

The corresponding data for  $50 \text{ g.Liquid}^{-1}$  of LRA is shown in Figure 5.12. Once again there is drop in flux caused by the large dead volume. Due to the high amount of solids the candle filter cannot process as much volume of feed, making cake volume more important than pressure or time in limiting the process. At this LRA concentration it is the RVLf device that shows more accurate scale up compared to the microscale data. Note should be taken that the candle filter runs required larger volumes than the other scales and were carried out on different dates using larger scale equipment during mixing steps as described in Section 2.5.4 (compared to Sections 2.5.2 and 2.5.3).



**Figure 5.11.** Flux and pressure profiles for LRA adsorbant ( $10\text{g}\cdot\text{L}_{\text{liquid}}^{-1}$ ) removal from a plasmid DNA solution in a candle filter ( $120\text{ cm}^2$ ). Solid lines represent the custom microwell filter plate ( $0.8\text{ cm}^2$ ) predictions and dashed lines represent the RVLF ( $9\text{ cm}^2$ ) predictions, both according to Equation 2.23. Error bars for the y-axis represent one standard deviation ( $n=11$ ) over the range denoted by the x-axis error bars. Experiment carried out as described in Sections 2.5.4.7 and 5.4.2.2.



**Figure 5.12.** Flux and pressure profiles for LRA adsorbant ( $50\text{g}\cdot\text{L}_{\text{liquid}}^{-1}$ ) removal from a plasmid DNA solution in a candle filter ( $120\text{cm}^2$ ). Solid lines represent the custom microwell filter plate ( $0.8\text{cm}^2$ ) predictions and dashed lines represent the RVLF ( $9\text{cm}^2$ ) predictions, both according to Equations 2.23. Error bars for the y-axis represent one standard deviation ( $n=11$ ) over the range denoted by the x-axis error bars. Experiment carried out as described in Sections 2.5.4.7 and 5.4.2.2.

The scale-up factors in terms of filtration area for the microscale custom filter plate to the candle filter is 150, however in terms of volume the process has been scaled by a factor of 600 ( $50 \text{ g.L}_{\text{liquid}}^{-1}$ ) and 2040 ( $10\text{g.L}_{\text{liquid}}^{-1}$ ). In addition the data has been scaled from a simple constant pressure vertical flow through NFF process to an upflow candle filter with a more complicated flow pattern.

### 5.4.3 Scale-up summary

The trend for reducing cake resistance at higher concentration is repeated at all the scales. Figure 5.13 shows the striking difference in specific cake resistance between the two concentrations tested and the agreement of all three scales of filtration equipment. Scale-up of flux and pressure behaviour is not shown to be perfect at such large scale-up factors, but this figure illustrates that the trend is repeated upon scale-up allowing small scale results to focus future large scale tests.

The complexity of the lysate feed would have caused problems for conventional laboratory scale normal flow filtration devices due to the settling nature of the feed (Reynolds *et al.*, 2003). In this work both the lysate and LRA results from the microscale are scaled successfully without any issues relating to the settling of the feeds under gravity and stratification of the cake formed.

The lysate clarification and LRA removal steps are the key filtration problems posed by this process sequence. Further investigation to optimising these steps is required at both microscale and pilot scales. The sizing and costing of filtration equipment for this process will be dominated by these two processes.

## 5.5 Summary

A whole process sequence involving 7 individual process steps (4 filtration based) has been run using automated microscale techniques using experimental design to focus the experiments. A total of 72 combinations of 8 different process parameters in parallel, collecting several hundred scaleable data points and highlighting the

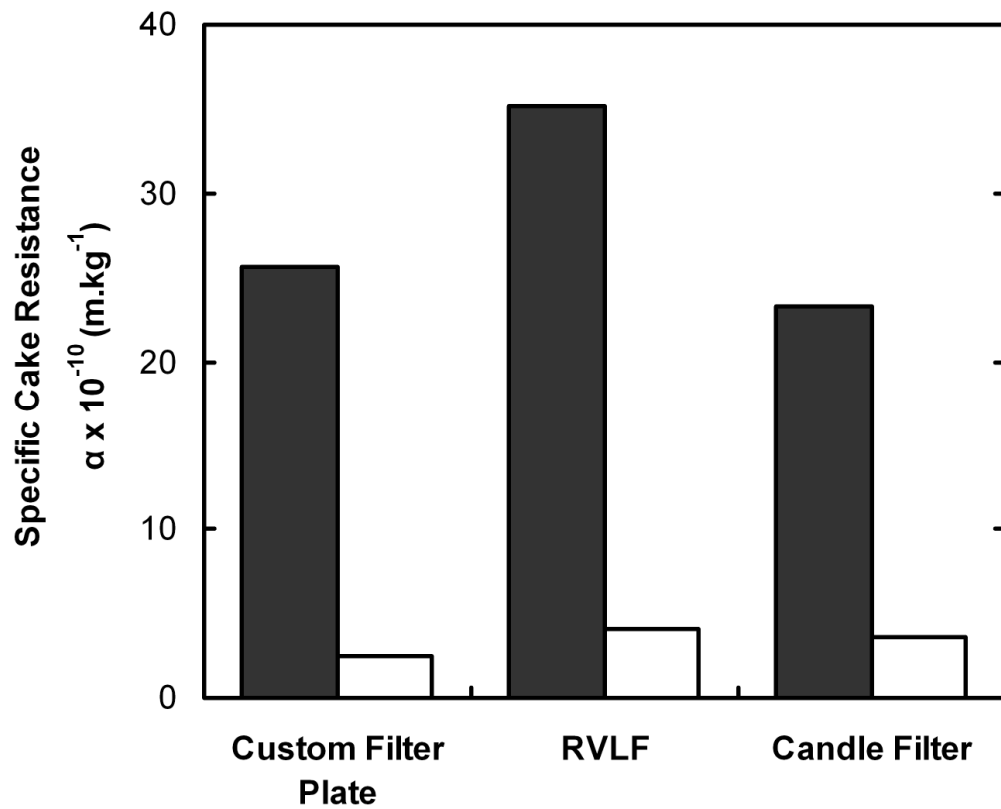


**Figure 5.13.** Specific cake resistance values for LRA removal at concentrations of  $10 \text{ g.Liquid}^{-1}$  (dark bars) and  $50 \text{ g.Liquid}^{-1}$  (light bars). Results from various scales compared: custom microwell filter plate ( $0.8 \text{ cm}^2$ ), RVLf ( $9 \text{ cm}^2$ ), candle filter ( $120 \text{ cm}^2$ ). Experiments carried out as described in Section 5.4.2.

important factors and most difficult processing steps required to generate purified plasmid DNA through a non-chromatographic process (Figures 5.2 to 5.6, Appendix D).

Microscale tests were able to predict large scale performance at volumetric scale-up factors up to 2040 (Figures 5.9 to 5.12). Scale up predictions were made from the custom microwell filter plate ( $0.8 \text{ cm}^2$ ) to a rotating vertical leaf filter ( $9 \text{ cm}^2$ ) and a candle filter ( $120 \text{ cm}^2$ ) where the flow is directed upwards. All these represent a significant change in format as well as scale.

The general trends of performance highlighted by the microwell techniques are shown to be scaleable through laboratory scale to pilot scale filtration (Figure 5.13). This illustrates that the microscale techniques developed in this thesis are capable of determining quantitative, scaleable data from whole microwell process sequences.

## 6.0 Overall conclusions and future work

### 6.1 Overall conclusions

A high throughput method for the study of normal flow microfiltration operations has been established using a custom designed 8-24 well filter plate (0.8 cm<sup>2</sup>) and a commercial 96-well Multiscreen filter plate (0.3 cm<sup>2</sup>). Integration of this new approach with a typical robotic platform has enabled automation of the experimental procedure and led to the following main conclusions:

- Membrane resistance values can be accurately quantified using either filter plate design (Table 3.1). The accuracy of these measurements has helped to determine that plate position does not affect experimental results and applied pressure difference does not vary across either plate (Figure 3.3, Section 3.3.3).
- Each of the two filter plate formats has been used to demonstrate that cell condition following fermentation, buffer type and media composition are all important factors influencing the specific cake resistance of *E.coli* TOP10 cells (Figure 3.5, Table 3.2 and Figure 3.6). The microscale method therefore allows parallel quantification of the impact of upstream process conditions on normal flow microfiltration performance.
- The filter plates both generate comparable data to conventional laboratory scale equipment (Figure 3.8). The custom plate, optimised for bioprocess studies, demonstrates approximately 25% lower variation in specific cake resistance values compared with the commercial filter plate.
- Automated microscale microfiltration techniques have been combined with factorial experimentation to identify the key factors and interactions which influence protein transmission and specific cake resistance during filtration of a model *E.coli*-lysozyme mixture. The initial factorial scouting experiments (Section 4.3) identified pH and ionic strength to be the most

significant factors and showed the existence of a strong 2-factor interaction (Figures 4.3 and 4.4) between them.

- The pH and ionic strength interaction was further investigated using response surface methodology and the custom microwell filter plate. A window of operation was generated showing optimum operating conditions (Figure 4.7). The pH and ionic strength values necessary to achieve an optimum transmission above 95% and a specific cake resistance below  $80 \times 10^{12} \text{ m.kg}^{-1}$  were  $\text{pH } 5.5 \pm 0.1$  and  $153 \pm 8 \text{ mM}$ .
- The microscale flux and protein transmission values calculated from microscale data were shown to scale-up (17X) to conventional laboratory scale equipment. The results confirmed that the optimum permeate flux and protein transmission conditions developed at microscale are valid.
- A whole process sequence for pDNA purification involving 7 individual process steps (4 filtration based) has been run using automated microscale techniques using experimental design to focus the experiments. A total of 72 combinations of 8 different process parameters in parallel, collecting several hundred scaleable data points and highlighting the important factors and most difficult processing steps required to generate purified plasmid DNA through a non-chromatographic process (Figures 5.2 to 5.6, Appendix D).
- Microscale tests were able to predict large scale performance at volumetric scale-up factors up to 2040 (Figures 5.9 to 5.12). Scale up predictions were made from the custom microwell filter plate ( $0.8 \text{ cm}^2$ ) to a rotating vertical leaf filter ( $9 \text{ cm}^2$ ) and a candle filter ( $120 \text{ cm}^2$ ) where the flow is directed upwards. All these represent a significant change in format as well as scale.
- The general trends of performance highlighted by the microwell techniques have been shown to be scaleable through laboratory scale to pilot scale filtration (Figure 5.13).

This illustrates that the microscale techniques developed in this thesis are capable of determining quantitative, scaleable data for early stage evaluation of whole microwell process sequences.

## 6.2 Future work

There are several evident improvements on this work that could be carried out to complete this phase of the microscale filtration development:

- Strengthen the plasmid DNA analysis and repeat the experiments from Chapter 5, evaluating the process sequence for all responses.
- Study flux and transmission for an industrially relevant extracellular protein. For example antibody fragment producing *E.coli* strains (García-Arrazola *et al.*, 2005) or monoclonal antibody producing mammalian cell cultures (CMC Biotech Working Group, 2009). Incorporate a full mass balance to determine the amount of protein bound to the filter and the plastic surfaces used.
- Demonstrate the full utility of the custom microwell filter plate to screen multiple membrane types by investigating a wider range of membrane types than seen in Chapter 4.
- Develop similar methods to quantify the standard blocking behaviour of a protein solution, for example in virus filtration (Kuriyel and Zydney, 2000).

The techniques and custom filter plate developed in this thesis provide a strong framework for the automated operation of microscale filtration. However, progressions of the current design could further enhance the strengths and remove some of the limitations:

- The existing custom filter plate design improves the volume to area ratio over existing commercial designs. This remains an area for improvement as it still does not match full scale process volume to area ratios and high flux processes will be too quick to easily quantify. Improvements to the filter insert design could reduce filter area (smaller disc diameter, e.g. 0.3 cm<sup>2</sup>) while maximising reservoir volume (24 deep square well format), allowing a potential increase of more than 6-fold to the volume to area ratio.
- Developing an automated seal system to allow positive pressure to be applied and thus increasing the upper range of pressure differences

available would limit current restrictions and increase the design space that can be investigated. This would lead to improved capabilities for investigating cake compression phenomena.

- Increase in the data confidence and quality should be investigated by using a three point method instead of the existing two point method. Modifications to the vacuum manifold to allow three plates in parallel could easily be made. This would increase sample throughput, but would also generate an extra data point and allow a more sensitive detection of curvature and deviation from the model.
- Further improvement in the data quality could be achieved by collecting continuous data from the microscale work. This would allow improved data analysis and model fitting without restrictions imposed by a low number of data points. Potential methods for this include the use of individual miniature load cells to measure continuous mass over time or monitoring the pressure of sealed individual collection wells to estimate the increase in permeate volume in real time as attempted by Chandler and Zydney (2004).
- Constant flow operation, which is the mode of operation at industrial scale for many filters (Ball, 2000), would allow continuous data collection since the performance could be tracked with individual pressure sensors on each well. As with applying positive pressure, significant obstacles would need to be overcome in order to seal the wells when changing plates, allowing full integration of a constant flow approach into an automated robotic platform.

In addition this work has helped to lay the foundation for more progressive microscale bioprocess research which will expand the ability to investigate a wider variety of process sequences:

- Expand the microscale microfiltration work from normal flow to tangential flow format, enabling parallel and automated study of tangential flow filtration processes.

- Develop a suite of microscale unit operations, right through to the purification and polishing steps, all capable of integration on the deck of an automation robot.

With these improved capabilities in place then the overall target of automated microscale process development will move closer to a reality.

## 7.0 References

- Abbott NL and Hatton TA (1988) Liquid-liquid-extraction for protein separations. *Chem Eng Prog* 84: 31-41.
- Abbott A and Pearson H (2004) Fear of human pandemic grows as bird flu sweeps through Asia. *Nature* 427: 472-473.
- Akbari A, Desclaux S, Remigy JC, Aptel P (2002) Treatment of textile dye effluents using a new photografted nanofiltration membrane. *Desalination* 149(1-3): 101-107.
- Alton E (2007) Progress and Prospects: Gene Therapy Clinical Trials (Part 1). *Gene Ther* 14: 1439-1447.
- American Water Works Association (2005) Microfiltration and ultrafiltration membranes for drinking water, 1<sup>st</sup> Ed. Denver: AWWA.
- Anderlei T, Zang W, Papaspyrou M, Büchs J (2004) Online respiration activity measurement (OTR, CTR, RQ) in shake flasks. *Biochem Eng J* 17: 187–194.
- Ayazi Shamlou P, Dunnill P, Hoare M, Ison AP, Keshavarz-Moore E, Lye GJ, Turner MK, Titchener-Hooker NJ, Woodley JM, Buckland BC (1998) UCL Biochemical Engineering (Editorial). *Biotechnol Bioeng* 60(5): 527-533.
- Badmington F, Honig E, Payne M, Wilkins R (1995) Vmax Testing for Practical Microfiltration Train Scale-Up in Biopharmaceutical Processing. *Pharmaceutical Tech* 19: 64-76.
- Bailey SM and Meagher MM (2000) Separation of soluble protein from inclusion bodies in *Escherichia coli* lysate using crossflow microfiltration. *J Membr Sci* 166(1): 137-146.
- Baker RW (2002) Future Directions of Membrane Gas Separation Technology. *Ind Eng Chem Res* 41(6): 1393–1411.
- Baker RW (2004) Membrane technology and applications, 2nd Ed. Chichester: Wiley.
- Ball P (2000) Scale-up and scale-down of membrane-based separation processes. *Membrane Technology* 117: 10-13.

Baneyx F and Mujacic M (2004) Recombinant protein folding and misfolding in *Escherichia coli*. *Nat Biotechnol* 22(11): 1399-1408.

Baneyx F (1999) Recombinant protein expression in *Escherichia coli*. *Curr Opin Biotech* 10(5): 411-421.

Batas B, Schiraldi C, Chaudhuri JB (1999) Inclusion body purification and protein refolding using microfiltration and size exclusion chromatography. *J Biotechnol* 68(2-3): 149-158.

Belfort G, Davis RH, Zydney AL (1994) The behavior of suspensions and macromolecular solutions in crossflow microfiltration. *J Membr Sci* 96(1-2): 1-58.

Belter PA, Cussler EL, Hu W (1988) *Bioseparations: downstream processing for biotechnology*. New York: Wiley.

Bentham AC, Ireton MJ, Hoare M, Dunnill P (1988) Protein precipitate recovery using microporous membranes. *Biotechnol Bioeng* 31(9): 984-994.

Beynon RJ and Easterby JS (1996) *Buffer Solutions: The Basics*. Oxford: IRL Press at Oxford University Press.

Bolton G, LaCasse D, Kuriyel R (2006) Combined models of membrane fouling: Development and application to microfiltration and ultrafiltration of biological fluids. *J Membr Sci* 277(1-2): 75-84.

Bouzerar R, Jaffrin MY, Ding L, Paullier P (2000) Influence of geometry and angular velocity on performance of a rotating disk filter. *AIChE J* 46(2): 257-265.

Bowen WR, Calvo JI, Hernández A (1995) Steps of membrane blocking in flux decline during protein microfiltration. *J Membr Sci* 101(1-2): 153-165.

Bowen WR and Gan Q (1991) Properties of microfiltration membranes: Adsorption of bovine serum albumin at polyvinylidene fluoride membranes. *J Colloid Interf Sci* 144(1): 254-262.

Box GEP and Behnken DW (1960) Some New Three Level Designs for the Study of Quantitative Variables. *Technometrics* 2(4): 455-475.

Box GEP and Hunter JS (1957) Multi-factor experimental designs for exploring response surfaces. *Ann Math Statist* 28(1): 195-241.

Box GEP and Wilson KB (1951) On the experimental attainment of optimum conditions. *J R Stat Soc Series B* 13(1): 1-45.

Box GEP, Hunter JS, Hunter WG (2005) *Statistics for experimenters: design, innovation, and discovery*, 2<sup>nd</sup> Ed. New York: Wiley.

Box GEP (1990) Must we randomize our experiment? *Quality Engineering* 2: 497-502.

Boychyn M, Yim SSS, Ayazi Shamlou P, Bulmer M, More J, Hoare M (2004) Characterization of flow intensity in continuous centrifuges for the development of laboratory mimics. *Chem Eng Sci* 56(16): 4759-4770.

Burnouf T and Radosevich M (2003) Nanofiltration of plasma-derived biopharmaceutical products. *Haemophilia* 9(1): 24-37.

Carnes AE (2005) Fermentation Design for the Manufacture of Therapeutic Plasmid DNA. *BioProc Int* 3(9): 36-42.

Carpenter JF, Pikal MJ, Chang BS, Randolph TW (1997) Rational Design of Stable Lyophilized Protein Formulations: Some Practical Advice. *Pharmaceut Res* 14(8): 969-975.

Carta G and Jungbauer A (2010) *Protein Chromatography: Process Development and Scale-Up*. Weinheim: Wiley-VCH.

Carter J and Lutz H (2002) An overview of viral filtration in biopharmaceutical manufacturing, *Eur J Parenteral Sci* 7(3): 72-78.

Chandler M and Zydney A (2004) High throughput screening for membrane process development. *J Membr Sci* 237: 181-188.

Charlton HR, Relton JM, Slater NKH (1999) Characterization of a generic monoclonal antibody harvesting system for adsorption of DNA by depth filters and various membranes. *Bioseparation* 8: 281-291.

Cheyran M (1998) *Ultrafiltration and microfiltration handbook*. Lancaster: Technomic Publishing Company.

Chhatre S, Jones C, Francis R, O'Donovan K, Titchener-Hooker N, Newcombe A, Keshavarz-Moore E (2006) The Integrated Simulation and Assessment of the Impacts of Process Change in Biotherapeutic Antibody Production. *Biotechnol Progr* 22(6): 1612-1620.

Claas ECJ, Osterhaus ADME, van Beek R, De Jong JC, Rimmelzwaan GF, Senne DA, Krauss S, Shortridge KF, Webster RG (1998) Human influenza A H5N1 virus related to a highly pathogenic avian influenza virus. *Lancet* 351: 472-477.

CMC Biotech Working Group (2009) A-Mab: a case study in bioprocess development, CASSS, “[http://www.casss.org/associations/9165/files/A-Mab\\_Case\\_Study\\_Version\\_2-1.pdf](http://www.casss.org/associations/9165/files/A-Mab_Case_Study_Version_2-1.pdf)”.

Cregg JM, Cereghino JL, Shi J, Higgins DR (2000) Recombinant protein expression in *Pichia pastoris*. *Mol Biotechnol* 16(1): 23-52.

Cutler P (2004) Protein purification protocols, 2<sup>nd</sup> Ed. Totowa: Humana Press.

Darcy H (1856) *Les Fontaines Publiques de la Ville de Dijon*. Paris: Victor Dalmont.

Davies JL, Baganz F, Ison AP, Lye GJ (2000) Studies on the interaction of fermentation and microfiltration operations: erythromycin recovery from *Saccharopolyspora erythraea* fermentation broths. *Biotechnol Bioeng* 69: 429-439.

Demain AL and Davies JE (1999) *Manual of Industrial Microbiology and Biotechnology*, 2<sup>nd</sup> Ed. Washington DC: ASM Press.

DiMasi JA, Hansen RW, Grabowski HG (2003) The price of innovation: new estimates of drug development costs. *J Health Econ* 22: 151-185.

Diogo MM, Queiroz JA, Prazeres DMF (2005) Chromatography of plasmid DNA. *J Chromatogr A* 1069(1): 3-22.

Doig SD, O’Sullivan ML, Patel S, Ward JM, Woodley JM (2001) Large scale production of cyclohexanone monooxygenase from *Escherichia coli* TOP10 pQR239. *Enzyme Microb. Technol* 28: 265-274.

Doig SD, Pickering SCR, Lye GJ, Woodley JM (2002) The use of microscale processing technologies for quantification of biocatalytic Baeyer-Villiger oxidation kinetics. *Biotechnol Bioeng* 80: 42-49.

Doig SD, Baganz F, Lye GJ (2006) High throughput screening and process optimisation, in: Ratledge C and Kristiansen B (Eds), *Basic Biotechnology*, 3<sup>rd</sup> Ed. Cambridge: Cambridge University Press.

Duetz WA, Rüedi L, Hermann R, O’Connor K, Büchs J, Witholt B (2000) Methods for intense aeration, growth, storage and replication of bacterial strains in microtitre plates. *Appl Environ Microbiol* 66: 2641-2646.

Duetz WA and Witholt B (2001) Effectiveness of orbital shaking for the aeration of suspended bacterial cultures in square-deepwell microtiter plates. *Biochem Eng J* 7: 113–115.

Duclos-Osello C, Li W, Ho C (2006) A three mechanism model to describe fouling of microfiltration membranes. *J Membr Sci* 280: 856-866.

Elmahdi I, Baganz F, Dixon K, Harrop T, Sugden D, Lye GJ (2003) pH control in microwell fermentations of *S. erythraea* CA340: influence on biomass growth kinetics and erythromycin biosynthesis. *Biochem Eng J* 16: 299–310.

Fane AG, Fell CJD, Waters AG (1983) Ultrafiltration of protein solutions through partially permeable membranes – the effect of adsorption and solution environment. *J Membr Sci* 16: 211-224.

Feng X and Robert Y. M. Huang (1997) Liquid Separation by Membrane Pervaporation: A Review. *Ind Eng Chem Res* 36(4): 1048-1066.

Ferreira GNM, Monteiro GA, Prazeres DMF, Cabral JMS (2000) Downstream processing of plasmid DNA for gene therapy and DNA vaccine applications. *Trends Biotechnol* 18(9): 380-388.

Ferreira-Torres C, Micheletti M, Lye GJ (2005) Microscale process evaluation of recombinant biocatalyst libraries: application to Baeyer–Villiger monooxygenase catalysed lactone synthesis. *Bioprocess Biosyst Eng* 28(2): 83-93.

Fisher RA (1925) *Statistical Methods for Research Workers*. Edinburgh: Oliver & Boyd.

Fisher RA (1935) *The Design of Experiments*. Edinburgh: Oliver & Boyd.

Foley G (2006) A review of factors affecting filter cake properties in dead-end microfiltration of microbial suspensions. *J Membr Sci* 274: 38-46.

Fries A and Hunter WG (1980) Minimum Aberration  $2^{k-p}$  Designs. *Technometrics* 22(4): 601-608.

Fritzmann C, Löwenberga J, Wintgens T, Melina T (2007) State-of-the-art of reverse osmosis desalination. *Desalination* 216(1-3): 1-76.

García-Arazola R, Siu SC, Chan G, Buchanan I, Doyle B, Titchener-Hooker N, Baganz F (2005) Evaluation of a pH-stat feeding strategy on the production and recovery of Fab' fragments from *E.coli*. *Biochem Eng J* 23(3): 221-230.

Ghosh R (2002) Protein separation using membrane chromatography: opportunities and challenges. *J Chromatogr A* 952(1-2): 13-27.

Gill NK, Appleton M, Baganz F, Lye GJ (2008a) Design and characterisation of a miniature stirred bioreactor system for parallel microbial fermentations. *Biochem Eng J* 39(1): 164-176.

Gill NK, Appleton M, Baganz F, Lye GJ (2008b) Quantification of power consumption and oxygen transfer characteristics of a stirred miniature bioreactor for predictive fermentation scale-up. *Biotechnol Bioeng* 100(6): 1144–1155.

Goeddel DV, Heyneker HL, Hozumi T, Arentzen R, Itakura K, Yansura DG, Ross MJ, Miozzari G, Crea R, Seeburg PH (1979) Direct expression in *Escherichia coli* of a DNA sequence coding for human growth hormone. *Nature* 281(5732): 544-548.

Gonsalves VE (1950) A critical investigation on the viscose filtration process. *Rec Trav Chim Pays-Bas* 69: 873-903.

Grace HP (1956) Structure and performance of filter media. II. Performance of filter media in liquid service. *AIChE J* 2(3): 316–336.

Gray DE (Ed.) (1972) *American Institute of Physics Handbook*, 3<sup>rd</sup> Ed. New York: McGraw-Hill.

Gribbon P and Andreas S (2005) High-throughput drug discovery: What can we expect from HTS? *Drug Discov Today* 10(1): 17-22.

Griesenbach U (2007) Progress and Prospects: Gene Therapy Clinical Trials (Part 2). *Gene Ther* 14: 1555-1563.

Hansson M, Ståhl S, Hjorth R, Uhlén M, Moks T (1994) Single-Step Recovery of a Secreted Recombinant Protein by Expanded Bed Adsorption. *Nat Biotechnol* 12: 285-288.

Harre M, Tilstam U, Weinmann H (1999) Breaking the New Bottleneck: Automated Synthesis in Chemical Process Research and Development. *Org Process Res Dev* 3: 304-318.

Harrison AC and Walker DK (1998) Automated 96-well solid phase extraction for the determination of doramectin in cattle plasma. *J Pharmaceut Biomed* 16(5): 777–783.

Hermans PH and Bredée HL (1935) Zur kenntnis der filtrationsgesetze, *Rec Trav Chim Pays-Bas*, 54: 680-700.

Hermans PH and Bredée HL (1936) Principles of the mathematical treatment of constant-pressure filtration. *J Soc Chem Ind* 55:1-4.

Hermia J (1966) Étude analytique des lois de filtration à pression constante. *Rev Univ Mines* 2: 45–51.

Hermia J (1982) Constant pressure blocking filtration laws - application to power-law non-newtonian fluids. *Trans Inst Chem Eng* 60: 183-187.

Higgins SJ and Hames BD (Eds) (1999) *Protein expression: a practical approach*. Oxford: Oxford University Press.

Hilal N, Al-Zoubi H, Darwish NA, Mohamma AW, Abu Arabi M (2004) A comprehensive review of nanofiltration membranes: Treatment, pretreatment, modelling, and atomic force microscopy. *Desalination* 170(3): 281-308.

Ho RJY and Gibaldi M (2003) *Biotechnology and biopharmaceuticals: transforming proteins and genes into drugs*. Hoboken: Wiley-Liss.

Ho C and Zydney AL (2000) A Combined Pore Blockage and Cake Filtration Model for Protein Fouling during Microfiltration. *J Colloid Interf Sci* 232: 389-399.

Hoare M, Levy MS, Bracewell DG, Doig SD, Kong S, Titchener-Hooker N, Ward JM, Dunnill P (2005) Bioprocess Engineering Issues That Would Be Faced in Producing a DNA Vaccine at up to 100 m<sup>3</sup> Fermentation Scale for an Influenza Pandemic. *Biotechnol Prog* 21: 1577-1592.

Hoare M, Dunnill P, Bell DJ (1983) Reactor Design for Protein Precipitation and Its Effect on Centrifugal Separation. *Ann NY Acad Sci* 413: 254-269.

Hodgson PH, Leslie GL, Fane AG, Schneider RP, Fell CJD, Marshall KC (1993) Cake resistance and solute rejection in bacterial microfiltration: The role of the extracellular matrix. *J Membr Sci* 79(1): 35-53.

Humphrey A (1998) Shake Flask to Fermentor: What Have We Learned? *Biotechnol Progr* 14(1): 3-7.

Ishihara T, Yamamoto S (2005) Optimization of monoclonal antibody purification by ion-exchange chromatography: Application of simple methods with linear gradient elution experimental data. *J Chromatogr A* 1069(1): 99-106.

Jabs DA, Griffiths PD (2002) Fomivirsen for the treatment of cytomegalovirus retinitis. *Am J Ophthalmol* 133(4): 552-6.

- Jackson NB, Liddell JM, Lye GJ (2006) An automated microscale technique for the quantitative and parallel analysis of microfiltration operations. *J Membr Sci* 276: 31-41.
- Jin K, Thomas ORT, Dunnill P (1994) Monitoring recombinant inclusion body recovery in an industrial disc stack centrifuge. *Biotechnol Bioeng* 43(6): 455–460.
- John GT, Klimant I, Wittmann C, Heinzle E (2003) Integrated optical sensing of dissolved oxygen in microtitre plates: a novel tool for microbial cultivation. *Biotechnol Bioeng* 81(7): 829–836.
- Jornitz MW, Soelkner PG, Meltzer TH (2002) Sterile Filtration – A Review of the Past and Present Technologies. *PDA J Pharm Sci Technol* 56: 192-195.
- Junker BH (2004) Scale-up methodologies for *Escherichia coli* and yeast fermentation processes. *J Biosci Bioeng* 97(6): 347-364.
- Kahn DW, Butler MD, Cohen DL, Gordon M, Kahn JW, Winkler ME (2000) Purification of plasmid DNA by tangential flow filtration. *Biotechnol Bioeng* 69(1): 101–106.
- Kelley BD, Hatton TA (1991) The fermentation/downstream processing interface. *Bioseparation* 1(5-6): 333-349.
- Kendall D, Lye GJ, Levy MS (2002) Purification of plasmid DNA by an integrated operation comprising tangential flow filtration and nitrocellulose adsorption. *Biotechnol Bioeng* 79(7): 816–822.
- Klyushnichenko V (2003) Protein crystallization: From HTS to kilogram-scale. *Curr Opin Drug Discov Devel* 6: 848-854.
- Kong S, Titchener-Hooker N, Levy MS (2006) Plasmid DNA processing for gene therapy and vaccination: Studies on the membrane sterilisation filtration step. *J Membr Sci* 280(1-2): 824-831.
- Kostov Y, Harms P, Randers-Eichhorn L, Rao G (2001) Low-cost microbioreactor for high-throughput bioprocessing. *Biotechnol Bioeng* 72(3): 346–352.
- Kosvintsev S, Holdich RG, Cumming IW, Starov VM (2002) Modelling of dead-end microfiltration with pore blocking and cake formation. *J Membr Sci* 208: 181-192.
- Kumar S, Wittmann C, Heinzle E (2004) Review: Minibioreactors. *Biotechnol Lett* 26(1): 1-10.

- Kurnik RT, Yu AW, Blank GS, Burton AR, Smith D, Athalye AM, van Reis R (1995) Buffer exchange using size exclusion chromatography, countercurrent dialysis, and tangential flow filtration: Models, development, and industrial application. *Biotechnol Bioeng* 45(2): 149-157.
- Kuriyel R and Zydney AL (2000) Sterile filtration and virus filtration, in: Desai M (Ed.), *Downstream Processing of Proteins: Methods and Protocols*, Vol 9. Totowa: Humana Press.
- Lamping SR, Zhang H, Allen B, Ayazi-Shamlou P (2002) Design of a prototype miniature bioreactor for high throughput automated bioprocessing, *Chem Eng Sci* 58(3): 747-758.
- Lander RJ, Winters MA, Meacle FJ, Buckland BC, Lee AL (2002) Fractional precipitation of plasmid DNA from lysate by CTAB. *Biotechnol Bioeng* 79(7): 776-784.
- Lander KS (2002) In-situ product removal to enhance the productivity of Baeyer-Villiger monooxygenase bioconversion processes, PhD Thesis, University of London.
- Lee SS, Burt A, Russotti G, Buckland B (2004) Microfiltration of recombinant yeast cells using a rotating disk dynamic filtration system. *Biotechnol Bioeng* 48(4): 386-400.
- Lee CT, Buswell AM, Middelberg APJ (2002) The influence of mixing on lysozyme renaturation during refolding in an oscillatory flow and a stirred-tank reactor. *Chem Eng Sci* 57(10): 1679-1684.
- Levy MS, Collins IJ, Tsai JT, Ayazi Shamlou P, Ward JM, Dunnill P (2000) Removal of contaminant nucleic acids by nitrocellulose filtration during pharmaceutical-grade plasmid DNA processing. *J Biotechnol* 76(2-3): 197-205.
- Light WG, Tran TV (1981) Improvement of Thin-Channel Design for Pressure-Driven Membrane Systems. *Ind Eng Chem Proc Des Dev* 20(1): 33-40.
- Ling Y, Wong HH, Thomas CJ, Williams DRG, Middelberg APJ (1998) Pilot-scale extraction of PHB from recombinant *E. coli* by homogenization and centrifugation. *Bioseparation* 7(1): 9-15.
- Luque S, Mallubhotla H, Gehlert G, Kuriyel R, Dzengeleski S, Pearl S, Belfort G (1999) A new coiled hollow-fiber module design for enhanced microfiltration performance in biotechnology. *Biotechnol Bioeng* 65(3): 247-257.

- Lutz H (2009) Rationally defined safety factors for filter sizing. *J Membr Sci* 341: 268-278.
- Lye GJ, Ayazi-Shamlou P, Baganz F, Dalby PA, Woodley JM (2003) Accelerated design of bioconversion processes using automated microscale processing techniques. *Trends Biotechnol* 21(1): 29-37.
- Maiorella B, Inlow D, Shauger A, Harano D (1988) Large-Scale Insect Cell-Culture for Recombinant Protein Production. *Nature Biotechnol* 6: 1406-1410.
- Mannall GJ, Titchener-Hooker NJ, Chase HA, Dalby PA (2006) A critical assessment of the impact of mixing on dilution refolding. *Biotechnol Bioeng* 93(5): 955-963.
- McCarthy AA, O'Shea DG, Murray BT, Walsh PK, Foley G (1998) Effect of cell morphology on dead-end filtration of the dimorphic yeast *Kluyveromyces marxianus* var. *marxianus* NRRLy2415. *Biotechnol Prog* 14: 279-285.
- McCue JT, Kemp G, Low D, Quiñones-García I (2003) Evaluation of protein-A chromatography media. *J Chromatogr A* 989(1): 139-153.
- Micheletti M and Lye GJ (2006) Microscale bioprocess optimisation. *Curr Opin Biotech* 17(6): 611-618.
- Montgomery DC (2008) Design and analysis of experiments, 7<sup>th</sup> Ed. Hoboken: Wiley.
- Mülhardt C (2007) Molecular biology and genomics. Burlington: Academic Press.
- Myers RH, Montgomery DC, Anderson-Cook CM (2009) Response surface methodology: process and product optimization using designed experiments, 2<sup>nd</sup> Ed. Hoboken: Wiley.
- Nakanishi K, Tadokoro T, Matsuno R (1987) On the specific resistance of cakes and microorganisms. *Chem Eng Comm* 62: 187-201.
- Nassehi V, Hanspal NS, Waghode AN, Ruziwa WR, Wakeman RJ (2005) Finite-element modelling of combined free/porous flow regimes: simulation of flow through pleated cartridge filters. *Chem Eng Sci* 60(4): 995-1006.
- Nealon AJ, Willson KE, Pickering SCR, Clayton TM, O'Kennedy R, Titchener-Hooker NJ, Lye GJ (2005) Use of operating windows in the assessment of integrated robotic systems for the measurement of bioprocess kinetics. *Biotechnol Prog* 21: 283-291.

- Ng EWM, Shima DT, Calias P, Cunningham Jr ET, Guyer DR, Adamis AP (2006) Pegaptanib, a targeted anti-VEGF aptamer for ocular vascular disease. *Nat Rev Drug Disc* 5: 123-132.
- Ohmori K and Glatz CE (1999) Effects of pH and ionic strength on microfiltration of *C. Glutamicum*. *J Membr Sci* 153: 23-32.
- Okamoto Y, Ohmori K, Glatz CE (2001) Harvest time effects on membrane cake resistance of *Escherichia coli* broth. *J Membr Sci* 190: 93-106.
- Perry RH and Green DW (1997) *Perry's chemical engineers' handbook*, 7<sup>th</sup> Ed. New York: McGraw-Hill.
- Persson A, Jönsson A, Zacchi G (2003) Transmission of BSA during cross-flow microfiltration: influence of pH and salt concentration. *J Membr Sci* 223(1-2): 11-21.
- Pierce JJ, Turner C, Keshavarz-Moore E, Dunnill P (1997) Factors determining more efficient large-scale release of a periplasmic enzyme from *E. coli* using lysozyme. *J. Biotechnol* 58: 1-11.
- Plackett RL and Burman JP (1946) The design of optimum multifactorial experiments. *Biometrika* 33: 305-325.
- Placzek MR, Chung I, Macedo HM, Ismail S, Blanco TM, Lim M, Cha JM, Fauzi I, Kang Y, Yeo DCL, Ma CYJ, Polak JM, Panoskaltis N, Mantalaris A (2009) Stem cell bioprocessing: fundamentals and principles. *J R Soc Interface* 6(32): 209-232.
- Poiseuille LM (1840) Recherches expérimentales sur le mouvement des liquides dans les tubes de très petits diamètres. *Comptes Rendus Acad Sc* 11: 961-967.
- Pollard M (2001) *Process Development Automation: An Evolutionary Approach*. *Org Process Res Dev* 5: 273-282.
- Prazeres DMF, Ferreira GNM, Monteiro GA, Cooney CL, Cabral JMS (1999) Large-scale production of pharmaceutical-grade plasmid DNA for gene therapy: problems and bottlenecks. *Trends Biotechnol* 17(4): 169-174.
- Puskeiler R, Kaufmann K, Weuster-Botzet D (2005) Development, parallelization, and automation of a gas-inducing milliliter-scale bioreactor for high-throughput bioprocess design (HTBD). *Biotechnol Bioeng* 89(5): 512-523.
- Queiroz JA, Tomaz CT, Cabral JMS (2001) Hydrophobic interaction chromatography of proteins. *J Biotechnol* 87(2): 143-159.

- Raghavan S, Jan D, Chilkunda R (1996) Modification of polyvinylidene fluoride membrane and method of filtering, US Pat 5,531,900.
- Rathone AS and Mhatre R (2009) *Quality by Design for Biopharmaceuticals: Principles and Case Studies*. Hoboken: Wiley.
- Reichert J and Pavlou A (2004) Monoclonal antibodies market. *Nat Rev Drug Disc* 3: 383-384.
- Reichert JM, Rosensweig CJ, Faden LB, Dewitz MC (2005) Monoclonal antibody successes in the clinic. *Nat Biotechnol* 23: 1073-1078.
- Reynolds T, Bochyn M, Sanderson T, Bulmer M, More J, Hoare M (2003) Scale-Down of Continuous Filtration for Rapid Bioprocess Design: Recovery and Dewatering of Protein Precipitate Suspensions. *Biotech Bioeng* 83: 454-464.
- Riesmeier R, Kroner KH, Kula M (1990) Harvest of microbial suspensions by microfiltration. *Desalination* 77: 219-233.
- Roque AC, Lowe CR (2008) Affinity chromatography: history, perspectives, limitations and prospects. *Methods Mol Biol* 421: 1-21.
- Rosenberg E, Hepbildikler S, Kuhne W, Winter G (2009) Ultrafiltration concentration of monoclonal antibody solutions: Development of an optimized method minimizing aggregation. *J Membr Sci* 342(1-2): 50-59.
- Russo E (2003) Special Report: The birth of biotechnology. *Nature* 421: 456-457.
- Russotti G, Osawa AE, Sitrin RD, Buckland BC, Adams WR, Lee SS (1995) Pilot-scale harvest of recombinant yeast employing microfiltration: a case study. *J Biotechnol* 42: 235-246.
- Ruth BF (1935) Studies in Filtration III. Derivation of General Filtration Equations. *Ind Eng Chem* 27(6): 708-723.
- Ruth BF, Montillon GH, Montonna RE (1933a) Studies in Filtration - I. Critical Analysis of Filtration Theory. *Ind Eng Chem* 25(1): 76-82.
- Ruth BF, Montillon GH, Montonna RE (1933b) Studies in Filtration - II. Fundamental Axiom of Constant-Pressure Filtration. *Ind Eng Chem* 25(2): 153-161.

Sablani SS, Goosen MFA, Al-Belushi R, Wilf M (2001) Concentration polarization in ultrafiltration and reverse osmosis: a critical review. *Desalination* 141(3): 269-289.

Shukla AA, Hubbard B, Tressel T, Guhan S, Low D (2007) Downstream processing of monoclonal antibodies – Application of platform approaches. *J Chromatogr B* 848(1): 28-39.

Shusta EV, Raines RT, Pluckthun A, Wittrup KD (1998) Increasing the secretory capacity of *Saccharomyces cerevisiae* for production of single-chain antibody fragments. *Nat Biotechnol* 16: 773-777.

Singhvi R, Schorr C, O'Hara C, Xie L, Wang DIC (1996) Clarification of Animal Cell Culture Process Fluids Using Depth Microfiltration. *BioPharm* 9(4): 35-41.

Song L (1998) Flux decline in crossflow microfiltration and ultrafiltration: mechanisms and modeling of membrane fouling. *J Membr Sci* 139(2): 183-200.

Staub JM, Garcia B, Graves J, Hajdukiewicz PTJ, Hunter P, Nehra N, Paradkar V, Schlittler M, Carroll JA, Spatola L, Ward D, Ye G, Russell DA (2000) High-yield production of a human therapeutic protein in tobacco chloroplasts. *Nat Biotechnol* 18: 333-338.

Sutherland K (2008) *Filters and filtration handbook*, 5<sup>th</sup> Ed. Oxford: Butterworth-Heinemann.

Tarleton ES and Wakeman RJ (1994) Understanding flux decline in crossflow microfiltration. II: Effects of process parameters. *Chem Eng Res Des* 72: 431-440.

Tracey EM and Davis RH (1994) Protein Fouling of Track-Etched Polycarbonate Microfiltration Membranes. *J Colloid Interf Sci* 167(1): 104-116.

Ulbricht M, Schuster O, Ansorge W, Ruetering M, Steiger P (2007) Influence of the strongly anisotropic cross-section morphology of a novel polyethersulfone microfiltration membrane on filtration performance. *Sep Purif Technol* 57(1): 63-73.

van Reis R and Zydney A (2001) Membrane separations in biotechnology. *Curr Opin Biotech* 12: 208-211.

van Reis R and Zydney A (2007) Bioprocess membrane technology. *J Membr Sci* 297: 16-50.

van Reis R, Goodrich EM, Yson CL, Frautschy LN, Dzengeleski S, Lutz H (1997) Linear Scale Ultrafiltration. *Biotechnol Bioeng* 55, p737-746.

- van Reis R, Brake JM, Charkoudian J, Burns DB, Zydney AL (1999) High-performance tangential flow filtration using charged membranes. *J Membr Sci* 159(1-2): 133-142.
- Vandezande P, Gevers LEM, Paul JS, Vankelecom IFJ, Jacobs PA (2005) High throughput screening for rapid development of membranes and membrane processes, *J Membr Sci* 250: 305-310.
- Verma IM and Weitzman MD (2005) Gene Therapy: Twenty-First Century Medicine. *Annu Rev Biochem* 74: 711-738.
- Walsh G (2002) *Proteins: biochemistry and biotechnology*. Hoboken: Wiley.
- Walsh G (2005) Biopharmaceuticals: recent approvals and likely directions. *Trends Biotechnol* 23(11): 553-558.
- Walther W and Stein U (2000) Viral vectors for gene transfer: a review of their use in the treatment of human diseases. *Drugs* 60(2): 249-271.
- Welch CJ, Shaimi M, Biba M, Chilenski JR, Szumigala RH, Dolling U, Mathre DJ, Reider PJ (2002) Microplate evaluation of process adsorbents. *J Sep Sci* 25(13): 847-850.
- Werner RG (2004) Economic aspects of commercial manufacture of biopharmaceuticals. *J Biotechnol* 113: 171-182.
- Wheelwright SM (1989) The design of downstream processes for large-scale protein purification. *J Biotechnol* 11(2-3): 89-102.
- Winters MA, Richter JD, Sagar SL, Lee AL, Lander RJ (2003) Plasmid DNA Purification by Selective Calcium Silicate Adsorption of Closely Related Impurities. *Biotechnol Progr* 19(2): 440-447.
- Witholt B, Heerikhuizen HV, De-Leij L (1976) How does lysozyme penetrate through the bacterial outer membrane? *Biochim Biophys Acta* 443: 534-544.
- Woodley JM and Titchener-Hooker NJ (1996) The use of windows of operation as a bioprocess design tool. *Bioprocess Biosyst Eng* 14(5): 263-268.
- Wu CF and Hamada M (2000) *Experiments: planning, analysis, and parameter design optimization*. New York: Wiley.

- Wutzel H and Samhaber WM (2009) Porous polymer nanoparticle layers. *Desalination* 240(1-3): 27-35.
- Yamagishi H, Crivello JV, Belfort G (1995) Development of a novel photochemical technique for modifying poly (arylsulfone) ultrafiltration membranes. *J Membr Sci* 105(3): 237-247.
- Yates F and Mather K (1963) Ronald Aylmer Fisher. *Biographical Memoirs of Fellows of the Royal Society of London* 9: 91-120.
- Yates F (1937) *The design and analysis of factorial experiments*, Technical Communication 35. Harpenden: Imperial Bureau of Soil Science.
- Zeman LJ and Zydney AL (1996) *Microfiltration and ultrafiltration: principles and applications*. New York: Marcel Dekker.
- Zhang J and Lynch J (2005) A high throughput ultrafiltration assay for the determination of unbound drug concentrations in human plasma. *Drug Plus International*, September 2005, p23-26.
- Zhou YH and Titchener-Hooker NJ (1999) Visualizing integrated bioprocess designs through “windows of operation”. *Biotechnol Bioeng* 65(5): 550-557.
- Zhou W, Chen C, Buckland B, Aunins J (1997) Fed-batch culture of recombinant NS0 myeloma cells with high monoclonal antibody production. *Biotechnol Bioeng* 55(5): 783-792.
- Zydney AL and Colton CK (1986) A concentration polarization model for the filtrate flux in cross-flow microfiltration of particulate suspensions. *Chem Eng Commun* 47(1-3): 1-21.
- Zydney AL and Ho C (2002) Scale-up of microfiltration systems: fouling phenomena and  $V_{\max}$  analysis. *Desalination* 146: 75-81.
- Zydney AL and Ho C (2003) Effect of Membrane Morphology on System Capacity During Normal Flow Microfiltration. *Biotech Bioeng* 83(5): 537-543.

## **A.0 Appendix A: Calibration curves**

### **A.1 Dry cell weight**

As described in Section 2.4.2 the optical density (OD) at 600nm and 1cm path length was calibrated to calculated *E.coli* dry cell weight (DCW). Figure A.1(a) shows that the early stages of fermentation provide a different ratio of OD to DCW. To calibrate the OD to DCW for completed fermentations the data from after 4 h was used. Several dilutions ranging from 1:10 to 1:30 were used to get the data into the linear range of the detector. It was assumed that the open circle data points were not within the linear range and these were not used to correlate the data.

### **A.2 Lysozyme concentration**

For each set of samples run on the reverse phase HPLC column as described in Section 2.6.1, a standard curve was generated using a 2g.L<sup>-1</sup> standard solution four times serially diluted 1 in 2. A typical plot of the integrated lysozyme peak area against the concentration of lysozyme is shown in Figure A.2. The very strong linear response is always seen with coefficient of determination ( $R^2$ ) values close to unity, showing the accuracy of the HPLC injection volume, HPLC method and serial dilution technique.

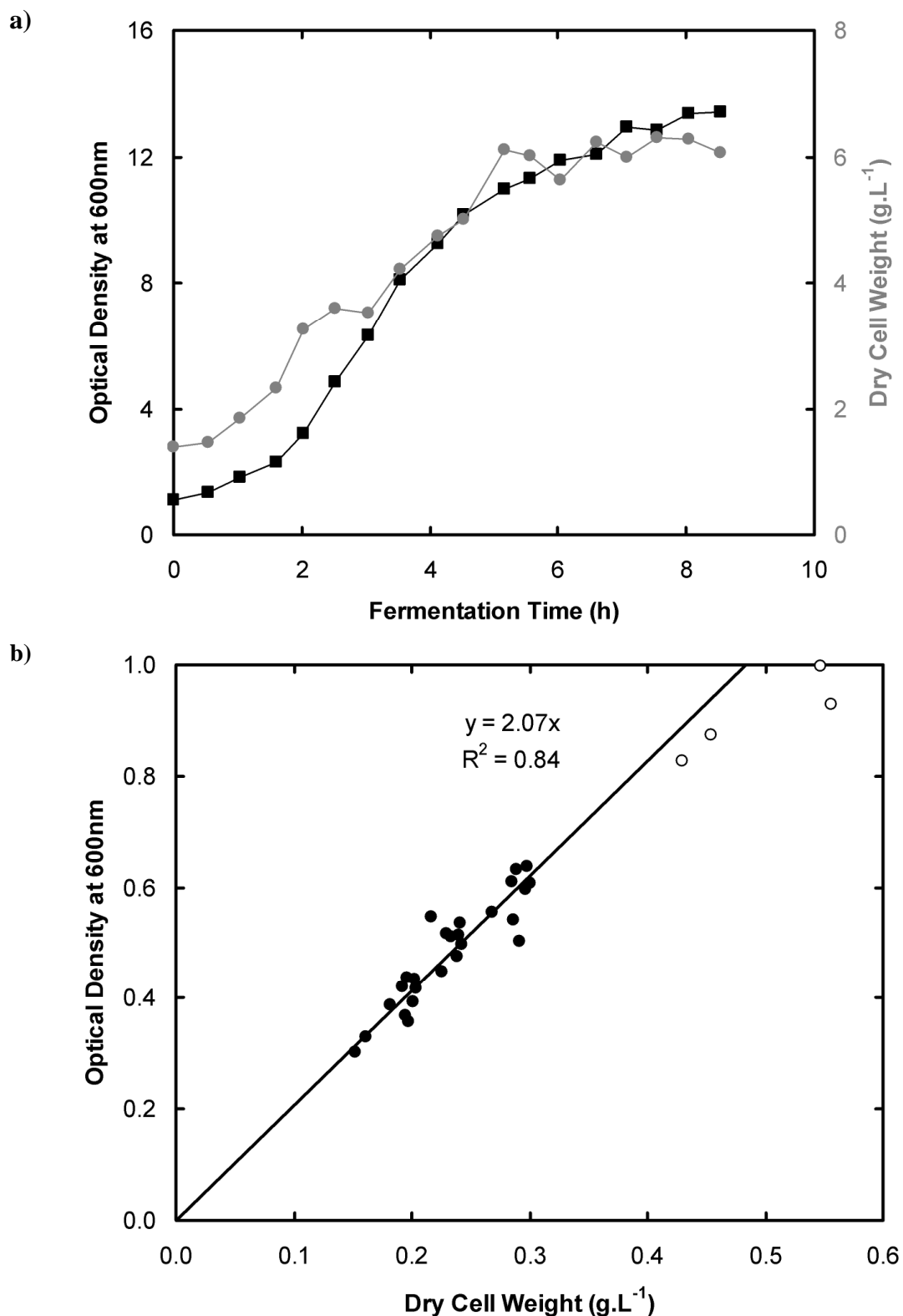


**Figure A.1.** (a) Typical *E.coli* shake flask fermentation growth curve and (b) the calibration of optical density to *E.coli* dry cell weight. Only growth curve data after 4h were used to generate the calibration curve. Open circles represent data outside the calibration range which were not used to generate the line of best fit. Experiments carried out as described in Section 2.4.1 and Section 2.4.2. Further details discussed in Section A.1.

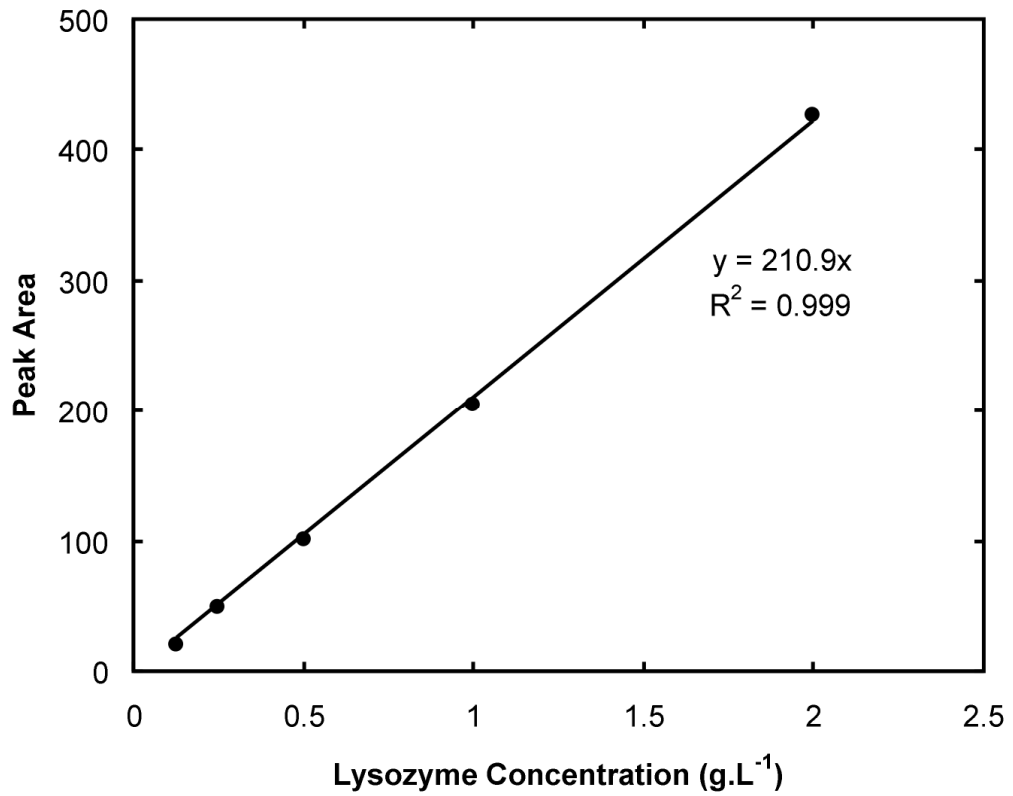


**Figure A.2.** Typical Lysozyme HPLC calibration curve showing the strong linear response over the concentration range tested. Assay carried out as described in Section 2.6.1. Further details discussed in Section A.2.

## B.0 Appendix B: Microscale calculation examples

### B.1 Example *E.coli* specific cake resistance calculation

Using the equations developed in Section 3.4.1 the raw mass and time data generated from the custom microwell filter plate can be used to estimate specific cake resistance and predict laboratory scale flux performance. Figure B.1 shows the example data progression from (a) the raw data to (b) linearised plots to (c) specific cake resistances and to (d) flux predictions. It demonstrates the data treatment for two data sets comparing *E.coli* cells resuspended in either freshly prepared yeast extract solution or the original broth supernatant. This section details the calculations required for the sample data in Figure B.1. The full data set for this experiment is summarised in Section 3.4.4.

#### B.1.1 Raw data

The shared raw data as well as specific data for yeast extract solution and cell broth supernatant are given in this section. The key raw data of mass and time is shown in Figure B.1(a).

##### B.1.1.1 Shared raw data

Time interval 1	$t_1 = 60 \text{ s}$
Time interval 2	$t_2 = 300 \text{ s}$
Dynamic permeate viscosity	$\mu = 0.001 \text{ N.s.m}^{-2}$
Effective filtration area	$A = 7.85 \times 10^{-5} \text{ m}^2$
Dry solids concentration	$c = 4.4 \text{ g.L}^{-1} = 4.4 \text{ kg.m}^{-3}$
Transmembrane pressure	$\Delta P = 60.0 \text{ kPa} = 6.00 \times 10^4 \text{ N.m}^{-2}$
Permeate density	$\rho_p = 1.00 \text{ g.mL}^{-1} = 1000 \text{ kg.m}^{-3}$

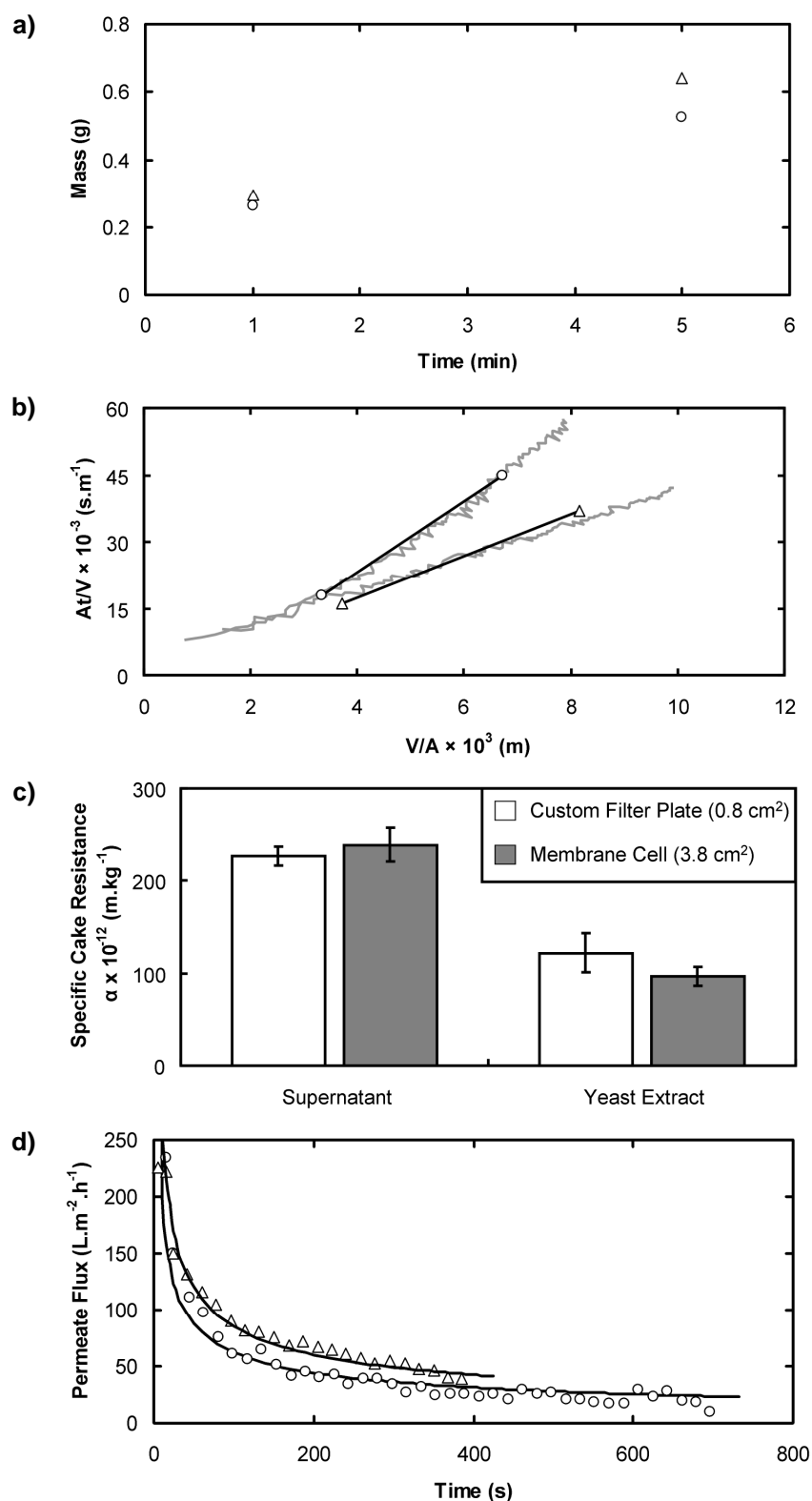


**Figure B.1.** The data progression from (a) example custom microwell filter plate raw mass and time data, to (b) linearised cake formation plots, through (c) specific cake resistance data, to (d) predicted laboratory scale flux decay curves. Data compares *E.coli* resuspended in (○) original broth supernatant compared to (△) freshly prepared yeast extract solution. Grey lines (b) represent laboratory scale membrane cell (3.8 cm<sup>2</sup>) results. Solid lines in (d) show the custom microwell filter plate (0.8 cm<sup>2</sup>) predictions of the membrane cell data. Described in detail in Appendix Section B.1.

## B.1.1.2 Yeast extract solution

Measured mass 1	$m_1 = 0.293 \text{ g}$
Measured mass 2	$m_2 = 0.640 \text{ g}$

## B.1.1.3 Cell broth supernatant

Measured mass 1	$m_1 = 0.262 \text{ g}$
Measured mass 2	$m_2 = 0.527 \text{ g}$

**B.1.2 Linearised cake formation data**

In order to fit the data to a linearised plot, as shown in Figure B.1(b), the data is manipulated into the form indicated by Equation 1.20.

## B.1.2.1 Yeast extract solution

$$\frac{V_1}{A} = \frac{0.293 \text{ g} \times 10^{-6} \text{ m}^3 \cdot \text{mL}^{-1}}{1.00 \text{ g} \cdot \text{mL}^{-1} \times 7.85 \times 10^{-5} \text{ m}^2} = 3.73 \times 10^{-3} \text{ m}$$

$$\frac{V_2}{A} = \frac{0.640 \text{ g} \times 10^{-6} \text{ m}^3 \cdot \text{mL}^{-1}}{1.00 \text{ g} \cdot \text{mL}^{-1} \times 7.85 \times 10^{-5} \text{ m}^2} = 8.15 \times 10^{-3} \text{ m}$$

$$\frac{At_1}{V_1} = \frac{60 \text{ s}}{3.72 \times 10^{-3} \text{ m}} = 16.1 \times 10^3 \text{ s} \cdot \text{m}^{-1}$$

$$\frac{At_2}{V_2} = \frac{300 \text{ s}}{8.15 \times 10^{-3} \text{ m}} = 36.8 \times 10^3 \text{ s} \cdot \text{m}^{-1}$$

## B.1.2.2 Cell broth supernatant

$$\frac{V_1}{A} = \frac{0.262 \text{ g} \times 10^{-6} \text{ m}^3 \cdot \text{mL}^{-1}}{1.00 \text{ g} \cdot \text{mL}^{-1} \times 7.85 \times 10^{-5} \text{ m}^2} = \mathbf{3.33 \times 10^{-3} \text{ m}}$$

$$\frac{V_2}{A} = \frac{0.527 \text{ g} \times 10^{-6} \text{ m}^3 \cdot \text{mL}^{-1}}{1.00 \text{ g} \cdot \text{mL}^{-1} \times 7.85 \times 10^{-5} \text{ m}^2} = \mathbf{6.71 \times 10^{-3} \text{ m}}$$

$$\frac{At_1}{V_1} = \frac{60 \text{ s}}{3.33 \times 10^{-3} \text{ m}} = \mathbf{18.0 \times 10^3 \text{ s} \cdot \text{m}^{-1}}$$

$$\frac{At_2}{V_2} = \frac{300 \text{ s}}{6.71 \times 10^{-3} \text{ m}} = \mathbf{44.7 \times 10^3 \text{ s} \cdot \text{m}^{-1}}$$

## B.1.3 Specific cake resistance

The mean specific cake resistance data is shown in Figure B.1(c) and the specific values for the example data sets are calculated in this section. Equation 3.6, described and developed in Section 3.4.1, is used as follows to calculate the specific cake resistance,  $\alpha$  ( $\text{m} \cdot \text{kg}^{-1}$ ):

$$\alpha = \frac{\left( \frac{t_2}{V_2} - \frac{t_1}{V_1} \right)}{(V_2 - V_1)} \cdot \frac{2A^2 \Delta P}{\mu c}$$

$$= \frac{\left( \frac{At_2}{V_2} - \frac{At_1}{V_1} \right)}{\left( \frac{V_2}{A} - \frac{V_1}{A} \right)} \cdot \frac{2\Delta P}{\mu c}$$

## B.1.3.1 Yeast extract solution

$$\alpha = \frac{(36.8 \times 10^3 \text{ s} \cdot \text{m}^{-1} - 16.1 \times 10^3 \text{ s} \cdot \text{m}^{-1})}{(8.15 \times 10^{-3} \text{ m} - 3.73 \times 10^{-3} \text{ m})} \times \frac{2 \times 6.00 \times 10^4 \text{ N} \cdot \text{m}^{-2}}{0.001 \text{ N} \cdot \text{s} \cdot \text{m}^{-2} \times 4.4 \text{ kg} \cdot \text{m}^{-3}}$$

$$\alpha = \mathbf{128 \times 10^{12} \text{ m} \cdot \text{kg}^{-1}}$$

## B.1.3.2 Cell broth supernatant

$$\alpha = \frac{(44.7 \times 10^3 \text{ s.m}^{-1} - 18.0 \times 10^3 \text{ s.m}^{-1})}{(6.71 \times 10^{-3} \text{ m} - 3.33 \times 10^{-3} \text{ m})} \times \frac{2 \times 6.00 \times 10^4 \text{ N.m}^{-2}}{0.001 \text{ N.s.m}^{-2} \times 4.4 \text{ kg.m}^{-3}}$$

$$\alpha = 216 \times 10^{12} \text{ m.kg}^{-1}$$

## B.1.4 Flux predictions

The scale-up and prediction of larger scale flux is detailed in Section 2.8.11. Using the modified cake filtration constant,  $K_c'$  ( $\text{N.s.m}^{-4}$ ), Equation 2.20 predicts the flux up until the time (calculated by Equation 2.21) that a fixed volume has been filtered. The modified cake filtration constant is calculated as follows using Equation 3.7:

$$\alpha = 2A^2 \Delta P \frac{\left( \frac{t_2}{V_2} - \frac{t_1}{V_1} \right)}{(V_2 - V_1)}$$

$$= 2\Delta P \frac{\left( \frac{At_2}{V_2} - \frac{At_1}{V_1} \right)}{\left( \frac{V_2}{A} - \frac{V_1}{A} \right)}$$

The detailed flux decline predictions over time are shown in Figure B.1(d) and in more detail in Figure 3.7. For example flux calculations here, Equation 2.21 is adapted to calculate the average flux,  $J_{average}$  ( $\text{m.s}^{-1}$ ), required to process a fixed volume.

$$t_{final} = \frac{V_{final}}{A} \left( \frac{K_c' V_{final}}{2A\Delta P} + \frac{1}{J_0} \right)$$

$$J_{average} = \frac{V_{final}}{t_{final} A}$$

$$J_{average} = \frac{1}{\left( \frac{K_c'}{2\Delta P} \cdot \frac{V_{final}}{A} + \frac{1}{J_0} \right)}$$

The following values are taken from Table 3.1 and Figure 3.2(b):

$$\frac{V_{final}}{A} = 1.05 \text{ mL.cm}^{-2} = 1.05 \times 10^{-7} \text{ m}$$

$$J_0 = 4820 \text{ L.m}^{-2}.\text{h}^{-1} = 1.34 \times 10^{-3} \text{ m.s}^{-1}$$

#### B.1.4.1 Yeast extract solution

$$K_c' = 2 \times 6.00 \times 10^4 \text{ N.m}^{-2} \times \frac{(36.8 \times 10^3 \text{ s.m}^{-1} - 16.1 \times 10^3 \text{ s.m}^{-1})}{(8.15 \times 10^{-3} \text{ m} - 3.73 \times 10^{-3} \text{ m})}$$

$$K_c' = 5.62 \times 10^{11} \text{ N.s.m}^{-4}$$

$$J_{average} = \frac{1}{\left( \frac{5.62 \times 10^{11} \text{ N.s.m}^{-4}}{2 \times 6.00 \times 10^4 \text{ N.m}^{-2}} \times 1.05 \times 10^{-2} \text{ m} + \frac{1}{1.34 \times 10^{-3} \text{ m.s}^{-1}} \right)}$$

$$J_{average} = 2.00 \times 10^{-5} \text{ m.s}^{-1}$$

$$J_{average} = 72.1 \text{ L.m}^{-2}.\text{h}^{-1}$$

#### B.1.4.2 Cell broth supernatant

$$K_c' = 2 \times 6.00 \times 10^4 \text{ N.m}^{-2} \times \frac{(44.7 \times 10^3 \text{ s.m}^{-1} - 18.0 \times 10^3 \text{ s.m}^{-1})}{(6.71 \times 10^{-3} \text{ m} - 3.33 \times 10^{-3} \text{ m})}$$

$$K_c' = 9.49 \times 10^{11} \text{ N.s.m}^{-4}$$

$$J_{average} = \frac{1}{\left( \frac{9.49 \times 10^{11} \text{ N.s.m}^{-4}}{2 \times 6.00 \times 10^4 \text{ N.m}^{-2}} \times 1.05 \times 10^{-2} \text{ m} + \frac{1}{1.34 \times 10^{-3} \text{ m.s}^{-1}} \right)}$$

$$J_{average} = 1.19 \times 10^{-5} \text{ m.s}^{-1}$$

$$J_{average} = 43.0 \text{ L.m}^{-2}.\text{h}^{-1}$$

### B.1.5 Summary

The calculations outlined in this section take the raw data from Section B.1.1 through to quantitative, scalable flux predictions that successfully forecast a 40 % decrease in average flux for the cells resuspended in yeast extract solution compared to cell broth supernatant.

## B.2 Example LRA specific cake resistance calculation

To evaluate the specific cake resistance of complex suspensions with low resistance and a propensity to form stratified cakes a different approach was required, as detailed in Section 5.2.2. Figure B.2 shows the data progression for example data sets of  $10 \text{ g.L}^{-1}_{\text{liquid}}$  vs  $50 \text{ g.L}^{-1}_{\text{liquid}}$  LRA suspensions from (a) the raw mass data and (b) the pressure profile to (c) the specific cake resistance. Calculations are completed using Equation 5.1 and Equation 5.2.

### B.2.1 Shared raw data

The following data is common to both concentrations, which were tested in parallel on the same plate and therefore subjected to the same pressure profile.

Effective filtration area	$A = 7.85 \times 10^{-5} \text{ m}^2$
Integrated pressure	$\int \Delta P . dt = 6.69 \times 10^5 \text{ Pa.s}$
Dynamic permeate viscosity	$\mu = 0.001 \text{ N.s.m}^{-2}$
Permeate density	$\rho_p = 1.00 \text{ g.mL}^{-1} = 1000 \text{ kg.m}^{-3}$

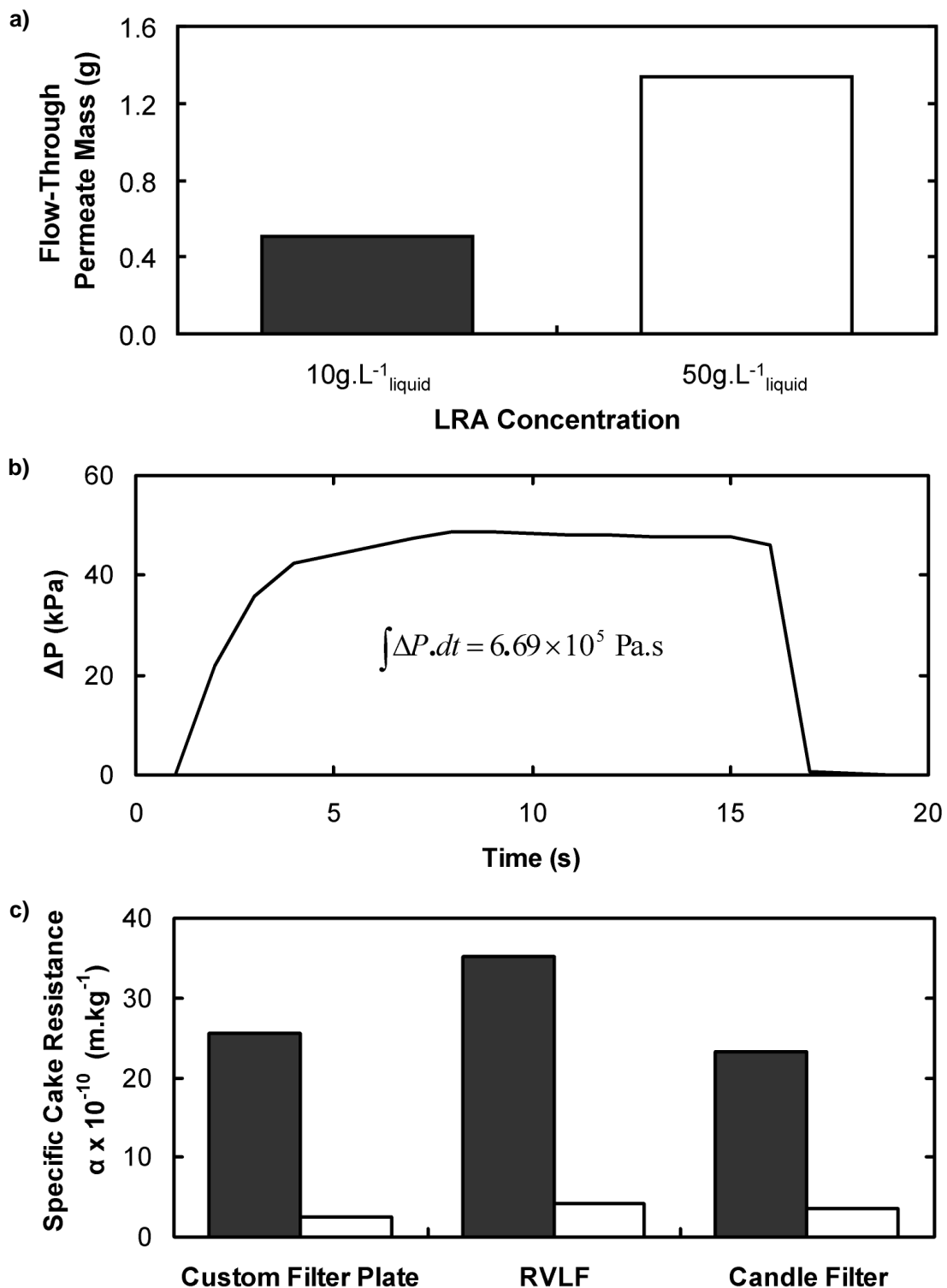


**Figure B.2.** The data progression from (a) example custom microwell filter plate flow-through permeate mass and (b) pressure profile during flow-through to (c) specific cake resistance data comparing the custom microwell plate calculated trend to laboratory scale rotating vertical leaf filter (RVLf) and pilot scale candle filter results. LRA specific cake resistance compared at concentrations of 10g.L<sub>liquid</sub><sup>-1</sup> (dark bars) and 50g.L<sub>liquid</sub><sup>-1</sup> (light bars). Described in detail in Appendix Section B.2.

**B.2.2** 10g.L<sup>-1</sup> liquid LRA

Measured flow-through mass	<b><math>m = 0.507 \text{ g}</math></b> $= 0.507 \text{ g} \times 10^{-3} \text{ kg.g}^{-1} = 5.07 \times 10^{-4} \text{ kg}$
Mass of solids per unit volume of liquid	$\rho_0 = 10 \text{ g.L}^{-1} = 10 \text{ kg.m}^{-3}$
Flow-through volume	$V_t = \frac{5.07 \times 10^{-4} \text{ kg}}{1000 \text{ kg.m}^{-3}} = 5.07 \times 10^{-7} \text{ m}^3$
Liquid in original feed sample	$V_c = 2.83 \text{ mL} \times 10^{-6} \text{ m}^3.\text{mL}^{-1} = 2.83 \times 10^{-6} \text{ m}^3$

Specific cake resistance:

$$\alpha = \frac{A^2 \int \Delta P . dt}{\mu \rho_0 V_t V_c}$$

$$\alpha = \frac{(7.85 \times 10^{-5} \text{ m}^2)^2 \times 6.69 \times 10^5 \text{ Pa.s}}{0.001 \text{ N.s.m}^{-2} \times 10 \text{ kg.m}^{-3} \times 5.07 \times 10^{-7} \text{ m}^3 \times 2.83 \times 10^{-6} \text{ m}^3}$$

$$\alpha = 28.8 \times 10^{10} \text{ m.kg}^{-1}$$

Modified cake filtration constant:

$$K_c = \frac{A^2 \int \Delta P . dt}{V_t V_c}$$

$$K_c = \frac{(7.85 \times 10^{-5} \text{ m}^2)^2 \times 6.69 \times 10^5 \text{ Pa.s}}{5.07 \times 10^{-7} \text{ m}^3 \times 2.83 \times 10^{-6} \text{ m}^3}$$

$$K_c = 2.88 \times 10^9 \text{ N.s.m}^{-4}$$

**B.2.3** 50g.L<sup>-1</sup> liquid LRA

Measured flow-through mass	<b><math>m = 1.340 \text{ g}</math></b> $= 1.340 \text{ g} \times 10^{-3} \text{ kg.g}^{-1} = 1.34 \times 10^{-3} \text{ kg}$
Mass of solids per unit volume of liquid	$\rho_0 = 50 \text{ g.L}^{-1} = 50 \text{ kg.m}^{-3}$
Flow-through volume	$V_t = \frac{1.34 \times 10^{-3} \text{ kg}}{1000 \text{ kg.m}^{-3}} = 1.34 \times 10^{-6} \text{ m}^3$

Liquid in original feed sample  $V_c = 2.14 \text{ mL} \times 10^{-6} \text{ m}^3 \cdot \text{mL}^{-1} = 2.14 \times 10^{-6} \text{ m}^3$

Specific cake resistance:

$$\alpha = \frac{A^2 \int \Delta P \cdot dt}{\mu \rho_0 V_t V_c}$$

$$\alpha = \frac{(7.85 \times 10^{-5} \text{ m}^2)^2 \times 6.69 \times 10^5 \text{ Pa} \cdot \text{s}}{0.001 \text{ N} \cdot \text{s} \cdot \text{m}^{-2} \times 50 \text{ kg} \cdot \text{m}^{-3} \times 1.34 \times 10^{-6} \text{ m}^3 \times 2.14 \times 10^{-6} \text{ m}^3}$$

$$\alpha = \mathbf{2.88 \times 10^{10} \text{ m} \cdot \text{kg}^{-1}}$$

Modified cake filtration constant:

$$K_c = \frac{A^2 \int \Delta P \cdot dt}{V_t V_c}$$

$$K_c = \frac{(7.85 \times 10^{-5} \text{ m}^2)^2 \times 6.69 \times 10^5 \text{ Pa} \cdot \text{s}}{1.34 \times 10^{-7} \text{ m}^3 \times 2.14 \times 10^{-6} \text{ m}^3}$$

$$K_c = 1.44 \times 10^9 \text{ N} \cdot \text{s} \cdot \text{m}^{-4}$$

#### B.2.4 Summary

The example data filtration progression here shows that more permeate mass flows through the cake formed by the higher concentration LRA suspension (Figure B.2(a)) under the same applied pressure (Figure B.2(b)) leading to a predicted 10-fold decrease in the specific cake resistance which is a trend replicated at laboratory and pilot scales (Figure B.2.(c)).

---

## **C.0 Appendix C: Chapter 4 data**

### **C.1 *E.coli* and lysozyme factorial data**

Table C.1 contains all of the specific cake resistance and lysozyme transmission raw data and calculations from each individual custom microwell filtration experiment carried out during the factorial screening experiments in Chapter 4. The detailed explanations of the experimental methods are found in Section 2.4.3, Section 2.7.1.1 and Section 3.4 and the results are examined and presented in detail in Section 4.3.

### **C.2 *E.coli* and lysozyme response surface data**

Table C.2 contains all of the specific cake resistance and lysozyme transmission raw data and calculations from each individual custom microwell filtration experiment carried out during the response surface experiments in Chapter 4. In addition the specific cake resistance data for the response surface in the absence of lysozyme is shown in Table C.3. The detailed explanations of the experimental methods are found in Section 2.4.3, Section 2.7.2 and Section 3.4 and the results are examined and presented in detail in Section 4.4.

**Table C.1.** Raw data and calculations for the factorial screening experiments described in detail in Section 4.3. Specific cake resistance,  $\alpha$ , and lysozyme transmission are quoted as the mean  $\pm$  one standard deviation. Data is given for each individual well including duplicates of the 16 factorial runs and the 4 sets of 4 centre point combinations. Plate positions on the two custom microwell filter plate layouts used are given in the form  $MX_Y$  where M is the row (A-D), X is the column number (1-6), and Y is the plate number (1-2).

Design Factors	Factorial Run Number	1		2		3		4		5		6		7		8		9		10		11		12					
	A = pH		5	7	5	7	5	7	5	7	5	7	5	7	5	7	5	7	5	7	5	7	5	7	5	7			
	B = Ionic Strength (mM)		100	100	200	200	100	100	200	200	100	100	200	200	100	100	200	200	100	100	200	200	100	100	200	200			
	C = YE Concentration ( $\text{g}\cdot\text{L}^{-1}$ )		0	0	0	0	10	10	10	10	0	0	0	0	0	0	0	0	0	0	0	0	0	0	0	0			
	D = Pressure Difference (kPa)		40	40	40	40	40	40	40	40	40	40	40	40	40	40	40	40	40	40	40	40	40	40	40	40			
E = Membrane Type	Qualitative	PVDF	Cellulose Nitrate	Cellulose Nitrate	PVDF	Cellulose Nitrate	Cellulose Nitrate	PVDF	Cellulose Nitrate	Cellulose Nitrate	PVDF	Cellulose Nitrate	Cellulose Nitrate	PVDF	Cellulose Nitrate	Cellulose Nitrate	PVDF	Cellulose Nitrate	Cellulose Nitrate	PVDF	Cellulose Nitrate	Cellulose Nitrate	PVDF	Cellulose Nitrate	Cellulose Nitrate				
Feed	Optical Density ( $\text{OD}_{600\text{nm}}$ )		14.5	14.5	14.5	14.5	14.5	14.5	14.5	14.5	14.5	14.5	14.5	14.5	14.5	14.5	14.5	14.5	14.5	14.5	14.5	14.5	14.5	14.5	14.5				
	Dry Cell Weight ( $\text{g}_{\text{DCW}}\cdot\text{L}^{-1}$ )		7.00	7.00	7.00	7.00	7.00	7.00	7.00	7.00	7.00	7.00	7.00	7.00	7.00	7.00	7.00	7.00	7.00	7.00	7.00	7.00	7.00	7.00	7.00				
Raw Data	Plate Position		A5 <sub>1</sub>	C2 <sub>1</sub>	B1 <sub>1</sub>	C6 <sub>1</sub>	A3 <sub>1</sub>	C4 <sub>1</sub>	B2 <sub>1</sub>	D5 <sub>1</sub>	B6 <sub>1</sub>	D3 <sub>1</sub>	A1 <sub>1</sub>	D4 <sub>1</sub>	A6 <sub>1</sub>	D2 <sub>1</sub>	B3 <sub>1</sub>	C5 <sub>1</sub>	A6 <sub>2</sub>	C4 <sub>2</sub>	A4 <sub>2</sub>	D1 <sub>2</sub>	B2 <sub>2</sub>	D5 <sub>2</sub>	B4 <sub>2</sub>	C6 <sub>2</sub>			
	$t_1$ (s)		90	90	90	90	90	90	90	90	90	90	90	90	90	90	90	90	90	90	90	90	90	90	90	90	90		
	Cuvette Before <sub>1</sub> (g)		2.131	2.131	2.130	2.131	2.131	2.130	2.131	2.131	2.130	2.131	2.130	2.131	2.130	2.131	2.130	2.131	2.130	2.131	2.131	2.131	2.131	2.131	2.130	2.131	2.130	2.131	
	Cuvette After <sub>1</sub> (g)		2.595	2.585	3.123	3.118	2.522	2.526	2.425	2.406	2.696	2.706	2.777	2.793	2.613	2.614	2.560	2.524	2.658	2.659	3.171	3.131	2.452	2.463	2.450	2.473	2.450	2.473	
	<b>Cuvette V<sub>1</sub> (mL)</b>		<b>0.464</b>	<b>0.455</b>	<b>0.993</b>	<b>0.987</b>	<b>0.392</b>	<b>0.396</b>	<b>0.295</b>	<b>0.276</b>	<b>0.566</b>	<b>0.575</b>	<b>0.646</b>	<b>0.663</b>	<b>0.481</b>	<b>0.483</b>	<b>0.429</b>	<b>0.394</b>	<b>0.528</b>	<b>0.529</b>	<b>1.039</b>	<b>1.001</b>	<b>0.322</b>	<b>0.334</b>	<b>0.320</b>	<b>0.343</b>	<b>0.320</b>	<b>0.343</b>	
	Insert Before <sub>1</sub> (g)		7.682	7.658	7.751	7.658	7.676	7.698	7.744	7.664	7.771	7.676	7.734	7.685	7.641	7.675	7.729	7.724	7.639	7.648	7.630	7.649	7.669	7.671	7.674	7.691	7.674	7.691	
	Insert After <sub>1</sub> (g)		7.195	7.193	6.724	6.656	7.272	7.284	7.435	7.383	7.198	7.083	7.053	7.008	7.143	7.168	7.291	7.325	7.124	7.103	6.582	6.653	7.352	7.358	7.347	7.337	7.347	7.337	
	<b>Insert V<sub>1</sub> (mL)</b>		<b>0.488</b>	<b>0.464</b>	<b>1.027</b>	<b>1.002</b>	<b>0.404</b>	<b>0.414</b>	<b>0.309</b>	<b>0.281</b>	<b>0.573</b>	<b>0.592</b>	<b>0.681</b>	<b>0.677</b>	<b>0.498</b>	<b>0.507</b>	<b>0.439</b>	<b>0.399</b>	<b>0.515</b>	<b>0.545</b>	<b>1.049</b>	<b>0.996</b>	<b>0.317</b>	<b>0.313</b>	<b>0.327</b>	<b>0.355</b>	<b>0.327</b>	<b>0.355</b>	
	$t_2$ (s)		300	300	300	300	300	300	300	300	300	300	300	300	300	300	300	300	300	300	300	300	300	300	300	300	300	300	
	Cuvette Before <sub>2</sub> (g)		2.130	2.130	2.131	2.130	2.131	2.131	2.131	2.130	2.130	2.130	2.131	2.131	2.131	2.130	2.131	2.130	2.130	2.130	2.130	2.130	2.130	2.130	2.130	2.130	2.130	2.131	2.131
	Cuvette After <sub>2</sub> (g)		2.912	2.910	3.822	3.768	2.739	2.737	2.592	2.564	3.116	3.114	3.244	3.265	3.056	2.991	2.859	2.791	2.976	2.961	3.898	3.804	2.645	2.671	2.589	2.623	2.589	2.623	
	<b>Cuvette V<sub>2</sub> (mL)</b>		<b>0.781</b>	<b>0.780</b>	<b>1.692</b>	<b>1.638</b>	<b>0.609</b>	<b>0.606</b>	<b>0.462</b>	<b>0.433</b>	<b>0.986</b>	<b>0.984</b>	<b>1.114</b>	<b>1.135</b>	<b>0.925</b>	<b>0.861</b>	<b>0.728</b>	<b>0.661</b>	<b>0.846</b>	<b>0.831</b>	<b>1.768</b>	<b>1.674</b>	<b>0.516</b>	<b>0.540</b>	<b>0.459</b>	<b>0.493</b>	<b>0.459</b>	<b>0.493</b>	
	Insert Before <sub>2</sub> (g)		7.690	7.696	7.751	7.719	7.776	7.733	7.684	7.669	7.697	7.686	7.676	7.652	7.682	7.666	7.676	7.646	7.695	7.739	7.653	7.648	7.689	7.617	7.656	7.655	7.656	7.655	
	Insert After <sub>2</sub> (g)		6.891	6.906	6.062	6.071	7.159	7.116	7.204	7.230	6.700	6.699	6.544	6.510	6.745	6.797	6.921	6.990	6.863	6.888	5.892	5.966	7.162	7.077	7.202	7.168	7.202	7.168	
<b>Insert V<sub>2</sub> (mL)</b>		<b>0.798</b>	<b>0.790</b>	<b>1.689</b>	<b>1.648</b>	<b>0.617</b>	<b>0.617</b>	<b>0.479</b>	<b>0.439</b>	<b>0.997</b>	<b>0.987</b>	<b>1.132</b>	<b>1.141</b>	<b>0.937</b>	<b>0.869</b>	<b>0.756</b>	<b>0.655</b>	<b>0.832</b>	<b>0.850</b>	<b>1.761</b>	<b>1.681</b>	<b>0.527</b>	<b>0.540</b>	<b>0.454</b>	<b>0.486</b>	<b>0.454</b>	<b>0.486</b>		
<b><math>\Delta P</math> (Average <math>t_1 \rightarrow t_2</math>) (mbar)</b>		<b>428.6</b>	<b>428.6</b>	<b>428.6</b>	<b>428.6</b>	<b>428.6</b>	<b>428.6</b>	<b>428.6</b>	<b>428.6</b>	<b>428.6</b>	<b>428.6</b>	<b>428.6</b>	<b>428.6</b>	<b>428.6</b>	<b>428.6</b>	<b>428.6</b>	<b>428.6</b>	<b>668.5</b>	<b>668.5</b>	<b>668.5</b>	<b>668.5</b>	<b>668.5</b>	<b>668.5</b>	<b>668.5</b>	<b>668.5</b>	<b>668.5</b>	<b>668.5</b>		
$\alpha$ Calculations	Cuvette $\alpha$ (Eq. 3.6) $\times 10^{-12}$ ( $\text{m}\cdot\text{kg}^{-1}$ )		45.1	43.3	9.4	10.7	91.4	95.8	155.8	175.4	26.1	27.5	21.0	20.6	23.4	32.4	51.0	63.7	68.2	74.5	13.4	15.6	183.1	162.3	315.2	271.8	315.2	271.8	
	Insert $\alpha$ (Eq. 3.6) $\times 10^{-12}$ ( $\text{m}\cdot\text{kg}^{-1}$ )		46.5	43.1	10.3	10.8	93.2	99.5	148.7	174.1	25.6	29.0	22.2	21.2	24.0	35.0	45.8	68.2	69.2	72.4	14.0	15.1	159.3	138.9	357.3	325.0	357.3	325.0	
	$\alpha$ (Average of Cuvette and Insert Values) $\times 10^{-12}$ ( $\text{m}\cdot\text{kg}^{-1}$ )		45.8	43.2	9.8	10.7	92.3	97.7	152.3	174.8	25.8	28.2	21.6	20.9	23.7	33.7	48.4	66.0	68.7	73.4	13.7	15.4	171.2	150.6	336.2	298.4	336.2	298.4	
	<b>Average <math>\alpha \times 10^{-12}</math> (<math>\pm 1</math> SD)</b> ( $\text{m}\cdot\text{kg}^{-1}$ )		<b>44.5 <math>\pm</math> 1.8</b>	<b>43.2 <math>\pm</math> 1.8</b>	<b>10.3 <math>\pm</math> 0.6</b>	<b>10.7 <math>\pm</math> 0.6</b>	<b>95.0 <math>\pm</math> 3.8</b>	<b>97.7 <math>\pm</math> 3.8</b>	<b>163.5 <math>\pm</math> 15.9</b>	<b>174.8 <math>\pm</math> 15.9</b>	<b>27.0 <math>\pm</math> 1.7</b>	<b>28.2 <math>\pm</math> 1.7</b>	<b>21.2 <math>\pm</math> 0.5</b>	<b>20.9 <math>\pm</math> 0.5</b>	<b>28.7 <math>\pm</math> 7.1</b>	<b>33.7 <math>\pm</math> 7.1</b>	<b>57.2 <math>\pm</math> 12.4</b>	<b>66.0 <math>\pm</math> 12.4</b>	<b>71.1 <math>\pm</math> 3.4</b>	<b>73.4 <math>\pm</math> 3.4</b>	<b>14.5 <math>\pm</math> 1.2</b>	<b>15.4 <math>\pm</math> 1.2</b>	<b>160.9 <math>\pm</math> 14.6</b>	<b>150.6 <math>\pm</math> 14.6</b>	<b>317.3 <math>\pm</math> 26.8</b>	<b>298.4 <math>\pm</math> 26.8</b>	<b>317.3 <math>\pm</math> 26.8</b>	<b>298.4 <math>\pm</math> 26.8</b>	
Lysozyme	Feed (Integrated Area)		421.9	421.9	421.9	421.9	421.9	421.9	421.9	421.9	421.9	421.9	421.9	421.9	421.9	421.9	421.9	421.9	421.9	421.9	421.9	421.9	421.9	421.9	421.9	421.9	421.9	421.9	
	Permeate (Integrated Area)		385.8	419.9	330.1	343.2	314.4	344.0	391.9	392.1	318.3	353.7	171.4	187.4	357.1	402.7	280.1	256.8	385.5	377.5	369.7	380.1	385.9	406.1	289.3	303.9	289.3	303.9	
	<b>Transmission (<math>\pm 1</math> SD)</b> (%)		<b>95.5 <math>\pm</math> 5.7</b>	<b>97.6 <math>\pm</math> 5.7</b>	<b>79.8 <math>\pm</math> 2.2</b>	<b>81.0 <math>\pm</math> 2.2</b>	<b>78.0 <math>\pm</math> 5.0</b>	<b>81.0 <math>\pm</math> 5.0</b>	<b>92.9 <math>\pm</math> 0.0</b>	<b>92.9 <math>\pm</math> 0.0</b>	<b>79.6 <math>\pm</math> 5.9</b>	<b>81.0 <math>\pm</math> 5.9</b>	<b>42.5 <math>\pm</math> 2.7</b>	<b>42.5 <math>\pm</math> 2.7</b>	<b>90.0 <math>\pm</math> 7.6</b>	<b>90.0 <math>\pm</math> 7.6</b>	<b>63.6 <math>\pm</math> 3.9</b>	<b>63.6 <math>\pm</math> 3.9</b>	<b>90.4 <math>\pm</math> 1.3</b>	<b>90.4 <math>\pm</math> 1.3</b>	<b>88.9 <math>\pm</math> 1.7</b>	<b>88.9 <math>\pm</math> 1.7</b>	<b>93.9 <math>\pm</math> 3.4</b>	<b>93.9 <math>\pm</math> 3.4</b>	<b>70.3 <math>\pm</math> 2.4</b>	<b>70.3 <math>\pm</math> 2.4</b>	<b>70.3 <math>\pm</math> 2.4</b>	<b>70.3 <math>\pm</math> 2.4</b>	

Continued on page 227...

Table C.1 continued from page 226.

Design Factors	Factorial Run Number	13	14	15	16	C <sub>1</sub>	C <sub>2</sub>	C <sub>3</sub>	C <sub>4</sub>	C <sub>5</sub>	C <sub>6</sub>	C <sub>7</sub>	C <sub>8</sub>	C <sub>9</sub>	C <sub>10</sub>	C <sub>11</sub>	C <sub>12</sub>	C <sub>13</sub>	C <sub>14</sub>	C <sub>15</sub>	C <sub>16</sub>			
	A = pH		5	7	5	7	6				6				6				6					
B = Ionic Strength	(mM)	100	100	200	200	150				150				150				150						
C = YE Concentration	(g.L <sup>-1</sup> )	10	10	10	10	5				5				5				5						
D = Pressure Difference	(kPa)	70	70	70	70	40				40				70				70						
E = Membrane Type	Qualitative	PVDF	Cellulose Nitrate	Cellulose Nitrate	PVDF	Cellulose Nitrate				PVDF				Cellulose Nitrate				PVDF						
Feed	Optical Density	(OD <sub>600nm</sub> )	14.5	14.5	14.5	14.5	14.5				14.5				14.5				14.5					
	Dry Cell Weight	(g <sub>DCW</sub> .L <sup>-1</sup> )	7.00	7.00	7.00	7.00	7.00				7.00				7.00				7.00					
Raw Data	Plate Position		A1 <sub>2</sub> D3 <sub>2</sub>	B5 <sub>2</sub> C2 <sub>2</sub>	A3 <sub>2</sub> D6 <sub>2</sub>	B1 <sub>2</sub> C5 <sub>2</sub>	A2 <sub>1</sub> A4 <sub>1</sub> D1 <sub>1</sub> D6 <sub>1</sub>	B4 <sub>1</sub> B5 <sub>1</sub> C1 <sub>1</sub> C3 <sub>1</sub>	B6 <sub>2</sub> C1 <sub>2</sub> C3 <sub>2</sub> D2 <sub>2</sub>	A2 <sub>2</sub> A5 <sub>2</sub> B3 <sub>2</sub> D4 <sub>2</sub>														
	t <sub>1</sub>	(s)	90	90	90	90	90				90				90				90					
	Cuvette Before <sub>1</sub>	(g)	2.131 2.130	2.130 2.130	2.130 2.130	2.130 2.130	2.131 2.131	2.131 2.131	2.131 2.131	2.131 2.131	2.131 2.130	2.130 2.130	2.130 2.130	2.131 2.130	2.131 2.130	2.130 2.130	2.131 2.131	2.130 2.130	2.131 2.131	2.130 2.130	2.130 2.130	2.130 2.130	2.130 2.130	2.130 2.130
	Cuvette After <sub>1</sub>	(g)	2.672 2.708	2.797 2.758	2.648 2.663	2.525 2.521	2.815 2.819	2.875 2.887	2.794 2.802	2.749 2.794	2.853 2.837	2.828 2.842	2.760 2.817	2.765 2.786										
	Cuvette V <sub>1</sub>	(mL)	<b>0.541 0.578</b>	<b>0.667 0.628</b>	<b>0.518 0.533</b>	<b>0.394 0.390</b>	<b>0.685 0.688</b>	<b>0.744 0.756</b>	<b>0.663 0.672</b>	<b>0.619 0.664</b>	<b>0.723 0.707</b>	<b>0.698 0.711</b>	<b>0.630 0.687</b>	<b>0.635 0.656</b>										
	Insert Before <sub>1</sub>	(g)	7.681 7.658	7.672 7.668	7.655 7.620	7.630 7.654	7.681 7.758	7.650 7.784	7.674 7.713	7.702 7.748	7.666 7.649	7.664 7.658	7.702 7.651	7.651 7.647										
	Insert After <sub>1</sub>	(g)	7.132 7.070	7.011 7.019	7.122 7.090	7.246 7.267	6.972 7.045	6.883 6.996	6.994 7.025	7.051 7.065	6.935 6.940	6.944 6.939	7.056 6.948	7.024 6.978										
	Insert V <sub>1</sub>	(mL)	<b>0.548 0.588</b>	<b>0.661 0.648</b>	<b>0.533 0.530</b>	<b>0.384 0.388</b>	<b>0.708 0.712</b>	<b>0.767 0.788</b>	<b>0.680 0.689</b>	<b>0.651 0.683</b>	<b>0.731 0.709</b>	<b>0.720 0.719</b>	<b>0.646 0.704</b>	<b>0.627 0.670</b>										
	t <sub>2</sub>	(s)	300	300	300	300	300				300				300				300					
	Cuvette Before <sub>2</sub>	(g)	2.131 2.130	2.131 2.131	2.130 2.131	2.130 2.131	2.130 2.131	2.130 2.131	2.130 2.131	2.130 2.131	2.130 2.131	2.130 2.131	2.130 2.131	2.130 2.131	2.130 2.131	2.130 2.131	2.130 2.131	2.130 2.131	2.130 2.131	2.130 2.131	2.130 2.131	2.130 2.131	2.130 2.131	
	Cuvette After <sub>2</sub>	(g)	3.148 3.171	3.265 3.210	3.030 3.063	2.863 2.826	3.226 3.221	3.344 3.364	3.229 3.281	3.214 3.261	3.316 3.311	3.311 3.307	3.266 3.317	3.272 3.281										
	Cuvette V <sub>2</sub>	(mL)	<b>1.017 1.041</b>	<b>1.134 1.079</b>	<b>0.900 0.933</b>	<b>0.733 0.694</b>	<b>1.097 1.091</b>	<b>1.214 1.233</b>	<b>1.099 1.150</b>	<b>1.084 1.131</b>	<b>1.185 1.180</b>	<b>1.180 1.177</b>	<b>1.136 1.186</b>	<b>1.142 1.150</b>										
	Insert Before <sub>2</sub>	(g)	7.690 7.665	7.692 7.644	7.632 7.702	7.659 7.701	7.677 7.706	7.691 7.653	7.691 7.705	7.662 7.719	7.712 7.723	7.655 7.646	7.716 7.625	7.728 7.722										
	Insert After <sub>2</sub>	(g)	6.644 6.609	6.546 6.537	6.720 6.769	6.900 7.013	6.544 6.605	6.438 6.400	6.577 6.536	6.549 6.574	6.514 6.520	6.459 6.464	6.565 6.428	6.592 6.559										
	Insert V <sub>2</sub>	(mL)	<b>1.045 1.057</b>	<b>1.146 1.108</b>	<b>0.912 0.934</b>	<b>0.759 0.688</b>	<b>1.133 1.102</b>	<b>1.252 1.253</b>	<b>1.113 1.169</b>	<b>1.113 1.146</b>	<b>1.198 1.203</b>	<b>1.196 1.182</b>	<b>1.151 1.198</b>	<b>1.137 1.163</b>										
ΔP (Average t <sub>1</sub> → t <sub>2</sub> )	(mbar)	668.5	668.5	668.5	668.5	428.6				428.6				668.5				668.5						
α Calculations	Cuvette α (Eq. 3.6) × 10 <sup>-12</sup>	(m.kg <sup>-1</sup> )	31.9 33.7	32.7 35.2	49.0 45.0	62.8 77.8	26.1 27.0	20.3 19.7	23.8 20.0	21.4 20.9	32.7 31.6	30.5 32.4	28.2 28.7	28.2 29.5										
	Insert α (Eq. 3.6) × 10 <sup>-12</sup>	(m.kg <sup>-1</sup> )	29.1 32.9	30.5 33.9	49.7 44.2	50.3 79.9	24.4 28.3	19.0 20.3	23.9 19.8	21.5 21.2	32.1 29.2	31.2 32.7	28.3 29.2	27.9 29.5										
	α (Average of Cuvette and Insert Values) × 10 <sup>-12</sup>	(m.kg <sup>-1</sup> )	30.5 33.3	31.6 34.5	49.4 44.6	56.6 78.8	25.3 27.7	19.6 20.0	23.8 19.9	21.4 21.1	32.4 30.4	30.9 32.6	28.2 29.0	28.0 29.5										
	Average α × 10 <sup>-12</sup> (± 1 SD)	(m.kg <sup>-1</sup> )	<b>31.9 ± 2.0</b>	<b>33.1 ± 2.1</b>	<b>47.0 ± 3.4</b>	<b>67.7 ± 15.7</b>	<b>23.1 ± 4.0</b>				<b>21.6 ± 1.6</b>				<b>31.6 ± 1.1</b>				<b>28.7 ± 0.7</b>					
Lysozyme	Feed (Integrated Area)		421.9	421.9	421.9	421.9	421.9				421.9				421.9				421.9					
	Permeate (Integrated Area)		391.2 405.2	128.4 129.5	361.4 361.1	348.0 345.9	243.1 241.9	260.4 244.7	310.0 302.1	297.7 317.0	239.1 238.0	242.3 223.2	290.4 300.0	276.1 297.0										
	Transmission (± 1 SD)	(%)	<b>94.4 ± 2.3</b>	<b>30.6 ± 0.2</b>	<b>85.6 ± 0.1</b>	<b>82.2 ± 0.3</b>	<b>58.7 ± 2.0</b>				<b>72.7 ± 2.0</b>				<b>55.9 ± 2.0</b>				<b>68.9 ± 2.5</b>					

**Table C.2.** Raw data and calculations for the response surface experiments described in detail in Section 4.4. Specific cake resistance,  $\alpha$ , and lysozyme transmission are quoted as the mean  $\pm$  one standard deviation. Data is given for each individual well including replicates at the same pH and ionic strength. Plate positions on the two custom microwell filter plate layouts used are given in the form MX where M is the row (A-D) and X is the column number (1-6).

		A2	D3	A5	C3	B2	B1	C4	B3	D5	C6	A3	B4	D1	D4	A4	C1	D6	C2	A6	B5	B6	D2	A1	C5
<b>Feed</b>	Plate Position																								
	pH	5		5.29		5.29	5.29		6		6	6				6	6		6.71		6.71	6.71		7	
	Ionic Strength (mM)	150		100		150	200		79.3		100	150				200	220.7		100		150	200		150	
	Optical Density (OD <sub>600nm</sub> )	16.1	15.4	16.7	17.4	16.0	15.7	15.5	16.1	14.7	16.5	16.6	17.2	16.0	15.6	16.5	15.9	16.0	14.6	16.3	16.5	15.9	16.5	15.4	15.0
	Dry Cell Weight (g <sub>DCW</sub> ·L <sup>-1</sup> )	7.77	7.44	8.09	8.39	7.74	7.59	7.48	7.80	7.12	7.98	8.03	8.31	7.72	7.54	7.98	7.69	7.71	7.03	7.87	7.96	7.67	7.98	7.43	7.24
<b>Raw Data</b>	t <sub>1</sub> (s)	90		90		90	90		90		90	90				90	90		90		90	90		90	
	Cuvette Before <sub>1</sub> (g)	2.131	2.131	2.130	2.131	2.131	2.131	2.131	2.131	2.130	2.132	2.131	2.131	2.131	2.131	2.130	2.131	2.131	2.131	2.131	2.132	2.131	2.131	2.131	2.132
	Cuvette After <sub>1</sub> (g)	2.487	2.411	2.530	2.578	2.479	2.471	2.392	3.337	3.285	3.036	2.694	2.704	2.710	2.706	2.536	2.430	2.421	3.065	3.276	2.655	2.415	2.480	2.616	2.611
	Cuvette V <sub>1</sub> (mL)	0.356	0.280	0.400	0.447	0.349	0.340	0.261	1.207	1.155	0.904	0.563	0.573	0.579	0.575	0.406	0.300	0.290	0.934	1.145	0.524	0.283	0.349	0.486	0.479
	Insert Before <sub>1</sub> (g)	7.714	7.674	7.701	7.726	7.710	7.666	7.623	7.679	7.706	7.644	7.664	7.680	7.679	7.648	7.605	7.690	7.649	7.704	7.647	7.684	7.665	7.678	7.701	7.684
	Insert After <sub>1</sub> (g)	7.379	7.318	7.293	7.255	7.330	7.301	7.332	6.427	6.495	6.709	7.096	7.071	7.071	7.055	7.214	7.366	7.379	6.708	6.451	7.146	7.319	7.318	7.186	7.177
	Insert V <sub>1</sub> (mL)	0.335	0.356	0.408	0.471	0.380	0.365	0.291	1.252	1.211	0.934	0.568	0.609	0.607	0.593	0.391	0.324	0.270	0.996	1.196	0.538	0.346	0.360	0.515	0.507
	t <sub>2</sub> (s)	270		270		270	270		270		270	270				270	270		270		270	270		270	
	Cuvette Before <sub>2</sub> (g)	2.130	2.131	2.130	2.131	2.131	2.131	2.130	2.131	2.130	2.131	2.130	2.130	2.130	2.131	2.130	2.130	2.130	2.130	2.131	2.131	2.130	2.130	2.130	2.131
	Cuvette After <sub>2</sub> (g)	2.683	2.683	2.736	2.750	2.718	2.634	2.557	4.037	4.030	3.544	3.079	3.047	2.992	3.061	2.728	2.565	2.554	3.673	3.908	2.991	2.594	2.607	2.940	2.875
	Cuvette V <sub>2</sub> (mL)	0.553	0.552	0.606	0.619	0.587	0.504	0.428	1.905	1.899	1.413	0.949	0.917	0.862	0.930	0.598	0.435	0.424	1.543	1.777	0.860	0.464	0.477	0.810	0.744
	Insert Before <sub>2</sub> (g)	7.742	7.747	7.719	7.651	7.695	7.647	7.759	7.736	7.653	7.667	7.670	7.682	7.652	7.739	7.671	7.726	7.711	7.697	7.692	7.686	7.723	7.689	7.727	7.705
	Insert After <sub>2</sub> (g)	7.203	7.163	7.078	6.999	7.083	7.152	7.300	5.773	5.696	6.237	6.732	6.728	6.792	6.775	7.084	7.265	7.296	6.107	5.865	6.802	7.245	7.199	6.886	6.928
Insert V <sub>2</sub> (mL)	0.539	0.585	0.641	0.652	0.612	0.495	0.459	1.964	1.957	1.429	0.939	0.954	0.860	0.964	0.586	0.460	0.415	1.589	1.827	0.884	0.478	0.490	0.840	0.777	
$\Delta P$ (Average t <sub>1</sub> → t <sub>2</sub> ) (mbar)	574.2		574.2		574.2	574.2		574.2		574.2	574.2				574.2	574.2		574.2		574.2	574.2		574.2		
<b><math>\alpha</math> Calculations</b>	Cuvette $\alpha$ (Eq. 3.6) $\times 10^{-12}$ (m.kg <sup>-1</sup> )	109.1	59.0	94.2	115.0	77.9	155.4	162.4	8.7	8.6	15.9	28.5	34.1	51.1	35.4	106.8	219.2	223.0	13.0	10.4	37.6	135.3	215.6	43.6	64.9
	Insert $\alpha$ (Eq. 3.6) $\times 10^{-12}$ (m.kg <sup>-1</sup> )	103.2	86.9	75.4	104.2	80.5	215.2	157.3	8.4	8.5	16.6	30.7	33.5	60.2	32.5	104.5	208.9	201.0	13.5	10.4	35.6	214.3	204.2	43.0	61.7
	$\alpha$ (Average of Cuvette and Insert Values) $\times 10^{-12}$ (m.kg <sup>-1</sup> )	106.1	72.9	84.8	109.6	79.2	185.3	159.8	8.5	8.5	16.3	29.6	33.8	55.6	34.0	105.7	214.0	212.0	13.3	10.4	36.6	174.8	209.9	43.3	63.3
	Average $\alpha \times 10^{-12}$ ( $\pm 1$ SD) (m.kg <sup>-1</sup> )	89.5 $\pm$ 23.5		97.2 $\pm$ 17.6		79.2	172.6 $\pm$ 18		8.5 $\pm$ 0		16.3	38.2 $\pm$ 11.8				105.7	213 $\pm$ 1.4		11.8 $\pm$ 2		36.6	192.4 $\pm$ 24.8		53.3 $\pm$ 14.1	
<b>Lysozyme</b>	Feed (Integrated Area)	753.0		753.0		753.0	753.0		753.0		753.0	753.0				753.0	753.0		753.0		753.0	753.0		753.0	
	Permeate (Integrated Area)	733.0	663.5	723.9	734.6	725.8	717.4	722.3	557.4	507.7	660.0	700.6	702.5	697.0	681.9	721.4	692.4	651.5	615.0	642.4	690.4	709.5	694.6	590.8	606.9
	Transmission ( $\pm 1$ SD) (%)	92.7 $\pm$ 6.5		96.8 $\pm$ 1.0		95.8	95.6 $\pm$ 0.5		70.7 $\pm$ 4.7		90.3	92.4 $\pm$ 1.2				93.9	89.2 $\pm$ 3.8		83.5 $\pm$ 2.6		93.0	93.2 $\pm$ 1.4		79.5 $\pm$ 1.5	

**Table C.3.** Raw data and calculations for the response surface experiments in the absence of lysozyme described in detail in Section 4.4. Specific cake resistance,  $\alpha$ , is quoted as the mean  $\pm$  one standard deviation. Data is given for each individual well including replicates at the same pH and ionic strength. Plate positions on the two custom microwell filter plate layouts used are given in the form MX where M is the row (A-D) and X is the column number (1-6).

Plate Position		A1	B5	B3	D6	A3	C2	D5	B1	C5	A2	B4	C1	A4	D4	D3	A5	C3	B2	C6	C4	B6	D2	D1	A6
Feed	pH	5		5.29		5.29	5.29		6		6	6				6	6		6.71		6.71	6.71		7	
	Ionic Strength (mM)	150		100		150	200		79.3		100	150				200	220.7		100		150	200		150	
	Optical Density (OD <sub>600nm</sub> )	15.5	16.0	16.3	16.3	15.7	15.1	16.0	16.8	16.5	16.9	16.3	15.9	16.3	16.0	15.3	15.4	15.8	16.9	16.9	16.9	16.5	16.8	15.4	16.2
	Dry Cell Weight (g <sub>DCW</sub> ·L <sup>-1</sup> )	7.49	7.72	7.86	7.89	7.57	7.31	7.75	8.12	7.99	8.16	7.89	7.67	7.89	7.72	7.41	7.46	7.62	8.15	8.16	8.15	7.95	8.13	7.45	7.81
	t <sub>1</sub> (s)	90		90		90	90		90		90	90				90	90		90		90	90		90	
Cuvette Before <sub>1</sub> (g)	2.131	2.131	2.130	2.130	2.130	2.130	2.131	2.131	2.131	2.130	2.131	2.130	2.130	2.131	2.131	2.131	2.130	2.130	2.131	2.129	2.130	2.130	2.131	2.130	2.130
Cuvette After <sub>1</sub> (g)	2.456	2.447	2.461	2.434	2.467	2.406	2.408	2.489	2.474	2.487	2.436	2.441	2.462	2.423	2.390	2.398	2.377	2.456	2.452	2.426	2.375	2.378	2.403	2.443	
Cuvette V <sub>1</sub> (mL)	0.326	0.317	0.331	0.303	0.337	0.275	0.277	0.358	0.344	0.356	0.305	0.310	0.331	0.292	0.259	0.268	0.246	0.325	0.323	0.296	0.245	0.247	0.273	0.313	
Insert Before <sub>1</sub> (g)	7.755	7.730	7.752	7.761	7.749	7.721	7.704	7.703	7.745	7.712	7.705	7.762	7.768	7.732	7.673	7.688	7.757	7.764	7.659	7.708	7.766	7.695	7.668	7.681	
Insert After <sub>1</sub> (g)	7.404	7.360	7.373	7.396	7.376	7.394	7.376	7.305	7.349	7.338	7.347	7.378	7.394	7.371	7.361	7.387	7.474	7.396	7.293	7.376	7.482	7.409	7.346	7.352	
Insert V <sub>1</sub> (mL)	0.351	0.370	0.379	0.365	0.372	0.327	0.328	0.398	0.396	0.373	0.358	0.384	0.374	0.361	0.313	0.301	0.283	0.369	0.367	0.332	0.284	0.286	0.322	0.329	
t <sub>2</sub> (s)	360		360		360	360		360		360	360				360	360		360		360	360		360		
Cuvette Before <sub>2</sub> (g)	2.131	2.131	2.130	2.131	2.130	2.131	2.131	2.131	2.130	2.130	2.131	2.130	2.131	2.130	2.131	2.131	2.130	2.131	2.131	2.131	2.130	2.130	2.131	2.131	
Cuvette After <sub>2</sub> (g)	2.671	2.709	2.702	2.748	2.712	2.655	2.605	2.798	2.802	2.729	2.722	2.697	2.630	2.677	2.599	2.623	2.589	2.734	2.730	2.701	2.594	2.607	2.648	2.671	
Cuvette V <sub>2</sub> (mL)	0.541	0.578	0.572	0.618	0.582	0.524	0.474	0.667	0.672	0.599	0.591	0.567	0.499	0.547	0.469	0.492	0.458	0.603	0.599	0.571	0.464	0.477	0.518	0.540	
Insert Before <sub>2</sub> (g)	7.707	7.721	7.710	7.675	7.799	7.786	7.724	7.781	7.682	7.717	7.697	7.691	7.703	7.678	7.711	7.716	7.793	7.721	7.763	7.739	7.748	7.675	7.700	7.699	
Insert After <sub>2</sub> (g)	7.162	7.090	7.099	6.986	7.199	7.218	7.206	7.038	6.962	7.088	7.071	7.068	7.139	7.068	7.195	7.216	7.280	7.073	7.116	7.123	7.248	7.168	7.140	7.136	
Insert V <sub>2</sub> (mL)	0.545	0.632	0.611	0.689	0.600	0.568	0.518	0.743	0.720	0.629	0.626	0.623	0.564	0.610	0.515	0.500	0.513	0.648	0.647	0.616	0.500	0.508	0.561	0.563	
$\Delta P$ (Average t <sub>1</sub> → t <sub>2</sub> ) (mbar)	574.3		574.3		574.2	574.3		574.3		574.3	574.3				574.3	574.3		574.3		574.3	574.3		574.3		
$\alpha$ Calculations	Cuvette $\alpha$ (Eq. 3.6) × 10 <sup>-12</sup> (m.kg <sup>-1</sup> )	171.4	118.9	133.8	81.9	134.7	140.4	202.0	81.8	74.0	124.3	98.9	124.3	239.9	125.8	192.4	168.1	184.4	100.2	101.3	103.1	166.0	148.3	142.1	152.1
	Insert $\alpha$ (Eq. 3.6) × 10 <sup>-12</sup> (m.kg <sup>-1</sup> )	196.3	114.9	136.4	76.2	147.1	144.6	201.9	65.3	74.4	112.5	108.2	132.5	189.1	125.8	193.7	200.7	154.7	96.9	96.4	95.9	165.9	155.7	144.8	141.5
	$\alpha$ (Average of Cuvette and Insert Values) × 10 <sup>-12</sup> (m.kg <sup>-1</sup> )	183.8	116.9	135.1	79.0	140.9	142.5	202.0	73.6	74.2	118.4	103.5	128.4	214.5	125.8	193.1	184.4	169.5	98.6	98.8	99.5	165.9	152.0	143.5	146.8
	Average $\alpha$ × 10 <sup>-12</sup> (± 1 SD) (m.kg <sup>-1</sup> )	150.4 ± 47.3		107.1 ± 39.7		140.9	172.2 ± 42.0		73.9 ± 0.5		118.4	143.0 ± 48.9				193.1	177.0 ± 10.5		98.7 ± 0.2		99.5	159.0 ± 9.8		145.1 ± 2.3	

---

## **D.0 Appendix D: Chapter 5 data**

### **D.1 Lysis clarification data**

Table D.1 contains all of the raw data and flux calculations from each individual custom microwell filtration experiment carried out during the factorial screening experiments in Chapter 5. The detailed explanations of the experimental methods are found in Section 2.5.2.2 and the results are examined and presented in detail in Section 5.3.1. In addition, flux data were taken from flow-through tests run at lower pressures is included. These were intended to be used to investigate compressibility, but the random nature of the results indicated that no compressibility could be quantified within this range. In Chapter 5 only the high pressure flow-through data is considered and only this data has been included in this appendix. The lack of compressibility of the feed is confirmed in the slope of the scalability data in Figure 5.7.

### **D.2 LRA removal data**

Table D.2 contains all of the specific cake resistance raw data and calculations from each individual custom microwell filtration experiment carried out during the factorial screening experiments in Chapter 5. The detailed explanations of the experimental methods are found in Section 2.5.2.8 and the results are examined and presented in detail in Section 5.3.3.

**Table D.1.** Raw data and calculations for the lysis clarification factorial screening experiments described in detail in Section 5.3.1 according to the methods in Section 2.5.2.2. Flux and clarification percentages are quoted as the mean  $\pm$  one standard deviation. Data is given for each individual well including duplicates of the 64 factorial runs and the 8 centre points. Plate positions on the six custom microwell filter plate layouts used are given in the form  $MX_Y$  where M is the row (A-D), X is the column number (1-6), and Y is the plate number (1-6).

Design Factors	Subset Analysis Factorial Run Number	1								2								3							
	Main Factorial Run Number	1		17		33		49		2		18		34		50		3		19		35		51	
	A = Celpure Grade (P grade)	P300		P300		P300		P300		P65		P65		P65		P65		P300		P300		P300		P300	
	B = Lysis Neutralisation Mixing Speed (rpm)	1200		1200		1200		1200		1200		1200		1200		1200		400		400		400		400	
	C = Celpure Concentration for Lysis Concentration ( $\text{g}\cdot\text{L}_{\text{lysate}}^{-1}$ )	50		50		50		50		50		50		50		50		50		50		50		50	
D = Number of Permeate Recycles During Lysis Clarification (#)	2		2		2		2		2		2		2		2		2		2		2		2		
Raw Data	Plate Position	A <sub>3<sub>6</sub></sub>	C <sub>3<sub>6</sub></sub>	A <sub>4<sub>6</sub></sub>	C <sub>4<sub>6</sub></sub>	B <sub>3<sub>6</sub></sub>	D <sub>3<sub>6</sub></sub>	B <sub>4<sub>6</sub></sub>	D <sub>4<sub>6</sub></sub>	A <sub>3<sub>4</sub></sub>	C <sub>3<sub>4</sub></sub>	A <sub>4<sub>4</sub></sub>	C <sub>4<sub>4</sub></sub>	B <sub>3<sub>4</sub></sub>	D <sub>3<sub>4</sub></sub>	B <sub>4<sub>4</sub></sub>	D <sub>4<sub>4</sub></sub>	A <sub>5<sub>5</sub></sub>	C <sub>5<sub>5</sub></sub>	A <sub>6<sub>5</sub></sub>	C <sub>6<sub>5</sub></sub>	B <sub>5<sub>5</sub></sub>	D <sub>5<sub>5</sub></sub>	B <sub>6<sub>5</sub></sub>	D <sub>6<sub>5</sub></sub>
	Cuvette Before (g)	2.175	2.172	2.170	2.172	2.172	2.171	2.176	2.176	2.172	2.171	2.172	2.173	2.172	2.173	2.172	2.172	2.174	2.176	2.172	2.171	2.171	2.176	2.172	2.173
	Cuvette After (g)	4.473	3.920	4.590	3.821	3.470	3.986	4.574	3.917	4.064	4.049	4.067	3.583	3.951	4.013	4.036	4.052	3.260	3.574	3.515	3.690	3.471	3.272	4.267	3.939
	<b>Cuvette V (mL)</b>	<b>2.299</b>	<b>1.748</b>	<b>2.419</b>	<b>1.649</b>	<b>1.298</b>	<b>1.814</b>	<b>2.398</b>	<b>1.741</b>	<b>1.892</b>	<b>1.878</b>	<b>1.895</b>	<b>1.411</b>	<b>1.779</b>	<b>1.840</b>	<b>1.865</b>	<b>1.879</b>	<b>1.086</b>	<b>1.398</b>	<b>1.343</b>	<b>1.519</b>	<b>1.301</b>	<b>1.097</b>	<b>2.096</b>	<b>1.766</b>
	t (s)	61		61		61		61		141		141		141		141		84		84		84		84	
	$\Delta P$ (Average over t) (mbar)	488.0		488.0		488.0		488.0		598.6		598.6		598.6		598.6		552.3		552.3		552.3		552.3	
	Optical Density $\times 10^3$ ( $\text{OD}_{600\text{nm}}$ )	7.2	-	7.5	-	7.2	-	6.4	-	4.2	-	5.2	-	5.1	-	7.1	-	5.2	-	7.5	-	8.1	-	7.1	-
Calculations	Flux normalised to 60kPa (Eq. 2.?) ( $\text{L}\cdot\text{m}^{-2}\cdot\text{h}^{-1}$ )	2124	1615	2235	1523	1199	1676	2216	1609	617	612	617	460	580	599	608	612	644	829	796	901	771	650	1242	1047
	<b>Average Flux (<math>\pm 1\text{SD}</math>)</b> ( $\text{L}\cdot\text{m}^{-2}\cdot\text{h}^{-1}$ )	<b>1775 <math>\pm</math> 375</b>								<b>588 <math>\pm</math> 53</b>								<b>860 <math>\pm</math> 202</b>							
	Clarification (%)	99.986		99.985		99.986		99.987		99.992		99.990		99.990		99.986		99.990		99.985		99.984		99.986	
	<b>Average Clarification (<math>\pm 1\text{SD}</math>)</b> (%)	<b>99.986 <math>\pm</math> 0.001</b>								<b>99.989 <math>\pm</math> 0.002</b>								<b>99.986 <math>\pm</math> 0.003</b>							
Design Factors	Subset Analysis Factorial Run Number	4								5								6							
	Main Factorial Run Number	4		20		36		52		5		21		37		53		6		22		38		54	
	A = Celpure Grade (P grade)	P65		P65		P65		P65		P300		P300		P300		P300		P65		P65		P65		P65	
	B = Lysis Neutralisation Mixing Speed (rpm)	400		400		400		400		1200		1200		1200		1200		1200		1200		1200		1200	
	C = Celpure Concentration for Lysis Concentration ( $\text{g}\cdot\text{L}_{\text{lysate}}^{-1}$ )	50		50		50		50		30		30		30		30		30		30		30		30	
D = Number of Permeate Recycles During Lysis Clarification (#)	2		2		2		2		2		2		2		2		2		2		2		2		
Raw Data	Plate Position	A <sub>5<sub>4</sub></sub>	C <sub>5<sub>4</sub></sub>	A <sub>6<sub>4</sub></sub>	C <sub>6<sub>4</sub></sub>	B <sub>5<sub>4</sub></sub>	D <sub>5<sub>4</sub></sub>	B <sub>6<sub>4</sub></sub>	D <sub>6<sub>4</sub></sub>	A <sub>1<sub>6</sub></sub>	C <sub>1<sub>6</sub></sub>	A <sub>2<sub>6</sub></sub>	C <sub>2<sub>6</sub></sub>	B <sub>1<sub>6</sub></sub>	D <sub>1<sub>6</sub></sub>	B <sub>2<sub>6</sub></sub>	D <sub>2<sub>6</sub></sub>	A <sub>3<sub>5</sub></sub>	C <sub>3<sub>5</sub></sub>	A <sub>4<sub>5</sub></sub>	C <sub>4<sub>5</sub></sub>	B <sub>3<sub>5</sub></sub>	D <sub>3<sub>5</sub></sub>	B <sub>4<sub>5</sub></sub>	D <sub>4<sub>5</sub></sub>
	Cuvette Before (g)	2.171	2.173	2.171	2.171	2.172	2.173	2.173	2.173	2.171	2.171	2.170	2.173	2.171	2.171	2.173	2.175	2.172	2.174	2.172	2.176	2.170	2.173	2.171	2.177
	Cuvette After (g)	3.642	3.376	3.360	3.648	3.590	3.274	3.501	3.662	3.709	4.533	4.473	3.730	4.339	4.084	4.135	4.540	3.413	3.340	3.402	3.229	3.265	3.373	3.344	3.239
	<b>Cuvette V (mL)</b>	<b>1.470</b>	<b>1.203</b>	<b>1.189</b>	<b>1.477</b>	<b>1.418</b>	<b>1.100</b>	<b>1.328</b>	<b>1.489</b>	<b>1.538</b>	<b>2.362</b>	<b>2.303</b>	<b>1.557</b>	<b>2.168</b>	<b>1.912</b>	<b>1.962</b>	<b>2.365</b>	<b>1.241</b>	<b>1.166</b>	<b>1.230</b>	<b>1.053</b>	<b>1.096</b>	<b>1.200</b>	<b>1.174</b>	<b>1.062</b>
	t (s)	141		141		141		141		61		61		61		61		84		84		84		84	
	$\Delta P$ (Average over t) (mbar)	598.6		598.6		598.6		598.6		488.0		488.0		488.0		488.0		552.3		552.3		552.3		552.3	
	Optical Density $\times 10^3$ ( $\text{OD}_{600\text{nm}}$ )	6.3	-	7.3	-	5.8	-	6.7	-	7.8	-	7.9	-	4.5	-	6.7	-	2.5	-	6.6	-	5.5	-	8.0	-
Calculations	Flux normalised to 60kPa (Eq. 2.?) ( $\text{L}\cdot\text{m}^{-2}\cdot\text{h}^{-1}$ )	479	392	387	481	462	359	433	485	1421	2182	2128	1438	2003	1767	1813	2185	736	691	729	624	649	711	696	630
	<b>Average Flux (<math>\pm 1\text{SD}</math>)</b> ( $\text{L}\cdot\text{m}^{-2}\cdot\text{h}^{-1}$ )	<b>435 <math>\pm</math> 50</b>								<b>1867 <math>\pm</math> 312</b>								<b>683 <math>\pm</math> 44</b>							
	Clarification (%)	99.987		99.985		99.988		99.987		99.984		99.984		99.991		99.987		99.995		99.987		99.989		99.984	
	<b>Average Clarification (<math>\pm 1\text{SD}</math>)</b> (%)	<b>99.987 <math>\pm</math> 0.001</b>								<b>99.987 <math>\pm</math> 0.003</b>								<b>99.989 <math>\pm</math> 0.005</b>							

Continued on page 232...

Table D.1 continued from page 231.

Design Factors	Subset Analysis Factorial Run Number		7								8								9								
	Main Factorial Run Number		7		23		39		55		8		24		40		56		9		25		41		57		
	A = Celpure Grade	(P grade)	P300	P300	P300	P300	P300	P300	P300	P300	P65	P65	P65	P65	P65	P65	P65	P65	P300	P300	P300	P300	P300	P300	P300	P300	
	B = Lysis Neutralisation Mixing Speed	(rpm)	400	400	400	400	400	400	400	400	400	400	400	400	400	400	400	400	1200	1200	1200	1200	1200	1200	1200	1200	
	C = Celpure Concentration for Lysis Concentration	(g.L <sub>lysate</sub> <sup>-1</sup> )	30	30	30	30	30	30	30	30	30	30	30	30	30	30	30	30	50	50	50	50	50	50	50	50	
D = Number of Permeate Recycles During Lysis Clarification	(#)	2	2	2	2	2	2	2	2	2	2	2	2	2	2	2	2	0	0	0	0	0	0	0	0		
Raw Data	Plate Position		A1 <sub>5</sub>	C1 <sub>5</sub>	A2 <sub>5</sub>	C2 <sub>5</sub>	B1 <sub>5</sub>	D1 <sub>5</sub>	B2 <sub>5</sub>	D2 <sub>5</sub>	A1 <sub>4</sub>	C1 <sub>4</sub>	A2 <sub>4</sub>	C2 <sub>4</sub>	B1 <sub>4</sub>	D1 <sub>4</sub>	B2 <sub>4</sub>	D2 <sub>4</sub>	A3 <sub>3</sub>	C3 <sub>3</sub>	A4 <sub>3</sub>	C4 <sub>3</sub>	B3 <sub>3</sub>	D3 <sub>3</sub>	B4 <sub>3</sub>	D4 <sub>3</sub>	
	Cuvette Before	(g)	2.170	2.172	2.172	2.171	2.169	2.171	2.170	2.174	2.172	2.172	2.172	2.173	2.170	2.173	2.171	2.172	2.172	2.173	2.173	2.167	2.171	2.173	2.172	2.172	
	Cuvette After	(g)	3.198	3.401	3.515	3.360	3.493	2.408	3.070	2.359	2.316	2.852	3.250	2.597	2.632	2.219	3.412	2.689	4.141	4.143	4.206	4.140	4.067	4.288	4.174	4.241	
	<b>Cuvette V</b>	<b>(mL)</b>	<b>1.028</b>	<b>1.229</b>	<b>1.343</b>	<b>1.189</b>	<b>1.325</b>	<b>0.237</b>	<b>0.900</b>	<b>0.184</b>	<b>0.144</b>	<b>0.680</b>	<b>1.077</b>	<b>0.424</b>	<b>0.462</b>	<b>0.046</b>	<b>1.241</b>	<b>0.517</b>	<b>1.968</b>	<b>1.970</b>	<b>2.033</b>	<b>1.973</b>	<b>1.896</b>	<b>2.116</b>	<b>2.002</b>	<b>2.070</b>	
	t	(s)	84	84	84	84	84	84	84	84	141	141	141	141	141	141	141	141	57	57	57	57	57	57	57	57	
	ΔP (Average over t)	(mbar)	552.3	552.3	552.3	552.3	552.3	552.3	552.3	552.3	598.6	598.6	598.6	598.6	598.6	598.6	598.6	598.6	513.0	513.0	513.0	513.0	513.0	513.0	513.0	513.0	
	Optical Density ×10 <sup>3</sup>	(OD <sub>600nm</sub> )	5.4	-	6.0	-	6.6	-	9.6	-	6.4	-	6.5	-	10.1	-	11.2	-	12.0	-	11.1	-	9.7	-	11.5	-	
Calculations	Flux normalised to 60kPa (Eq. 2.?)	(L.m <sup>-2</sup> .h <sup>-1</sup> )	609	729	796	704	785	141	533	109	47	221	351	138	151	15	404	168	1851	1853	1912	1856	1783	1990	1883	1946	
	<b>Average Flux (± 1SD)</b>	<b>(L.m<sup>-2</sup>.h<sup>-1</sup>)</b>	<b>551 ± 277</b>								<b>187 ± 136</b>								<b>1884 ± 64</b>								
	Clarification	(%)	99.989	99.988	99.987	99.981	99.987	99.987	99.980	99.978	99.976	99.978	99.981	99.977	99.976	99.978	99.981	99.977	99.976	99.978	99.981	99.977	99.976	99.978	99.981	99.977	
	<b>Average Clarification (± 1SD)</b>	<b>(%)</b>	<b>99.986 ± 0.004</b>								<b>99.983 ± 0.005</b>								<b>99.978 ± 0.002</b>								
Design Factors	Subset Analysis Factorial Run Number		10								11								12								
	Main Factorial Run Number		10		26		42		58		11		27		43		59		12		28		44		60		
	A = Celpure Grade	(P grade)	P65	P65	P65	P65	P65	P65	P65	P65	P300	P300	P300	P300	P300	P300	P300	P300	P65	P65	P65	P65	P65	P65	P65		
	B = Lysis Neutralisation Mixing Speed	(rpm)	1200	1200	1200	1200	1200	1200	1200	1200	400	400	400	400	400	400	400	400	400	400	400	400	400	400	400	400	
	C = Celpure Concentration for Lysis Concentration	(g.L <sub>lysate</sub> <sup>-1</sup> )	50	50	50	50	50	50	50	50	50	50	50	50	50	50	50	50	50	50	50	50	50	50	50	50	
D = Number of Permeate Recycles During Lysis Clarification	(#)	0	0	0	0	0	0	0	0	0	0	0	0	0	0	0	0	0	0	0	0	0	0	0	0		
Raw Data	Plate Position		A1 <sub>3</sub>	C1 <sub>3</sub>	A2 <sub>3</sub>	C2 <sub>3</sub>	B1 <sub>3</sub>	D1 <sub>3</sub>	B2 <sub>3</sub>	D2 <sub>3</sub>	A5 <sub>2</sub>	C5 <sub>2</sub>	A6 <sub>2</sub>	C6 <sub>2</sub>	B5 <sub>2</sub>	D5 <sub>2</sub>	B6 <sub>2</sub>	D6 <sub>2</sub>	A1 <sub>2</sub>	C1 <sub>2</sub>	A2 <sub>2</sub>	C2 <sub>2</sub>	B1 <sub>2</sub>	D1 <sub>2</sub>	B2 <sub>2</sub>	D2 <sub>2</sub>	
	Cuvette Before	(g)	2.172	2.172	2.172	2.172	2.172	2.173	2.173	2.172	2.172	2.171	2.172	2.172	2.172	2.171	2.172	2.172	2.172	2.173	2.171	2.172	2.171	2.173	2.172	2.172	2.172
	Cuvette After	(g)	3.156	3.208	3.152	3.131	3.171	3.261	3.150	3.194	4.051	3.936	3.603	3.592	3.967	3.772	3.915	3.522	3.023	3.132	3.039	2.968	2.952	2.921	3.057	2.941	
	<b>Cuvette V</b>	<b>(mL)</b>	<b>0.984</b>	<b>1.037</b>	<b>0.980</b>	<b>0.959</b>	<b>0.999</b>	<b>1.088</b>	<b>0.977</b>	<b>1.022</b>	<b>1.880</b>	<b>1.765</b>	<b>1.432</b>	<b>1.420</b>	<b>1.795</b>	<b>1.601</b>	<b>1.744</b>	<b>1.350</b>	<b>0.850</b>	<b>0.960</b>	<b>0.867</b>	<b>0.797</b>	<b>0.780</b>	<b>0.749</b>	<b>0.885</b>	<b>0.768</b>	
	t	(s)	57	57	57	57	57	57	57	57	61	61	61	61	61	61	61	61	61	61	61	61	61	61	61	61	
	ΔP (Average over t)	(mbar)	513.0	513.0	513.0	513.0	513.0	513.0	513.0	513.0	520.3	520.3	520.3	520.3	520.3	520.3	520.3	520.3	520.3	520.3	520.3	520.3	520.3	520.3	520.3	520.3	
	Optical Density ×10 <sup>3</sup>	(OD <sub>600nm</sub> )	3.6	-	10.5	-	10.3	-	8.2	-	10.7	-	3.4	-	12.1	-	10.7	-	13.9	-	8.9	-	14.8	-	13.4	-	
Calculations	Flux normalised to 60kPa (Eq. 2.?)	(L.m <sup>-2</sup> .h <sup>-1</sup> )	926	975	921	902	939	1023	919	961	1629	1529	1240	1231	1556	1387	1511	1169	737	832	751	691	676	649	767	666	
	<b>Average Flux (± 1SD)</b>	<b>(L.m<sup>-2</sup>.h<sup>-1</sup>)</b>	<b>946 ± 39</b>								<b>1407 ± 174</b>								<b>721 ± 62</b>								
	Clarification	(%)	99.993	99.979	99.979	99.984	99.979	99.993	99.976	99.979	99.972	99.982	99.970	99.973	99.972	99.982	99.970	99.973	99.972	99.982	99.970	99.973	99.972	99.982	99.970	99.973	
	<b>Average Clarification (± 1SD)</b>	<b>(%)</b>	<b>99.984 ± 0.006</b>								<b>99.982 ± 0.008</b>								<b>99.975 ± 0.005</b>								

Continued on page 233...

Table D.1 continued from page 232.

Design Factors	Subset Analysis Factorial Run Number		13								14								15								
	Main Factorial Run Number		13		29		45		61		14		30		46		62		15		31		47		63		
	A = Celpure Grade	(P grade)	P300	P300	P300	P300	P300	P300	P300	P300	P65	P65	P65	P65	P65	P65	P65	P65	P65	P65	P300	P300	P300	P300	P300	P300	
	B = Lysis Neutralisation Mixing Speed	(rpm)	1200	1200	1200	1200	1200	1200	1200	1200	1200	1200	1200	1200	1200	1200	1200	1200	1200	1200	400	400	400	400	400	400	
	C = Celpure Concentration for Lysis Concentration	(g.L <sub>lysate</sub> <sup>-1</sup> )	30	30	30	30	30	30	30	30	30	30	30	30	30	30	30	30	30	30	30	30	30	30	30	30	
D = Number of Permeate Recycles During Lysis Clarification	(#)	0	0	0	0	0	0	0	0	0	0	0	0	0	0	0	0	0	0	0	0	0	0	0	0		
Raw Data	Plate Position		A3 <sub>2</sub>	C3 <sub>2</sub>	A4 <sub>2</sub>	C4 <sub>2</sub>	B3 <sub>2</sub>	D3 <sub>2</sub>	B4 <sub>2</sub>	D4 <sub>2</sub>	A5 <sub>1</sub>	C5 <sub>1</sub>	A6 <sub>1</sub>	C6 <sub>1</sub>	B5 <sub>1</sub>	D5 <sub>1</sub>	B6 <sub>1</sub>	D6 <sub>1</sub>	A3 <sub>1</sub>	C3 <sub>1</sub>	A4 <sub>1</sub>	C4 <sub>1</sub>	B3 <sub>1</sub>	D3 <sub>1</sub>	B4 <sub>1</sub>	D4 <sub>1</sub>	
	Cuvette Before	(g)	2.171	2.172	2.173	2.171	2.172	2.172	2.172	2.172	2.171	2.172	2.173	2.172	2.172	2.172	2.171	2.173	2.173	2.172	2.172	2.171	2.172	2.170	2.172	2.172	2.172
	Cuvette After	(g)	4.309	4.278	4.381	3.960	4.303	4.921	4.219	3.985	3.280	3.279	3.286	3.204	3.372	3.058	3.090	3.078	3.132	2.582	3.627	2.895	3.518	3.259	3.577	3.850	
	<b>Cuvette V</b>	<b>(mL)</b>	<b>2.138</b>	<b>2.105</b>	<b>2.208</b>	<b>1.790</b>	<b>2.131</b>	<b>2.748</b>	<b>2.047</b>	<b>1.812</b>	<b>1.108</b>	<b>1.107</b>	<b>1.113</b>	<b>1.032</b>	<b>1.199</b>	<b>0.886</b>	<b>0.919</b>	<b>0.905</b>	<b>0.959</b>	<b>0.409</b>	<b>1.454</b>	<b>0.725</b>	<b>1.346</b>	<b>1.089</b>	<b>1.405</b>	<b>1.678</b>	
	t	(s)	61	61	61	61	61	61	61	61	74	74	74	74	74	74	74	74	74	74	74	74	74	74	74	74	
	ΔP (Average over t)	(mbar)	520.3	520.3	520.3	520.3	520.3	520.3	520.3	520.3	515.7	515.7	515.7	515.7	515.7	515.7	515.7	515.7	515.7	515.7	515.7	515.7	515.7	515.7	515.7	515.7	
	Optical Density ×10 <sup>3</sup>	(OD <sub>600nm</sub> )	10.5	-	4.3	-	13.5	-	11.0	-	2.1	-	4.7	-	6.6	-	4.5	-	4.0	-	7.1	-	14.1	-	9.4	-	
Calculations	Flux normalised to 60kPa (Eq. 2.?)	(L.m <sup>-2</sup> .h <sup>-1</sup> )	1853	1824	1914	1551	1846	2381	1774	1570	799	798	802	744	864	639	663	652	691	295	1048	522	970	784	1012	1209	
	<b>Average Flux (± 1SD)</b>	<b>(L.m<sup>-2</sup>.h<sup>-1</sup>)</b>	<b>1839 ± 256</b>								<b>745 ± 84</b>								<b>817 ± 304</b>								
	Clarification	(%)	99.979	99.991	99.973	99.978	99.996	99.991	99.987	99.991	99.992	99.986	99.972	99.981													
	<b>Average Clarification (± 1SD)</b>	<b>(%)</b>	<b>99.980 ± 0.008</b>								<b>99.991 ± 0.004</b>								<b>99.983 ± 0.009</b>								
Design Factors	Subset Analysis Factorial Run Number		16								Centre Points																
	Main Factorial Run Number		16		32		48		64		C <sub>1</sub>		C <sub>2</sub>		C <sub>3</sub>		C <sub>4</sub>		C <sub>5</sub>		C <sub>6</sub>		C <sub>7</sub>		C <sub>8</sub>		
	A = Celpure Grade	(P grade)	P65	P65	P65	P65	P65/P300	P65/P300	P65/P300	P65/P300	P65/P300	P65/P300	P65/P300	P65/P300	P65/P300	P65/P300	P65/P300	P65/P300	P65/P300	P65/P300	P65/P300	P65/P300	P65/P300	P65/P300	P65/P300	P65/P300	
	B = Lysis Neutralisation Mixing Speed	(rpm)	400	400	400	400	800	800	800	800	800	800	800	800	800	800	800	800	800	800	800	800	800	800	800	800	
	C = Celpure Concentration for Lysis Concentration	(g.L <sub>lysate</sub> <sup>-1</sup> )	30	30	30	30	40	40	40	40	40	40	40	40	40	40	40	40	40	40	40	40	40	40	40	40	
D = Number of Permeate Recycles During Lysis Clarification	(#)	0	0	0	0	1	1	1	1	1	1	1	1	1	1	1	1	1	1	1	1	1	1	1	1		
Raw Data	Plate Position		A1 <sub>1</sub>	C1 <sub>1</sub>	A2 <sub>1</sub>	C2 <sub>1</sub>	B1 <sub>1</sub>	D1 <sub>1</sub>	B2 <sub>1</sub>	D2 <sub>1</sub>	A5 <sub>6</sub>	C5 <sub>6</sub>	A6 <sub>6</sub>	C6 <sub>6</sub>	B5 <sub>6</sub>	D5 <sub>6</sub>	B6 <sub>6</sub>	D6 <sub>6</sub>	A5 <sub>3</sub>	C5 <sub>3</sub>	A6 <sub>3</sub>	C6 <sub>3</sub>	B5 <sub>3</sub>	D5 <sub>3</sub>	B6 <sub>3</sub>	D6 <sub>3</sub>	
	Cuvette Before	(g)	2.174	2.172	2.173	2.172	2.172	2.171	2.172	2.172	2.175	2.176	2.171	2.171	2.176	2.176	2.172	2.173	2.173	2.173	2.173	2.171	2.172	2.172	2.173	2.171	2.173
	Cuvette After	(g)	2.529	2.705	2.876	2.582	2.311	2.573	2.748	2.851	3.097	3.154	3.039	3.155	3.083	3.221	3.104	3.259	3.392	3.362	3.301	3.372	3.333	3.223	3.435	3.392	
	<b>Cuvette V</b>	<b>(mL)</b>	<b>0.355</b>	<b>0.533</b>	<b>0.703</b>	<b>0.409</b>	<b>0.139</b>	<b>0.402</b>	<b>0.576</b>	<b>0.679</b>	<b>0.923</b>	<b>0.978</b>	<b>0.867</b>	<b>0.983</b>	<b>0.908</b>	<b>1.045</b>	<b>0.932</b>	<b>1.087</b>	<b>1.219</b>	<b>1.189</b>	<b>1.130</b>	<b>1.200</b>	<b>1.161</b>	<b>1.051</b>	<b>1.264</b>	<b>1.219</b>	
	t	(s)	74	74	74	74	74	74	74	74	61	61	61	61	61	61	61	61	61	57	57	57	57	57	57	57	
	ΔP (Average over t)	(mbar)	515.7	515.7	515.7	515.7	515.7	515.7	515.7	515.7	488.0	488.0	488.0	488.0	488.0	488.0	488.0	488.0	488.0	513.0	513.0	513.0	513.0	513.0	513.0	513.0	
	Optical Density ×10 <sup>3</sup>	(OD <sub>600nm</sub> )	8.0	-	4.4	-	10.2	-	10.3	-	5.3	-	5.4	-	6.9	-	7.0	-	8.9	-	6.6	-	7.7	-	4.9	-	
Calculations	Flux normalised to 60kPa (Eq. 2.?)	(L.m <sup>-2</sup> .h <sup>-1</sup> )	256	384	506	295	100	290	415	490	852	904	801	909	839	965	861	1004	1146	1118	1063	1128	1092	988	1189	1147	
	<b>Average Flux (± 1SD)</b>	<b>(L.m<sup>-2</sup>.h<sup>-1</sup>)</b>	<b>342 ± 135</b>								<b>1000 ± 128</b>																
	Clarification	(%)	99.984	99.991	99.980	99.979	99.989	99.989	99.986	99.986	99.982	99.987	99.985	99.990													
	<b>Average Clarification (± 1SD)</b>	<b>(%)</b>	<b>99.984 ± 0.006</b>								<b>99.987 ± 0.003</b>																

**Table D.2.** Raw data and calculations for the LRA removal factorial screening experiments described in detail in Section 5.3.3 according to the methods in Section 2.5.2.8. Data is given for each individual well including all of the 64 factorial runs and the 8 centre points. Plate positions on the three custom microwell filter plate layouts used are given in the form  $MX_Y$  where M is the row (A-D), X is the column number (1-6), and Y is the plate number (1-3).

Factorial Run Number		1	2	3	4	5	6	7	8	9	10	11	12	13	14	15	16	17	18	
Design Factors	A = Celpure Grade (P grade)	P300	P65																	
	B = Lysis Neutralisation Mixing Speed (rpm)	1200	1200	400	400	1200	1200	400	400	1200	1200	400	400	1200	1200	400	400	1200	1200	
	C = Celpure Concentration for Lysis Concentration ( $g.L_{lysate}^{-1}$ )	50	50	50	50	30	30	30	30	50	50	50	50	30	30	30	30	50	50	
	D = Number of Permeate Recycles During Lysis Clarification (#)	2	2	2	2	2	2	2	2	0	0	0	0	0	0	0	0	2	2	
	E = Celpure Concentration for Precipitate Removal ( $g.L_{liquid}^{-1}$ )	10	10	10	10	10	10	10	10	10	10	10	10	10	10	10	10	2	2	
	F = Dissolution Mixing Speed (rpm)	High	High																	
	G = LRA Concentration ( $g.L_{liquid}^{-1}$ )	33.3	6.7	6.7	33.3	6.7	33.3	33.3	6.7	6.7	33.3	33.3	6.7	33.3	6.7	6.7	33.3	33.3	6.7	
	H = LRA Adsorption Time (h)	24	2	2	24	24	2	2	24	24	2	2	24	24	2	2	24	2	24	
Raw Data	Plate Position	A5 <sub>2</sub>	A1 <sub>1</sub>	A2 <sub>1</sub>	A6 <sub>2</sub>	B5 <sub>2</sub>	A3 <sub>1</sub>	A4 <sub>1</sub>	B6 <sub>2</sub>	C5 <sub>2</sub>	A5 <sub>1</sub>	A6 <sub>1</sub>	C6 <sub>2</sub>	D5 <sub>2</sub>	B1 <sub>1</sub>	B2 <sub>1</sub>	D6 <sub>2</sub>	B3 <sub>1</sub>	A1 <sub>3</sub>	
	Cuvette Before (g)	2.130	2.129	2.130	2.130	2.130	2.129	2.130	2.130	2.129	2.129	2.130	2.129	2.130	2.130	2.130	2.131	2.130	2.129	
	Cuvette After (g)	2.939	3.382	2.992	2.928	2.788	3.267	2.967	3.868	2.766	2.692	2.777	2.819	2.904	3.999	3.366	2.705	3.001	2.759	
	Cuvette V <sub>t</sub> (mL)	<b>0.809</b>	<b>1.254</b>	<b>0.861</b>	<b>0.798</b>	<b>0.658</b>	<b>1.138</b>	<b>0.837</b>	<b>1.738</b>	<b>0.636</b>	<b>0.563</b>	<b>0.647</b>	<b>0.689</b>	<b>0.774</b>	<b>1.869</b>	<b>1.236</b>	<b>0.575</b>	<b>0.871</b>	<b>0.630</b>	
	t (s)	27	42	42	27	27	42	42	27	27	42	42	27	27	42	42	27	42	27	
	ΔP (Average over t) (mbar)	206.4	102.3	102.3	206.4	206.4	102.3	102.3	206.4	206.4	102.3	102.3	206.4	206.4	102.3	102.3	206.4	102.3	206.4	
$\alpha$ (Eq. 5.1) $\times 10^{-10}$ ( $m.kg^{-1}$ )	<b>8.5</b>	<b>21.2</b>	<b>30.8</b>	<b>8.6</b>	<b>52.3</b>	<b>4.7</b>	<b>6.3</b>	<b>19.8</b>	<b>54.0</b>	<b>9.4</b>	<b>8.2</b>	<b>49.9</b>	<b>8.9</b>	<b>14.2</b>	<b>21.5</b>	<b>12.0</b>	<b>6.1</b>	<b>54.5</b>		
$K_c$ (Eq. 5.2) $\times 10^{-8}$ ( $s.m^{-2}$ )	<b>28.3</b>	<b>14.1</b>	<b>20.5</b>	<b>28.7</b>	<b>34.9</b>	<b>15.5</b>	<b>21.1</b>	<b>13.2</b>	<b>36.0</b>	<b>31.4</b>	<b>27.3</b>	<b>33.3</b>	<b>29.6</b>	<b>9.5</b>	<b>14.3</b>	<b>39.9</b>	<b>20.3</b>	<b>36.4</b>		

Factorial Run Number		19	20	21	22	23	24	25	26	27	28	29	30	31	32	33	34	35	36	
Design Factors	A = Celpure Grade (P grade)	P300	P65																	
	B = Lysis Neutralisation Mixing Speed (rpm)	400	400	1200	1200	400	400	1200	1200	400	400	1200	1200	400	400	1200	1200	400	400	
	C = Celpure Concentration for Lysis Concentration ( $g.L_{lysate}^{-1}$ )	50	50	30	30	30	30	50	50	50	50	30	30	30	30	50	50	50	50	
	D = Number of Permeate Recycles During Lysis Clarification (#)	2	2	2	2	2	2	0	0	0	0	0	0	0	0	2	2	2	2	
	E = Celpure Concentration for Precipitate Removal ( $g.L_{liquid}^{-1}$ )	2	2	2	2	2	2	2	2	2	2	2	2	2	2	10	10	10	10	
	F = Dissolution Mixing Speed (rpm)	High	Low	Low	Low	Low														
	G = LRA Concentration ( $g.L_{liquid}^{-1}$ )	6.7	33.3	6.7	33.3	33.3	6.7	6.7	33.3	33.3	6.7	33.3	6.7	6.7	33.3	33.3	6.7	6.7	33.3	
	H = LRA Adsorption Time (h)	24	2	2	24	24	2	2	24	24	2	2	24	24	2	2	24	24	2	
Raw Data	Plate Position	A2 <sub>3</sub>	B4 <sub>1</sub>	B5 <sub>1</sub>	A3 <sub>3</sub>	A4 <sub>3</sub>	B6 <sub>1</sub>	C1 <sub>1</sub>	A5 <sub>3</sub>	A6 <sub>3</sub>	C2 <sub>1</sub>	C3 <sub>1</sub>	B1 <sub>3</sub>	B2 <sub>3</sub>	C4 <sub>1</sub>	C5 <sub>1</sub>	B3 <sub>3</sub>	B4 <sub>3</sub>	C6 <sub>1</sub>	
	Cuvette Before (g)	2.130	2.129	2.131	2.129	2.130	2.129	2.130	2.129	2.130	2.130	2.129	2.130	2.130	2.129	2.130	2.130	2.129	2.131	
	Cuvette After (g)	3.091	3.863	2.542	3.798	3.263	2.480	3.080	2.712	3.404	3.338	3.100	3.654	3.664	2.558	3.406	3.741	3.226	2.747	
	Cuvette V <sub>t</sub> (mL)	<b>0.961</b>	<b>1.733</b>	<b>0.412</b>	<b>1.669</b>	<b>1.133</b>	<b>0.351</b>	<b>0.950</b>	<b>0.583</b>	<b>1.274</b>	<b>1.208</b>	<b>0.972</b>	<b>1.524</b>	<b>1.534</b>	<b>0.428</b>	<b>1.276</b>	<b>1.611</b>	<b>1.097</b>	<b>0.616</b>	
	t (s)	27	42	42	27	27	42	42	27	27	42	42	27	27	42	42	27	27	42	
	ΔP (Average over t) (mbar)	206.4	102.3	102.3	206.4	206.4	102.3	102.3	206.4	206.4	102.3	102.3	206.4	206.4	102.3	102.3	206.4	206.4	102.3	
$\alpha$ (Eq. 5.1) $\times 10^{-10}$ ( $m.kg^{-1}$ )	<b>35.8</b>	<b>3.1</b>	<b>64.4</b>	<b>4.1</b>	<b>6.1</b>	<b>75.6</b>	<b>27.9</b>	<b>11.8</b>	<b>5.4</b>	<b>21.9</b>	<b>5.5</b>	<b>22.6</b>	<b>22.4</b>	<b>12.4</b>	<b>4.2</b>	<b>21.3</b>	<b>31.4</b>	<b>8.6</b>		
$K_c$ (Eq. 5.2) $\times 10^{-8}$ ( $s.m^{-2}$ )	<b>23.9</b>	<b>10.2</b>	<b>42.9</b>	<b>13.7</b>	<b>20.2</b>	<b>50.4</b>	<b>18.6</b>	<b>39.3</b>	<b>18.0</b>	<b>14.6</b>	<b>18.2</b>	<b>15.0</b>	<b>14.9</b>	<b>41.3</b>	<b>13.9</b>	<b>14.2</b>	<b>20.9</b>	<b>28.7</b>		

Continued on page 235...

Table D.2 continued from page 234.

Design Factors	Factorial Run Number		<b>37</b>	<b>38</b>	<b>39</b>	<b>40</b>	<b>41</b>	<b>42</b>	<b>43</b>	<b>44</b>	<b>45</b>	<b>46</b>	<b>47</b>	<b>48</b>	<b>49</b>	<b>50</b>	<b>51</b>	<b>52</b>	<b>53</b>	<b>54</b>
	A = Celpure Grade	(P grade)	P300	P65																
	B = Lysis Neutralisation Mixing Speed	(rpm)	1200	1200	400	400	1200	1200	400	400	1200	1200	400	400	1200	1200	400	400	1200	1200
	C = Celpure Concentration for Lysis Concentration	(g.L <sub>lysate</sub> <sup>-1</sup> )	30	30	30	30	50	50	50	50	30	30	30	30	50	50	50	50	30	30
	D = Number of Permeate Recycles During Lysis Clarification	(#)	2	2	2	2	0	0	0	0	0	0	0	0	2	2	2	2	2	2
	E = Celpure Concentration for Precipitate Removal	(g.L <sub>liquid</sub> <sup>-1</sup> )	10	10	10	10	10	10	10	10	10	10	10	10	2	2	2	2	2	2
	F = Dissolution Mixing Speed	(rpm)	Low																	
	G = LRA Concentration	(g.L <sub>liquid</sub> <sup>-1</sup> )	6.7	33.3	33.3	6.7	6.7	33.3	33.3	6.7	33.3	6.7	6.7	33.3	33.3	6.7	6.7	33.3	6.7	33.3
	H = LRA Adsorption Time	(h)	2	24	24	2	2	24	24	2	2	24	24	2	24	24	2	2	24	24
Raw Data	Plate Position		D1 <sub>1</sub>	B5 <sub>3</sub>	B6 <sub>3</sub>	D2 <sub>1</sub>	D3 <sub>1</sub>	C1 <sub>3</sub>	C2 <sub>3</sub>	D4 <sub>1</sub>	D5 <sub>1</sub>	C3 <sub>3</sub>	C4 <sub>3</sub>	D6 <sub>1</sub>	C5 <sub>3</sub>	A1 <sub>2</sub>	A2 <sub>2</sub>	C6 <sub>3</sub>	D1 <sub>3</sub>	B1 <sub>2</sub>
	Cuvette Before	(g)	2.130	2.129	2.129	2.130	2.129	2.130	2.130	2.130	2.131	2.129	2.129	2.130	2.130	2.131	2.130	2.131	2.130	2.130
	Cuvette After	(g)	3.098	4.437	3.207	3.505	2.947	3.659	2.941	3.298	2.489	3.714	3.372	3.800	3.721	3.204	3.317	3.411	3.659	2.764
	Cuvette V <sub>t</sub>	(mL)	<b>0.968</b>	<b>2.308</b>	<b>1.078</b>	<b>1.376</b>	<b>0.818</b>	<b>1.529</b>	<b>0.812</b>	<b>1.168</b>	<b>0.358</b>	<b>1.585</b>	<b>1.243</b>	<b>1.670</b>	<b>1.590</b>	<b>1.073</b>	<b>1.187</b>	<b>1.281</b>	<b>1.529</b>	<b>0.634</b>
	t	(s)	42	27	27	42	42	27	27	42	42	27	27	42	27	42	42	27	27	42
	ΔP (Average over t)	(mbar)	102.3	206.4	206.4	102.3	102.3	206.4	206.4	102.3	102.3	206.4	206.4	102.3	206.4	102.3	102.3	206.4	206.4	102.3
	$\alpha$ (Eq. 5.1) × 10 <sup>-10</sup>	(m.kg <sup>-1</sup> )	<b>27.4</b>	<b>3.0</b>	<b>6.4</b>	<b>19.3</b>	<b>32.4</b>	<b>4.5</b>	<b>8.5</b>	<b>22.7</b>	<b>14.8</b>	<b>21.7</b>	<b>27.7</b>	<b>3.2</b>	<b>4.3</b>	<b>24.7</b>	<b>22.3</b>	<b>5.4</b>	<b>22.5</b>	<b>8.4</b>
	$K_c$ (Eq. 5.2) × 10 <sup>-8</sup>	(s.m <sup>-2</sup> )	<b>18.3</b>	<b>9.9</b>	<b>21.3</b>	<b>12.9</b>	<b>21.6</b>	<b>15.0</b>	<b>28.2</b>	<b>15.1</b>	<b>49.4</b>	<b>14.5</b>	<b>18.4</b>	<b>10.6</b>	<b>14.4</b>	<b>16.5</b>	<b>14.9</b>	<b>17.9</b>	<b>15.0</b>	<b>27.9</b>

Design Factors	Factorial Run Number		<b>55</b>	<b>56</b>	<b>57</b>	<b>58</b>	<b>59</b>	<b>60</b>	<b>61</b>	<b>62</b>	<b>63</b>	<b>64</b>	<b>C<sub>1</sub></b>	<b>C<sub>2</sub></b>	<b>C<sub>3</sub></b>	<b>C<sub>4</sub></b>	<b>C<sub>5</sub></b>	<b>C<sub>6</sub></b>	<b>C<sub>7</sub></b>	<b>C<sub>8</sub></b>	
	A = Celpure Grade	(P grade)	P300	P65	P65 / P300																
	B = Lysis Neutralisation Mixing Speed	(rpm)	400	400	1200	1200	400	400	1200	1200	400	400	800								
	C = Celpure Concentration for Lysis Concentration	(g.L <sub>lysate</sub> <sup>-1</sup> )	30	30	50	50	50	50	30	30	30	30	40								
	D = Number of Permeate Recycles During Lysis Clarification	(#)	2	2	0	0	0	0	0	0	0	0	1								
	E = Celpure Concentration for Precipitate Removal	(g.L <sub>liquid</sub> <sup>-1</sup> )	2	2	2	2	2	2	2	2	2	2	6								
	F = Dissolution Mixing Speed	(rpm)	Low	Medium																	
	G = LRA Concentration	(g.L <sub>liquid</sub> <sup>-1</sup> )	33.3	6.7	6.7	33.3	33.3	6.7	33.3	6.7	6.7	33.3	20.0								
	H = LRA Adsorption Time	(h)	2	24	24	2	2	24	24	2	2	24	13								
Raw Data	Plate Position		B2 <sub>2</sub>	D2 <sub>3</sub>	D3 <sub>3</sub>	C1 <sub>2</sub>	C2 <sub>2</sub>	D4 <sub>3</sub>	D5 <sub>3</sub>	D1 <sub>2</sub>	D2 <sub>2</sub>	D6 <sub>3</sub>	A3 <sub>2</sub>	A4 <sub>2</sub>	B3 <sub>2</sub>	B4 <sub>2</sub>	C3 <sub>2</sub>	C4 <sub>2</sub>	D3 <sub>2</sub>	D4 <sub>2</sub>	
	Cuvette Before	(g)	2.130	2.130	2.129	2.129	2.129	2.130	2.131	2.130	2.130	2.130	2.130	2.130	2.130	2.131	2.129	2.130	2.129	2.129	2.130
	Cuvette After	(g)	3.824	3.026	3.561	2.921	3.012	3.564	3.143	3.103	2.698	3.112	2.725	2.864	2.966	2.848	2.840	2.916	2.823	2.861	
	Cuvette V <sub>t</sub>	(mL)	<b>1.694</b>	<b>0.896</b>	<b>1.432</b>	<b>0.792</b>	<b>0.882</b>	<b>1.434</b>	<b>1.012</b>	<b>0.973</b>	<b>0.568</b>	<b>0.982</b>	<b>0.595</b>	<b>0.734</b>	<b>0.835</b>	<b>0.720</b>	<b>0.710</b>	<b>0.787</b>	<b>0.694</b>	<b>0.731</b>	
	t	(s)	42	27	27	42	42	27	27	42	42	27	22	22	22	22	22	22	22	22	
	ΔP (Average over t)	(mbar)	102.3	206.4	206.4	102.3	102.3	206.4	206.4	102.3	102.3	206.4	259.5	259.5	259.5	259.5	259.5	259.5	259.5	259.5	
	$\alpha$ (Eq. 5.1) × 10 <sup>-10</sup>	(m.kg <sup>-1</sup> )	<b>3.1</b>	<b>38.4</b>	<b>24.0</b>	<b>6.7</b>	<b>6.0</b>	<b>24.0</b>	<b>6.8</b>	<b>27.2</b>	<b>46.7</b>	<b>7.0</b>	<b>19.7</b>	<b>16.0</b>	<b>14.1</b>	<b>16.3</b>	<b>16.5</b>	<b>14.9</b>	<b>16.9</b>	<b>16.1</b>	
	$K_c$ (Eq. 5.2) × 10 <sup>-8</sup>	(s.m <sup>-2</sup> )	<b>10.4</b>	<b>25.6</b>	<b>16.0</b>	<b>22.3</b>	<b>20.0</b>	<b>16.0</b>	<b>22.6</b>	<b>18.2</b>	<b>31.1</b>	<b>23.3</b>	<b>39.5</b>	<b>32.0</b>	<b>28.1</b>	<b>32.6</b>	<b>33.1</b>	<b>29.8</b>	<b>33.8</b>	<b>32.1</b>	

### D.3 Example plasmid DNA gels

The failed gel results from the post-LRA analysis are shown in Figure D.1. Also included for reference are successful example gels generated during trial runs on different salt concentrations for the precipitate dissolution (Figure D.2) and a post LRA sample using similar procedures and the same plasmid source during a pilot plant study for masters student training (Figure D.3). These highlight some of the likely causes of failure by the differences in the gel performances. The possible interference of LRA particles present in the samples (see Section 5.3.3) may be the cause of the dots of staining retained in the wells in Figure D.1. These are in contrast to the random specs present in an imperfectly cast gel (Figure D.2) which still yields all the necessary information. Another clear problem with the pDNA factorial gels is the high concentration of the denatured pDNA standard which was clearly not at the correct dilution and may have caused lighter bands in the more dilute samples not to show up correctly. It is not known for sure what caused the problems with the gel results and even worse errors were unfortunately seen with the spare set of samples retained due to errors in the procedure. There were definite signs of the presence of nucleic acids since there were clearly visible pellets in each sample during the isopropanol precipitation and the gels generated showed some staining in almost all the samples.

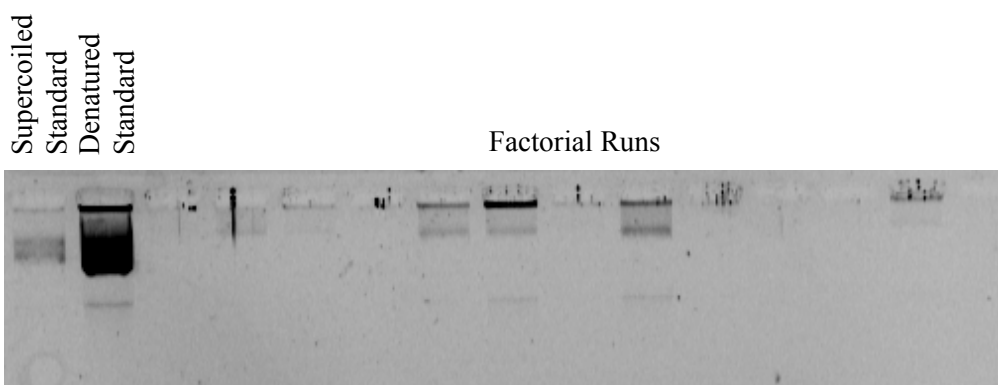


**Figure D.1.** Example gel from the post LRA samples for factorial analysis, showing the very light bands and contamination, including poor standards in the first two lanes.

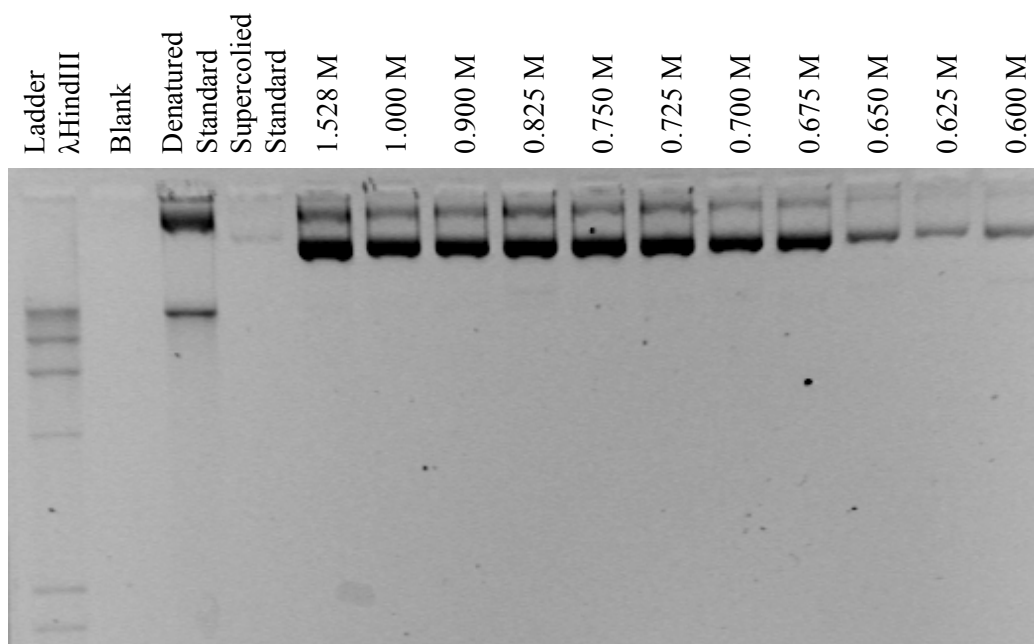


**Figure D.2.** Example gel from successful scouting tests looking at the effect of sodium chloride concentration in precipitate dissolution on the relative concentration of supercoiled and open circular plasmid DNA.

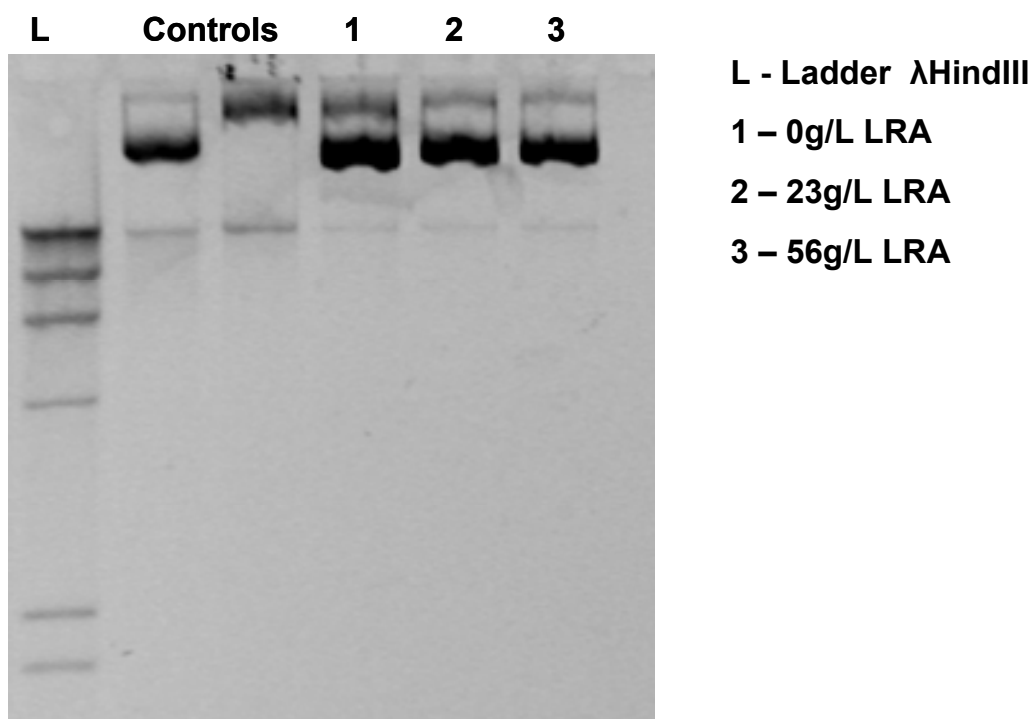


**Figure D.3.** Example gel from a pilot plant study including an LRA adsorption step. Experiments carried out by masters students in a pilot plant week study under my supervision. Gels were performed by other post-graduate students during the study. Controls are supercoiled plasmid standard (first) and denatured plasmid (second).

## E.0 Appendix E: Quantification of low specific cake resistances

During the whole microscale plasmid DNA process sequence described in Chapter 5, the precipitate recovery and removal steps (Section 2.5.2.4 and 2.5.2.5) generated cakes of such low resistance that gravity alone was capable of permeating liquid through the cake. In such circumstances the existing methods will not allow quantification of the cake resistance. Adjustments that could potentially be made to allow quantification include increasing the volume per unit area feed challenge (not possible with the whole process sequence volumes and the current custom filter plate design) or change the flow through solution to a more viscous fluid (deviation from process fluids risks possible adverse interactions with the cake components). The solution attempted was quickly thought up during the experimental execution and implemented on the precipitate recovery process only.

The amount of water permeated during a fixed time (13 minutes) was measured using a starting volume of 2mL added directly to the wells in sequence and the removal of these wells from the plate in the same sequence after the elapsed time. The volume of liquid remaining on the feed side of the filter cake is directly proportional to the applied pressure at that point in time and will decrease exponentially over time, allowing the calculation of a specific cake resistance.

### E.1 Method for quantification of low specific cake resistances

Combining equations 1.1 and 1.17 generates the following expression for the flow of a solution through a filter cake pre-deposited onto a membrane surface:

$$\frac{dV}{dt} = \frac{A \cdot \Delta P}{\mu \left( R_m + \left[ \alpha \rho_0 \left( \frac{V_c}{A} \right) \right]_{precipitate} \right)} \quad (\text{E.1})$$

where  $V$  is the flow through filtrate volume ( $\text{m}^3$ ),  $t$  is time (s),  $A$  is filtration area ( $\text{m}^2$ ),  $\Delta P$  is pressure difference (Pa),  $\mu$  is the flow through solution viscosity (Pa.s),  $R_m$  is resistance of the membrane ( $\text{m}^{-1}$ ),  $\alpha$  is specific cake resistance per unit dry cake mass ( $\text{m.kg}^{-1}$ ),  $\rho_0$  is the mass of dry solids per unit volume of filtrate ( $\text{kg.m}^{-3}$ ) and  $V_c$  is the volume of feed added to deposit the cake ( $\text{m}^3$ ). The terms under the subscript 'precipitate' were values during the generation of the precipitate cake. The membrane resistance here is considered to be the applied pre-coat with an appropriate term for its cake resistance added. The wire mesh filter is assumed to provide negligible resistance. The numerator of Equation E.1 is equal to the force applied to the membrane which can be represented using the flow through solution density,  $\rho_{fi}$  ( $\text{kg.m}^{-3}$ ), the acceleration due to gravity,  $g$  ( $\text{m.s}^{-2}$ ) and the volume of the flow-through solution remaining above the cake:

$$\frac{dV}{dt} = \frac{\rho g (V_i - V)}{\mu \left( \left[ \alpha \rho_0 \left( \frac{V_c}{A} \right) \right]_{precoat} + \left[ \alpha \rho_0 \left( \frac{V_c}{A} \right) \right]_{precipitate} \right)} \quad (\text{E.2})$$

where  $V_i$  is initial flow-through volume above the cake ( $\text{m}^3$ ). Equation E.2 is integrated to account for the diminishing force due to the weight of the flow through solution as it decays exponentially. Rearranging the integrated form allows the modified cake filtration constant,  $K_c'$  ( $\text{N.s.m}^{-4}$ ), or specific cake resistance,  $\alpha$  ( $\text{m.kg}^{-1}$ ), to be evaluated for the precipitate cake.

$$K_c' = \mu \alpha \rho_0 = \frac{1}{V_c} \left( \frac{\rho_{fi} g t A}{\ln \left( \frac{V_i}{V_i - V} \right)} - [K_c' V_c]_{precoat} \right) \quad (\text{E.3})$$

$$\alpha = \frac{1}{\mu \rho_0 V_c} \left( \frac{\rho_{fi} g t A}{\ln \left( \frac{V_i}{V_i - V} \right)} - [\mu \alpha \rho_0 V_c]_{precoat} \right) \quad (\text{E.4})$$

## E.2 Evaluation of precipitate removal results

The results for the specific cake resistance were difficult to evaluate for the precipitate cake alone. Indications were that the resistances of the precipitate cakes themselves were very small and were obscured by the variability in the pre-coat cake resistance. A more accurate data set could have been generated if the individual pre-coat resistances were calculated using the same method before application of the precipitate suspension.

Factorial analysis was carried out for the cake resistance of the pre-coat combined with the precipitate cake. Since the volumes added for cake deposition were the same it was possible to combine the cake resistances in Equation E.2 and produce a simpler integrated form for specific cake resistance quantification:

$$\alpha_{combined} = \frac{1}{\mu\rho_0V_c} \cdot \frac{\rho_{ft}gtA}{\ln\left(\frac{V_i}{V_i-V}\right)} \quad (E.4)$$

Where  $\rho_0$  is now the sum of both precoat and precipitate values. The raw data generated is detailed in Table E.1. The factorial analysis (Figure E.1) shows that the dominant variable is Celpure grade (A) with the resistance to flow and therefore the liquid collected by the force of gravity being dependant on the grade of Celpure used. Increasing lysis neutralisation mixing speed (B) increases cake resistance, although it is not clear why as higher clarification is achieved at higher mixing speeds (Figure 5.5). There is a marginally significant filter aid effect as increasing the Celpure concentration (E) gives a slight reduction in cake resistance. This effect may have been clearer if the measurement of pre-coat resistance, which should not be affected by the precipitate cake, had been removed from the total result.

In general the factorial analysis indicates that there is merit in this measurement method, but does not verify it. The method was able to distinguish between cakes of different Celpure grade and quantity, with the overall resistance at different concentration being approximately equivalent.

**Table E.1.** The raw data and specific cake resistance calculations from evaluation of the low specific cake resistances during the precipitate recovery stage of a plasmid DNA purification step. Experiments carried out as described in Section 2.5.2.4 and Section E.1.

<b>Design Factors</b>	<b>Subset Analysis Factorial Run Number</b>		<b>1</b>		<b>2</b>		<b>3</b>		<b>4</b>		<b>5</b>		<b>6</b>		<b>7</b>		<b>8</b>		<b>9</b>		<b>10</b>		<b>11</b>		<b>12</b>	
	Main Factorial Run Number		1	33	2	34	3	35	4	36	5	37	6	38	7	39	8	40	9	41	10	42	11	43	12	44
	A = Celpure Grade	(P grade)	P300		P65		P300		P65		P300		P65		P300		P65		P300		P65		P300		P65	
	B = Lysis Neutralisation Mixing Speed	(rpm)	1200		1200		400		400		1200		1200		400		400		1200		1200		400		400	
	C = Celpure Concentration for Lysis Concentration	(g.L <sub>lysate</sub> <sup>-1</sup> )	50		50		50		50		30		30		30		30		50		50		50		50	
	D = Number of Permeate Recycles During Lysis Clarification	(#)	2		2		2		2		2		2		2		2		0		0		0		0	
E = Celpure Concentration for Precipitate Removal	(g.L <sub>liquid</sub> <sup>-1</sup> )	10		10		10		10		10		10		10		10		10		10		10		10		
<b>Raw Data</b>	Plate Position		C3 <sub>3</sub>	C4 <sub>3</sub>	C1 <sub>3</sub>	C2 <sub>3</sub>	C5 <sub>2</sub>	C6 <sub>2</sub>	C1 <sub>2</sub>	C2 <sub>2</sub>	C3 <sub>2</sub>	C4 <sub>2</sub>	C5 <sub>1</sub>	C6 <sub>1</sub>	C3 <sub>1</sub>	C4 <sub>1</sub>	C1 <sub>1</sub>	C2 <sub>1</sub>	A3 <sub>3</sub>	A4 <sub>3</sub>	A1 <sub>3</sub>	A2 <sub>3</sub>	A5 <sub>2</sub>	A6 <sub>2</sub>	A1 <sub>2</sub>	A2 <sub>2</sub>
	t	(s)	600	600	600	600	780	780	780	780	780	780	780	780	780	780	780	780	600	600	600	600	780	780	780	780
	Cuvette Before	(g)	2.154	2.155	2.156	2.154	2.155	2.156	2.155	2.154	2.155	2.154	2.159	2.155	2.155	2.155	2.155	2.154	2.155	2.156	2.154	2.157	2.156	2.156	2.156	2.153
	Cuvette After	(g)	3.056	3.140	2.628	2.752	3.451	3.518	2.893	2.834	3.649	3.731	2.903	2.750	3.658	3.784	2.923	3.006	3.111	2.844	2.772	2.787	3.605	3.582	2.970	2.953
	Cuvette V <sub>t</sub>	(mL)	0.902	0.986	0.472	0.598	1.296	1.363	0.738	0.679	1.494	1.577	0.744	0.595	1.503	1.629	0.768	0.853	0.956	0.688	0.618	0.631	1.449	1.426	0.814	0.800
	α (Eq. E.5) × 10 <sup>-9</sup>	(m.kg <sup>-1</sup> )	19.7	17.4	43.7	33.2	14.7	13.4	33.3	36.9	11.1	9.9	32.9	43.4	11.0	9.1	31.6	27.6	18.1	28.0	31.9	31.1	11.9	12.3	29.3	30.0
<b>Average α × 10<sup>-9</sup> (± 1SD)</b>	<b>(m.kg<sup>-1</sup>)</b>	<b>18.5 ± 1.6</b>		<b>38.5 ± 7.5</b>		<b>14.0 ± 0.9</b>		<b>35.1 ± 2.6</b>		<b>10.5 ± 0.9</b>		<b>38.2 ± 7.4</b>		<b>10.0 ± 1.3</b>		<b>29.6 ± 2.9</b>		<b>23.0 ± 7.0</b>		<b>31.5 ± 0.6</b>		<b>12.1 ± 0.3</b>		<b>29.7 ± 0.5</b>		
<b>Design Factors</b>	<b>Subset Analysis Factorial Run Number</b>		<b>13</b>		<b>14</b>		<b>15</b>		<b>16</b>		<b>17</b>		<b>18</b>		<b>19</b>		<b>20</b>		<b>21</b>		<b>22</b>		<b>23</b>		<b>24</b>	
	Main Factorial Run Number		13	45	14	46	15	47	16	48	17	49	18	50	19	51	20	52	21	53	22	54	23	55	24	56
	A = Celpure Grade	(P grade)	P300		P65		P300		P65		P300		P65		P300		P65		P300		P65		P300		P65	
	B = Lysis Neutralisation Mixing Speed	(rpm)	1200		1200		400		400		1200		1200		400		400		1200		1200		400		400	
	C = Celpure Concentration for Lysis Concentration	(g.L <sub>lysate</sub> <sup>-1</sup> )	30		30		30		30		50		50		50		50		30		30		30		30	
	D = Number of Permeate Recycles During Lysis Clarification	(#)	0		0		0		0		2		2		2		2		2		2		2		2	
E = Celpure Concentration for Precipitate Removal	(g.L <sub>liquid</sub> <sup>-1</sup> )	10		10		10		10		2		2		2		2		2		2		2		2		
<b>Raw Data</b>	Plate Position		A3 <sub>2</sub>	A4 <sub>2</sub>	A5 <sub>1</sub>	A6 <sub>1</sub>	A3 <sub>1</sub>	A4 <sub>1</sub>	A1 <sub>1</sub>	A2 <sub>1</sub>	D3 <sub>3</sub>	D4 <sub>3</sub>	D1 <sub>3</sub>	D2 <sub>3</sub>	D5 <sub>2</sub>	D6 <sub>2</sub>	D1 <sub>2</sub>	D2 <sub>2</sub>	D3 <sub>2</sub>	D4 <sub>2</sub>	D5 <sub>1</sub>	D6 <sub>1</sub>	D3 <sub>1</sub>	D4 <sub>1</sub>	D1 <sub>1</sub>	D2 <sub>1</sub>
	t	(s)	780	780	780	780	780	780	780	780	600	600	600	600	780	780	780	780	780	780	780	780	780	780	780	780
	Cuvette Before	(g)	2.155	2.154	2.159	2.156	2.160	2.155	2.155	2.158	2.156	2.153	2.156	2.154	2.155	2.156	2.154	2.156	2.156	2.156	2.158	2.156	2.156	2.160	2.155	2.157
	Cuvette After	(g)	3.617	3.470	2.999	3.056	3.486	3.658	2.957	2.985	3.301	2.926	2.935	2.964	3.691	3.791	3.151	3.395	3.632	3.654	3.205	3.098	3.841	3.847	3.193	3.130
	Cuvette V <sub>t</sub>	(mL)	1.463	1.315	0.840	0.900	1.326	1.503	0.803	0.828	1.145	0.773	0.779	0.810	1.537	1.636	0.997	1.239	1.476	1.499	1.047	0.942	1.685	1.687	1.039	0.973
	α (Eq. E.5) × 10 <sup>-9</sup>	(m.kg <sup>-1</sup> )	11.7	14.3	28.1	25.6	14.1	11.0	29.9	28.7	23.4	40.8	40.3	38.4	17.7	15.2	37.5	26.8	19.3	18.7	34.9	40.6	14.0	14.0	35.3	38.8
<b>Average α × 10<sup>-9</sup> (± 1SD)</b>	<b>(m.kg<sup>-1</sup>)</b>	<b>13.0 ± 1.9</b>		<b>26.9 ± 1.8</b>		<b>12.5 ± 2.2</b>		<b>29.3 ± 0.8</b>		<b>32.1 ± 12.3</b>		<b>39.4 ± 1.4</b>		<b>16.4 ± 1.8</b>		<b>32.1 ± 7.6</b>		<b>19.0 ± 0.4</b>		<b>37.8 ± 4.0</b>		<b>14.0 ± 0.0</b>		<b>37.1 ± 2.5</b>		
<b>Design Factors</b>	<b>Subset Analysis Factorial Run Number</b>		<b>25</b>		<b>26</b>		<b>27</b>		<b>28</b>		<b>29</b>		<b>30</b>		<b>31</b>		<b>32</b>		<b>C<sub>1</sub></b>	<b>C<sub>2</sub></b>	<b>C<sub>3</sub></b>	<b>C<sub>4</sub></b>	<b>C<sub>5</sub></b>	<b>C<sub>6</sub></b>	<b>C<sub>7</sub></b>	<b>C<sub>8</sub></b>
	Main Factorial Run Number		25	57	26	58	27	59	28	60	29	61	30	62	31	63	32	64	P65 / P300							
	A = Celpure Grade	(P grade)	P300		P65		P300		P65		P300		P65		P300		P65		800							
	B = Lysis Neutralisation Mixing Speed	(rpm)	1200		1200		400		400		1200		1200		400		400		40							
	C = Celpure Concentration for Lysis Concentration	(g.L <sub>lysate</sub> <sup>-1</sup> )	50		50		50		50		30		30		30		30		1							
	D = Number of Permeate Recycles During Lysis Clarification	(#)	0		0		0		0		0		0		0		0		6							
E = Celpure Concentration for Precipitate Removal	(g.L <sub>liquid</sub> <sup>-1</sup> )	2		2		2		2		2		2		2		2										
<b>Raw Data</b>	Plate Position		B3 <sub>3</sub>	B4 <sub>3</sub>	B1 <sub>3</sub>	B2 <sub>3</sub>	B5 <sub>2</sub>	B6 <sub>2</sub>	B1 <sub>2</sub>	B2 <sub>2</sub>	B3 <sub>2</sub>	B4 <sub>2</sub>	B5 <sub>1</sub>	B6 <sub>1</sub>	B3 <sub>1</sub>	B4 <sub>1</sub>	B1 <sub>1</sub>	B2 <sub>1</sub>	A5 <sub>3</sub>	A6 <sub>3</sub>	B5 <sub>3</sub>	B6 <sub>3</sub>	C5 <sub>3</sub>	C6 <sub>3</sub>	D5 <sub>3</sub>	D6 <sub>3</sub>
	t	(s)	600	600	600	600	780	780	780	780	780	780	780	780	780	780	780	780	600	600	600	600	600	600	600	600
	Cuvette Before	(g)	2.155	2.156	2.154	2.154	2.156	2.154	2.157	2.157	2.156	2.155	2.154	2.155	2.153	2.154	2.152	2.153	2.156	2.157	2.155	2.155	2.156	2.157	2.156	2.155
	Cuvette After	(g)	3.159	3.838	2.914	2.860	3.685	3.806	3.264	3.249	3.778	3.599	3.233	3.320	3.586	3.569	3.307	3.283	2.933	2.804	3.020	3.121	2.924	2.969	2.983	3.197
	Cuvette V <sub>t</sub>	(mL)	1.004	1.682	0.761	0.707	1.529	1.652	1.107	1.093	1.622	1.444	1.079	1.165	1.433	1.415	1.155	1.130	0.777	0.648	0.865	0.966	0.768	0.812	0.827	1.043
	α (Eq. E.5) × 10 <sup>-9</sup>	(m.kg <sup>-1</sup> )	28.5	10.8	41.6	45.6	17.9	14.8	32.1	32.7	15.5	20.2	33.3	29.6	20.5	21.1	30.0	31.1	30.1	61.4	42.4	36.4	49.6	46.1	45.0	32.6
<b>Average α × 10<sup>-9</sup> (± 1SD)</b>	<b>(m.kg<sup>-1</sup>)</b>	<b>19.7 ± 12.5</b>		<b>43.6 ± 2.9</b>		<b>16.3 ± 2.2</b>		<b>32.4 ± 0.5</b>		<b>17.9 ± 3.3</b>		<b>31.5 ± 2.6</b>		<b>20.8 ± 0.4</b>		<b>30.5 ± 0.7</b>		<b>43.0 ± 10.1</b>								



### **E.3 Scale-up of precipitate recovery**

The RVLf scale-up test was carried out as described in Section 2.5.3.4 using a precipitate suspension with P300 grade Celpure filter aid at  $2 \text{ g.L}^{-1}_{\text{liquid}}$ . Preparation for the RVLf experiments were carried out using Celpure P300, 1200 rpm lysis neutralisation mixing speed and a Celpure concentration of  $50 \text{ g.L}^{-1}_{\text{lysate}}$  during lysate clarification with no recycles. Assuming exactly 2mL of Celpure 300 pre-coat solution was added at  $10 \text{ g.L}^{-1}_{\text{liquid}}$ , the calculated modified cake filtration constant from the microwell data was actually slightly negative at these conditions. Using just a 20% lower value for the celpure pre-coat would turn a negative value into a precise prediction of the RVLf results. This is because the precipitate is so low fouling that the pressure only increases approximately one kPa over the course of 10 minutes constant flow filtration.

### **E.4 Summary**

This appendix puts forward a potential solution to the problem of quantifying the specific cake resistances. It appears that it does a good job of differentiating relative performance for some feeds but may have a limited use given the very low impact of such feeds on the overall process demands.